Opposite effects of *mstnb* and *inhbaa* on cardiomyocyte proliferation during development and repair

Dissertation
zur Erlangung des Doktorgrades
der Naturwissenschaften

vorgelegt beim Fachbereich 15
der Johann Wolfgang Goethe -Universität
in Frankfurt am Main

Von
Deepika Dogra
aus Noida, Indien

Frankfurt 2017
(D30)

vom Fachbereich Biowissenschaften (FB15) der Johann Wolfgang Goethe - Universität als Dissertation angenommen.

Dekan: Prof. Dr. Meike Piepenbring

Gutachter: Prof. Dr. Didier Y. R. Stainier

Prof. Dr. Virginie Lecaudey

Datum der Disputation:

SUPERVISED BY

Dr. Sven Reischauer, Ph.D.
Department of Developmental Genetics
Max Planck Institute for Heart and Lung Research
Bad Nauheim, Germany

REVIEWERS

Prof. Dr. Didier Y. R. Stainier, Ph.D.
Department of Developmental Genetics
Max Planck Institute for Heart and Lung Research
Bad Nauheim, Germany

and

Prof. Dr. Virginie Lecaudey, Ph.D.
Department of Developmental Biology of Vertebrates
Institute of Cell Biology and Neuroscience
Johann Wolfgang Goethe University
Frankfurt am Main, Germany

ERKLÄRUNG

Ich erkläre hiermit, dass ich mich bisher keiner Doktorprüfung im Mathematisch-Naturwissenschaftlichen Bereich unterzogen habe.

Frankfurt am Main, den .....

(Unterschrift)

Versicherung

Ich erkläre hiermit, dass ich die vorgelegte Dissertation über

Opposite effects of *mstnb* and *inhbaa* on cardiomyocyte proliferation during development and repair.

selbständig angefertigt und mich anderer Hilfsmittel als der in ihr angegebenen nicht bedient habe, insbesondere, dass alle Entlehnungen aus anderen Schriften mit Angabe der betreffenden Schrift gekennzeichnet sind.

Ich versichere, die Grundsätze der guten wissenschaftlichen Praxis beachtet, und nicht die Hilfe einer kommerziellen Promotionsvermittlung in Anspruch genommen zu haben.

Vorliegende Ergebnisse der Arbeit werden in folgendem Publikationsorgan veröffentlicht:

Dogra D., et al. Opposite effects of TGF-β ligands on cardiomyocyte proliferation during development and repair. *(Manuskript in Arbeit)*

Frankfurt am Main, den .....

(Unterschrift)

The most important thing in life is to stop saying 'I wish' and start saying 'I will'.

Consider nothing impossible, then treat possibilities as probabilities.

Charles Dickens

Table of Contents

Abbreviations

µg	microgram
µl	microlitre
µm	micrometer
4-HT	4-Hydroxytamoxifen
ACVR	Activin Receptor
AFOG	Acid Fuchsin Orange G
ARE	Activin Response Element
ATP	Adenosine triphosphate
BMP	Bone Morphogenetic Protein
BOD	Biochemical Oxygen Demand
bp	basepair
BSA	Bovine Serum Albumin
ca	constitutively active
$CaCl_2$	Calcium chloride
CAD	Coronary Artery Disease
CDKN2B	Cyclin Dependent Kinase Inhibitor 2B
cDNA	Complementary DNA
CDS	Coding sequence
CFP	Cyan Fluorescent Protein
cm	Centimeter
$CuSO_4$	Copper sulphate
CVD	Cardiovascular Diseases
Cxcl12	C-X-C Motif Chemokine Ligand 12
Cxcr4	C-X-C Motif Chemokine Receptor 4
DAPI	4',6-diamidino-2-phenylindole
ddH_2O	Double distilled water
DEPC	Diethyl pyrocarbonate
dkk1b	*dickkopf1b*
DMSO	Dimethyl sulfoxide
dn	Dominant negative
DNA	Deoxyribonucleic acid
DNase	Deoxyribonuclease
dNTP	Nucleoside triphosphate
dpa	days post amputation
dpci	days post cryoinjury
dpf	days post fertilization
DTA	Diphtheria toxin
E.coli	Escherichia coli
ECM	Extracellular matrix
EDM	Embryo Disruption Medium
EDTA	Ethylenediaminetetraacetic acid
EdU	5-ethynyl-2′-deoxyuridine
EGF	Epidermal Growth Factor
EGFP	Enhanced Green Fluorescent Protein
embCMHC	embryonic Cardiac Myosin Heavy Chain
EMT	Epithelial–mesenchymal transition
Erk	Extracellular signal–regulated kinases
FC	Fold Change
FGF	Fibroblast Growth Factor

Fgfr	Fibroblast growth factor receptor
FOXH1	Forkhead box H1
g	gram
GATA4	GATA binding protein 4
GDF	Growth Differentiation Factor
GOF	gain-of-function
Gsc	Goosecoid
H&E	Hematoxylin and Eosin
H_2O_2	Hydrogen peroxide
HAND2	Heart- and neural crest derivatives-expressed protein 2
HCl	Hydrochloric acid
HER2	human epidermal growth factor receptor 2
hESC-CMs	Human Embryonic-stem-cell-derived Cardiomyocytes
hey2	Hairy/enhancer-of-split related with YRPW motif protein 2
HIF1	Hypoxia-Inducible Factor1
hpci	hours post cryoinjury
hpf	hours post fertilization
HRMA	High Resolution Melt Analysis
IGF	Insulin-like Growth Factor
IHC	Immunohistochemistry
IL6	Interleukin 6
inhbaa	*inhibin-betaAa*
IPTG	Isopropyl β-D-1-thiogalactopyranoside
Jak1	Janus Kinase 1
JNK	c-Jun N-terminal kinases
kb	kilobase
KCl	Potassium chloride
KH_2PO_4	Monopotassium phosphate
L	Litre
LB	Lysogeny Broth
LMA	Low Melting Agarose
LMD	Laser Microdissection
LOF	loss-of-function
M	Molar
MAPK	Mitogen-activated protein kinases
MCM5	Minichromosome Maintenance Complex Component 5
MEF2C	Myocyte Enhancer Factor 2C
mg	milligram
$MgCl_2$	Magnesium chloride
$MgSO_4$	Magnesium sulphate
MI	Myocardial Infarction
miRNA	microRNA
ml	millilitre
mm	millimeter
MO	Morpholino
mpf	Months post fertilization
mRNA	Messenger RNA

mstnb	*myostatin b*
Mtz	Metronidazole
myl7	*myosin light chain 7*
Na_2HPO_4	Disodium phosphate
NaCl	Sodium chloride
NaOH	Sodium hydroxide
NBT/BCIP	nitro-blue tetrazolium/5-bromo-4-chloro-3'-indolyphosphate
NFκB	Nuclear Factor Kappa-light-chain-enhancer of activated B cells
ng	nanogram
nm	nanometer
Nrg	Neuregulin
NTR	Nitroreductase
OCT	Optimal Cutting Temperature
OCT4	Octamer-binding transcription factor 4
OE	Overexpression
P	Postnatal Day
PAI-1	Plasminogen activator inhibitor-1
PBS	Phosphate-buffered saline
PCNA	Proliferating cell nuclear antigen
PCR	Polymerase Chain Reaction
PDGF	Platelet-Derived Growth Factor
PFA	Paraformaldehyde
pH	Negative log of hydrogen ion concentration
pg	pictogram
PI3K	Phosphatidylinositol-4,5-bisphosphate 3-kinase
PTU	1-phenyl-2-thiourea
RA	Retinoic Acid
raldh2	*retinaldehyde dehydrogenase 2*
RCF	Relative Centrifugal Field
RFP	Red Fluorescent Protein
RNA	Ribonucleic acid
RNase	Ribonuclease
rpl13	*60S ribosomal protein L13*
RPM	Revolutions Per Minute
RT	Room Temperature
RT-qPCR	Real-Time quantitative PCR
RVD	Repeat Variable Diresidue
s	second
s.e.m.	standard error of mean
SBE	Smad Binding Element
SOX2	(sex determining region Y)-box 2
Stat3	Signal transducer and activator of transcription 3
TALEN	Transcription activator-like effector nucleases
tcf21	*transcription factor 21*
TCF3	Transcription Factor 3

TGFBR	TGF-β Receptor
TGF-β	Transforming Growth Factor beta
TRAP	Translating Ribosome Affinity Purification
Tricaine	Ethyl-m-aminobenzoate methanesulfonate
U	Unit
UV	Ultra Violet
VEGF	Vascular Endothelial Growth Factor
V	Volt
WHO	World Health Organization
wt	Wild-type
wt1b	*wilms tumor 1b*
X-gal	5-bromo-4-chloro-3-indolyl-D-galactopyranoside

1. Introduction

1.1 Myocardial Infarction (MI)

Cardiovascular diseases (CVD) including myocardial infarction (MI) are one of the major causes of mortality worldwide, leading to arrhythmia and heart failure (Mozaffarian et al., 2016). MI (also known as heart attack) refers to the damage and death of heart muscle due to the prolonged lack of oxygen supply mainly caused by coronary artery disease (CAD). The occurrence of MI due to CAD involves the complete blockage of a coronary artery caused by a rupture of an atherosclerotic plaque (**Figure 1.1**). Mammalian heart cannot regenerate after MI as the injured heart muscle is replaced by irreversible fibrotic scar, which leads to the loss of cardiac contractility and ultimately causes heart failure (Laflamme and Murry, 2011; Steinhauser and Lee, 2011). Thus there is an urgent need to develop regenerative therapies to treat the ailing human heart.

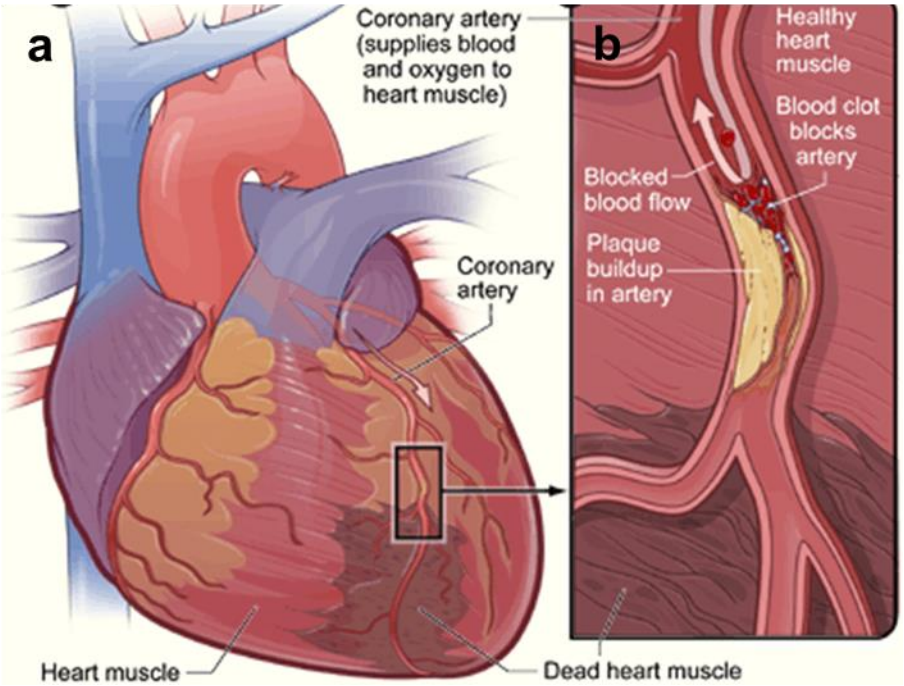

Figure 1.1. Schematic of myocardial infarction (MI) in the human heart. (**a**) Injured heart muscle of a patient suffering from MI, due to coronary artery disease (CAD). (**b**) Detailed view of blockage in the coronary artery. Modified images are adapted from nurseslabs.com.

1.2 Therapeutic strategies

Current therapeutic strategies for the treatment of damaged cardiac muscle focus on introducing stem cell-derived cardiomyocytes in the injured heart, stimulating cardiomyocyte division and trans-differentiation of other cell types into cardiomyocytes, explained in details below.

1.2.1 Introduction of stem cell-derived cardiomyocytes

Pluripotent stem cells were used to generate human embryonic-stem-cell-derived cardiomyocytes (hESC-CMs), which were transplanted to a non-primate (monkey) heart suffering from MI. The intramyocardial delivery of hESC-CMs led to remuscularization of the infarcted heart. The transplanted hESC-CMs matured overtime, were perfused by host vasculature and also electrically coupled to the host heart. However, non-fatal cardiac arrhythmias were observed in the hESC-CM-engrafted primates, indicating a downfall of this MI treatment therapy which needs to be overcome (Chong et al., 2014; Chong and Murry, 2014). Another group of researchers have shown that temporal modulation of Wnt signaling cascade can stimulate robust cardiac induction in human pluripotent stem cells (Lian et al., 2012).

1.2.2 Promotion of cardiomyocyte proliferation

Within the first two weeks of birth in mice and about 10-20 years in humans, the cardiomyocytes transit from cell-cycle activity to a non-cycling state (Bergmann et al., 2009; Mollova et al., 2013; Soonpaa et al., 1996; Walsh et al., 2010). Moreover, the capacity of scarless cardiac regeneration appears to be present in mice only until the neonatal stage, which indicates an association between cardiomyocyte cell-cycle activity and the regenerative capacity of injured heart (Porrello et al., 2011). Thus, another approach which has directed the attention of research community is the enhancement of endogenous regenerative mechanisms, by inducing cardiomyocyte proliferation. To regain the proliferative ability of the adult cardiomyocytes, genetic modulation of cell-cycle checkpoints has been performed, such as cyclin B1-CDC2 overexpression and p21/p27 knockdown *in vitro* (Bicknell et al., 2004; Di Stefano et al., 2011), however cell cycle factors do not universally induce cell division but may only promote cardiomyocyte DNA synthesis and multinucleation (Soonpaa and Field, 1997). The other method to promote cardiomyocyte proliferation is to recapitulate the developmental signaling pathways in the adult cardiomyocytes. In this context, the administration of Neuregulin (Nrg) and Oncostatin M has been shown to stimulate

cardiomyocyte proliferation (Bersell et al., 2009; Kubin et al., 2011) and few other signaling pathways have also been targeted for inducing endogenous cardiomyocyte proliferation (Senyo et al., 2014).

1.2.3 Trans-differentiation to cardiomyocytes

Another strategy to repair the injured mammalian heart is to trans-differentiate non-cardiomyocytes (such as fibroblasts) into cardiomyocytes. In recent years, researchers have shown that the non-cardiomyocytes in injured mouse hearts can be reprogrammed into cardiomyocyte-like cells *in vivo* by local delivery of four transcription factors, GATA4, MEF2C, HAND2 and TBX5 after coronary ligation (Qian et al., 2012; Song et al., 2012). *in vivo* administration of these transcription factors led to improvement in the scar area and cardiac function following MI, showing that this approach holds great therapeutic potential.

Although the above mentioned approaches offer hope for the treatment of injured patient hearts, they all have a number of drawbacks, preventing the generation of successful therapeutic strategies (Hudson and Porrello, 2013).

1.3 Cardiac Regeneration

It has been discussed since last many years that the mammalian heart lacks the ability to undergo cardiac regeneration following MI as the cardiomyocytes are terminally differentiated (Porrello and Olson, 2014). However, this traditional view has not been supported in recent years by enormous amount of studies being carried out on human and other mammalian cardiac samples (Beltrami et al., 2001; Bergmann et al., 2009; Senyo et al., 2013). Unfortunately, the low degree of cell turnover in the mammalian heart is insufficient to replace billions of damaged cardiomyocytes post myocardial injury. Surprisingly, neonatal mice have been shown to regenerate their heart following cardiac injury, contrary to the post-natal mammalian heart, indicating that the cardiomyocytes lose their proliferative capacity during development (Porrello et al., 2011). Unlike the adult mammalian heart, many lower vertebrates such as newts and zebrafish possess the ability to undergo complete cardiac regeneration following MI (Poss et al., 2002; Witman et al., 2011) (**Figure 1.2**). This remarkable ability of zebrafish (Danio rerio) promotes it as an ideal model to explore the molecular mechanisms underlying the process of cardiac regeneration, in order to recapitulate the successful regeneration in the heart failure patients. In addition to its heart, the zebrafish

can regenerate multiple injured tissues, including fins, maxillary barbell, hair cells, spinal cord, brain, pancreas, liver and kidney (Kikuchi, 2014). The ease of genetic manipulations in zebrafish has helped to develop various genetic tools, such as loss- and gain-of-function transgenesis, in order to understand the role of various genes and signaling pathways involved in cardiac regeneration.

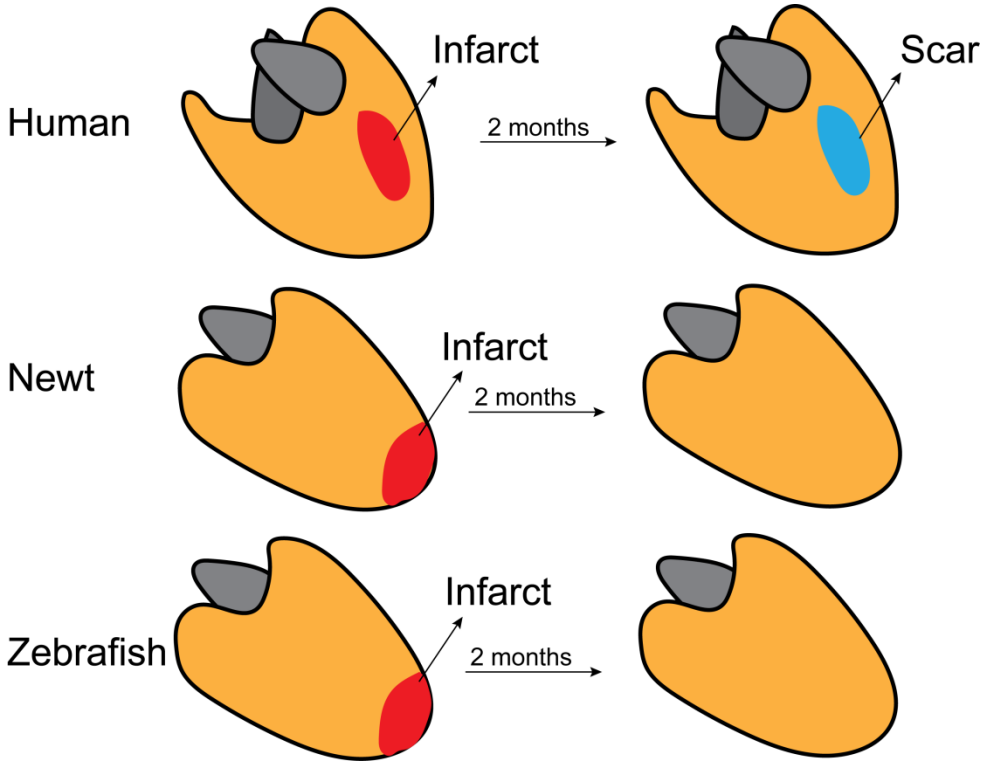

Figure 1.2. The regenerative capacities of the hearts of different organisms post MI. The mammalian (human) heart is unable to regenerate after injury and the dead tissue is replaced by a fibrotic scar, whereas in zebrafish and newts, the infarct is completely resolved within a span of about 2 months.

1.4 Zebrafish cardiac injury models for studying cardiac regeneration

There are three well-established models of injury for studying cardiac regeneration in zebrafish, namely ventricular resection, cryoinjury and genetic cardiomyocyte ablation.

1.4.1 Ventricular resection

The mechanical ventricular resection is one of the well-established cardiac injury techniques, which has been used to study the process of cardiac regeneration in multiple organisms, including the zebrafish (Dickover et al., 2013; Poss et al., 2002). In this injury model, an incision is made with a pair of scissors in the chest of the zebrafish to expose the heart for

ventricular resection (**Figure 1.3**). This technique can lead to 15-20% of the ventricular apex resection and several groups have shown that within a span of several weeks, the new myocardium is able to replace the transected ventricular apex (Jopling et al., 2010; Kikuchi et al., 2010; Poss et al., 2002). Previously, a detailed analysis of the resected ventricle has been performed (Poss et al., 2002), which shows that after several seconds of profuse bleeding from the ventricle, a large clot of erythrocytes is formed. Beginning 2-4 days post amputation (dpa), these erythrocytes are replaced by fibrin, whose expression is more prominent at 7-9 dpa. From 9-30 dpa, the new cardiac muscle surrounds, penetrates and eventually replaces the clot. By 60 dpa, the fibrin clot completely disappears and the ventricles look grossly normal on histological sections (**Figure 1.4**).

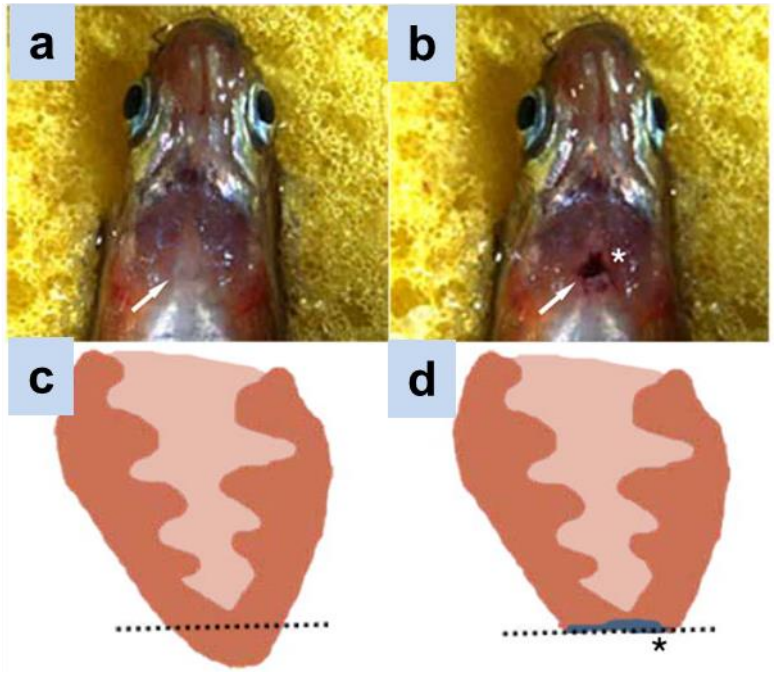

Figure 1.3. Inducing cardiac injury by ventricular apex resection in the adult zebrafish. (**a, b**) Anesthetized adult zebrafish mounted ventral side up, prior to resection (a) and after resection (b). White arrows point to the heart. (**c, d**) Schematic of ventricular section before (c) and after resection (d). Dashed lines mark the plane of resection and asterisks mark scar after resection. Modified images are adapted from Dickover et al., 2013.

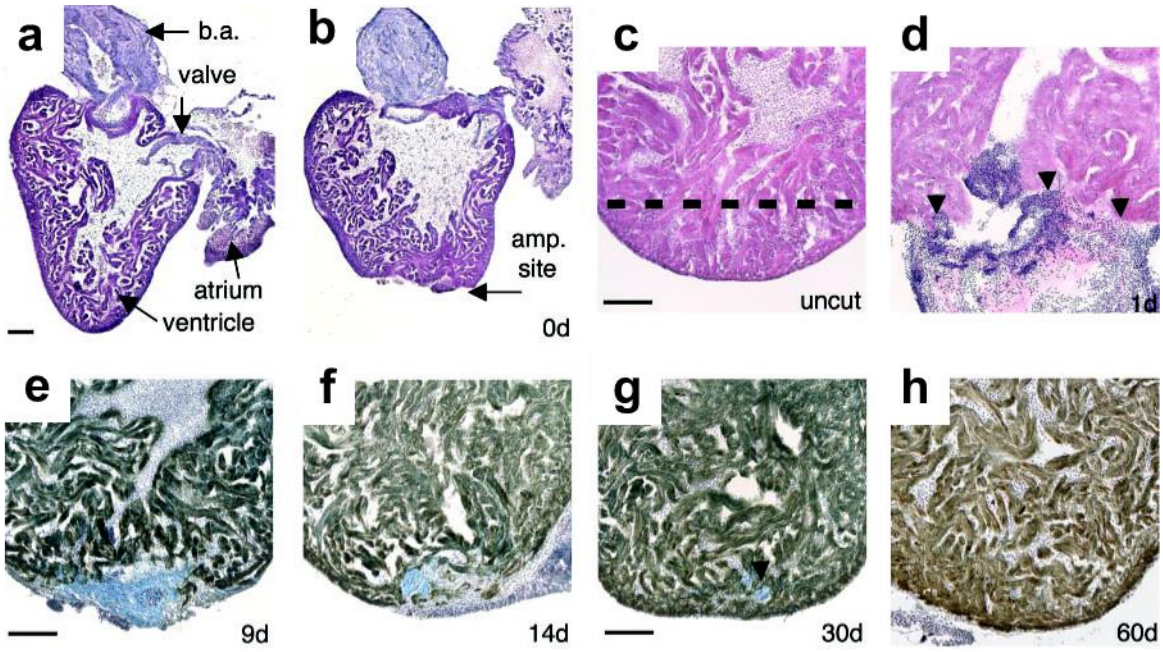

Figure 1.4. Regeneration of ventricular myocardium in the resected zebrafish heart. (**a-d**) Hematoxylin and Eosin (H&E) staining of uninjured zebrafish heart (a), after ventricular resection (b), intact ventricular apex at higher magnification indicating approximate amputation plane with dashed line (c) and 1d ventricle showing a large clot filled with erythrocytes, as pointed by arrowheads (d). (**e-h**) the heart section is stained for the presence of myosin heavy chain to identify healthy cardiac muscle (brown) and with aniline blue to identify fibrin (blue). 9d heart section showing the presence of fibrin (e), 14d heart section showing diminished fibrin and reconstituting cardiac muscle (f), newly regenerated cardiac wall with traces of fibrin left at 30d (g) and completely regenerated heart section with no signs of injury at 60d (h). Scale bars, 100 µm. d, days post amputation. Modified images are adapted from Poss et al., 2002.

1.4.2 Cryoinjury

In mammals, the most frequently used model to study cardiac regeneration has been coronary artery ligation or cryoinjury-induced tissue destruction, to mimic acute ischemia. Thus, several groups have established a similar cryoinjury technique in the adult zebrafish, as it allows a comparative interpretation of results obtained from the mammalian and non-mammalian species (Chablais and Jaźwińska, 2012; González-Rosa and Mercader, 2012). This injury method is based on rapidly freezing-thawing the ventricular tissue, which causes a massive death of ~20% of cardiomyocytes at the ventricular apex. A small incision is made through the chest with the scissors to expose the heart and the ventricular apex is frozen by applying the pre-cooled cryoprobe till the time it gets thawed (Chablais and Jaźwińska, 2012; González-Rosa and Mercader, 2012) (**Figure 1.5, 1.6**). Similar to previously published studies (Chablais et al., 2011; González-Rosa et al., 2011), I have performed a detailed

analysis of cryoinjured hearts by performing Acid Fuchsin Orange G (AFOG) staining on heart sections at various time points post cardiac injury. There is a process of scar formation and regression, as the scar tissue gets replaced by newly regenerated myocardium and the damaged cardiac muscle gets regenerated within 2 months. At 4 days post cryoinjury (dpci), a damaged myocardium is observed, which further gets replaced by a scar network comprising of fibrin and collagen (21 dpci), and newly regenerated myocardium is observed by the end of 2 months (45 dpci) (**Figure 1.7**).

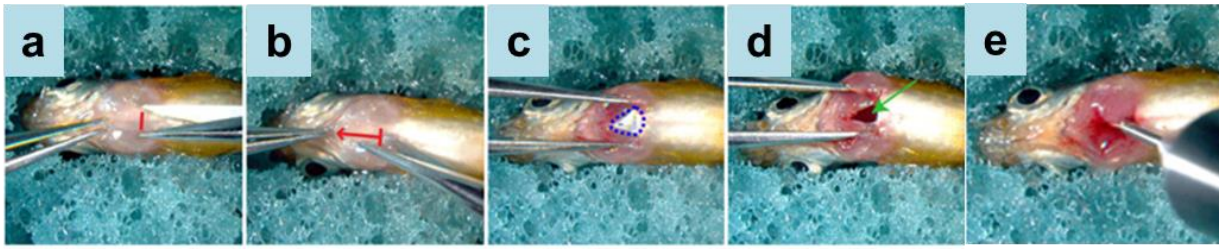

Figure 1.5. Inducing cardiac injury by cryoinjury in the adult zebrafish ventricle. (**a**) A small cut is made through the skin and muscles lying between the two pectoral fin (as shown by red line). (**b**) The incision is made by making the cut with scissors following the red arrow. (**c**) After making the cut, silver coating of pericardium is seen underneath the skin (encircled by the dashed line). (**d**) The pericardium is opened by using forceps and beating heart is exposed for inducing injury. (**e**) The precooled cryoprobe is gently inserted into the chest to touch the heart and kept on the heart until it thaws. Modified images are adapted from Chablais and Jaźwińska, 2012.

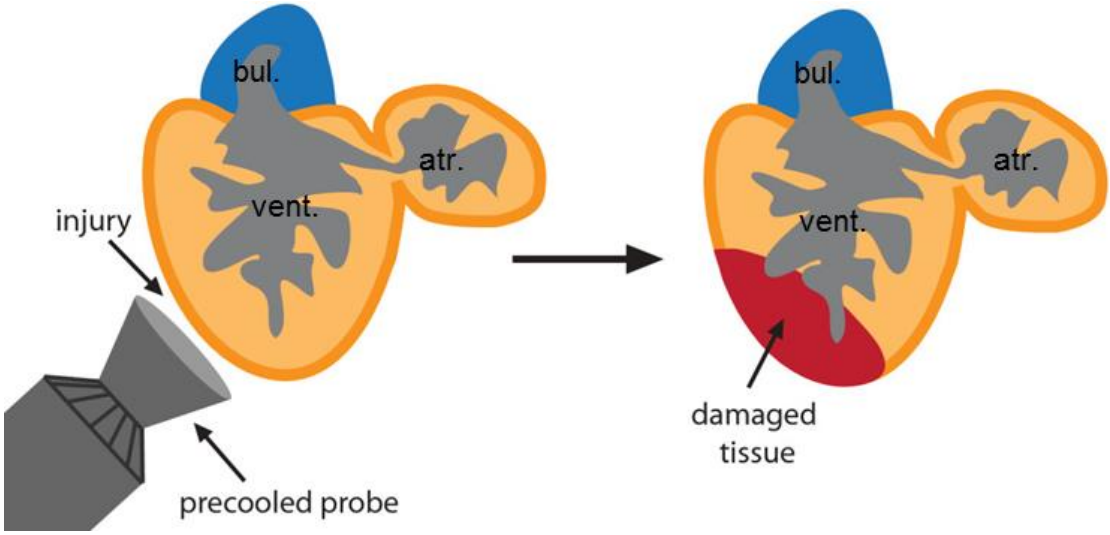

Figure 1.6. Schematic showing the induction of cryoinjury in the adult zebrafish heart. The precooled cryoprobe is placed on the ventricular apex, leading to a damaged cardiac tissue. Bul., bulbus arteriosus; vent., ventricle; atr., atrium. Modified images are adapted from Chablais et al., 2011.

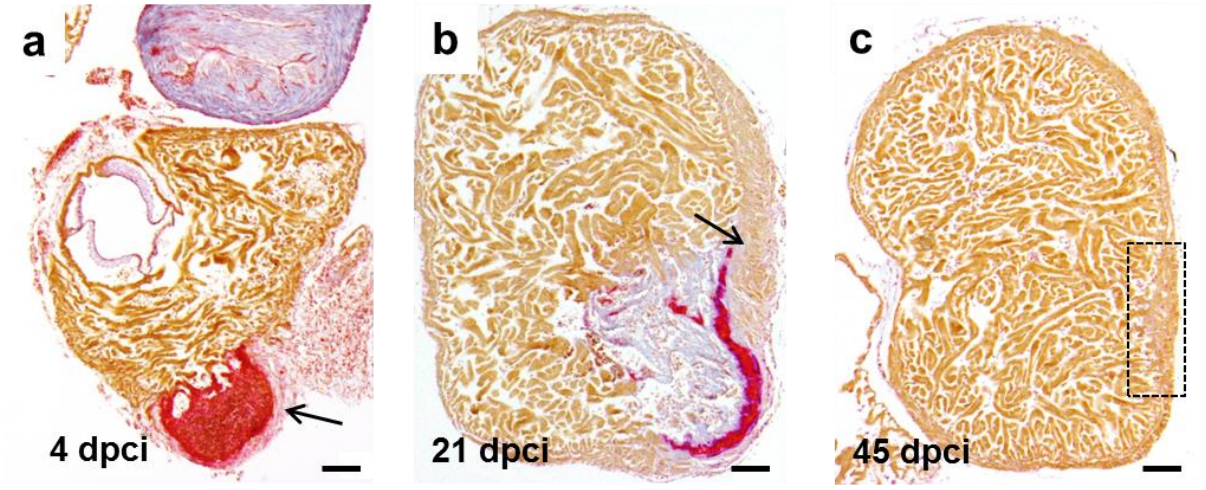

Figure 1.7. Scar formation and clearance post cryoinjury in adult zebrafish heart. (**a**) AFOG stained 4 dpci heart section, with damaged myocardium stained red (indicated by arrow). (**b**) AFOG stained 21 dpci heart section, with a scar network comprising of fibrin (stained red) and collagen (stained blue), along with regenerating cardiac muscle as indicated by arrow. (**c**) AFOG stained 45 dpci heart section, with newly formed cardiac muscle (within the dotted region) showing no sign of scarring. Scale bars, 100 µm. dpci, days post cryoinjury.

1.4.3 Genetic cardiomyocyte ablation

Genetic cardiomyocyte ablation is achieved by using a double transgenic system in zebrafish, which includes *Tg(myl7:CreER)*, where the expression of tamoxifen inducible CreER is driven by cardiomyocyte-specific promoter, *myosin light chain, 7 (myl7,* previously known as *cmlc2)* and *Tg(bactin2:loxp-mCherry-STOP-loxp-DTA),* Diptheria toxin A (DTA) expressing switch line under the ubiquitous promoter, *bactin 2* (Dickover et al., 2013; Wang et al., 2011). On tamoxifen induction, the cardiomyocyte-specific expression of DTA blocks the protein synthesis, resulting in destruction of over 60% of the ventricular myocardium (Wang et al., 2011) (**Figure 1.8**). The genetically resected hearts regenerate faster than the mechanically resected hearts, which could be because the mechanical resection majorly disrupts the cardiac structure and destroys other cell-types in the heart which may be crucial for efficient cardiac regeneration (Dickover et al., 2013). DTA-inducible cardiomyocyte ablation model involves the technical issue of crossing two transgenic lines to generate the double transgenic fish. Thus, a better genetic cell ablation model has been established, which requires the usage of only one transgenic line by utilizing bacterial nitroreductase (NTR) enzyme (Curado et al., 2007; Dickover et al., 2013). The transgenic line *Tg(myl7:NTR)* has been generated which drives NTR expression in zebrafish hearts, under cardiomyocyte-specific promoter, *myosin light chain, 7 (myl7,* previously known as *cmlc2)* (Curado et al., 2007). Thus, cardiomyocytes

can be efficiently ablated by the treatment of this transgenic line with the drug, metronidazole (Mtz) (**Figure 1.9**). Moreover, in order to study the regeneration of damaged myocardium, Mtz can be washed out to discontinue the genetic ablations (Anderson et al., 2009).

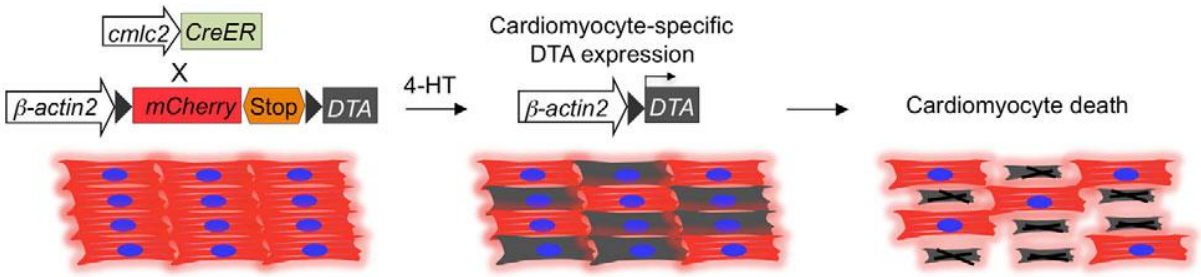

Figure 1.8. Zebrafish cardiomyocyte genetic ablation using DTA. Schematic showing transgenes used in zebrafish cardiomyocyte ablation. Tamoxifen (4-HT) induction causes DTA expression specifically in the cardiomyocytes. Modified imageas are adapted from Wang et al., 2011.

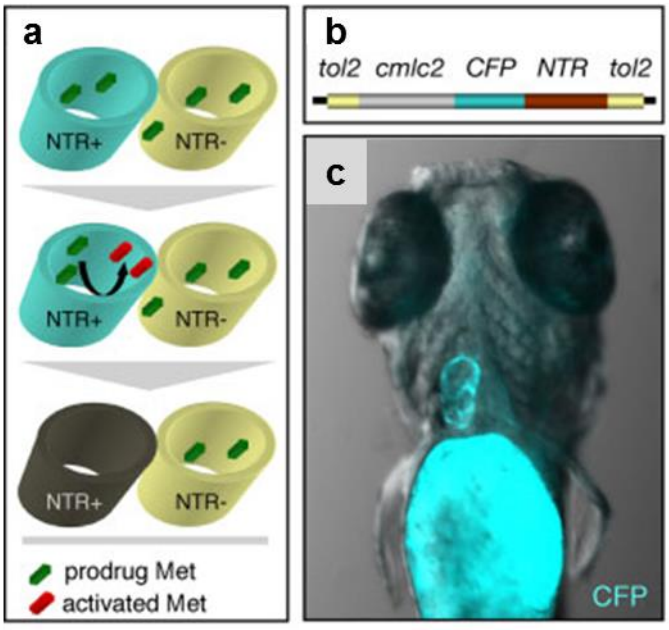

Figure 1.9. Zebrafish cardiomyocyte genetic ablation using Nitroreductase/Metronidazole (NTR/Mtz) cell ablation system. (**a**) Mechanism of NTR/Mtz cell ablation model- when an NTR-expressing cell (NTR in cyan) is exposed to Mtz (green), it converts the latter to cytotoxic agent (red). This causes damage and death of NTR^{+} cell. (**b**) Construct used to generate the *Tg(myl7:CFP-NTR)*^{s890} transgenic line, containing *myl7:CFP-NTR* sequences flanked by *tol2* sequences. (**c**) Brightfield combined with fluorescent imaging of 4 days post fertilization (dpf) larva, showing stable expression of Cyan Fluorescent Protein-NTR (CFP-NTR) in cardiomyocytes. Modified images are adapted from Curado et al., 2007.

1.5 Cellular responses during cardiac regeneration

Cardiac injury in zebrafish induced by any of the models explained above, induces organ-wide injury responses from all the three layers of the heart, i.e., myocardium, endocardium and epicardium, as explained below.

1.5.1 Myocardium

The possible sources of regenerated cardiomyocytes in the zebrafish heart have been postulated to be either stem cell population or proliferation of uninjured cardiomyocytes present near the site of injury (Kikuchi, 2014). Previously, it has been suggested that there exists a non-cardiomyocyte source for regenerating cardiac muscle (Lepilina et al., 2006). However, two research groups have shown that the spared cardiomyocytes in the vicinity of the injured area undergo dedifferentiation and proliferation to give rise to new cardiac muscle (Jopling et al., 2010; Kikuchi et al., 2010). Both studies have used genetic fate-mapping techniques to examine the contribution of cardiomyocytes to the regenerating zebrafish hearts. Two transgenic lines were used, one line driving the expression of 4-hydroxytamoxifen (4-HT)-inducible Cre recombinase (CreER) gene under cardiomyocyte-specific *myl7* promoter and the other line in which the expression of enhanced green fluorescent protein (EGFP) reporter can be induced in CreER expressing cells after excising loxP sites by tamoxifen treatments. Using these two transgenic lines, a majority of the cardiomyocytes expressing *myl7* were pre-labelled with EGFP by 4-HT treatments before performing the injury and 30 days post amputation (dpa) injured hearts were used to perform regeneration experiments. It was shown that the vast majority of regenerated myocardium comprises of EGFP-expressing cardiomyocytes, suggesting that the existing *myl7*$^{+}$ cardiomyocytes, but not *myl7*$^{-}$ non-cardiomyocytes, are the primary source for newly regenerated zebrafish cardiac muscle (Kikuchi, 2014). It has been further suggested that cardiomyocyte dedifferentiation is the prerequisite of proliferation, as shown by disorganized sarcomeric structures in mitotic cardiomyocytes. It is noteworthy that mammalian cardiomyocytes are also thought to dedifferentiate after MI (Kubin et al., 2011), which makes dedifferentiation a common injury response amongst the mammalian and zebrafish cardiomyocytes.

The cardiac transcription factor, Gata4 has been reported to be expressed in a subpopulation of cardiomyocytes in the compact myocardium post cardiac injury and the overexpression of dominant-negative form of Gata4 blocks cardiomyocyte proliferation specifically in the

compact myocardium, suggesting that gata-4 stimulated cardiomyocyte proliferation is essential for efficient cardiac regeneration (Kikuchi et al., 2010; Gupta et al., 2013). Apart from cardiomyocyte dedifferentiation and proliferation, another crucial event during cardiac regeneration, i.e., the migration of cardiomyocytes into the injury site has been shown to be regulated by the Cxcl12-Cxcr4 system (Itou et al., 2012) and needs to be studied in more details.

1.5.2 Endocardium

The endocardial cells are the first to respond to cardiac injury. Within one hour post injury, the endocardial cells throughout the heart undergo morphological changes, including rounding up and detachment from the myocardium. Additionally, the expression of developmental marker gene, *retinal aldehyde dehydrogenase 2 (raldh2)*, involved in retinoic acid (RA) signaling, is induced in the whole endocardium at 3 hours post injury (Kikuchi et al., 2011). The inhibition of RA signaling has been shown to suppress cardiac regeneration; however, how endocardial- or epicardial-induced RA signaling controls cardiomyocyte proliferation still remains unanswered.

1.5.3 Epicardial cells

Epicardial cells have been shown to reactivate the expression of genes associated with epicardial development, such as *tbx18, wt1b* and *raldh2* and also show proliferative properties from 3 days post injury (Kikuchi et al., 2011; Lepilina et al., 2006; Schnabel et al., 2011). Genetic lineage-tracing studies and transplantation experiments have revealed that tcf21-expressing epicardial cells give rise to perivascular cells and myofibroblasts, not to cardiomyocytes (Kikuchi et al., 2011b). In a recent study, the injury-activated epicardial cells have been shown to deposit the extracellular matrix protein, fibronectin, which has a pro-regenerative effect (Wang et al., 2013). It has been further suggested that fibronectin does not regulate cardiomyocyte proliferation, rather is required for cardiomyocyte migration and integration into the injury area during cardiac regeneration. Further investigation into the molecular functions of epicardium is required.

1.6 Signaling pathways involved in cardiac regeneration

Various pathways such as RA signaling, fibroblast growth factor (FGF) signaling, bone morphogenetic protein (BMP) signaling, interleukin 6 (Il6) signaling, epidermal growth factor (EGF) signaling and others have been implicated in the process of cardiac regeneration in zebrafish and are crucial for diverse processes including cardiomyocyte proliferation, scar deposition, neovascularization and epicardial responses after injury (Fang et al., 2013; Kikuchi, 2014; Kikuchi et al., 2011b; Marín-Juez et al., 2016; Wu et al., 2016).

1.6.1 RA signaling

RA signaling has been shown to be essential for cardiac development during embryogenesis, showing early patterning roles as well as later mitogenic roles (Hoover et al., 2008; Kastner et al., 1994; Ryckebusch et al., 2008). Moreover, the role of RA signaling has been established during cardiac regeneration as within 3 hours of ventricular injury, the entire endocardium undergoes morphological changes and induces the expression of RA-synthesizing enzyme (*raldh2*). The expression of *raldh2* becomes localized to the endocardium at the site of injury as early as 24 hours post injury, and is also observed in epicardial tissue at 3 dpa (Kikuchi et al., 2011b; Lepilina et al., 2006) (**Figure 1.10a-e**). Further on, the transgenic inhibition of RA receptors or expression of RA-degrading enzyme blocks injury-induced cardiomyocyte proliferation during zebrafish cardiac regeneration (Kikuchi et al., 2011b) (**Figure 1.10f-i**).

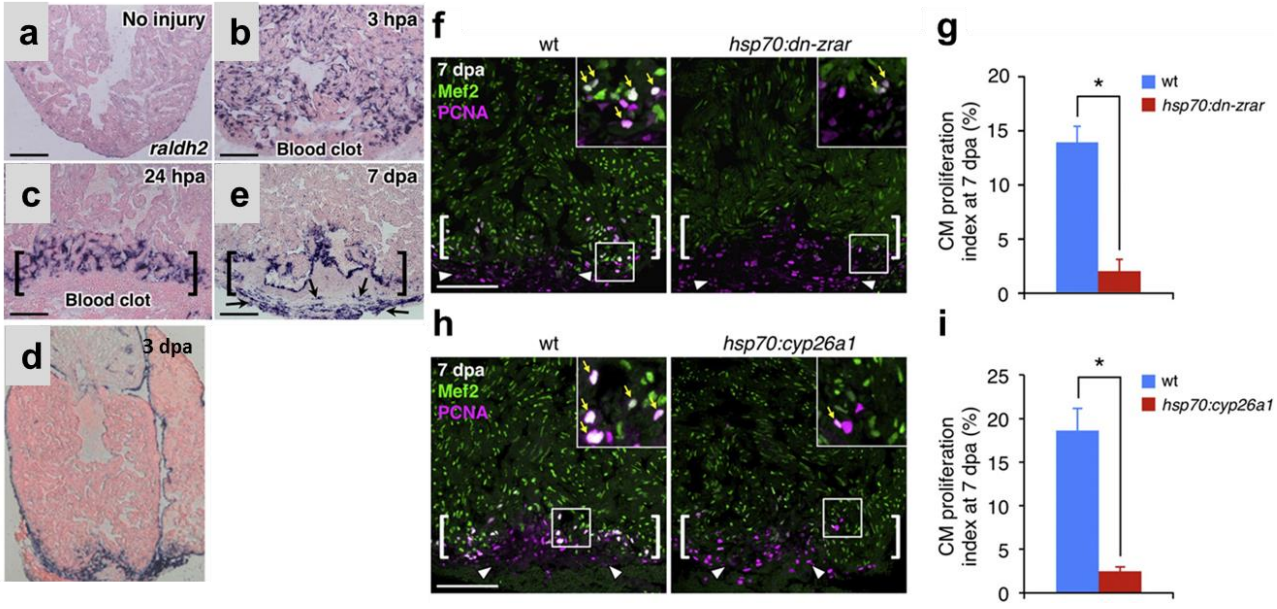

Figure 1.10. Role of RA signaling during zebrafish cardiac regeneration. (**a-e**) *raldh2* expression analysis by *in situ* hybridization on uninjured (a), 3 hpa (b), 24 hpa (c), 3 dpa (d) and 7 dpa (e) heart sections. Brackets include injured site and arrows point to epicardial cells. (**f, g**) Assessment (f) and quantification (g) of cardiomyocyte proliferation in PCNA (cell stage marker) and Mef2 (cardiomyocyte marker) stained 7 dpa heart sections of wt and *hsp70:dn-zrar* transgenic fish. (**h, i**) Assessment (h) and quantification (i) of cardiomyocyte proliferation in PCNA and Mef2 stained 7 dpa heart sections of wild-type (wt) and *hsp70:cyp26a1* transgenic fish. Brackets include injured site and arrowheads point to proliferating epicardial cells. Scale bars, 100 µm. hpa, hours post amputation; dpa, days post amputation. Modified images are adapted from Kikuchi et al., 2011b and Lepilina et al., 2006.

1.6.2 FGF signaling

FGF signaling has been reported to be involved in both mammalian and non-mammalian cardiac regeneration previously (Lepilina et al., 2006; Rubin et al., 2013). During zebrafish cardiac regeneration, the expression of the ligand *fgf17b* is shown to be induced in the myocardium, while the expression of receptors *fgfr2* and *fgfr4* is induced in the epicardial-derived cells (**Figure 1.11**). Blocking FGF signaling by the expression of dominant-negative fgf receptor leads to disturbed epicardial EMT, coronary vascularization failure and ultimately arrests cardiac regeneration as assessed by the persistence of scarring at a later time point (Lepilina et al., 2006) (**Figure 1.12**).

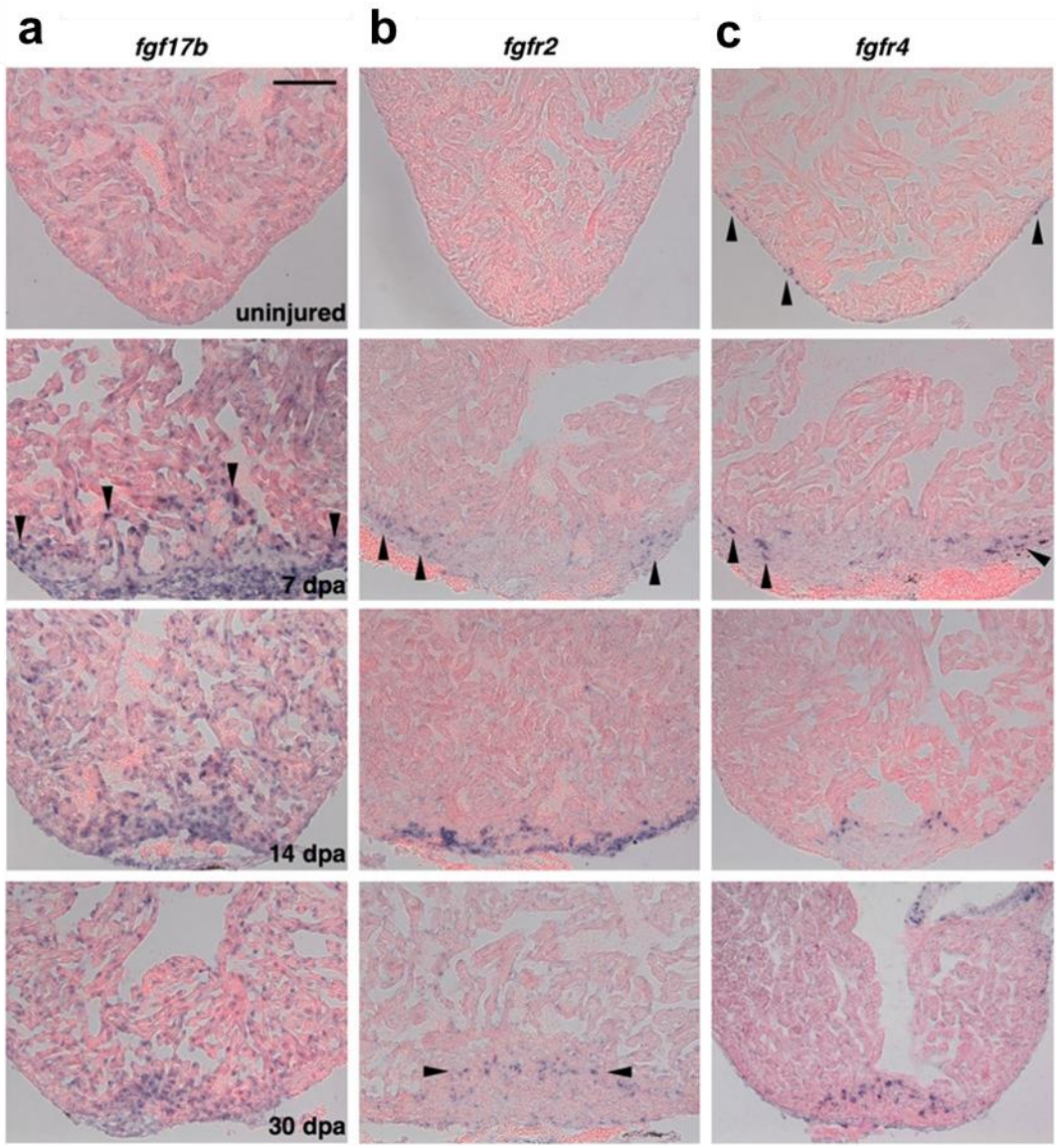

Figure 1.11. Expression analysis of FGF signaling members during zebrafish cardiac regeneration. (**a**) Expression analysis of *fgf17b* by *in situ* hybridization; weak perinuclear expression in uninjured heart, starting at 7 dpa, myofibers at the apical edge of the regenerating tissue and other cells within and surrounding the injury area showed enhanced *fgf17b* expression (arrowheads), which persisted through 30 dpa. (b) Expression analysis of *fgfr2* by *in situ* hybridization; no expression in uninjured heart, mild expression in the epicardial cells near injury site at 7 dpa (arrowheads), which enhanced at 14 dpa and faint expression in isolated cells within the regenerated tissue at 30 dpa. (c) Expression analysis of *fgfr4* by *in situ* hybridization; faint expression in epicardial cells in uninjured heart, induced expression in cells near the injury site at 7 dpa (arrowheads) and 14 dpa, which persisted at 30 dpa. Scale bar, 100 µm. dpa, days post amputation. Modified images are adapted from Lepilina et al., 2006.

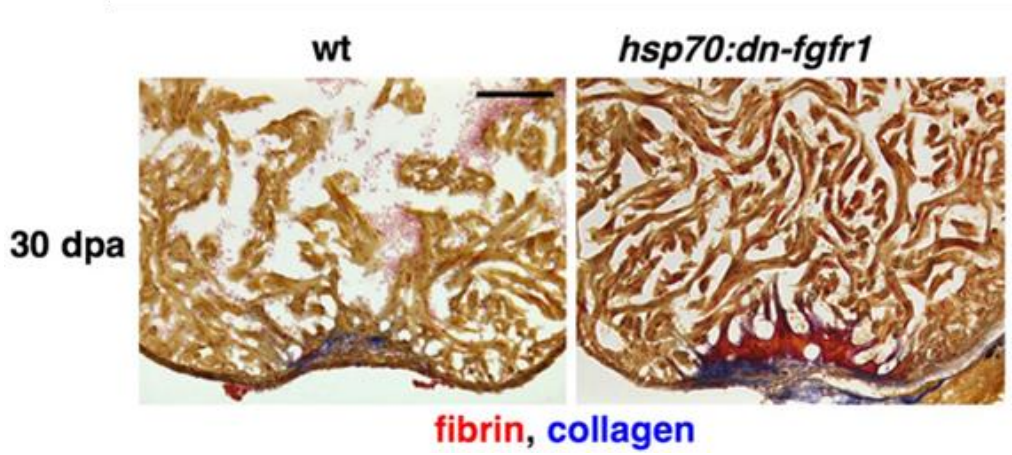

Figure 1.12. Role of FGF signaling during zebrafish cardiac regeneration. AFOG stained 30 dpa hearts, with wild-type (wt) heart showing small amount of scarring left whereas *hsp70:dn-fgfr1* (transgenic line expressing dominant-negative fgf receptor1, under heat shock promoter) hearts retain significant amounts of fibrin (orange) and collagen (blue). Scale bar, 100 µm. dpa, days post amputation. Modified images are adapted from Lepilina et al., 2006.

1.6.3 BMP signaling

BMP signaling pathway is a part of the TGF-β superfamily and functions by acting through the downstream signal transducers, Smad1/5/8 (Miyazono et al., 2010). Apart from the role of BMP signaling pathway in cardiac development (Ahuja et al., 2016; Yuasa and Fukuda, 2009), a recent study has shown its significance during zebrafish cardiac regeneration (Wu et al., 2016). *in situ* hybridization analysis of the expression of BMP ligands, receptor and target genes has shown their upregulation at 3 days post cryoinjury in multiple cell-types located in the border zone between injured area and healthy myocardium (**Figure 1.13**). Furthermore, the genetic or chemical inhibition of BMP signaling leads to reduced cardiac dedifferentiation and proliferation, and ultimately blocks cardiac regeneration. On the other hand, overexpression of *bmp2b* is sufficient to enhance cardiac regeneration in the injured zebrafish hearts as shown by reduced scar area in injured hearts (Wu et al., 2016) (**Figure 1.14**).

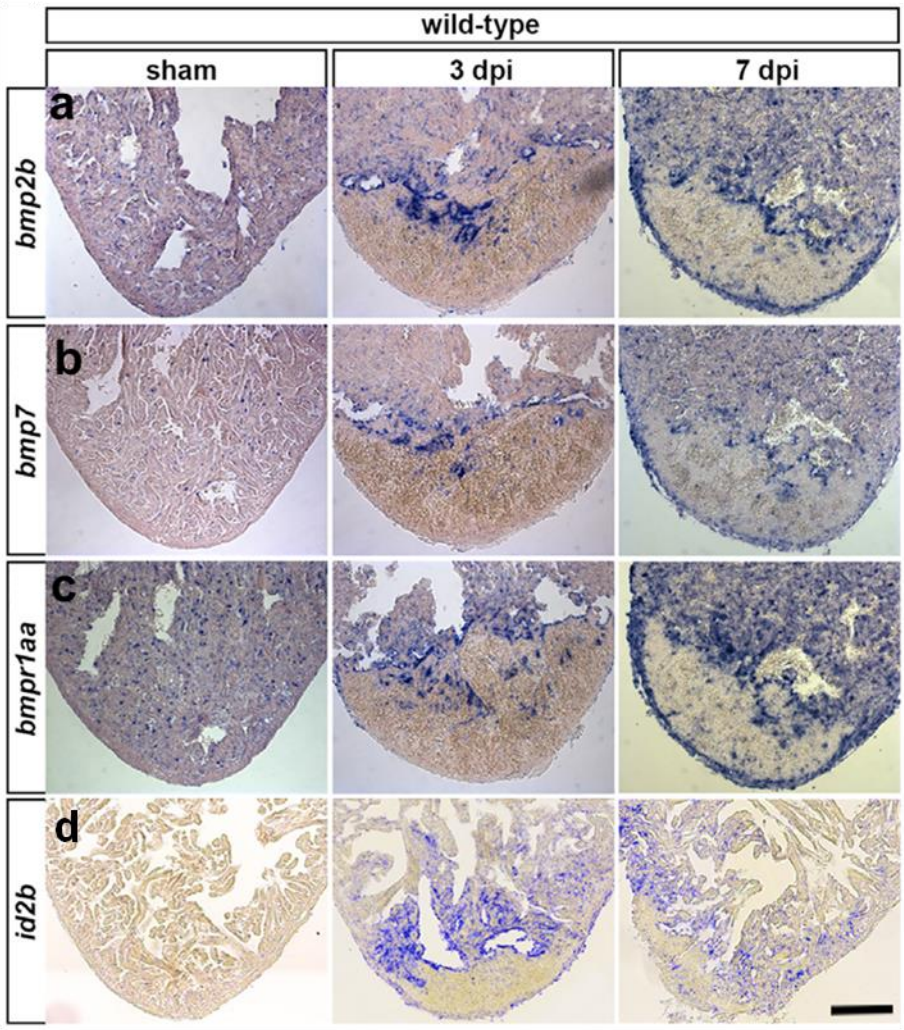

Figure 1.13. Expression analysis of BMP signaling members during zebrafish cardiac regeneration. (**a, b, c**) *in situ* hybridization for the expression analysis of BMP ligands (*bmp2b* and *bmp7*) and BMP receptor (*bmpr1aa*), showing enhanced expression post cardiac injury in the injury border zone at 3 dpi, which further expanded to the epicardium covering the wound at 7 dpi. (**d**) *in situ* hybridization for the expression analysis of BMP target gene *id2b*, showing upregulation in the injury border zone at 3 dpi, which persisted at 7 dpi. Scale bar, 100 µm. dpi, days post cryoinjury. Modified images are adapted from Wu et al., 2016.

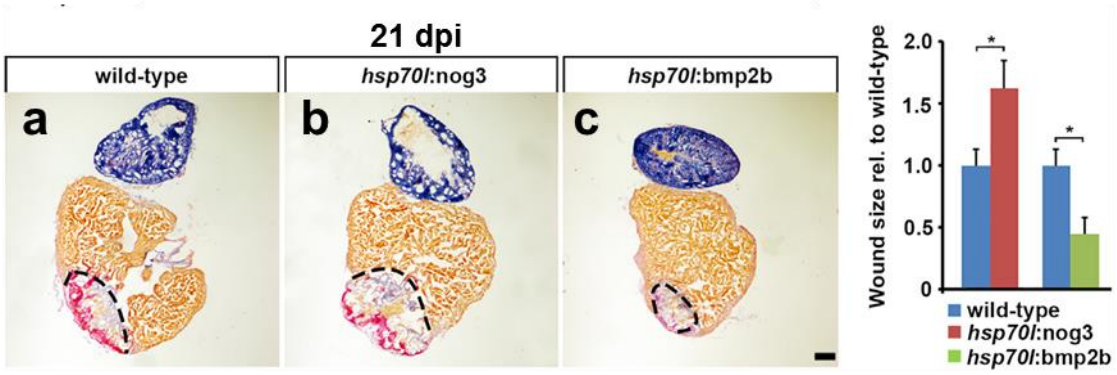

Figure 1.14. Role of BMP signaling during zebrafish cardiac regeneration. (**a-c**) AFOG staining showing wound size (shown by dashed lines) in wild-type, *hsp70l:nog3* (transgenic line with heat-shock-inducible expression of BMP inhibitor *noggin 3*), *hsp70l:bmp2b* (transgenic line with heat-shock-inducible expression of BMP ligand encoding gene, *bmp2b*) cryoinjured heart sections at 21 dpi. Significantly increased wound size is observed in *hsp70l:nog3* hearts, whereas *hsp70l:bmp2b* hearts show reduced wound size compared to wild-types. Wound tissue size relative to the whole ventricle and normalized to heat-shocked wild-type siblings is plotted as bar graph. Error bars represent s.e.m., Student's t-test, *p= 0.002 (nog3) and *p= 0.016 (bmp2b). Scale bar, 100 µm. dpi, days post cryoinjury. Modified images are adapted from Wu et al., 2016.

1.6.4 IL6 cytokine or Jak1/Stat3 signaling

The IL6 cytokine signaling is initiated by dimerization of the Interleukin 6 signal transducer (Il6st, or glycoprotein 130) upon IL6 cytokine binding to its receptor. On IL6st dimerization, the Janus kinase 1(Jak1) gets activated and phosphorylates IL6st, creating a docking site for Signal transducer and activator of transcription 3 (Stat3). After phosphorylation, Stat3 dimerizes, dissociates from the receptor and translocates to the nucleus for transcriptional activation of target genes involved in cell growth and survival (Heinrich et al., 2003; Hirano et al., 2000; Schindler and Jr, 1995). By profiling translating RNAs in zebrafish cardiomyocytes during cardiac regeneration (using translating ribosome affinity purification (TRAP) technology), the induction of several Jak1/Stat3 pathway members has been reported post cardiac injury. Enhanced expression levels *of il6st, jak1, stat3,* and the Jak1/Stat3 pathway target gene, *suppressor of cytokine signaling 3b (socs3b)* have been observed in 1 day post amputation (dpa) cardiomyocytes (Fang et al., 2013) (**Figure 1.15**). Another study has previously shown the induction of the expression of other members of this pathway, *jak2a and stat2* at 7 dpa (Jopling et al., 2012). Cardiomyocyte-specific transgenic Stat3 inhibition, by generating dominant-negative Stat3 (dnStat3) significantly reduces cardiomyocyte proliferation and also leads to disturbed cardiac regeneration (Fang et al., 2013) (**Figure 1.16**).

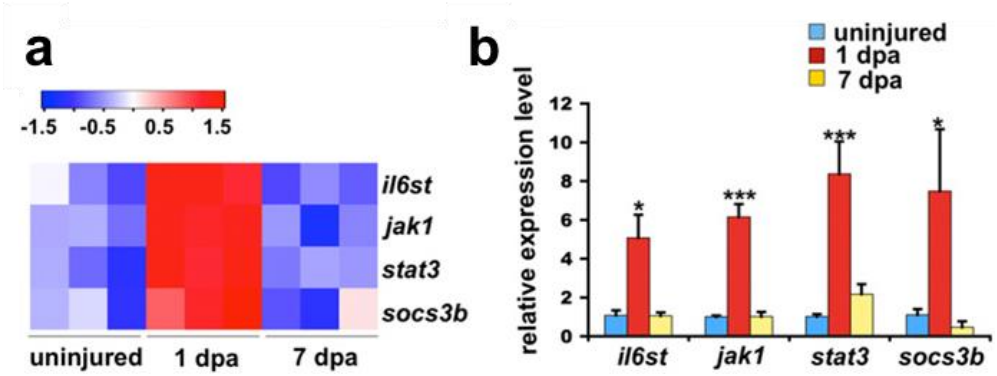

Figure 1.15. Expression analysis of Jak1/Stat3 signaling members during zebrafish cardiac regeneration. (**a**) Heat map from microarray indicating increased levels of Jak1/Stat3 pathway members post cardiac injury at 1 dpa and 7 dpa. (**b**) Real-Time quantitative PCR (RT-qPCR) using RNA immunoprecipitated from *myl7:*TRAP zebrafish cardiac ventricles, validating the upregulation of Jak1/Stat3 pathway members post cardiac injury. Expression levels were normalized to that of β-actin2, and further normalized to that of the uninjured sample. Data are mean ± s.e.m., *P < 0.05, **P < 0.01, ***P < 0.001, Student t test (unpaired, two-tailed). dpa, days post amputation. Modified images are adapted from Fang et al., 2013.

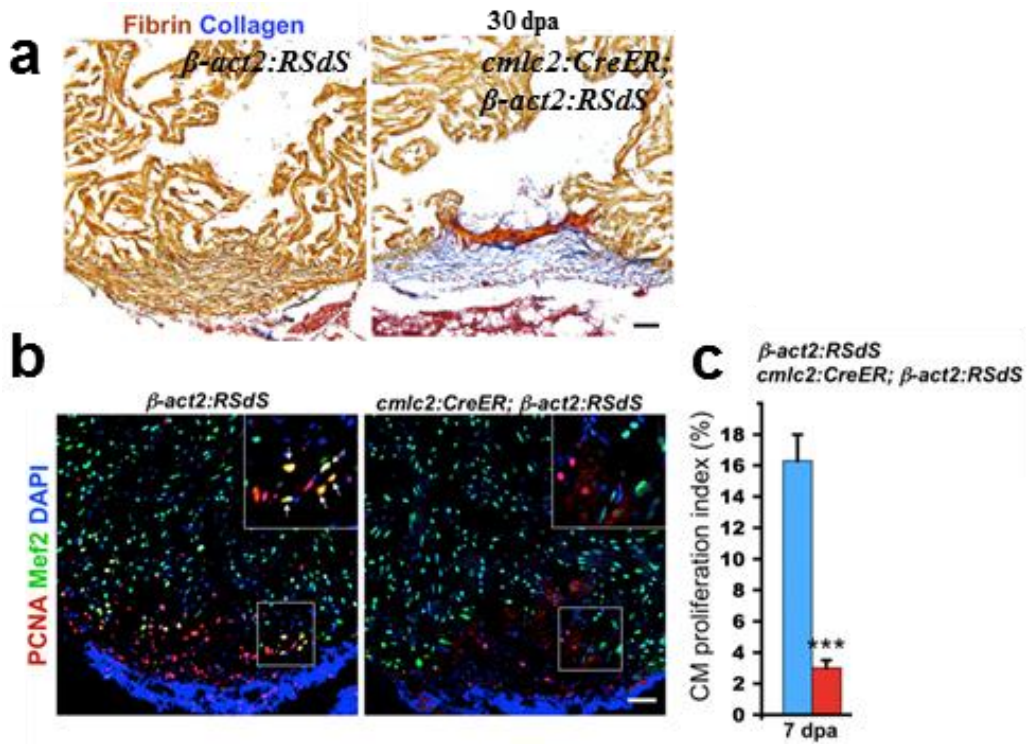

Figure 1.16. Role of Jak1/Stat3 signaling during zebrafish cardiac regeneration. (**a**) AFOG staining performed on injured heart sections of *cmlc2:CreER;β-act2:RSdS* (dnStat3) and *β-act2:RSdS* (control) at 30 dpa, showing scar retention and blocked muscle regeneration in dnStat3-expressing fish. (**b**) Immunostained 7 dpa *cmlc2:CreER;β-act2:RSdS* (dnStat3) and *β-act2:RSdS* (control) ventricles with antibodies against PCNA (cell-stage marker) and Mef2 (cardiomyocyte marker). (**c**) Quantification of cardiomyocyte proliferation showing reduced proliferation in dnStat3-expressing fish. Data are mean ± s.e.m., *P < 0.05, ***P < 0.001. Student t test (unpaired, two-tailed). Scale bars, 50 μm. dpa, days post amputation. Modified images are adapted from Fang et al., 2013.

1.6.5 EGF signaling

Interestingly, only the EGF family ligand, Nrg and its central co-receptor ERBB have so far been reported to possess mitogenic activity on cardiomyocytes, not only after injury, but also on the healthy myocardium of fish and mammals *in vivo* (Bersell et al., 2009; D'Uva et al.,

2015; Gemberling et al., 2015; Liu et al., 2010). It has been shown that cardiomyocyte-specific knockout of *Erbb2* leads to disturbed cardiomyocyte proliferation during embryonic and neonatal stages of murine development. The induction of constitutively active ERBB2 (caERBB2) in mice cardiomyocytes results in cardiomegaly, as observed by excessive cardiac hypertrophy, dedifferentiation and proliferation. Further on, transient caERBB2 induction post MI triggers cardiomyocyte dedifferentiation, proliferation and cardiac regeneration in juvenile and adult stages (D'Uva et al., 2015) (**Figure 1.17**). Another study has reported that *in vivo* genetic inactivation of ERBB4 in adult mice reduces cardiomyocyte proliferation, whereas the overexpression of ERBB4 enhances the same process. Additionally, NRG1 injections in adult mice induces cardiomyocyte proliferation as well as myocardial regeneration post cardiac injury (Bersell et al., 2009). A recent study that identified the role Nrg/ErbB signaling during zebrafish cardiac regeneration detects the injury-induced upregulation of *nrg1* (Gemberling et al., 2015) (**Figure 1.18**). Next, the myocardial overexpression of Nrg1 has been shown to induce cardiomyocyte dedifferentiation, excessive muscle hyperplasia, epicardial activation and cardiomegaly in uninjured zebrafish heart, as well as enhanced cardiomyocyte proliferation post cardiac injury (Gemberling et al., 2015) (**Figure 1.19, 1.20**). Consequently, Nrg treatment is a subject of ongoing research to evaluate its therapeutic potential (Polizzotti et al., 2015).

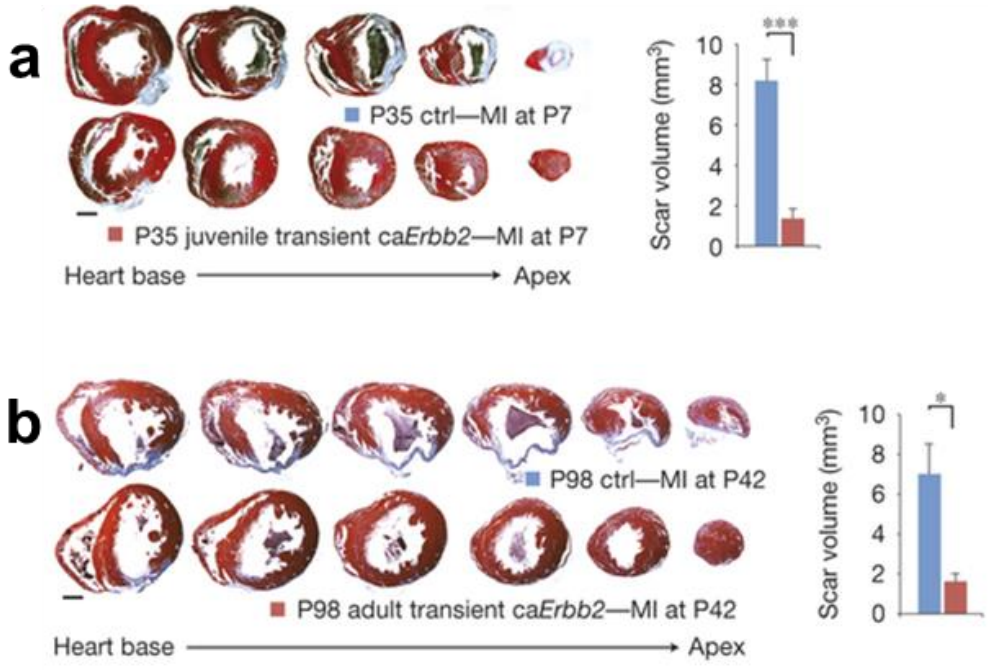

Figure 1.17. Transient ERBB2 induction triggers cardiac regeneration in juvenile and adult mice. (**a**) Scar quantification based on Masson's trichrome staining of 1 month post MI (P35) control and juvenile caErbb2

mice, with *caErbb2* heart showing significantly reduced scarring. (**b**) Scar quantification based on Masson's trichrome staining of 2 months post MI (P98) control and adult *caErbb2* mice, with *caErbb2* heart showing significantly reduced scarring. Data are presented as mean (error bars show s.e.m.); statistical significance was calculated using two-tailed unpaired t-test, *P <0.05, **P <0.01. Scale bars, 1 mm. Modified images are adapted from D'Uva et al., 2015.

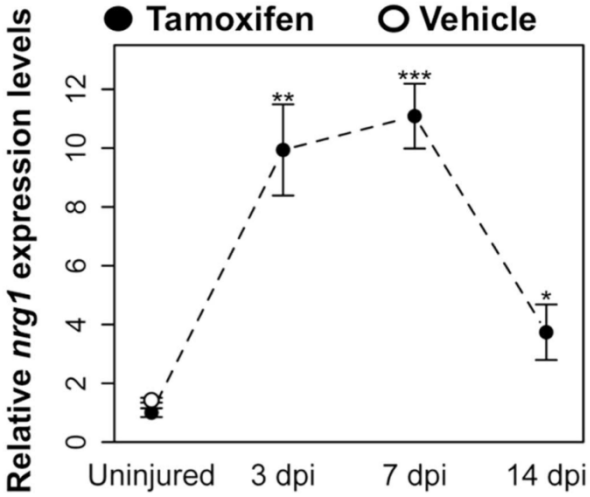

Figure 1.18. Induction of Nrg1 post cardiac injury in adult zebrafish. Time course of *nrg1* induction in zebrafish cardiac ventricles after cardiomyocyte genetic ablation. *nrg1* mRNA levels were analyzed by performing RT-qPCR at 3, 7 and 14 days post ablation injury in tamoxifen-treated *myl7:CreER; β-act2:RSDTA* animals (leading to DTA expression under *myl7* promoter and cardiomyocyte ablation) relative to control *myl7:CreER* animals (closed circles). *myl7:CreER; β-act2:RSDTA* (open circle) vehicle-treated animals served as an additional control. Data are presented as mean ± s.e.m. *p < 0.05, **p < 0.01, ***p < 0.001, Student's t-test, two-tailed. dpi, days post ablation injury. Modified images are adapted from Gemberling et al., 2015.

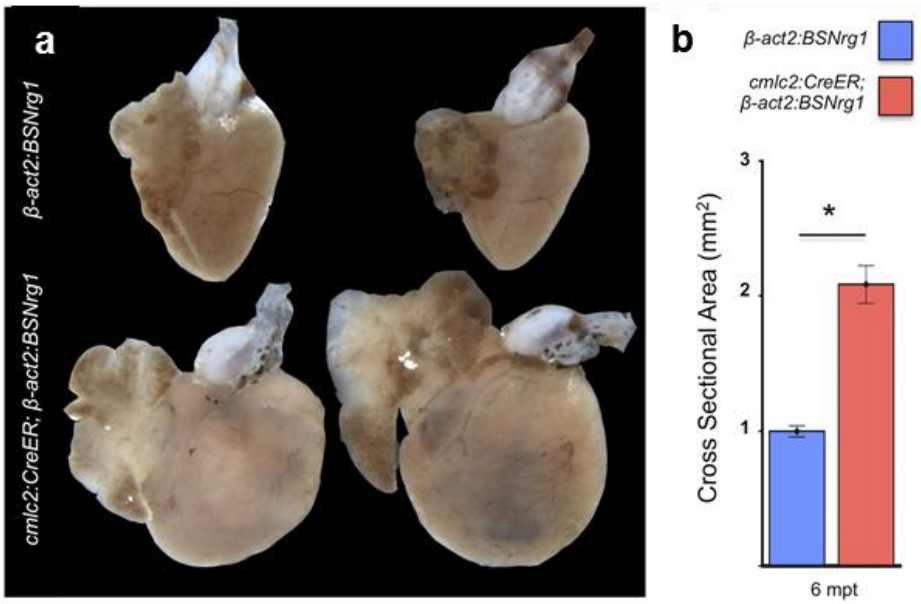

Figure 1.19. Overexpression of Nrg1 induces cardiac hyperplasia, leading to cardiomegaly in adult zebrafish. (**a**) Whole-mount images of *cmlc2:CreER; β-act2:BSNrg1*(tamoxifen-induced *nrg1* overexpression) and control ventricles at 6 months post-tamoxifen treatment, showing enlarged heart size due to *nrg1* overexpression. (**b**) Quantification of the cross-sectional surface area of *cmlc2:CreER; β-act2:BSNrg1* and control ventricles 6 months post-treatment, showing cardiomegaly effects of *nrg1* overexpression. Data are represented as mean ± s.e.m. *p < 0.05, Student's t-test, two-tailed. Modified images are adapted from Gemberling et al., 2015.

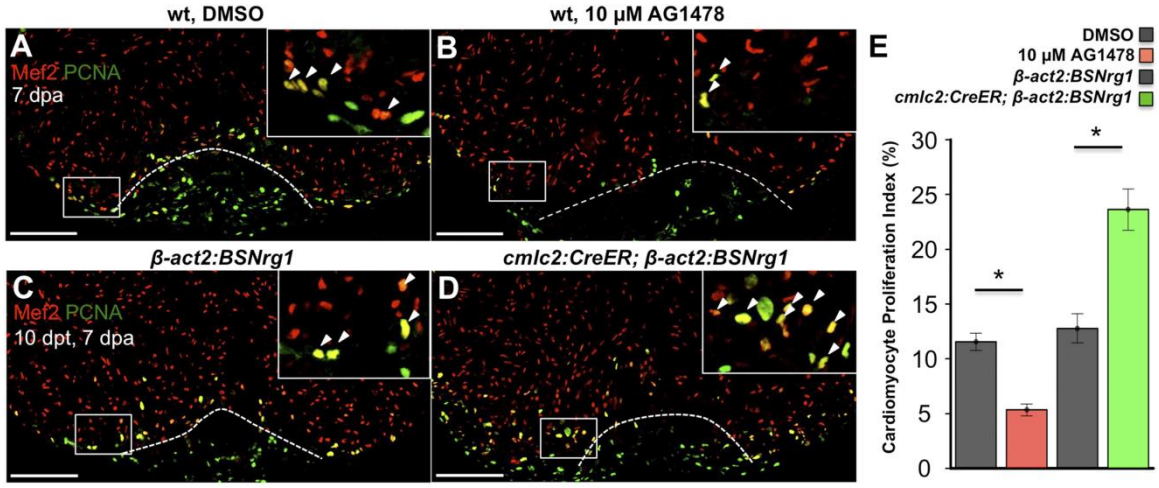

Figure 1.20. Overexpression of Nrg1 promotes cardiomyocyte proliferation during zebrafish cardiac regeneration. (**A, B**) PCNA (cell stage marker) and Mef2c (cardiomyocyte marker) immunostained 7 dpa heart sections of animals treated from 6 to 7 dpa, with DMSO (A) or 10 μM AG1478 (a small molecule inhibitor of Erbb receptors) (B). (**C, D**) PCNA and Mef2c immunostained 7 dpa heart sections of control *β-act2:BSNrg1* (C) or *cmlc2:CreER; β-act2:BSNrg1*(tamoxifen-induced *nrg1* overexpression) (D) animals treated with tamoxifen at 3 days before cardiac injury. (**E**) Quantification of cardiomyocyte proliferation at 7 dpa, revealing that Erbb inhibition suppresses cardiomyocyte proliferation and *nrg1* overexpression promotes this process. Data are represented as mean ± s.e.m. *p < 0.05, Mann–Whitney Ranked Sum Test. Scale bars, 100 μm. dpa, days post amputation. Modified images are adapted from Gemberling et al., 2015.

1.6.6 Other Signaling pathways

Apart from the above-mentioned pathways, there are also other signaling pathways which have been shown to play essential roles during zebrafish cardiac regeneration, including Insulin-like Growth Factor (IGF) signaling, Platelet-derived Growth Factor (PDGF) signaling, NFκB signaling, H_2O_2 signaling, Hypoxia-inducible factor 1 (HIF1) signaling, Notch signaling, VEGF signaling and microRNAs (miRNAs) (Karra et al., 2015; Kikuchi, 2014; Marín-Juez et al., 2016; Münch et al., 2017; Yin et al., 2012).

1.7 Transforming growth factor beta (TGF-β) signaling pathway

1.7.1 Smad-dependent canoninal TGF-β signaling

The vertebrate TGF-β superfamily has two subfamilies, the TGF-β/Activin subfamily (TGF-β subfamily hereafter) of ligands comprising of TGF-β, Activins, GDFs (including Myostatin) and Nodal ligands, leading to signal transduction via recruitment of Smad2/3 and the the BMP subfamily comprising of BMPs and other GDFs, functioning via downstream Smad1/5/8. The TGF-β subfamily of ligands bind to plasma membrane-associated serine/threonine kinase receptors, i.e., activin type 2 receptors (ACVR2A, ACVR2B, TGFBR2). This ligand-receptor association leads to the recruitment and activation of another set of transmembrane serine/threonine kinase receptors, i.e., activin type 1 receptors (ACVR1B, TGFBR1, ACVR1C). The activin type 1 receptors have a characteristic Gly-Ser (GS) domain upstream of their kinase domains, which gets phosphorylated by the ligand-receptor complex. Canonically, the activated type 1 receptors lead to the phosphorylation of the C-terminal serines at the serine-serine-X-serine (SSXS) motif of downstream signal transducers, Smad2 and Smad3 (Massagué and Gomis, 2006; Massagué, 2012; Sartori et al., 2014). After phosphorylation, these receptor-activated Smads (R-Smads) are released from the receptor complex and form a heterotrimeric complex of two R-Smads and one common Smad4, and further translocate to the nucleus. The nuclear Smad2/3–Smad4 complex interacts with other transcription factors and co-factors, further modulating the expression of target genes. The pathway also comprises of two inhibitory Smads (I-Smads), Smad6 and Smad7, which block the activation of R-Smads as well as compete with the common Smad4 (Massagué and Gomis, 2006; Massagué, 2012; Sartori et al., 2014) (**Figure 1.21**). The Smad proteins comprise of two conserved regions, namely, the N-terminal MH1 domain and the C-terminal MH2 domain, connected by a poorly conserved flexible linker region. The MH1 domain is highly conserved among the Smad2, Smad3 and Smad4, whereas I-Smads lack this domain. Smad2, Smad3 and Smad4 also have the N-terminal nuclear localization signals in their MH1 domains. The MH1 domain is responsible for DNA binding and interaction with transcription factors, whereas, the MH2 domain regulates receptor interaction, cytoplasmic anchoring and transcription of target genes (Brown et al., 2007; Derynck and Zhang, 2003; Massagué and Gomis, 2006). Although, Smad2 and Smad3 share about 66% amino acid sequence homology between their MH1 domains and about 96% amino acid sequence homology between their MH2 domains, they display divergent DNA-binding activities as well as functional roles (Denis et al., 2016; Liu et al., 2016; Morikawa et al., 2013; Míguez et al.,

2013; Petersen et al., 2010). Interestingly, the MH1 domain of Smad2 has extra 30 amino acids, which prevents its direct binding to DNA, unlike Smad3 which along with Smad4 can recognize Smad Binding Element (SBE) boxes present in the promoter region of target genes, such as *JunB* and *Plasminogen activator inhibitor-1 (PAI-1)* (Brown et al., 2007; Jonk et al., 1998; Stroschein et al., 1999). However, Smad2 and Smad4 along with other transcription factors like FAST1/2, bind to the activin response element (ARE) in the promoter region of target genes, such as *Goosecoid (Gsc)* and *Mix.2* (Chen et al., 1996; Labbé et al., 1998; Yingling et al., 1997).

The activin type 1 receptor-mediated C-terminal phosphorylation of Smads is the main event in Smad activation; however, it has been shown that other kinase pathways also regulate Smad signaling (Derynck and Zhang, 2003). Amongst many such pathways is the Erk mitogen-activated protein kinase (MAPK) pathway, stimulated by the activation of tyrosine kinase receptors and Ras, which also targets R-Smads. It has been reported that the stimulation of the MAPK signaling cascade by oncogenic mutations in Ras or by EGF receptor stimulation mediates the phosphorylation of specific residues in the linker region of Smad2/3 (Jia and Souchelnytstkyi, 2011; Kretzschmar et al., 1999). Phosphorylation of this linker region was shown to inhibit TGF-β-induced C-terminal phosphorylation and nuclear translocation of Smads, disturbing the transcriptional activation of their target genes (Jia and Souchelnytstkyi, 2011; Kretzschmar et al., 1999).

1.7.2 Smad-independent non-canoninal TGF-β signaling

Apart from Smad-mediated transcription, TGF-β also activates other signaling cascades such as the Erk, JNK and p38 MAPK kinase pathways (**Figure 1.21**). Slow activation of these pathways may result from Smad-dependent transcriptional responses in some cases, but the rapid activation in other cases suggests independence from Smad-associated transcription. Rapid Ras activation by TGF-β in epithelial cells may suggest the involvement of Ras in TGF-β-induced Erk MAPK signaling. JNK and p38 MAPK signaling pathways have been shown to be activated by various MAPK kinase kinases (MAPKKK) in response to multiple stimuli (Derynck and Zhang, 2003). TGF-β-induced activation of Erk and JNK pathways can lead to Smad phosphorylation and therefore regulate Smad activation. Furthermore, TGF-β-induced activation of Ras/Erk MAPK signaling can lead to the induction of TGFB1 expression, thereby amplifying the response of TGF-β and promoting secondary TGF-β-

associated responses. MAPK pathway activation by TGF-β may also affect transcription by directly affecting Smad-interacting transcription factors, indicating the convergence of TGF-β-induced Smad and MAPK pathways (Massagué, 2000). This convergence often results in cooperation between these pathways but there have been certain instances where these pathways have counteracted each other. Thus, the balance between direct interaction of Smad and MAPK kinase pathways defines cellular responses to TGF-β (Derynck and Zhang, 2003).

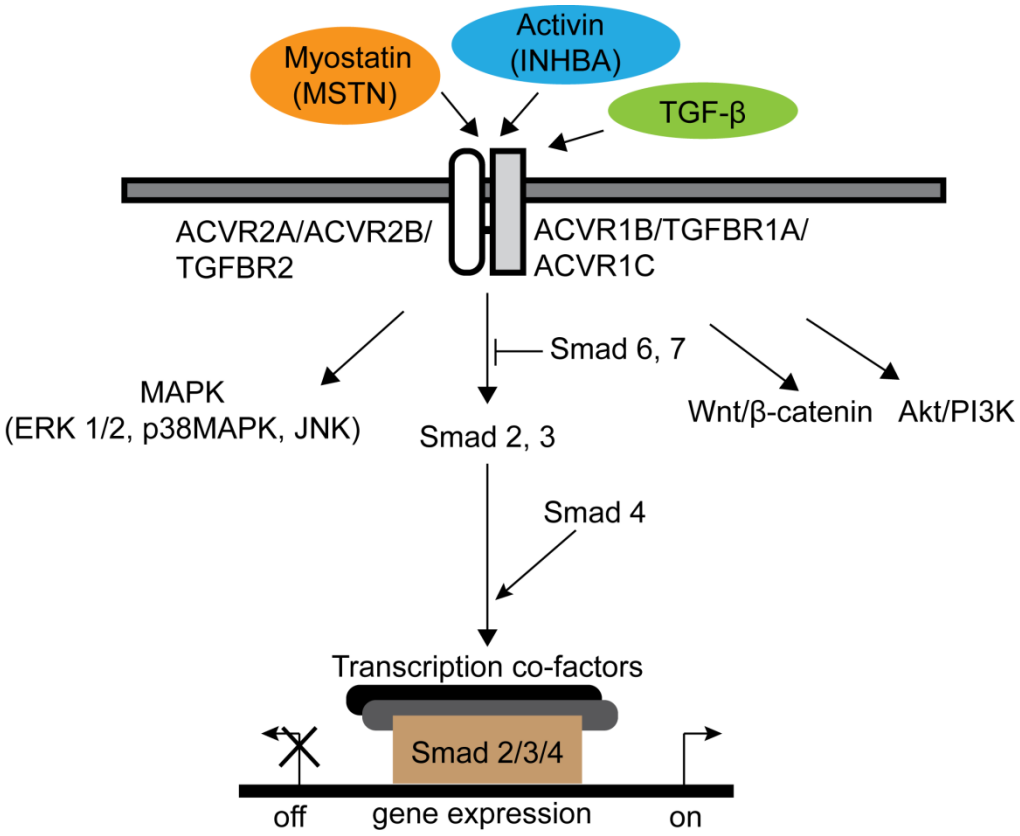

Figure 1.21. A simplified overview of Smad-dependent and Smad-indepenedent TGF-β signaling pathways. The ligands bind to a complex of transmemberane receptor serine/threonine kinases (type 2 and type 1 receptors), leading to the trans-phosphorylation of type 1 receptors by the type 2 receptor kinases. The activated type 1 receptors phosphorylate the R-Smads at C-terminal serines. These receptor-activated Smads form a complex with Smad4 and this Smad complex gets translocated to the nucleus, where they regulate the transcriptional activation or repression of their target genes. Modified image is adapted from Tsuchida et al., 2009.

1.8 Factors influencing the activity of TGF-β signaling

The function of TGF-β signaling has been shown to be dependent on cell-type as well as the conditions. The contextual dependence on the functional roles of this signaling pathway

makes it an interesting pathway to be explored. The number of target genes for a given TGF-β family member can range from just a few to hundreds. The effects of TGF-β signaling on transcription can be positive or negative, depending on the gene targeted as well as the cellular context. For instance, TGF-β suppresses the activation of inhibitor of differentiation 1 (ID1) in mammary epithelial cells (Kang et al., 2003), whereas it induces this gene in metastatic breast cancer cells (Padua et al., 2008). There exist three types of contextual determinants that shape the TGF-β transcriptional response in a cell. Firstly, within an epigenetic and transcriptional context, the extracellular and the intracellular composition of the TGF-β signal transduction system decides the response of a cell. The abundance and activity of various TGF-β ligands, receptors and regulators controls the nature of TGF-β nuclear signal and the co-existing cues further determine the response by Smad functional regulation and/or by activating non-canonical pathways. Next, the factors that cooperate with SMAD proteins to regulate transcription form the second set of determinants. Such factors include forkhead box H1 (FOXH1, a.k.a FAST1), a transcriptional factor that allows SMAD proteins to recognize AREs in the promoter region of SMAD target genes (Chen et al., 1997). Finally, the epigenetic status of the cell, including DNA methylation, histone modifications, etc., shapes the chromatin and decides what genes are accessible for expression and suspectible to regulation. Overall, these three classes of contextual determinants control the pleiotropic capacity of TGF-β signaling and give rise to specific responses in particular cell types and conditions (Massagué, 2012), which are explained in more details in the following section.

1.9 Various functions of TGF-β signaling

1.9.1 Embryonic stem (ES) cell self-renewal and differentiation

The triad OCT4, SOX2 and NANOG have been shown to be the core transcriptional regulators which induce pluripotency in ES cells (Orkin and Hochedlinger, 2011; Young, 2011). The SMAD proteins have been recently reported to be playing important roles in the context of this network. BMP signaling stimulates ES cell self-renewal by directing SMAD1 to co-occupy the genome with STAT3, OCT4, SOX2 and NANOG, at the sites that contain the H3K4me3 mark of active transcription (Ying et al., 2003). The genes targeted include *Oct4, Sox2, Nanog* and *Id3*. The Nodal-activated SMAD3 is also directed by OCT4 to the neighbouring sites, which leads to the activation of a few of the target genes, including Nanog and the Nodal negative feedback regulators, *Lefty1, Lefty2* and *Smad7*. In the absence of

pluripotency inducing factors, the ES cells differentiate into mesendodermal cells of the primitive steak and ectodermal cells. Nodal promotes mesendodermal differentiation by inducing the expression of homeobox transcription factors, goosecoid homeobox *(GSC)* and mix paired-like homeobox *(MIXL1)* (Massagué, 2012; Xi et al., 2011).

1.9.2 Epithelial-Mesenchymal Transition (EMT)

EMT is not only a crucial morphogenetic event during gastrulation, embryonic tissue formation and regeneration, but the pathological forms of EMT are also involved during fibrosis and cancer. The enforced expression of EMT transcriptional regulators can transform the mammary epithelial cells into stem-like cells, thereby providing the breast cancer cells with a tumour-initiating phenotype. The interactive network of transcriptional repressors, including SNAIL1, SNAIL2, TCF3, TWIST, etc. can drive EMT (Nieto, 2011; Thiery et al., 2009). The TGF-β pathway has been shown to trigger EMT during cardiac development, renal fibrosis, palate fusion and many other processes (Massagué, 2012). WNT creates a favourable environment for TGF-β-induced EMT, as otherwise the epithelial cells would undergo growth arrest in response to TGF-β. In mammary epithelial cells, the SMAD proteins, which are activated by TGF-β, induce the expression of SNAIL1 and TWIST1 (Tan et al., 2012; Thuault et al., 2008). This is followed by the event of repression of epithelial cell junction gene expression by SMAD proteins and SNAIL1 (Vincent et al., 2009). On the other hand, BMPs antagonize EMT and favour mesenchymal-epithelial transition (MET) (Scheel et al., 2011). Also, the transcriptional effects of TGF-β are accompanied by TGFBR2-mediated PAR6 phosphorylation, in order to dissolve tight junctions and drive an invasive phenotype (Ozdamar et al., 2005; Viloria-Petit et al., 2009).

1.9.3 Tumour suppression and tumour progression

TGF-β has been reported to be a tumor suppressor in pre-malignant cells, whereas it acts as an enhancer of invasion and metastasis in the advanced carcinoma cells. Inactivating mutations in *TGFBR2* and *SMAD4* have been observed in the carcinoma transition of gastrointestinal and pancreatic tumours (Massagué, 2008). With the elimination of TGF-β pathway, the cancer cells can create a TGF-β rich microenvironment that favours tumour progression (Massagué, 2008; Yang et al., 2010). In case of breast cancer, melanomas and gliomas, the prevailing cancer clones retain intact SMAD signaling machinery and are disabled for TGF-β

tumour suppressive responses. Genetic loss of *CDKN2B* relieves cancer cells of the tumour suppressive SMAD target gene, and oncogenic drivers such as HER2 and PI3K weaken the tumour suppressor SMAD cofactors. Under such conditions, the cancer cells can utilize the SMAD pathway according to their will, for instance, the SMAD-driven EMT promotes metastatic seeding in breast cancer cells (Massagué, 2012). Therefore, the SMAD-mediated gene responses which would be non-oncogenic in a normal cellular context, can act as mediators of malignancy in cancer cells.

1.10 The role of TGF-β signaling in cardiac development and disease

1.10.1 Cardiac development

The ligand-specific function of TGF-β signaling has been studied in EMT during cardiac cushion formation in mice. It has been reported that TGFB2, not TGFB1 or TGFB3, mediates cardiac cushion EMT by promoting both the initiation and termination of this process during embryonic development (Azhar et al., 2009). In another study, an extensive analysis of the role of this signaling pathway in cardiac development has been carried out by ablating TGFBR1 in the myocardial, endocardial and epicardial lineages of the heart (Sridurongrit et al., 2008). It has been shown that TGFBR1-mediated signaling does not play an important role in the myocardium, rather it is crucial in the endocardium for the induction of EMT both *in vitro* and *in vivo*. Furthermore, the loss of epicardial TGFBR1-mediated signaling disturbed the cell-cell interactions between the epicardium and myocardium, resulting in thinner myocardium and a lack of EMT in TGFBR1-lacking epicardial cells was also observed (Sridurongrit et al., 2008).

1.10.2 Cardiac diseases

Cell culture studies have revealed that TGFB1 inhibits cardiomyocyte divison (Kardami, 1990), and stimulates hypertrophic growth (Villarreal and Dillmann, 1992), fibrosis (Eghbali et al., 1991; Villarreal and Dillmann, 1992) and re-expression of the fetal isoforms of the myofibrillar protein genes (Parker et al., 1990). In the adult heart, TGFβs not only regulate hypertrophic response, but are also involved in vascular remodeling and regulation of the renal renin-angiotensin system (Azhar et al., 2003).

1.10.3 Cardiac regeneration

The reported function of TGF-β signaling cascade in cardiac regeneration appears to be contradictory in the context of different species. In the diseased mammalian heart, enhanced TGF-β signaling via the upregulation of the expression of its various ligands, such as TGF-β (Hein et al., 2003; Li et al., 1997), Myostatin (MSTN) (Bish et al., 2010; Castillero et al., 2015) and Inhibin betaA (INHBA) (Yndestad et al., 2004), has been reported to induce pathological cardiac remodeling by stimulating cardiac hypertrophy, fibrosis, apoptosis and endothelial-mesenchymal transition (Euler-Taimor and Heger, 2006; Zeisberg et al., 2007). Furthermore, the cardiomyocyte-specific deletion of *Tgfbr2* suppresses pathological remodeling in response to sustained pressure overload, indicating the deleterious effects of the TGF-β signaling pathway on cardiac remodeling (Koitabashi et al., 2011). On the other hand, in zebrafish, TGF-β signaling pathway has been reported to be essential for cardiac regeneration as global inhibition of this signaling cascade by using chemical inhibitor of activin type 1 receptors, negatively affects cardiomyocyte proliferation (**Figure 1.22**) and scar clearance post cardiac injury (**Figure 1.23**), thereby leading to a compromised cardiac regeneration (Chablais and Jazwinska, 2012).

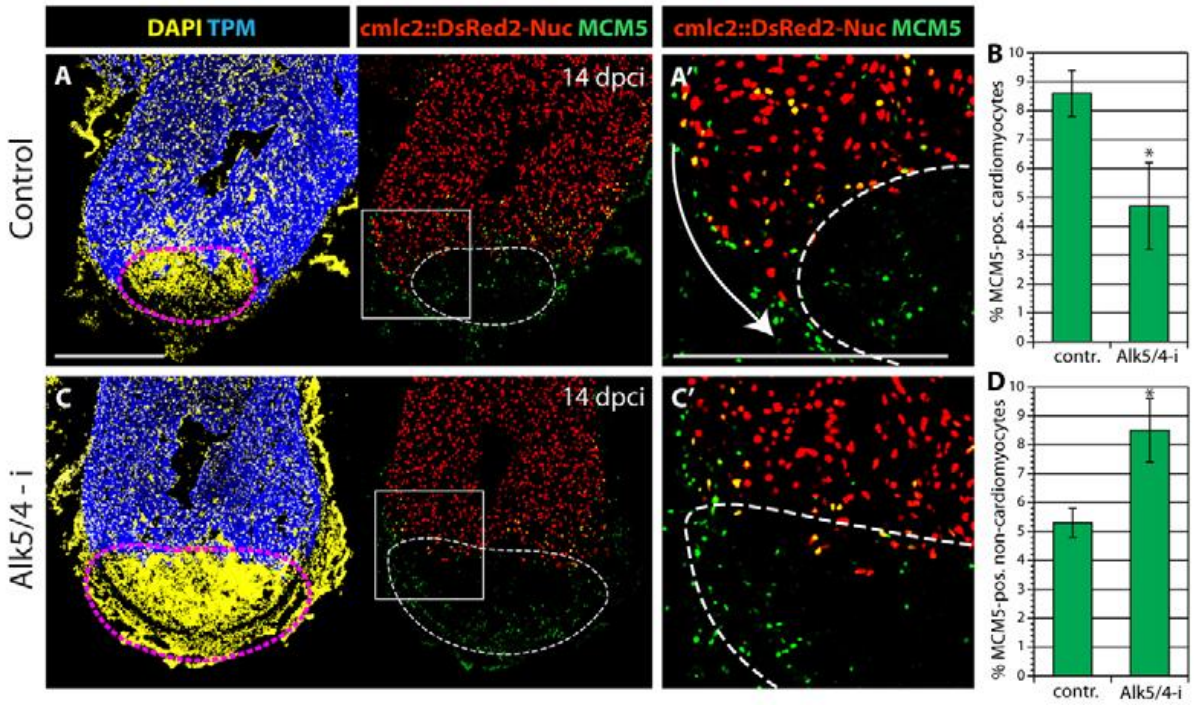

Figure 1.22. The effect of TGF-β signaling on cardiomyocyte proliferation. (A, A', C, C') Heart sections of transgenic *myl7:DsRed-Nuc* (red) fish immunostained for Tropomyosin (blue) and MCM5 (green) to detect mitotic cells, followed by DAPI staining (yellow) at 14 dpci. Proliferating cardiomyocytes are identified by co-expression of DsRed2 and MCM5. The postinfarcts are encircled by dashed lines. (A', C') Higher magnifications of the boxed areas in A, C. (A, A') In control hearts, proliferating cardiomyocytes are located in

the vicinity of the injury site. Non-cardiac Mcm5-positive cells are distributed predominantly at the post-infarct wall. (C,C') Exposure to Alk5/4-i attenuates cardiomyocyte proliferation and expansion. (**B**) The ratio of Mcm5-positive DsRed2-positive nuclei to all DsRed2-positive nuclei demonstrates a reduction of proliferating cardiomyocytes after drug treatment (n=10). (**D**) The ratio of Mcm5-positive to DAPI-positive nuclei shows enhanced proliferation of non-cardiac cells after drug treatment (n=10). Error bars indicate s.e.m.; n=10; *P<0.05, t-test. Scale bars: 300µm. dpci, days post cryoinjury. Modified image is adapted from Chablais and Jazwinska, 2012.

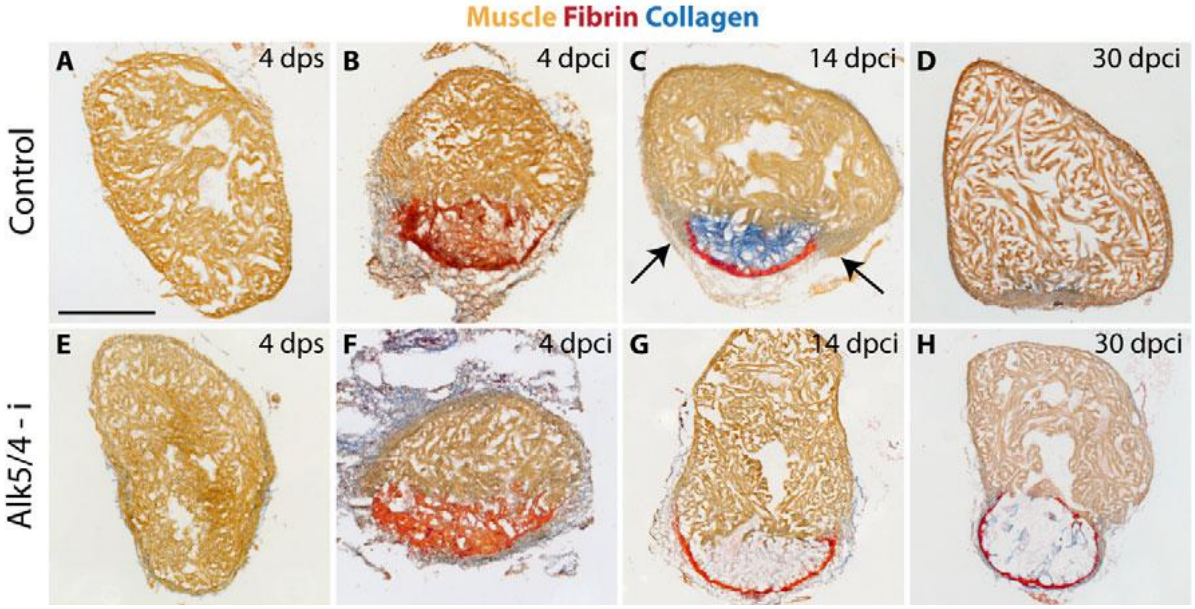

Figure 1.23. The inhibition of TGF-β signaling blocks heart regeneration resulting in the infarct bulging phenotype. AFOG staining of heart sections was performed on (A-D) control and (E-H) Alk5/4-i treated heart sections. (**A, E**) Control and inhibitor-treated ventricles after sham operation (4 dps) consist of healthy myocardium. (**B, F**) At 4 dpci, similar infarcts (red) are detected in both groups. (**C, G**) Hearts at 14 dpci. (C) Control hearts contain abundant fibrillar collagen in the injury area. A layer of fibrin (red) covers the margin of the infarct. New myocardium begins to invade the scar tissue (arrows). (G) Exposure to Alk5/4-i suppresses collagen deposition and no myocardial invasion is observed. (**D**) In control hearts, the scar is nearly completely resolved and replaced with new muscle. (**H**) Alk5/4-i suppressed cardiac regeneration and the infarct is surrounded by a collagen-deficient fibrin layer. The injury area bulges beyond the ventricular circumference. Scale bar: 300µm. dps, days post sham injury; dpci, days post cryoinjury. Modified image is adapted from Chablais and Jazwinska, 2012.

1.11 Myostatin

Myostatin (MSTN, also known as GDF8) is one of the TGF-β family ligands and is a well-known negative regulator of skeletal muscle growth. Mstn has two paralogs in the zebrafish, namely, *mstna* and *mstnb*. It is produced as a precursor protein that contains a signal

sequence, an N-terminal propeptide domain, and a C-terminal domain which acts as the active ligand. Proteolytic processing between the propeptide domain and the C-terminal domain releases mature Myostatin, which dimerizes to form active protein. After cleavage, the unprocessed and mature active Myostatin remain associated and Myostatin must be released from the latent complex in order to elicit its biological activity (Hill et al., 2002; McPherron et al., 1997).

MSTN has been shown to be highly expressed in skeletal muscle, and is also produced in heart and fat tissue in detectable amounts (McPherron and Lee, 1997; Sharma et al., 1999). MSTN acts by binding to activin type 2 receptor ACVR2B preferably compared to ACVR2A, and forms a heteromeric complex with the type 1 receptor ACVR1B/TGFBR1, thereby inducing phosphorylation of downstream Smads to activate a TGF-β-like signaling pathway (Lee and McPherron, 2001; Rebbapragada and Benchabane, 2003; Tsuchida et al., 2009).

Inactivation of *Mstn* by targeted deletion (**Figure 1.24**) or naturally occurring mutations (**Figure 1.25**) causes an enormous increase in skeletal muscle mass in various species, including humans, mice and cattle (McPherron and Lee, 1997; McPherron et al., 1997; Rodgers and Garikipati, 2008). It is also shown to negatively regulate the satellite cell activation and self-renewal through the downregulation of Pax7 (McCroskery et al., 2003). Through the up-regulation of p21 and inhibition of Cdk2 activity, MSTN inhibits or prevents the progression of myoblasts from the G1 to S phase of cell cycle, thereby maintaining the quiescence of satellite cells (Carnac et al., 2007). There have been several reports supporting the essential role of MSTN in regulating cardiac hypertrophy in mammals (Biesemann et al., 2014; Haidet et al., 2008; Whittemore et al., 2003). Amongst these reports, a recent study shows that myostatin not only prevents cardiac hypertrophy by stimulating the expression of regulator of G-protein signaling 2, a GTPase-activating protein that restricts Gaq and Gas signaling, but also regulates myocardial metabolism by suppressing the activation of AMP-activated kinase in the heart (Biesemann et al., 2014). Further, the absence of myostatin has been reported to enhance murine skeletal muscle regeneration, as muscles of senescent *Mstn*$^{-/-}$ mice regenerate robustly from both chronic and acute injury, and also the early markers of regeneration are enhanced (Wagner et al., 2005). A recently developed monoclonal antibody (REGN1033) against MSTN shows therapeutic potential in the treatment of skeletal muscular atrophy, as the antibody-treated mice show increased muscle fiber size, muscle mass and force production (Latres et al., 2015).

Although several studies have reported that the expression of myoostatin is upregulated after MI as seen in mammalian system (Bish et al., 2010; Castillero et al., 2015), but its role in cardiac regeneration remains unknown.

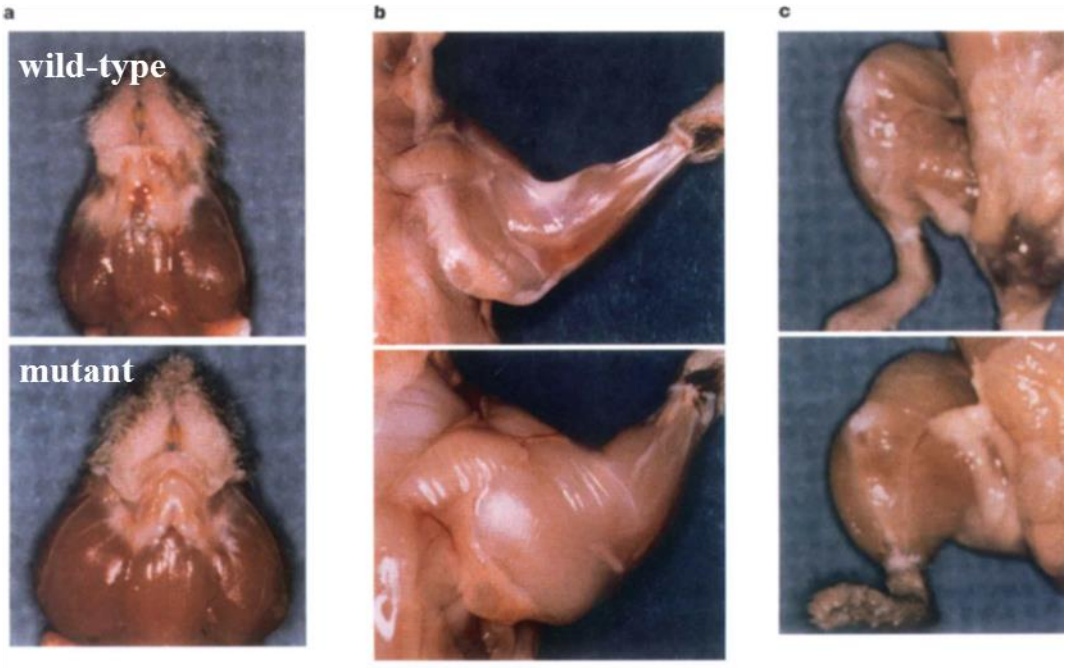

Figure 1.24. Increased skeletal muscle mass in *Mstn* null mice (bottom panels) compared to wild-type littermates (top panels). Facial **(a)**, upper limb **(b)** and lower limb **(c)** muscles of skinned animals, showing an enormous increase in the skeletal muscle mass of *Mstn* null mice. Modified image is adapted from McPherron et al., 1997.

Figure 1.25. A fullblood Belgian Blue bull showing the double muscling phenotype due to a mutation in myostatin. Modified image is adapted from McPherron and Lee, 1997.

1.12 Activin A

Activins are formed by dimers of two inhibin β subunits (4 subunits have been identified so far, including βA, βB, βC and βE). Homodimers of inhibin βA or βB subunits form activin A and activin B, respectively, or heterodimeric activin AB form activing AB. Activin A is another ligand of the TGF-β signaling pathway and has two paralogs in zebrafish, i.e., Inhibin-betaAa ((*Inhbaa*) or Activin-betaAa (*Actbaa*)) and Inhibin-betaAb (*Inhbab*). Activin proteins are synthesized as large precursors, with the precursor chain consisting of an N-terminal signal peptide, followed by a prodomain and a C-terminal mature domain. During proteolytic processing, the cleavage of polypeptide sequence takes place between pro- and mature domains, releasing the mature signaling domain (Gentry et al., 1988; Wang et al., 2016). Once Activins bind to Activin type 2 receptors ACVR2A/ACVR2B, type 1 receptors ACVR1B/ACVR1C are recruited to the ligand/ACVR2 complex, leading to the phosphorylation of type 1 receptors by ACVR2 kinases (Tsuchida et al., 2009). Finally, the downstream Smads are phosphorylated by activated type 1 receptors (Tsuchida et al., 2009).

Activin was initially isolated from porcine ovarian follicular fluid and identified as an activating factor for the release of follicle stimulating hormone (Vale et al., 1986). Many other roles of this protein have further been discovered, including the regulation of embryogenesis, regulation of immune system, reproductive system development, regulation of immune system and wound healing (Antsiferova and Werner, 2012; Jones et al., 2004; Murry and Keller, 2008; Pangas et al., 2007). Moreover, high levels of Activin A have been detected during breast cancer and it has been shown to promote anchorage-independent growth, EMT, invasion, angiogenesis, and stemness of breast cancer cells (Bashir et al., 2015). Interestingly, *inhba* was also found to be strongly induced at the fin amputation site and was reported to be involved in wound healing and blastema proliferation during zebrafish fin regeneration (Jaźwińska et al., 2007). Intriguingly, the high expression levels of INHBA have been observed both in heart failure patients as well as rodent model system (Yndestad et al., 2004), however its role during cardiac regeneration still needs to be explored.

1.13 Aims of this project

As mentioned above, the TGF-β signaling pathway has been implicated to be involved in various developmental and disease conditions, but the role of its individual members in cardiac regeneration remains to be determined. In order to elucidate the role of individual TGF-β family ligands, microarray analysis of cryoinjured versus sham injured adult zebrafish hearts was performed. Using gene expression profiling, I identified that the two TGF-β genes, *myostatin b* (*mstnb*) and *inhibin beta Aa* (*inhbaa*) have opposite expression response to cryoinjury, which called for a detailed investigation of their specific functional roles during cardiac regeneration.

The project thus carried out had the following aims:

AIM-1: To perform spatio-temporal expression analysis of *mstnb* and *inhbaa* during cardiac regeneration.

AIM-2: To unravel the role of *mstnb* and *inhbaa* during cardiac regeneration by generating their loss-of-function mutants and gain-of-function transgenic lines.

AIM-3: To determine the molecular mechanisms underlying the specific expression patterns and functional roles of these two TGF-β family ligands during cardiac regeneration.

2. Materials

2.1 Lab equipments

2.1.1 PCR cyclers

Table 1: List of PCR machines used and their respective suppliers.

Machines	Supplier
PCR cycler, Mastercycler Pro	Eppendorf
Real-time PCR Cycler	BIORAD
Real-time PCR cycler	Illumina

2.1.2 Microscopes

Table 2: List of microscopes used and their respective suppliers.

Microscopes	Supplier
Confocal Microscope, LSM 700	Zeiss
Confocal Microscope, LSM 800	Zeiss
Embryo Microinjection, Stereomicroscope Stemi 2000	Zeiss
Stereomicroscope, Stereodiscovery V8	Zeiss
Stereomicroscope Stereodiscovery V8, with camera AxioCam MRc5	Zeiss
Stereomicroscope, MZ 16 F	Leica
Stereomicroscope, SMZ18	Nikon
Stereomicroscope, with camera SMZ25	Nikon

2.1.3 Centrifuges

Table 3: List of centrifuges used and their respective suppliers.

Centrifuges	Supplier
Centrifuge (slow speed, 1.5-2ml tubes)	Qualitron
Centrifuge (slow speed, 200 µl tubes)	Qualitron

Centrifuge 5415 D (1.5-2 ml tubes)	Eppendorf
Centrifuge 5418 (1.5-2 ml tubes)	Eppendorf
Centrifuge 5418 (1.5-2 ml tubes)	Eppendorf
Centrifuge 5417 R (200 µl tubes)	Eppendorf
Centrifuge 5810 R (15-50 ml tubes)	Eppendorf

2.1.4 Miscellaneous equipments

Table 4: List of miscellaneous equipments used and their respective suppliers.

Equipments	**Supplier**
Bacterial incubator	Heraeus
Bacterial incubator shaker	Infors HAT
Heating block	VWR
Latex gloves	Roth
Nitrile gloves	VWR
Vortex	Scientific Industries
Pipetteman	Gilson
Pipetboy	Integra
Pipette tips	Greiner bio-one
Pipette filter tips	Greiner bio-one
Pipette pump	Bel-Art Products
Agarose gel electrophoresis chamber	Peqlab
Combitips	Eppendorf
Dark reader transilluminator	Clare Chemical Research
Gel DOC EZ imager	BIORAD
Gel electrophoresis power supply	Peqlab
Microwave	Bosch
Multipipette Plus	Eppendorf
Laboratory film	Parafilm
Forceps	Dumont
Fumehood	Bense
Homogenizer	Bibby Scientific

LMD-6000	Leica
Hot plate	Janke & Kunkel Gmbh
Hot plate magnetic stirrer	VWR
Hybridization oven	VWR
Immedge pen	Vector Laboratories
Injection micromanipulator	World Precision Instruments
Injection needles	Harvard Apparatus
Injection needle puller	Sutter Instruments
Injection pump, PicoPump	World Precision Instruments
Zebrafish incubator	Binder
Zebrafish aquatic housing system	Tecniplast
Weighing balance	Sartorius
Water bath	Julabo
PICOSPRITZER III	Parker
Microscale	Novex
Mineral oil	Sigma
Pasteur pipette	Greiner bio-one
pH meter	Mettler Toledo
pH strips	Merck
Petridish	Greiner bio-one
qPCR adhesive seals	Illumina
qPCR plates, 48 well	Illumina
qPCR plates, 96 well	BIORAD
qPCR microseals	BIORAD
Rocker	Grant Instruments
Rotator	Stuart
Spectrophotometer, NANODROP 2000C	Thermo Scientific
Serum pipette	Greiner bio-one
Serological pipette	Greiner bio-one
Surgery scissors	Fine Science Tools
Scalpel	Braun
Magnetic stir bar	VWR

Microdish	ibidi
Microloader pipette tips	Eppendorf
Magnetic stirrer	HANNA instruments
Beakers	VWR
Glass bottles	VWR, Duran
Cocical flasks	VWR
Glass measuring cylinder	SCHOTT
Bacterial culture tubes	Sarstedt
Centrifuge tubes (500 µl)	Sarstedt
Centrifuge tubes (1.5 ml, 2 ml)	Sarstedt
Centrifuge tubes (15 ml, 50 ml)	Greiner bio-one
PCR tubes	Sarstedt
PCR tube strips	Sarstedt
Optical dishes	MatTek
19-guage needle	FINE-JECT
5 ml syringe	TERUMO
100 µm nylon mesh	FALCON
40 µm nylon mesh	FALCON
Qiashredder columns	Qiagen

2.2 Chemicals

Table 5: List of chemicals used and their respective suppliers.

Chemicals	**Supplier**
1-Phenyl-2-thiourea (PTU)	Sigma
5-ethynyl-2´-deoxyuridine (EdU)	Invitrogen
Acetic anhydride	Sigma
Acidic hemalum	Waldeck
AFOG staining kit	Gennova
Agarose	Peqlab
Agarose, low melting temperature	Sigma
Blocking reagent	Roche

Bouin's Solution	Sigma
Bovine Serum Albumin (BSA)	Sigma
Chloroform	Merck
Citric acid	Sigma
DEPC	Sigma
DIG labelling mix	Roche
Dimethyl Sulfoxide	Sigma
DMH1	Sigma
DNA Away	Molecular Bioproducts
DNA ladder	Thermo Scientific
dNTP	Thermo Scientific
Entellan	Merck
Eosin	Waldeck
Ethanol	Roth
Ethidium Bromide	Sigma
Ethylenediaminetetraacetic acid (EDTA)	Roth
Fetal Calf Serum	Biochrom
Formaldehyde	Santacruz
Formamide	Applichem
Gel loading dye	Thermo Scientific
Glycerol	Roth
Goat serum	Gibco
Isopropanol	Roth
Magnesium Chloride	Fluka
Magnesium Sulphate	Fluka
Methanol	Roth
Methylene blue	Sigma
Mineral oil	Sigma
NBT/BCIP stock solution	Roche
Nuclease-free water	Thermo Scientific
Paraformaldehyde (PFA)	Sigma
Paraplast	Leica

PD168393	Calbiochem
Phosphate Buffered Saline (PBS)	Sigma
Potassium Chloride	Merck
Potassium dihydrogen phosphate	Merck
Phenol Red	Sigma
RNase A	Roche
RNase ZAP	Sigma
SB431542	Calbiochem
Sheep serum	Sigma
SIS3	Calbiochem
Sodium Chloride	Roth
Sodium Citrate	Sigma
Sodium hydroxide	Sigma
Sodium phosphate monobasic monohydrate	Sigma
Sodium phosphate dibasic dodecahydrate	Sigma
Sucrose	Roth
SSC	Ambion
SYBR Safe	Invitrogen
Tricaine	Pharmaq
Triethanolamine	Sigma
TRIS	Sigma
Tris-EDTA	Cayman Chemicals
Triton X-100	Sigma
TRIzol reagent	Ambion
Tryptone	Fluka
Tween-20	Sigma
X-gal	Sigma
Yeast extract	Fluka

2.3 Enzymes

Table 6: List of enzymes used and their respective suppliers.

Enzymes	Supplier
AgeI-HF	NEB
BamHI	NEB
BsrGI	NEB
ClaI	NEB
EcoRV-HF	NEB
HindIII-HF	NEB
NheI-HF	NEB
NotI	NEB
Plasmid Safe DNase	Epicentre
Pronase	Roche
Proteinase K	Roche
RNasein	Promega
RQ1 RNase-Free DNase	Promega
SmaI	NEB
SP6 RNA Polymerase	Promega
T4 DNA Ligase	NEB
T3 RNA Polymerase	Promega
T7 RNA Polymerase	Promega
XbaI	NEB

2.4 PCR enzymes and mastermix

Table 7: List of PCR enzymes/mastermix used and their respective suppliers.

PCR enzyme/mastermix	Supplier
2x Dynamo Color Flash	ThermoFischer Scientific
PrimeSTAR Max DNA Polymerase	Takara
KAP2G 2x	KAPABIOSYSTEMS
Maxima SYBR Green qPCR master mix	ThermoFischer Scientific

PCR master mix	ThermoFischer Scientific
Phusion DNA Ploymerase	NEB

2.5 Kits

Table 8: List of kits used and their respective suppliers.

Kits	Supplier
Cold Fusion Cloning Kit	System Biosciences
Gel extraction kit	Thermo Scientific
Maxima cDNA synthesis kit	Thermo Scientific
Mini Prep Plasmid Isolation kit	Thermo Scientific
miRNeasy Micro Kit	Qiagen
mMessage mMachine kits (SP6, T7)	Ambion
PCR product cleanup (ExoSAP)	Jena Bioscience
PCR purification kit	Thermo Scientific
pGEM-T Easy Cloning kit	Promega
RNA clean and concentrator-5	Zymo Research
Superscript III first strand synthesis	Invitrogen

2.6 Antibiotics

Table 9: List of antibiotics and their respective concentrations used.

Antibiotics	Working concentrations
Ampicillin	100 µg/ml
Spectinomycin	50 µg/ml
Tetracycline	10 µg/ml

2.7 Antibodies

Table 10: List of antibodies used, along with their source and respective suppliers.

Antibodies	Source	Supplier

DsRed polyclonal antibody	Rabbit	Clontech
Fibronectin antibody	Rabbit	Sigma
GFP polyclonal antibody	Chicken	Aves Labs
MF-20 antibody	Mouse	eBioscience
N2.261antibody	Mouse	H.M. Blau, DSHB
PCNA monoclonal antibody	Mouse	Dako
phospho Smad3 monoclonal antibody	Rabbit	Abcam
Aldh1a2 (Raldh2) antibody	Rabbit	GeneTex
Goat Anti Mouse Alexa Fluor 647	Goat	Invitrogen
Goat Anti Mouse Alexa Fluor Cy3	Goat	Invitrogen
Goat Anti Rabbit Alexa Fluor 488	Goat	Invitrogen
Goat Anti Rabbit Alexa Fluor 568	Goat	Invitrogen
Goat Anti Rabbit Alexa Fluor 647	Goat	Invitrogen
Goat Anti Chicken Alexa Fluor 488	Goat	Invitrogen
Anti-Digoxigenin-AP, Fab fragments		Roche

2.8 Bacterial culture media

Table 11: List of bacterial culture media used, along with their suppliers and preparation recipes.

Bacterial strain	**Supplier/Recipe**
LB medium	Roth
LB agar	Roth
SOC medium	-The following components were dissolved

	in distilled water: Tryptone 2%, Yeast extract 0.5%, NaCl 0.05% and KCl 0.0186%. -pH was adjusted to 7, and 10 mM $MgCl_2$ and 20 mM D-glucose were added, followed by autoclaving.

2.9 Bacterial strains

Table 12: List of bacterial strains used and their application.

Bacterial strain	Application
Dh5α	Competent cells for cloning

2.10 Buffers and other solutions

Table 13: List of buffers and other solutions used, along with their composition.

Buffers and other solutions	Composition
Alkaline Tris Buffer	100mM Tris HCl pH 9.5 100mM NaCl, 50mM $MgCl_2$
DEPC Water	0.01% DEPC dissolved in distilled water and autoclaved
E3 embryo medium	3g Instant Ocean 0.75g Calcium sulphate dissolved in 10 L of distilled water
PBS	8g NaCl 0.2g KCl 1.44g Na_2HPO_4 0.24g KH_2PO_4 dissolved in 900 ml of distilled water, pH was adjusted to 7.4, volume was made up to 1000 ml with distilled water
PBT	0.1% Tween 20 in PBS
20x SSC	175.3g NaCl

	88.2g Sodium Citrate dissolved in 800 ml distilled water and pH was adjusted to 7, volume was made up to 1000 ml with distilled water.
EDM	L-15 medium 10% Fetal Calf Serum
DEPC-PBS	1 L PBS was filtered and 1 ml DEPC was added, followed by stirring for 1 hour and autoclaving.
1M (10x) Triethanolamine, pH 8.0	66.5 mL Triethanolamine and 20 mL concentrated HCl were added to 413.5ml DEPC-water.
50x Denhardt's Solution	2% BSA 2% Polyvinylpyrrolidone (PVP-40) 2% Ficoll 400. A slurry was prepared in DEPC-water and diluted.
Hybridization Solution for *in situ* hybridization	50% Formamide 5X SSC 0.3 mg/mL Yeast tRNA 0.1 mg/mL Heparin 1xDenhardt's Solution 0.1% Tween 20 5mM EDTA in DEPC-H2O.
Alkaline Phosphatase Buffer	100mM Tris pH 9.5 50mM $MgCl_2$ 100mM NaCl 0.1% Tween 20 made up to 500 ml with ddH_2O and filtered into clean bottle.
Permeabilization Buffer for whole mount IHC	PBS 0.3% Triton-X 1% DMSO

	1% BSA 0.1% Tween 20
Blocking Buffer-I for whole mount Immunohistochemistry (IHC)	PBS 1% DMSO 2% Fetal Calf Serum 1% BSA 0.1% Tween 20
Sodium Citrate antigen retrival buffer for IHC on sections	2.94 g of Tri-sodium citrate (dehydrate) was added to distilled water (made up to 1 L) and stirred to dissolve. pH was adjusted to 6.0 and 0.5 ml of Tween 20 was added.
Blocking Buffer-II for IHC on sections	1%BSA in PBS
Click IT EdU reaction mix	For 1 ml recation mix: 860 µl 1X Click-iT reaction buffer 40 µl $CuSO_4$ 2.5 µl Alexa Fluor azide 100 µl reaction buffer additive.

2.11 Oligonucleotides

2.11.1 Primers

Table 14: List of primer sequences used and their application.

Primer names	Primer sequences	Application
*mstnb*_qpcr_F	5'-CGTCACTTCAACCGAGACTG-3'	primers used for RT-qPCR
*mstnb*_qpcr_R	5'-ATTCTCCTGAACAGTAATTCGCC-3'	primers used for RT-qPCR
*inhbaa*_qpcr_F	5'-AGAACAGACGGAGATCATCAC-3'	primers used for RT-qPCR
*inhbaa*_qpcr_R	5'-GCAGTCGAAGGAAGATCCAG-3'	primers used for RT-qPCR
*inhbab*_qpcr_F	5'-GTCAAGCAGCACATCCTCAA-3'	primers used for RT-

		qPCR
*inhbab*_qpcr_R	5’-CCTCCGTCTTCCTCCATCTC-3’	primers used for RT-qPCR
*inhbb*_qpcr_F	5’-ACCAAATATCACTCATCCCATTCC-3’	primers used for RT-qPCR
*inhbb*_qpcr_R	5’-TGGAGTTACATCATCTGATTCGG-3’	primers used for RT-qPCR
*tgfb1a*_qpcr_F	5’-TTCCAGCAAGCTCAGAATAACAC-3’	primers used for RT-qPCR
*tgfb1a*_qpcr_R	5’-TGTCTGTTTCACGTCAAATGAGAG-3’	primers used for RT-qPCR
*tgfb1b*_qpcr_F	5’-CATTGACTTCCGCAAAGACC-3’	primers used for RT-qPCR
*tgfb1b*_qpcr_R	5’-ACAACTGTTCCACCTTATGCT-3’	primers used for RT-qPCR
*tgfb2*_qpcr_F	5’-CTACACAGAGACAGAAACAAAGG-3’	primers used for RT-qPCR
*tgfb2*_qpcr_R	5’-GAGCAGAAAGCAGTATCCAG-3’	primers used for RT-qPCR
*tgfb3*_qpcr_F	5’-CAAACAGAGCAACGAACCTG-3’	primers used for RT-qPCR
*tgfb3*_qpcr_R	5’-TGAGAAGCAGTATTTGGTGTC-3’	primers used for RT-qPCR
*acvr2aa*_qpcr_F	5’-CCAGTTCAGACGACATCAAACC-3’	primers used for RT-qPCR
*acvr2aa*_qpcr_R	5’-GTATGCCAACTTGTGATGCC-3’	primers used for RT-qPCR
*acvr2ab*_qpcr_F	5’-CCATGAGAAGGGTTCACTGAC-3’	primers used for RT-qPCR
*acvr2ab*_qpcr_R	5’-TAGATCACTCTTCAGCAGCAC-3’	primers used for RT-qPCR
*acvr2ba*_qpcr_F	5’-GACTCCTTTCTGCGGATAGAC-3’	primers used for RT-qPCR

*acvr2ba*_qpcr_R	5’-GACACAGACCTGAATGCTTGAG-3’	primers used for RT-qPCR
*acvr2bb*_qpcr_F	5’-CTTCTGATGGTCCTGTAGGT-3’	primers used for RT-qPCR
*acvr2bb*_qpcr_R	5’-TAAACCCTGATGCTTGACCC-3’	primers used for RT-qPCR
*acvr1ba*_qpcr_F	5’-ACTGATACTATAGACATTGCACCC-3’	primers used for RT-qPCR
*acvr1ba*_qpcr_R	5’-CATGGATACCTCCAGCATTACAC-3’	primers used for RT-qPCR
*tgfbr1a*_qpcr_F	5’-AAAGTTATCCCAGAGTTGCCT-3’	primers used for RT-qPCR
*tgfbr1a*_qpcr_R	5’-ACACGATGGTGGATGATTGAG-3’	primers used for RT-qPCR
*tgfbr1b*_qpcr_F	5’-GACATCGCTCCCAATCACAG-3’	primers used for RT-qPCR
*tgfbr1b*_qpcr_R	5’-TCATGAATACCTCCGATAGAGCAG-3’	primers used for RT-qPCR
*acvr1c*_qpcr_F	5’-TCAATCCAGAGCAACCACCT-3’	primers used for RT-qPCR
*acvr1c*_qpcr_R	5’-CACACTCCTAGCATGACACC-3’	primers used for RT-qPCR
*nppa*_qpcr_F	5’-ACGCATTCAGAGACACTCAG-3’	primers used for RT-qPCR
*nppa*_qpcr_R	5’-TTGCTGTCTTCATAATCTACGG-3’	primers used for RT-qPCR
*tcf21*_qpcr_F	5’-TCAGAATGTACAGGAAAGAGGC-3’	primers used for RT-qPCR
*tcf21*_qpcr_R	5’-CTTGGAGAGTTTGGTGTCCG-3’	primers used for RT-qPCR
*hey2*_qpcr_F	5’-GCAGCGAGAATAACTACTCTGG-3’	primers used for RT-qPCR
*hey2*_qpcr_R	5’-TTTCAATGATCCCTCTCCGCT-3’	primers used for RT-

		qPCR
*EGFP*_qpcr_F	5’-AAGCTGACCCTGAAGTTCATCTGC-3’	primers used for RT-qPCR
*EGFP*_qpcr_R	5’-CTTGTAGTTGCCGTCGTCCTTGAA-3’	primers used for RT-qPCR
*junba*_qpcr_F	5’-GCAATCCTAACACTAACCTCACAC-3’	primers used for RT-qPCR
*junba*_qpcr_R	5’-TCCTCTTTCAGAGTAACGAGCC-3’	primers used for RT-qPCR
*junbb*_qpcr_F	5’-CCACAAGATGAACCAGATGCC-3’	primers used for RT-qPCR
*junbb*_qpcr_R	5’-TTCAGCGTCGTGTAAATGGG-3’	primers used for RT-qPCR
*jun*_qpcr_F	5’-GGAAACTACTTTCTACGATGACTC-3’	primers used for RT-qPCR
*jun*_qpcr_R	5’-CTAGACTGGATGATGAGCCT-3’	primers used for RT-qPCR
*jund*_qpcr_F	5’-GCTTCGCATAAACAAGGATATACG-3’	primers used for RT-qPCR
*jund*_qpcr_R	5’-GTTGAGTATTCCCTCAGCATCC-3’	primers used for RT-qPCR
*zgc:153924*_qpcr_F	5’-GACGGGTAAGATGGAAACGC-3’	primers used for RT-qPCR
*zgc:153924*_qpcr_R	5’-TGCTCTTCTTCATCATCTTGTGG-3’	primers used for RT-qPCR
*serpine1*_qpcr_F	5’-CACACTGATGGAATGATTTCTGAG-3’	primers used for RT-qPCR
*serpine1*_qpcr_R	5’-CATCCTTAGACACGAACTCAC-3’	primers used for RT-qPCR
*serpine2*_qpcr_F	5’-GCACTAAAGGCCAGATTCCC-3’	primers used for RT-qPCR
*serpine2*_qpcr_R	5’-GCACTTTGTATGTGTTTCCGTC-3’	primers used for RT-qPCR

*serpine3*_qpcr_F	5’-AACTCCTGCCAGAATTTACCC-3’	primers used for RT-qPCR
*serpine3*_qpcr_R	5’-TGGTCATCAGCTTTACTTTGG-3’	primers used for RT-qPCR
*gsc*_qpcr_F	5’-TGTGCTTATTTCTCCAGTCCC-3’	primers used for RT-qPCR
*gsc*_qpcr_R	5’-TGAACCAAACCTCTACCTTCTC-3’	primers used for RT-qPCR
*mixl1*_qpcr_F	5’-GACAACGTCAGTTTGTTTACAC-3’	primers used for RT-qPCR
*mixl1*_qpcr_R	5’-GGAACCAGACCTGAATTCTC-3’	primers used for RT-qPCR
mxtx1_qpcr_F	5’-CTGCGAGCTACATTTGAAACAG-3’	primers used for RT-qPCR
mxtx1_qpcr_R	5’-GAACCAGACCTGTATGCGAG-3’	primers used for RT-qPCR
mxtx2_qpcr_F	5’-CACGTATTCAGGTATGGTTCCAG-3’	primers used for RT-qPCR
mxtx2_qpcr_R	5’-TGGATGTTGAAGGGTGACTC-3’	primers used for RT-qPCR
*rpl13*_qpcr_F	5’-TAAGGACGGAGTGAACAACCA-3’	primers used for RT-qPCR
*rpl13*_qpcr_R	5’-CTTACGTCTGCGGATCTTTCTG-3’	primers used for RT-qPCR
mstnb OE_PCR_F	5’-GAGGACTTTGGCTGGGACTG-3’	primers used for genotyping *mstnb* overexpression (OE) larvae by PCR
mstnb OE_PCR_R	5’-ATGGCCTTAGTACCCTCGGAC-3’	primers used for genotyping *mstnb* OE larvae by PCR
inhbaa OE_PCR_F	5’-TCCATGCTCTACTACAACGAGGAG-3’	primers used for genotyping *inhbaa*

		OE larvae by PCR
inhbaa OE_PCR_R	5'-ATGGCCTTAGTACCCTCGGAC-3'	primers used for genotyping *inhbaa* OE larvae by PCR
nrg2a OE_PCR_F	5'-CAGGTGCCTACCTTCCAGATCAC-3'	primers used for genotyping *nrg2a* OE larvae by PCR
nrg2a OE_PCR_R	5'-GCAGCCCATACTAGTAGGTCC-3'	primers used for genotyping *nrg2a* OE larvae by PCR
erbb2^{st61} _PCR_F	5'-TGAAGAATGCTGGTAGCTGG-3'	primers used for genotyping *erbb*^{st61} larvae by PCR-based restriction fragment length polymorphism (RFLP) analysis
erbb2^{st61} _PCR_R	5'-GGACTCAGCAAAGGACTTAC-3'	primers used for genotyping *erbb*^{st61} larvae by PCR-based RFLP analysis
*inhbaa*_F	5'-AGAGCGAGGACGAGGGAG-3'	primers used for genotyping *inhbaa*^{bns37} by High resolution melt analysis (HRMA)
*inhbaa*_R	5'- GTGTGTGATGTTGGGTCGCT-3'	primers used for genotyping *inhbaa*^{bns37} by HRMA
*mstnb*_F	5'-GTGTATTAATTGCATGTGGTCCAG-3'	primers used for genotyping *mstnb*^{bns5} by HRMA
*mstnb*_R	5'-GAACACTGCTCGCTTTCCTC-3'	primers used for genotyping *mstnb*^{bns5}

		by HRMA
*mstnb*_insitu_F	5’-CCCATTGTTCAAGTAGATCGG-3’	Primers used for amplification and cloning of *mstnb in situ* hybridization probe
*mstnb*_insitu_R	5’-ATTGTCCATTCCCGAGTCCA-3’	Primers used for amplification and cloning of *mstnb in situ* hybridization probe
*inhbaa*_insitu_F	5’-ATCATCACGT TCGCTGAAACC-3’	Primers used for amplification and cloning of *inhbaa in situ* hybridization probe
*inhbaa*_insitu_R	5’-GAGAGTTCGTCTTGAGGCAG-3’	Primers used for amplification and cloning of *inhbaa in situ* hybridization probe

2.11.2 Morpholinos (MO)

Table 15: List of MO sequences used and their application.

MO names and supplier	**MO Sequences**	**Application**
acvr2aa ATG MO, GeneTools (Philomath, OR)	5’-CCAGCTTTGTTGCAGGTCCCATTTT-3’	Used to knockdown *acvr2aa* gene.
acvr2ab splice MO, GeneTools (Philomath, OR)	5’-TGGCTGCACACAAACACAGATTAAT-3’	Used to knockdown *acvr2ab* gene.

acvr2ba ATG MO, GeneTools (Philomath, OR)	5'-TGAGCAGAGAAGCGAACATATTCCT-3'	Used to knockdown *acvr2ba* gene.
acvr2bb ATG MO, GeneTools (Philomath, OR)	5'-AGCCAGCCAGGGAACAAACATATTC-3'	Used to knockdown *acvr2bb* gene.
control MO, GeneTools (Philomath, OR)	5'-CCTCTTACCTCAGTTACAATTTATA-3'	Used as a control MO.

2.12 Plasmids

Table 16: List of plasmids used and their details.

Plasmids and their suppliers	**Antibiotic resistence**	**Application**
pCS2TAL3DD (Grunwald Lab (Utah))	Ampicillin	Expression vector to clone the final TALEN arm.
pCS2TAL3RR (Grunwald Lab (Utah))	Ampicillin	Expression vector to clone the final TALEN arm.
pHD(1-10), pNG(1-10), pNI(1-10), pNN(1-10) (Addgene)	Tetracycline	TALEN RVDs corresponding to a specific nucleobase: HD – C (Cytosine) NG – T (Thymine) NI – A (Adenine) NN – G (Guanine)
pLR-HD, pLR-NG, pLR-NI, pLR-NN (Addgene)	Spectinomycin	Last half repeat used for cloning TALEN arms.
pFUS_A (Addgene)	Spectinomycin	Used to assemble the first 10 RVDs for each TALEN arm.
pFUS_B(N-1) (Addgene)	Spectinomycin	Used to assemble 11th to (N-1) RVDs for each TALEN arm (N : Total

		number of RVDs).
pGEM-T (Promega)	Ampicillin	Used for synthesizing *in situ* hybridization probe, as a sub-cloning vector to generate the sticky ends.
pcDNA3.1 (Addgene)	Ampicillin	Used for cloning the CDS of gene of interest for mRNA synthesis.
myl7:LIFEACT-GFP (Reischauer et al., 2014)	Ampicillin	Used the plasmid backbone with cardiomyocyte-specific promoter to generate overexpression and constitutively active constructs.

2.13 Zebrafish lines

Table 17: List of published zebrafish lines used and their details.

Zebrafish lines and the publications in which they were described	**Details**
AB	wild-type
erbb2^{st61} (Lyons et al., 2005)	*erbb2* mutant
Tg(-0.8myl7:nlsDsRedExpress)hsc4 (Takeuchi et al., 2011)	Cardiomyocyte-specific reporter
Tg(myl7:LIFEACT-GFP)s974 (Reischauer et al., 2014)	Cardiomyocyte-specific reporter
Tg(myl7:nrg2a202-p2a-tdTomato)bns140 (Rasouli and Stainier, 2017)	*nrg2a* overexpression transgenic line
Tg(ARE:EGFP)fci100 (van Boxtel et al., 2015)	Activin Response Element (ARE) reporter line
Tg(12XSBE:EGFP)ia16 (Casari et al., 2014)	Smad Binding Element (SBE) reporter line

2.14 Zebrafish food

Table 18: List of zebrafish food used at various time points during zebrafish development and their supplier details.

Food	Age of fish	Supplier
Brine Shrimp	5 dpf –12dpf	Special diets services
SDS 100	>12dpf –1 month	Special diets services
SDS 200	>1 month –2 months	Special diets services
SDS 300	>2months –3 months	Special diets services
Topical Breeder mix and SDS 400	Adult fish (≥ 3months)	Special diets services

2.15 Softwares

Table 19: List of softwares used and their application.

Software	Application
Adobe illustrator	Image formatting
Fiji, Imaris and ZEN	Image processing
GraphPad Prism, MS Excel	Data analysis

3. Methods

3.1 Zebrafish maintenance and breeding

All zebrafish husbandry was performed under standard conditions in accordance with institutional (MPG), national and european ethical and animal welfare guidelines. All the strains of zebrafish (wild-type, transgenic and mutant) were maintained in Techniplast fish culture system. The temperature of water was kept between 26-28°C and the temperature of the fishroom was kept between 27-29°C. The zebrafish embryos and larvae upto 5 dpf were kept in egg water in BOD incubator at 28°C and later shifted to the fish culture system. For setting up mating, the male and female were put in breeding tank in the evening and were separated by dividers, in case the eggs were needed at specific time points. Next morning, dividers were removed and the fish would lay eggs within 30 minutes usually. The fertilized eggs which got settled at the bottom of the tank were collected and kept in clean egg water in 10 cm petri dishes.

3.2 Microinjections in zebrafish embryos

3.2.1 Preparing injection plates

The injection plates were prepared by pouring 2% agarose solution (prepared in egg water) in 10 cm petri dishes and putting a mold with lanes on the agarose solution until it solidified. Later the mold was removed and these plates were used for injections.

3.2.2 Preparing injection needles

Using injection needle puller, the injection needles of desired size were prepared from glass capillaries, as per manufacturer's instructions (SUTTER INSTRUMENT).

3.2.3 Injections

At the time of injections, the needle was loaded with ~5 µl of DNA/RNA/morpholino injection mix and the needle was fixed into injection manipulator. The injection pressure conditions were adjusted in the injection pump and the droplet size was calibrated using microscale. The one-cell stage eggs were aligned in the injection plate and were injected with injection mix (in the cell for DNA and in the yolk for RNA/morpholino).

3.3 Larval heart extraction

72 hours post fertilization (hpf) larvae expressing a fluorescent protein (for e.g., GFP) under the control of cardiomyocyte-specific myosin, light chain 7, regulatory (*myl7*) promoter were used for heart extraction, as described previously (Burns and MacRae, 2006), with slight modifications. Approximately 100 larvae were anesthetized and transferred to a 1.5 ml microfuge tube followed by washing them three times with embryo disruption medium (EDM) and finally resuspending in 1.25 ml EDM. Nearly 1 ml EDM containing larvae was drawn into the 19-guage needle and ejected back into the microfuge tube 30 times at the rate of 1 s per syringe motion. Fragmented larvae were passed through 100 µm nylon mesh and the flow-through was collected in a 30-mm polystyrene Petri dish. The microfuge tube, needle, syringe and mesh were washed with additional media that was added to the flow-through. Further, the flow-through was passed through the 40 µm nylon mesh. The 40 µm mesh was then inverted and the retained material was washed off with EDM into a 30 mm petri dish. Intact GFP^+ hearts were identified under fluorescent light and collected in a fresh EDM in order to avoid contamination. The hearts were further collected from the EDM and pooled in a 1.5 ml microfuge tube. Later the hearts were pelleted, the media was removed and the preparations were frozen in dry ice, before storing them at -80°C.

3.4 RNA isolation

3.4.1 RNA extraction using Trizol

A pool of 10-20 zebrafish embryos/larvae of desired developmental stages or 3-4 adult zebrafish hearts (or ventricles) were added to 500 µl of trizol reagent in 1.5 ml tube and homogenized using a homogenizer. The tissue homogenate was vortexed for 30 seconds and incubated at room temperature (RT) for 10 minutes. 100 µl of chloroform was added to the homogenate; the tube was vortexed gently for 2 minutes and incubated at RT for 5 minutes. This was followed by centrifugation for 15 minutes at 13,000 RPM at 4°C. The separated aqueous phase was transferred in a fresh tube and isopropanol was added in 1:1 volume. This solution was then incubated for 1 hour on ice and later centrifuged for 20 minutes at 13,000 RPM at 4°C. The supernatant was removed and pellet was washed with ice-cold 75% ethanol by centrifugation for 8 minutes. After this, the supernatant was removed and the pellet was

air dried for several minutes on bench. The dried pellet was finally resuspended in 25-30 µl of RNase-free water.

3.4.2 RNA extraction with miRNeasy Micro Kit

miRNeasy Micro kit (Qiagen) was used for RNA extraction from Laser microdissected (LMD) samples as well as extracted larval hearts. 700 µl of Qiazol was added to the sample in the tube, vortexed for 1 minute and incubated for 5 minutes at RT. The final sample was loaded on Qiashredder column (Qiagen) and centrifuged at full speed for 2 minutes for homogenization. The flow-through was transferred to fresh tube and 140 µl of chloroform was added to it, followed by shaking the tube vigorously for 15 seconds and incubating the mixture for 3 minutes at RT. Next, the sample was centrifuged for 15 minutes at 12,000 RCF at 4°C. The upper aqueous phase obtained was transferred to new tube and 525 µl of 100% ethanol was added and mixed by pipetting. 700 µl of sample was pipetted into the spin column and centrifuged at 8000 RCF for 30 seconds at RT. The flow-through was discarded and the above-mentioned step was repeated for the remaining sample. Then, 350µl of buffer RWT (prepared with isopropanol) was added to spin column, centrifuged at 8000 RCF for 30 seconds at RT and flow-through was discarded. Further, for each sample 10 µl of DNase I stock solution was added to 70 µl of buffer RDD and was mixed gently by inverting the tube (vortexing was avoided). The obtained DNA mix was pipetted directly onto the column and incubated for 15 minutes at RT. Then 500µl of buffer RWT was added to the column and centrifuged at 8000 RCF for 30 seconds at RT. The flow-through was reapplied to the column and centrifugation was repeated. The flow-through was discarded and 500 µl of buffer RPE (prepared with ethanol) was added to spin column and centrifuged at 8000 RCF for 30 seconds at RT. Then, the flow-though was discarded and 500 µl of 80% ethanol was added to the column and centrifuged at 8000 RCF for 30 seconds at RT**.** The flow-through was discarded and the column was placed on fresh tube. Further, the empty column was centrifuged at full speed for 5 minutes with its lid open. The flow-through was discarded and the column was placed to a fresh collection tube. 20 µl of nuclease-free water was added to the column and incubated for 1 minute, followed by centrifugation at full speed for 1 minute at RT. The centrifugation was repeated with the flow-through and the isolated RNA was stored at -80°C.

3.5 cDNA synthesis

cDNA synthesis from RNA was performed by using Maxima First Strand cDNA Synthesis Kit for RT-qPCR (Thermo Scientific). The reaction mix was made as follows:

Components	Reaction volume
Template RNA	500 ng-1µg
5X reaction mix	4 µl
Maxima enzyme mix	2µl
Nuclease-free water	Upto 20 µl

Table 3.1. Components of reaction mix for cDNA synthesis.

The components were mixed gently and incubated for 10 minutes at 25°C followed by 15 minutes at 50°C. The reaction was terminated by heating at 85°C for 5 minutes. The cDNA obtained was diluted to 200 ng/µl for RT-qPCR and other applications.

3.6 Real-Time quantitative PCR (RT-qPCR)

RT-qPCR was performed to analyze the gene expression levels relative to an endogenous control. RT-qPCR was performed using 2x Maxima SYBR Green qPCR Master Mix (2x DyNAmo color flash, Thermo Scientific) on CFX Connect Real-Time System (Biorad). SYBR Green was used as fluorescent dye for the quantification of PCR products, as it intercalates with dsDNA. The primers used for RT-qPCR are listed in Table 14 in materials section. *rpl13* was used as an internal control. The following reaction mix and reaction conditions were used for RT-qPCR:

Components	Reaction volume
2x Maxima Sybr Green qPCR Master Mix	5 µl
5 µm forward primer	1 µl
5 µm reverse primer	1 µl
cDNA	1 µl
Nuclease free water	2 µl
Total	10 µl

Table 3.2. Components of reaction mix for RT-qPCR.

Step	Temperature	Duration	No. of cycles
Polymerase activation	95°C	2 minutes	1
PCR cycling	95°C	5 seconds	39
	60°C	30 seconds	
HRMA	95°C	5 seconds	1
	65°C	5 seconds	
	95°C	5 seconds	

Table 3.3. Reaction conditions for RT-qPCR.

3.7 cDNA PCR amplification

The PCR reactions were carried out in Eppendorf Mastercycler Pro thermal cyclers. The primers were designed using PerlPrimer software and their specificity was checked with NCBI blast. The PCR amplification was carried out by using Kappa 2G Fast Ready Mix or Phusion HF DNA Polymerase. The following reaction mix was prepared for PCR reactions:

Components (Kappa 2G)	Reaction Volume
2X Kappa 2G Fast Ready Mix	10 µl
10 µM forward primer	1 µl
10 µM reverse primer	1 µl
cDNA	1 µl
Nuclease-free water	7 µl
Total	20 µl

Table 3.4. Components of PCR reaction mix (Kappa 2G polymerase).

Components (Phusion)	Reaction Volume
5X Phusion HF Buffer	4 µl
10 mM dNTPs	0.4 µl
10 µM forward primer	1 µl
10 µM reverse primer	1 µl

DMSO	0.6 µl
Template DNA	1 µl
Phusion DNA Polymerase	0.2 µl
Nuclease-free water	11.8 µl
Total	20 µl

Table 3.5. Components of PCR reaction mix (Phusion polymerase).

The following PCR cycle parameters were used and the reaction was held at 4°C at the end:

Step (Kappa 2G)	Temperature	Duration	No. of cycles
Initial Denaturation	95°C	7 minutes	1
Denaturation	95°C	20 seconds	30-35
Annealing	55-65°C(primer specific T_A)	25 seconds	
Extension	72°C	20 seconds	
Final Extension	72°C	7 minutes	1

Table 3.6. PCR cycler conditions used with Kappa 2G polymerase.

Step (Phusion)	Temperature	Duration	No. of cycles
Initial Denaturation	98°C	30 seconds	1
Denaturation	98°C	10 seconds	25-35
Annealing	45-72°C(primer specific T_A)	30 seconds	
Extension	72°C	30 seconds	
Final Extension	72°C	10 minutes	1

Table 3.7. PCR cycler conditions used with Phusion polymerase.

3.8 PCR product purification

The PCR products were purified using GeneJET PCR purification kit (Thermo Scientific). All the steps of centrifugation in this protocol were carried out at 14000 RPM. 1:1 volume of binding buffer was added to the PCR product and mixed thoroughly. The color of solution was checked and yellow color indicated an optimal pH for DNA binding. Upto 800 µl of

solution was transferred to the purification column and centrifuged for 1 minute. The flow-through was discarded. 700 µl of wash buffer was added to the purification column and centrifuged for 1 minute. Following this, the empty purification column was centrifuged for 1 minute to completely remove any residual wash buffer. Then the purification column was transferred to a clean 1.5 ml microcentrifuge tube and 30 µl of elution buffer was added to the purification column. After 1 minute of incubation, the purification column was centrifuged for 1 minute and the purified DNA obtained was stored at -20°C.

3.9 Agarose Gel Electrophoresis

Large DNA fragments of 5-10kb were resolved on 0.8% agarose gel and small DNA fragments of 0.2-1kb were resolved on 1.5%-2% agarose gel, containing SYBR safe for staining the DNA. The DNA samples along with appropriate ladder were loaded into the wells of the gel and the time duration of electrophoresis depended on the size of DNA to be resolved (mostly 30-40 minutes) at 100-120V. Later the gel was visualized under UV light in a gel doc imager system.

3.10 DNA gel extraction

The DNA gel extraction was performed using GeneJET Gel Extraction kit (Thermo Scientific). All the steps of centrifugation in this protocol were carried out at 14000 RPM. The desired PCR product or digested plasmid was extracted from the agarose gel. The gel slice containing the DNA fragment was excised using a clean scalpel and was transferred to a clean 1.5 ml tube. Further, the gel slice was weighed and 1:1 volume of binding buffer was added to it. This mixture was incubated at 50-60°C until the gel was completely dissolved. During this step, the tube was inverted in between and vortexed in order to make sure that the gel was dissolved. A yellow colored solution was an indication of optimal pH for DNA binding. Then, upto 800 µl of solubilized gel solution was transferred to the purification column and centrifuged for 1 minute. The flow-through was discarded and 700 µl of wash buffer was added to the purification column and centrifuged for 1 minute. Further, the empty purification column was centrifuged for 1 minute to completely remove any residual wash buffer. The purification column was then transferred to a clean 1.5 ml microcentrifuge tube and 30 µl of elution buffer was added to the purification column. After 1 minute of

incubation, the purification column was centrifuged for 1 minute and the purified DNA obtained was stored at -20°C.

3.11 Competent cells preparation

3.11.1 Day 1

Two 15 ml falcons were filled with 3 ml of liquid LB medium. E.coli competent cells from the stock were put in one of the falcons and the other falcon was used as a sterile control. The culture was grown overnight at 37°C.

3.11.2 Day 2

The sterile control was checked for any contamination. Three 500 ml flasks were filled with 200 ml liquid medium each and 0.5 µl-1 ml of the overnight culture. The flasks were then kept on shaker for 3-4 hours at 37°C. The centrifuge was pre-chilled to 4°C, before starting the protocol. The culture was chilled on ice for 20 minutes and was transferred to pre-chilled 50 ml falcons. The bacterial culture was then centrifuged for 10 minutes at 4000 RPM at 4°C. Following this, the supernatent was discarded and the pellet was dried by inverting the falcons on clean tissues. The dried culture was resuspended in 5 ml cold 0.1 M $CaCl_2$ and homogenized by pipetting with 1 ml pipette tips. The homogenate was chilled on ice for 5 minutes, followed by centrifugation for 5 minutes at 4000 RPM at 4°C. All the previous steps were repeated till the pellet was obtained again. The supernatent was discarded and the pellet was dried by inverting the falcons on tissues. 1 ml cold 0.1 M $CaCl_2$, 15% glycerol was added to dried pellet and falcons were kept on ice. The pellet was then resuspended and bacterial culture obtained was aliquoted. 20 µl of suspension was added to 1.5 ml eppendorfs and cells were snapfrozen by quickly placing the eppendorfs on chilled metal tube rack. The eppendorfs were transferred to pre-chilled stockboxes and stored at -80°C.

3.12 Transformation of competent cells

Competent cells stored at -80°C were thawed for 2-3 minutes on ice and 5 µl of vector-insert ligation mix was incubated with competent cells for 20 minutes on ice, followed by heat shock of 45 seconds at 42°C and 2 minutes of incubation on ice. Next, the cells were

incubated in shaker incubator for 1 hour at 37°C. Later, the cells were centrifuged at 11,000 RPM for 2 minutes and the cell pellet was plated on LB-agar plates (resistant to specific antibiotics).

3.13 DNA restriction digestion

The required DNA was digested by using appropriate restriction enzymes, under specific temperature conditions and incubation timings, as mentioned by the manufacturer (NEB). The following reaction mix was prepared for carrying out restriction digestion:

Components	Volume per reaction
10X Buffer	3 µl
DNA	1-3 µg
Restriction enzyme(s)	2U/µl
H20	Upto 30 µl

Table 3.8. Components of reaction mix for DNA restriction digestion.

3.14 Molecular cloning

3.14.1 TA Cloning

TA cloning was performed by using pGEMT Easy Vector system and PCR products were inserted in the pGEMT vector for synthesizing RNA probes for *in situ* hybridization and other cloning purposes. The ligation of vector and PCR products was carried out by preparing the following ligation mix:

Components	Reaction Volume
2X reaction buffer	5 µl
pGEMT Easy vector	1 µl
PCR product	as required
T4 DNA ligase	1 µl
Water	Upto 10 µl

Table 3.9. Components of reaction mix for pGEMT Easy cloning.

The reaction mix was mixed by pipetting and incubated for 1 hour at RT or overnight at 4°C. Later, the ligation mix was transformed using competent cells and plated on appropriate antibiotic-resistant plates.

3.14.2 Cold Fusion Cloning

Cold fusion cloning was used for generating overexpression constructs for *mstnb (myl7:mstnb-2A-H2B-EGFP, myl7:mstnb-2A-H2B-mcherry)* and *inhbaa (myl7:inhbaa-2A-H2B-EGFP, myl7:inhbaa-2A-H2B-mcherry)*, as well as constitutively active constructs for *smad2 (myl7:H2B-EGFP-2A-caSmad2), smad3a (myl7:H2B-EGFP-2A-caSmad3a)* and *smad3b (myl7:H2B-EGFP-2A-caSmad3b),* along with the control plasmid *(myl7:H2B-EGFP)*. The vector was linearized by restriction digestion with the required restriction enzymes and was purified by gel elution. All the inserts were PCR amplified with Phusion DNA polymerase by using appropriate primers for cold fusion and were eluted from gel. PCR primers for the inserts were designed to have atleast 15 bases of homology with the neighboring sequence at their 5' ends.

Primer design:

5'-- ~15 bp vector sequence --restriction enzyme site ----18-20 bp gene (insert)-specific sequence

The following reaction mix was prepared for cold fusion reaction:

Components	**Reaction volume**
Linearized vector (10-100 ng/µl) + PCR Insert(s) (20-200 ng/µl)	2.1µl
5x master mix	0.4 µl
Total	2.5 µl

Table 3.10. Components of reaction mix for cold fusion cloning.

The reaction mix was mixed gently by pipetting and was incubated for 5 minutes at RT, followed by 10 minutes incubation on ice. The competent cells were transformed with the cold fusion reaction mix and cultured on LB plates overnight at 37°C.

3.14.3 mRNA overexpression

Full length *mstnb* and *inhbaa* CDS was amplified from cDNA and cloned into pcDNA3.1.
For mRNA synthesis, *mstnb-2A-H2B-mcherry* and *inhbaa-2A-H2B-mcherry* CDS was cloned

into pcDNA3.1. mRNA was synthesized using the mMESSAGE mMACHINE kit and 100 pg of each mRNA was injected into *Tg(ARE:EGFP)* and *Tg(12XSBE:EGFP)* embryos at one-cell stage.

3.15 Plasmid DNA isolation

All the steps were carried out by using GeneJET Plasmid Miniprep Kit (Thermo Scientific) at RT and all the centrifugations were carried out at 14,000 RPM, unless otherwise stated. The bacterial culture was harvested by centrifugation at 8000 RPM for 2 minutes. Then, the supernatant was discarded and 250 µl of resuspension buffer was added to the pellet, followed by the resuspension of pellet by pipetting. Next, 250 µl of lysis buffer was added to the resuspended cell pellet and the tube was inverted 6-8 times. This was followed by adding 350µl of neutralization buffer and inverting the tube 6-8 times. Then, the solution was centrifuged for 5 minutes. The supernatant was transferred to the spin column provided in the kit and was centrifuged for 1 minute. The flow-through was discarded and 500 µl of wash buffer was added to the spin column, followed by centrifugation for 1 minute. The wash buffer was again added and same steps were followed till centrifugation. Later, empty column was centrifuged for 1 minute and the column was transferred to a fresh tube. 50 µl of pre-warmed (at 50°C) elution buffer was added to the column and incubated for 2 minutes on bench. This was followed by centrifugation for 2 minutes and the flow-through was collected and isolated plasmid was stored at -20°C.

3.16 Morpholinos (MO)

The following MOs were purchased from GeneTools (Philomath, OR) and injected at the one-cell stage at the indicated amounts in all experiments described. All doses were determined as optimal by titration (no toxic effects were observed).

MO	**Concentrations injected**
acvr2aa ATG MO	1.5 ng
acvr2ab splice MO	2 ng
acvr2ba ATG MO	1 ng
acvr2bb ATG MO	0.5 ng

control morpholino	concentrations similar to experimental MOs

Table 3.11. The concentrations of MOs used.

3.17 Transcription activator-like effector nucleases (TALEN) cloning

TALENs were designed using TALEN targeter (https://tale-nt.cac.cornell.edu/) and cloning was performed using golden gate TALEN assembly protocol (addgene) as described below:

3.17.1 TALEN cloning Day 1

The TALEN RVD sequence was chosen for the length of 12-21 RVDs in each TALEN arm. The plasmids for RVDs 1-10 (e.g. pNI1, pHD2, pNN3…) and destination vector pFUS_A were picked. Next, the plasmids for RVDs 11 upto N-1 and destination vector pFUS_B#N-1 were picked. Then the golden gate reaction #1 was mixed for each set of vectors separately (1-10 + pFUS_A; 11-(N-1) + pFUS_B(N-1)). The reaction mix included the following:

Components	**Reaction volume**
Each module vector	150 ng
pFUS vector	150 ng
BsaI	1 µl
T-4 DNA ligase	1 µl
10X DNA ligase buffer	2 µl
Water	Upto 20 µl

Table 3.12. Components of reaction mix for Golden gate reaction #1.

The ligation was carried at following conditions: 10X (37°C/ 5 minutes + 16°C/ 10 minutes) + 50°C/ 5 minutes + 80°C/ 5 minutes. This was followed by plasmid-safe nuclease treatment of 1 hour at 37°C (1 µl 10mM ATP + 1 µl plasmid-safe nuclease). Further, the competent cells were transformed with 5 µl of the golden gate reaction#1. Finally, the transformed cells were plated on spectinomycin plates along with 40µl of 20 mg/ml X-gal + 40 µl of 0.1 M IPTG.

3.17.2 TALEN cloning Day 2

4 white colonies were picked from each plate and checked by colony PCR using primers pCR8_F1 and pCR8_R1. The PCR program for colony PCR included annealing at 55°C, extension of 1.75 minutes and cycle 30-35. The correct clones were selected after resolving

PCR products on 1% agarose gel. The correct clones had a band around expected size which was 1.2 kb for vectors with 10 repeats, smearing and a ladder of bands starting at 200 bp and every 100 bp upto 500 bp. The positive clones were kept for overnight cultures at 37°C.

3.17.3 TALEN cloning Day 3

The plasmids (pFUS_A with first 10 repeats cloned (A) and pFUS_B with 11-(N-1) repeats cloned (B)) were isolated by performing miniprep with GeneJET Plasmid Miniprep Kit and sent for sequencing with primers pCR8_F1 and pCR8_R1 to confirm that the clones picked were correct. Golden gate reaction#2 was carried out for each TALEN arm separately. The reaction included the following:

Component	Reaction volume
Vector A and B	150 ng of each
Respective pLR vector	150 ng
Destination vector (pTAL 1, 2, 3 or 4)	75 ng
Esp3I	1 µl
T-4 DNA ligase	1 µl
10X DNA ligase buffer	2 µl
Water	20 µl

Table 3.13. Components of reaction mix for Golden gate reaction #2.

The ligation was carried out at 10X (37°C/ 5 minutes + 16°C/10 minutes) + 37°C/ 15 minutes + 80°C/ 5 minutes. Further, the competent cells were transformed with 5 µl of this ligation reaction. Next, the transformed cells were plated on ampicillin plates with X-gal and IPTG.

3.17.4 TALEN cloning Day 4

4 white colonies were picked from each plate and checked by colony PCR using primers TAL_F1 and TAL_R2. The PCR program for colony PCR included annealing at 55°C, extension for 3 minutes and 30-35X cycle. Further, the correct clones were selected after resolving PCR products on 1% agarose gel. The correct clones had a smear and the 'ladder' effect.

3.17.5 TALEN cloning Day 5

pTal vectors containing full-length TALEN were isolated by performing miniprep plasmid isolation protocol with GeneJET Plasmid Miniprep Kit, as described before.

3.17.6 TALEN vector linearization and purification

The TALEN vectors for both arms were linearized with NotI enzyme for 3 hours at 37°C, using the following reaction mix:

Components	Reaction volume
Plasmid	5 µg
NEBuffer 3.1	3 µl
BSA (10X)	3 µl
NotI enzyme	1 µl
Water	Upto 30 µl

Table 3.14. Components of reaction mix for TALEN vector restriction digestion.

The linearized and unlinearized vectors were resolved on 1% agarose gel to check whether linearization worked and the linearized vector was isolated by using GeneJET Gel Extraction Kit, as described before.

3.17.7 TALEN mRNA synthesis and RNA cleanup

TALEN mRNA was synthesized from linearized TALEN vectors with mMessage mMachine SP6 transcription kit (Ambion). The reaction mix was prepared as follows:

Components	Reaction volume
2X NTP/CAP	10 µl
10X reaction buffer	2 µl
Linear template DNA	1 µg
Enzyme mix	2 µl
Nuclease-free water	Upto 20 µl

Table 3.15. Components of reaction mix for TALEN mRNA synthesis.

The reaction mix was mixed thoroughly and incubated at 37°C for 2 hours. Later, 1 µl of TURBO DNase was added, mixed well and incubated for 15 minutes at 37°C.

The TALEN mRNA was column purified by using RNA Clean & Concentrator-5 Kit (Zymo Research), using the following protocol:

All the centrifugation steps were performed at 16,000 RCF at RT. 2 volumes of RNA binding buffer and 100% ethanol were added to the sample and mixed. Then the mixture was transferred to the spin column and centrifuged for 1 minute. The flow-through was discarded and 400 µl of RNA Prep buffer was added to the column, followed by centrifugation for 1 minute. Later, 700 µl of 80% ethanol was added to the column, centrifuged for 1 minute and the flow through was discarded. This step was repeated with 400 µl of ethanol and then, empty column was centrifuged for 1 minute. Finally the empty column was centrifuged for 1 minute and transferred to a fresh tube. 30 µl of nuclease-free water was added to the column and incubated for 2 minutes on bench. Then the column was centrifuged for 2 minutes and the flow-through was added again to the column and centrifuged for another 2 minutes. The RNA thus obtained was stored at -80°C.

3.18 DNA/RNA concentration measurements

The concentration of DNA or RNA was measured by using the Nanodrop ND-2000 spectrophotometer, by putting 1 µl of sample on the optical pedestal. The absorption at 260 nm was measured and the concentration of the sample was calculated by the program according to the Lambert-Beer law.

3.19 Genotyping

3.19.1 High Resolution Melt Analysis (HRMA)

For genotyping, genomic DNA was extracted and PCR was performed on the same, by using primers flanking the region of mutation. HRMA was performed on those PCR products, in order to distinguish different genotypes based on melting temperatures. The following reaction mix and reaction conditions were used for PCR and HRMA:

Components	**Reaction volume**
2x Maxima Sybr Green qPCR Master Mix	5 µl
10 µm forward primer	1 µl

10 µm reverse primer	1 µl
genomic DNA	1 µl
Nuclease free water	2 µl
Total	10 µl

Table 3.16. Components of reaction mix for PCR and HRMA.

Step	Temperature	Duration	No. of cycles
Polymerase activation	95°C	10 minutes	1
PCR cycling	95°C	10 seconds	30-35
	60°C	15 seconds	
HRMA	95°C	15 seconds	1
	55°C	15 seconds	
	95°C	15 seconds	

Table 3.17. PCR Reaction conditions for HRMA.

3.19.2 Genotyping by PCR and Restriction Fragment Length Polymorphism (RFLP)

For genotyping the immunostained larvae obtained by crossing different transgenic backgrounds, PCR was performed on genomic DNA by using the primers listed in Table 14 in materials section. *erbb2*^{st61} mutants were genotyped (Lyons et al., 2005) by using PCR-based RFLP analysis. PCR products obtained from genomic DNA samples (using primer pairs listed Table 14 in materials section) were digested with BsrGI, resulting in a genotype-specific DNA band pattern.

3.19.3 DNA sequencing

DNA plasmid or PCR product sequencing was performed by the Seqlab and GATC companies.

3.20 Cryoinjury and heart extraction

Procedures involving animals were approved by the veterinary department of the Regional Board of Darmstadt. Cryoinjury was performed on adult zebrafish hearts (4-6 months post fertilization (mpf)), as described previously (Chablais et al., 2011). The main equipment required for cryoinjury was cryoprobe which was about 0.8 mm in diameter, apart from this liquid nitrogen and sponge were used. The adult zebrafish was anaesthetized in 0.016% tricaine until the gills of the fish stopped moving. Meanwhile the tip of cryoprobe was kept to cool in liquid nitrogen. The fish was placed on a wet sponge with their ventral side up. Using a dissection scissor, a cut was made through the skin and muscles over the pericardial cavity and the silver colored epithelial layer of the hypodermis was teared gently using forceps. The beating ventricle was visible after opening the epithelial layer with the help of forceps. The tip of cryoprobe was touched at the apex of ventricle till it thawed, which took approximately 10 seconds. After removing the cryoprobe, the fish was transferred to fresh water and stimulated by squirting water into the gills with a plastic pipette until it started to breathe by itself. Later at the required time points, the fish was anaesthetized in 0.016% tricaine, the heart was extracted and rinsed with PBS before fixing.

3.21 Tissue fixation

Zebrafish embryos/larvae or adult zebrafish hearts were fixed in 4% PFA overnight at 4 °C. To prepare 1L of 4% PFA, 40 g of paraformaldehyde powder was added to 1L of 1X PBS solution. Further, 2 tablets of NaOH were added and the solution was kept on a stir plate in a ventilated hood at 65-68°C until the powder dissolved in approximately 30 minutes. Next, the pH was adjusted to 7.4 with 1N HCL. The solution thus obtained was aliquoted and stored in -20°C for several months or 4°C for few days.

3.22 Sample preparation for sectioning adult zebrafish hearts

3.22.1 Paraffin embedding

The hearts of adult zebrafish were extracted, washed with PBS and fixed with 4% PFA overnight at 4°C in microfuge tubes. Next day, the hearts were washed with PBS twice for 10 minutes at RT with slow agitation. This was followed by washing in 30% ethanol/H_20 for 10

minutes, 50% ethanol/H_20 for 10 minutes and 70% ethanol/H_20 twice for 10 minutes each. Further, the hearts were incubated in fresh 70% ethanol/PBS at 4°C overnight. The next day, the hearts were washed at RT in 80% ethanol/H_20 for 10 minutes, 90% ethanol/H_20 for 10 minutes, 95% ethanol/H_20 for 10 minutes, and 100% ethanol/H_20 thrice for 10 minutes each. The hearts were shifted to a plastic cassette and placed in xylene twice for 20 minutes in the hood. The cassette was transferred to 50% xylene/50% paraffin at 65°C for an hour, followed by incubation in paraffin for 2-3 hours at 65°C and later incubated in fresh paraffin for overnight at 65°C. Next day, the hearts were mounted in paraffin blocks and sectioned according to the desired section thickness as per the requirement of the assay.

3.22.2 Embedding for cryosectioning

The hearts of adult zebrafish were extracted, washed with PBS and fixed with 4% PFA overnight at 4°C in microfuge tubes. Next day, the hearts were washed with PBS twice for 10 minutes at RT with slow agitation. Then the hearts were shifted to 10% sucrose for 1-2 hours at 4°C and later moved to 30% sucrose till the time the hearts sank to the bottom of the tube. Then the hearts were mounted in OCT solution in the desired orientation and were snap frozen on dry ice. Finally, the mounted hearts were stored at -80°C, till the time they were cryosectioned.

3.23 Laser microdissection (LMD)

LMD (LMD-6000, Leica) was performed, on adult zebrafish heart cryosections, as per manufacturer's instructions to dissect the wall and trabecular tissues separately for RNA extraction. RNA was extracted from LMD samples using miRNeasy Micro Kit (Qiagen), as described before.

3.24 Microarray expression profiling

Total RNA was isolated from ~6 mpf sham operated and cryoinjured hearts 4 dpci (n=12 hearts each) using Trizol (Sigma). Dual color cDNA labeling and hybridization was performed by *MOgene* (commercial service) using the Agilent Zebrafish (V3) 4x44K platform. Microarray raw and normalized data has been submitted to NCBI-GEO under the accession number GSE89259.

3.25 Acid Fuschin Orange-G (AFOG) staining

The AFOG staining protocol was followed according to the manufacturer's instructions (Gennova) with slight modifications. The paraffin sections of adult zebrafish hearts were deparaffinized and rehydrated by putting the slides in xylene twice for 10 minutes each, followed by putting them in 100% ethanol twice for 2 minutes, 70% ethanol for 2 minutes, 30% ethanol for 2 minutes and distilled water twice for 2 minutes. The sections were fixed in Bouin's solution overnight in the fume hood or 2 hours at 60°C, followed by 1 hour incubation at RT. Further, the sections were rinsed under flowing tap water for 10 minutes. Few drops of reagent C (phosphomolybdic acid solution) were poured on the sections, left for 5 minutes and washed with distilled water. Later, few drops of reagent D (AFOG solution) were poured on the sections, left for 5 minutes and washed with distilled water. Finally the sections were dehydrated in increasing concentration of ethanol, cleared in xylene and mounted with entellan for imaging.

3.26 Hematoxylin and Eosin (H&E) staining

The staining was performed on adult zebrafish heart cryosections. The sections were kept at RT for atleast an hour before starting the staining. The slides were kept in hematoxylin solution for 10 minutes. After this, slides were kept under running tap water for approximately 2 minutes, until the sections became blue and then moved to distilled water for 1-2 minutes, until the water that comes from sections became clear. Further on, the slides were kept in eosin for 6 minutes. Then the slides were dipped in 100% ethanol twice and kept in xylene till mounting. Finally, the sections were mounted in entellan and imaged.

3.27 *in situ* hybridization

3.27.1 RNA probe synthesis

The CDS of gene of interest was amplified by performing PCR with appropriate primer pairs and the PCR product was purified by gel elution. The purified PCR product was cloned in pGem-T Easy vector. Correct clones were identified by sequencing and aligning with the available ensembl sequences. The vector was linearized by using appropriate restriction enzymes and purified by gel elution to obtain template DNA for synthesizing the antisense

RNA probe. The following reaction mix was prepared for RNA probe synthesis and was incubated for 2 hours at 37°C:

Components	**Volume per reaction**
Template DNA	5 µl
5X Transcription buffer	2 µl
DTT (0.1 M)	1 µl
DIG-RNA labeling mix (10X)	1 µl
RNAsein (40 U μl^{-1})	0.5 µl
T7 or SP6 RNA Polymerase (20 U μl^{-1})	0.5 µl
Total	10 µl

Table 3.18. Components of reaction mix for RNA probe synthesis.

Later, 2 µl of RNase-free DNase was added to the reaction mix and incubated for 30 minutes at 37°C. The probe synthesis reaction was stopped and RNA probe was column-purified and eluted in 30 µl of nuclease-free water using RNA Clean and Concentrator-5 kit, as described before. The eluted RNA probe was diluted in hybridization solution at 10X concentration and stored at -20°C.

3.27.2 *in situ* Hybridization Day 1: Pre-treatment and hybridization

- ✓ All the steps were performed at RT, unless otherwise stated.
- ✓ All the reagents and slide containers used were RNase-free.
- ✓ Freshly prepared 4% PFA in DEPC-PBS water was used.
- ✓ Slide containers were filled with prehyb solution and placed in 65°C incubator to warm before starting the protocol.
- ✓ Cryosections of 12 µm thickness were used for performing *in situ* hybridization.

in situ hybridization was performed as previously described (Bae et al., 2009), with slight modifications. The slides were kept at RT for 30 minutes and dried at 50°C for 15 minutes. Then, the sections were fixed in 4% PFA in DEPC-PBS for 20 minutes. Next, the sections were washed two times with DEPC-PBS for 5 minutes each. This was followed by treating the sections with 5 µg/ml Proteinase-K (Roche) at RT for 15 minutes. Then the sections were

washed with DEPC-PBS for 5 minutes. To stop Proteinase-K reaction, the sections were fixed in 4% PFA in DEPC-PBS for 15 minutes and then quickly rinsed in DEPC-water.

Acetylation: For 200mL 0.1M RNase-free triethanolamine-HCl pH 8.0, 500 µL acetic anhydride was added with constant stirring right before using. It was stirred for 1-2 minutes until "beading" disappeared, and then slides were put in for 10 min with stirring. Later, the slides were washed in DEPC-PBS for 5 minutes.

Prehybridization: Prehybridization was performed for 1-4 hours at 70°C in hybridization solution. Meanwhile, *in situ* hybridization box containing 50% formamide/5X SSC was kept in the 70°C incubator to pre-warm.

Hybridization: the hybridization solution was replaced with 1 ng/µl preheated probes (diluted in unused hybridization solution) and incubated overnight at 70°C.

3.27.3 *in situ* Hybridization Day 2: Washing and antibody binding

- ✓ Before starting the Day 2 of the protocol, all the solutions were kept in coplin jars in incubators with required temperatures.
- ✓ It was not necessary to use RNase-free solutions from Day 2 onwards.

The slides were transferred to coplin jars and washed with 2X SSC for 15 minutes at 65°C. Then the slides were washed with 2X SSC for 5 minutes at RT, followed by treatment with 10 µg/ml RNase A and 1 U/ml RNase T1 in 2X SSC for 30-45 minutes at 37°C (for preparing, 200 µl of 10 mg/ml stock of RNase A and 2 µl of 100 U/ml RNase T1 were added in 200 ml 2X SSC, and stirred to mix well). Next, the slides were washed two times with 2X SSC for 5 minutes each at RT, two times with 0.2X SSC for 30 minutes each at 65°C, 0.2X SSC for 2 minutes at RT and two times with PBT for 20 minutes each at RT. Blocking was performed in blocking buffer (PBT+10% inactivated sheep serum) for 1 hour at RT in an antibody humidity chamber. The blocking buffer was replaced with anti-digoxygenin antibody (diluted 1:2000 in blocking buffer) and incubated overnight at 4°C.

3.27.4 *in situ* Hybridization Day 3: Antibody visualization of digoxygenin

The slides were washed three times with PBT for 20-30 minutes each at RT. Afterwards, the slides were washed two times with Alkaline Phosphatase buffer for 5 minutes each at RT. 1 µl of NBT and 3.5µl of BCIP were added on slides for every 1 ml of Alkaline Phosphatase buffer and developed in dark for 2-20 hours, depending on the abundance of the RNA.

NBT/BCIP reaction mixture was replaced every 24 hours with fresh reaction mixture and slides were allowed to develop for around 3 days for weaker probes. Once the signal was observed, slides were washed twice in PBS at RT, to remove the substrates.

3.27.5 *in situ* Hybridization Day 4: Washing and mounting

The slides were fixed in 4% PFA/PBS for 15 minutes at RT, followed by rinsing three times with water. The sections were then incubated in 30% ethanol for 5 minutes, 70% ethanol for 5 minutes, 70% ethanol for 5 minutes and two times in 95% ethanol for 5 minutes each and two times in 100% ethanol for 5 minutes each. Later the sections were incubated three times in xylene for 5 minutes each and mounted in entellan.

3.27.6 *in situ* Hybridization: Imaging

Bright field images of stained sections were obtained with stereomicroscopes (SMZ25, Nikon and stereodiscovery V8, Zeiss).

3.28 Whole mount Immunohistochemistry (IHC) and EdU labeling on larvae

3.28.1 EdU Incubation

1 mM EdU was used to incubate embryos from 48 hpf to 72 hpf and larvae from 96 hpf to 120 hpf. Later, the larvae were transferred to fresh egg water for 10-15 minutes and rinsed two times in PBS. Further, the larvae were fixed in 4% PFA overnight at 4°C and used for staining and imaging.

3.28.2 Whole mounting IHC and EdU labeling

The PFA-fixed larvae were washed three times with PBT (PBS+0.1% Tween-20) for 10 minutes each, followed by incubation in permeabilization buffer for 3 hours at RT. This was followed by blocking the larvae in blocking buffer-I for atleast 1 hour at RT. After blocking, the larvae were incubated with primary antibody (diluted in blocking buffer-I) overnight at 4°C. Next day, the larvae were washed three times with PBT for 10 minutes each and incubated in secondary antibody (diluted 1:500 in PBT) for 2-3 hours at RT. Then, the larvae were washed three times with PBT for 10 minutes each. This was followed by EdU labeling by incubating the larvae in Click IT reaction mix for 30 minutes at RT in the dark. The stained larvae were washed three times with PBT for 10 minutes each. Further, the larvae

were incubated in DAPI (diluted 1:3000 in PBT) and finally washed three times with PBT for 5 minutes each. The stained larvae were mounted in 1.5% low melting agarose and imaged.

Primary antibody	Dilution used	Tissue/cell-type stained
DsRed	1:300	Cardiomyocytes
GFP	1:300	Cardiomyocytes overexpressing *mstnb, inhbaa, ca smad2, ca smad3a, ca smad3b*
pSmad3	1:300	Cells undergoing phosphorylation of Smad3

Table 3.19. Details of primary antibodies used in whole mount IHC.

3.29 IHC and EdU labeling on adult heart sections

All the stainings were performed on 12 µm thick cryosections. The antibody specific staining protocols are described below:

3.29.1 PCNA/DsRed, pSmad3/MF-20, N2.261/DsRed IHC

The slides were dried for atleast one hour at RT and boundaries were drawn around sections with a hydrophobic pen. The sections were fixed in 4% PFA for 30 minutes at RT. Meanwhile, water bath was switched on at 95°C and sodium citrate buffer was kept in water bath in coplin jar. The slides were rinsed in PBS and transferred to coplin jar containing citrate buffer. Sodium citrate antigen retrival was performed for 20 minutes. Then, the slides were transferred in PBS for 10 minutes on ice, followed by washing in PBS two times for 5 minutes each at RT. Later, permeabilization was carried out in 0.5% Triton-X for 15 minutes at RT. This was followed by blocking in blocking buffer-II for 1-2 hours at RT. Afterwards, the blocking buffer-II was replaced by primary antibody (diluted in blocking buffer II) and incubated overnight at 4°C. Next day, the slides were washed with PBT four times for 30 minutes each at RT. Then, the slides were incubated in secondary antibody (diluted 1:500 in blocking buffer II) overnight at 4°C or 2-3 hours at RT. This was followed by washing with PBT four times for 30 minutes each at RT. DAPI (diluted 1:3000 in PBT) staining was performed for 10 minutes at RT. Finally, the sections were mounted in mowiol and imaged.

Primary antibody	Dilution used	Tissue/cell-type stained
PCNA	1:200	Cells in S-phase of mitosis
pSmad3	1:200	Cells undergoing phosphorylation of Smad3
MF-20	1:500	Cardiomyocytes
N2.261	1:50	Dedifferentiated cardiomyocytes
DsRed	1:500	Cardiomyocytes

Table 3.20. Details of primary antibodies used in IHC on sections-I.

3.29.2 Raldh2/DsRed, Fibronectin/DsRed, Fibronectin/GFP IHC

The slides were dried for atleast one hour at RT and boundaries were drawn around sections with a hydrophobic pen. The sections were fixed in 4% PFA for 15 minutes at RT. This was followed by washing in PBTx (PBS+0.1%Triton-X) three times for 5 minutes each. Then, blocking was performed with blocking buffer-II for one hour at RT. Later, the blocking buffer-II was replaced by primary antibody (diluted in blocking buffer-II) and incubated overnight at 4°C. Next day, the slides were washed with PBTx four times for 20 minutes each. Then, slides were incubated in secondary antibody (diluted 1:500 in blocking buffer-II) overnight at 4°C or 2-3 hours at RT. This was followed by washing with PBTx four times for 20 minutes each. DAPI (diluted 1:3000 in PBT) staining was performed for 10 minutes at RT. The sections were mounted in mowiol and imaged.

Primary antibody	Dilution used	Tissue/cell-type stained
Aldh1a2 (Raldh2)	1:300	Cells expressing Raldh2
Fibronectin	1:300	Cells expressing Fibronectin

Table 3.21. Details of primary antibodies used in IHC on slides-II.

3.29.3 DsRed/EdU IHC

a) EdU incorporation

Adult fish were anaesthetized with 0.016% tricaine and 200 µg of EdU was injected intraperitoneally in each fish, with the total injection volume not more than 10 µl. After

injection, the fish were transferred to fresh water for recovery and were let to swim for 3 days. After 3 days of EdU incubation, the hearts were extracted, fixed overnight in 4% PFA at 4°C and sectioned for staining purposes.

b) IHC and EdU labeling

The slides were dried for atleast one hour at RT and boundaries were drawn around sections with a hydrophobic pen. The sections were fixed in 4% PFA for 15 minutes at RT. The slides were rinsed with PBS and permeabilized with 0.5% Triton-X for 20 minutes at RT. This was followed by blocking in blocking buffer II for one hour at RT. The blocking buffer-II was replaced by primary antibody (diluted in blocking buffer-II) and incubated overnight at 4°C. Next day, slides were washed with PBT three times for 10 minutes each. Then, the sections were incubated in secondary antibody (1:500 diluted in blocking buffer-II) overnight at 4°C or 2-3 hours at RT. Later, washing was performed with PBT three times for 10 minutes. This was followed by EdU labeling by incubating the sections in Click IT reaction mix for 30 minutes at RT in the dark. This was followed by washing with PBT three times for 10 minutes each. Next, DAPI (diluted 1:3000 in PBT) staining was performed for 10 minutes at RT. Finally, the sections were mounted in mowiol and imaged.

3.30 Chemical inhibitor treatments

3.30.1 ErBb2 signaling inhibition

The previously described ErBb2 signaling inhibitor, PD168393 (Calbiochem) (Reischauer et al., 2014) was used to treat the zebrafish larvae. 10 µM PD168393 in DMSO was added to egg water and the larvae were incubated from 86 hpf to 120 hpf. The control untreated larvae were incubated in 1% DMSO in egg water.

3.30.2 TGF-β signaling inhibition

The previously described TGF-β signaling inhibitors, Smad3 phosphorylation inhibitor (SIS3, Calbiochem) (Jinnin et al., 2006) and Activin type 1 receptor inhibitor (SB431542, Calbiochem) (Inman et al., 2002) were used to treat the zebrafish embryos or larvae. The embryos were treated with 3 µM SIS3 and 10 µM SB431542 from 36 hpf to 72 hpf. The larvae were treated with 10 µM PD168393 and 3 µM SIS3 from 84 hpf to 120 hpf. All

inhibitors were dissolved in DMSO and added to egg water. The control untreated fish were incubated in 1% DMSO in egg water.

3.31 Imaging

Confocal microscopy was performed to image fixed & immunostained adult heart sections and larvae, as well as for live imaging the larval hearts. The slides were mounted in mowiol and larvae were mounted in 1.5% low melting agarose (LMA), prior to imaging. Images were obtained as Z-stacks, with optical section thickness of 1 µm for larval hearts and 3 µm for adult heart sections.

Bright field microscopy was performed to obtain images of *in situ* hybridization and histological stained adult heart sections as well as whole mount larvae.

3.32 Image processing and Cell count

Image processing was performed by using ZEN software to obtain maximum intensity projections of adult heart sections from their Z-Stacks. Later, cell counting was performed by using Image J and Imaris softwares. The average of cell count from three representative sections of each heart was used to obtain dot plots for quantification.

Image processing and cell count of immunostained larval hearts was performed by using ZEN software. Cell count was performed on non-overlapping confocal planes of larval hearts. The average of cell count from all the representative optical planes of each heart was used to obtain dot plots for quantification.

3.33 Statistical analysis

GraphPad software was used to perform statistical analysis. Data are represented as mean ± s.e.m. and p-values were calculated by two-tailed Student's t-test (ns: no significant changes observed, *$P \leq 0.05$, **$P \leq 0.01$, ***$P \leq 0.001$, ***$P \leq 0.001$).

4. Results

Note: Parts of this chapter will be included in the article 'Opposite effects of TGF-β ligands on cardiomyocyte proliferation during development and repair' from Dogra, D. et al. (manuscript under revision). All the experiments and results mentioned in this thesis were performed by Deepika Dogra, unless otherwise stated. Parts of the histology experiments were performed in collaboration with Dr. Suchit Ahuja, *in situ* hybridization experiments were performed in collaboration with Dr. Hyun-Teak Kim and Seyed Javad Rasouli has provided the transgenic line *Tg(myl7:nrg2a202-p2a-tdTomato)bns140*. Prof. Dr. Didier Stainier and Dr. Sven Reischauer supervised this project and helped with the experimental design.

4.1 *mstnb* and *inhbaa* exhibit opposite expression response during cardiac regeneration in zebrafish.

To study cardiac regeneration, cryoinjury was performed on zebrafish heart, which is closely associated to mammalian MI as both conditions involve cell death and scarring (Chablais et al., 2011; González-Rosa et al., 2011). In order to determine the genes which are differentially regulated after cryoinjury, microarray was performed on 4 days post sham injured (dpsi) versus 4 days post cryoinjured (dpci) hearts (**Figure 4.1a**). Interestingly, the two TGF-β ligand encoding genes, *mstnb* and *inhbaa* showed opposing expression response after cryoinjury. *mstnb* was found to highly downregulated, whereas *inhbaa* was upregulated at 4 dpci (**Figure 4.1b,** raw data have been deposited in the NCBI-Gene Expression Omnibus Website - GSE89259). Further, to obtain more detailed temporal expression data, I quantified *mstnb* and *inhbaa* expression in sham and cryoinjured ventricles at different time points post injury using RT–qPCR. *mstnb* mRNA level was found to be reduced in the cryoinjured ventricles compared to sham injured ones, as early as 1 hour post cryoinjury (hpci) and remained downregulated throughout the phase of regeneration (Chablais et al., 2011), suggesting that a continuous reduction of *mstnb* expression is important for cardiac regeneration (**Figure 4.2a**). At 60 dpci, *mstnb* mRNA expression in the cryoinjured ventricles became similar to sham injured ventricles (**Figure 4.2a**). On the contrary, *inhbaa* mRNA levels started rising at 0 dpci, followed by a peak of its expression at 4 dpci (**Figure 4.2b**). During later time points, its expression reached similar to the sham levels (**Figure 4.2b**), indicating a principal role for *inhbaa* during the early phase of cardiac regeneration. To complement the temporal expression data, the spatio-temporal expression of *mstnb* and

inhbaa was studied by performing *in situ* hybridization on the sections of uninjured versus regenerating hearts at 4 dpci (**Figure 4.2c-f**; *in situ* hybridization experiments were performed in collaboration with Dr. Hyun-Taek Kim). The expression of *mstnb* was strongest in ventricular wall of uninjured hearts (**Figure 4.2c, c'**), which was reduced below detection levels at 4 dpci (**Figure 4.2d, d'**). The expression of *mstnb* in uninjured adult hearts was further examined by performing RT–qPCR on laser micro dissected (LMD) wall and trabecular tissues from adult zebrafish heart sections, confirming higher *mstnb* expression levels in the ventricular wall over trabecular tissue (**Figure 4.2g**). *tcf21* and *hey2 (*compact wall-specific genes) and *nppa* (trabeculae-specific gene) were used as positive controls for the RT-qPCR experiment (Han et al., 2016; Kikuchi et al., 2011a) (**Figure 4.2g**). Conversely, no expression of *inhbaa* was observed in uninjured ventricles (**Figure 4.2e, e'**), but its expression was prominent proximal to the injury site at 4 dpci (**Figure 4.2f, f'**). Altogether, the expression patterns of these two genes show clear spatio-temporal changes during cardiac regeneration, as assessed by the microarray profiling, RT-qPCR and *in situ* hybridization data. (Certain lines in this section 4.1 have been quoted verbatim from Dogra et al. (manuscript under revision)).

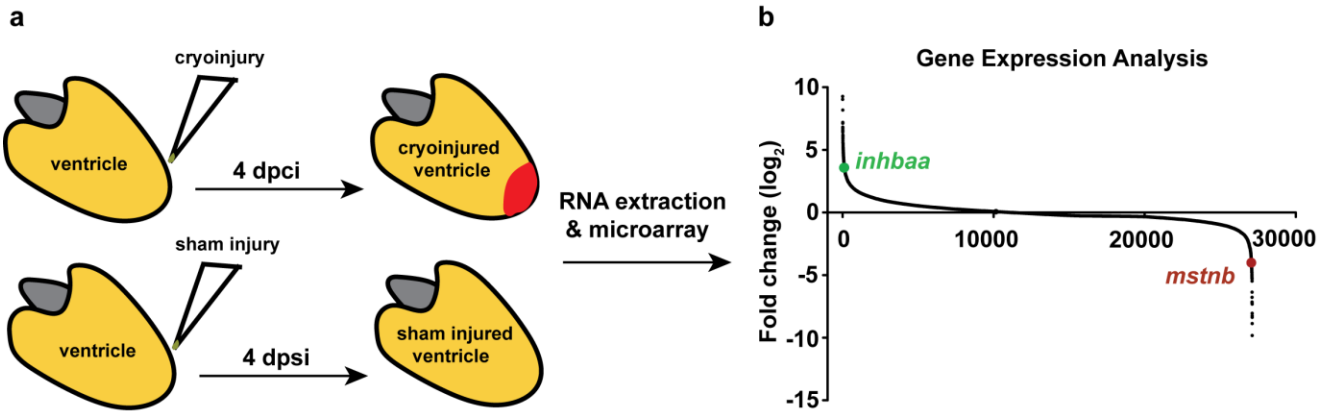

Figure 4.1. Microarray-based gene expression analysis. (**a**) Schematic representation of injury and sample preparation for microarray analysis (n=12 hearts). (**b**) Averaged transcriptional gene expression changes post cryoinjury as assessed by microarray analysis (*inhbaa* and *mstnb* indicated). Figure submitted in Dogra et al. (manuscript under revision).

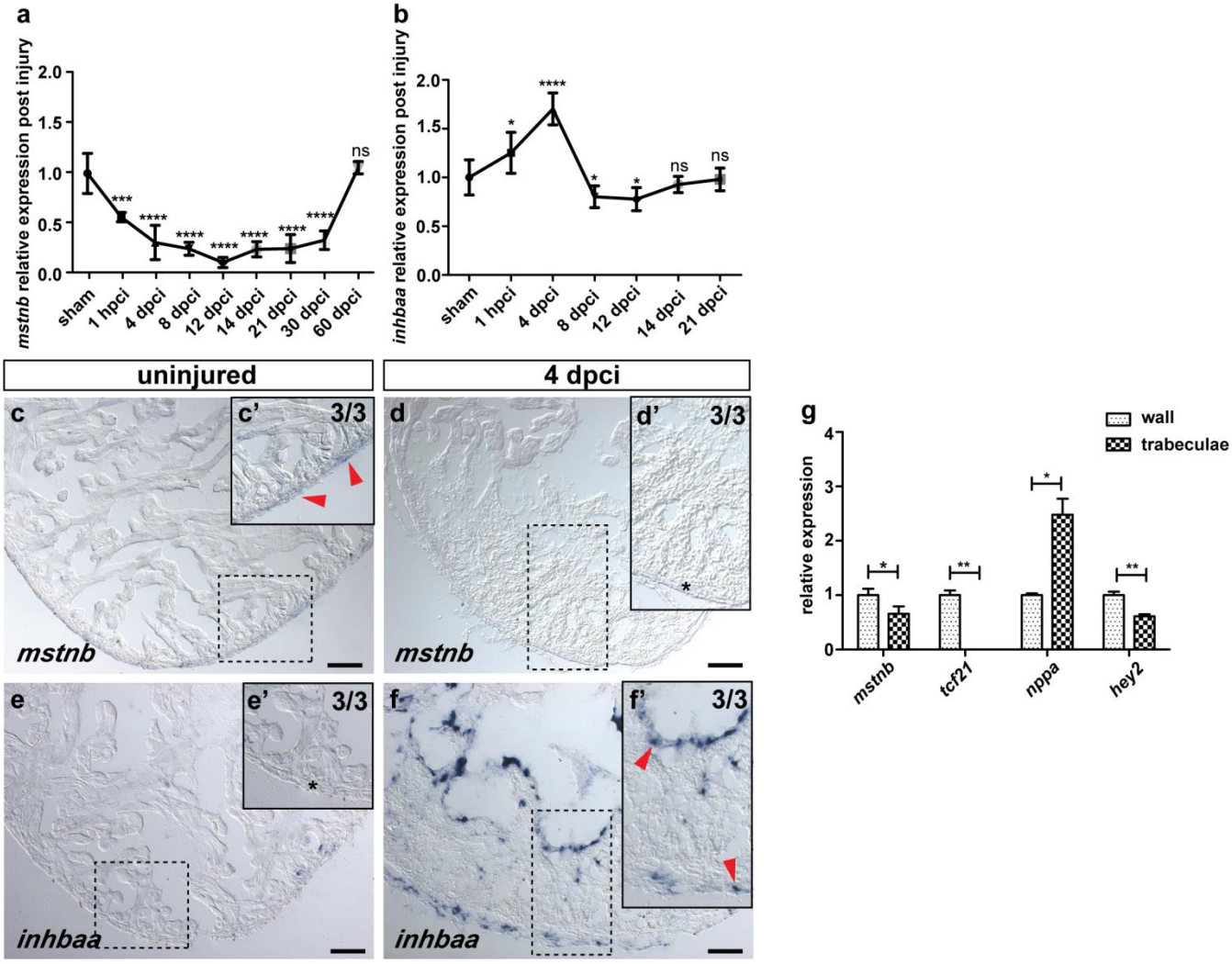

Figure 4.2. *mstnb* and *inhbaa* are inversely regulated during cardiac regeneration in zebrafish. (**a, b**) Temporal RT–qPCR analysis for *mstnb* and *inhbaa* expression post cryoinjury (n=2 x 3 cardiac ventricles assessed as 2 biological and 2 technical replicates for each time point). (**c-f**) *in situ* hybridization for *mstnb* and *inhbaa* expression on uninjured and 4 dpci adult zebrafish heart sections. (**c', d', e', f'**) Higher magnifications of outlined regions in c-f. RNA probe signal is indicated by red arrowheads and the absence of signal is indicated by asterisks. The numerators indicate the number of hearts with a particular pattern of signal and the denominators the total number of hearts analyzed. (**g**) RT–qPCR for *mstnb, tcf21* and *hey2* (wall-specific), *nppa* (trabeculae-specific) expression in LMD wall and trabecular tissues from adult zebrafish heart sections (n=3 hearts assessed in 2 technical replicates). Data are mean ± s.e.m., ns: no significant changes observed, *P ≤ 0.05, **P ≤ 0.01, ***P ≤ 0.001 and ****P ≤ 0.0001, Student's t-test, two-tailed. Scale bars, 50 µm. Figure submitted in Dogra et al. (manuscript under revision). *in situ* hybridization experiments in Figure 4.2c-f were performed in collaboration with Dr. Hyun-Taek Kim.

4.2 *mstnb* and *inhbaa* are the most regulated genes amongst various TGF-β subfamily members during cardiac regeneration.

Next, I performed RT-qPCR to determine the expression of genes encoding various TGF-β/Activin ligands and their receptors during cardiac regeneration. Even at a later time point (6 dpci), *inhbaa* and its paralogs *inhbb* and *tgfb3* were the only significantly induced TGF-β ligand genes, with *inhbaa* showing the most robust upregulation (**Figure 4.3a**). Likewise, only the expression of *mstnb* was seen to be significantly declined at 6 dpci, as compared to other ligand encoding genes (**Figure 4.3a**). Further, amongst the various TGF-β/Activin receptor-encoding genes, only *tgfbr1a*, *tgfbr1b* and *acvr1c* showed a significant increase in expression post cryoinjury, while the expression of other genes remained unchanged (**Figure 4.3b**). (Certain lines in this section 4.2 have been quoted verbatim from Dogra et al. (manuscript under revision)).

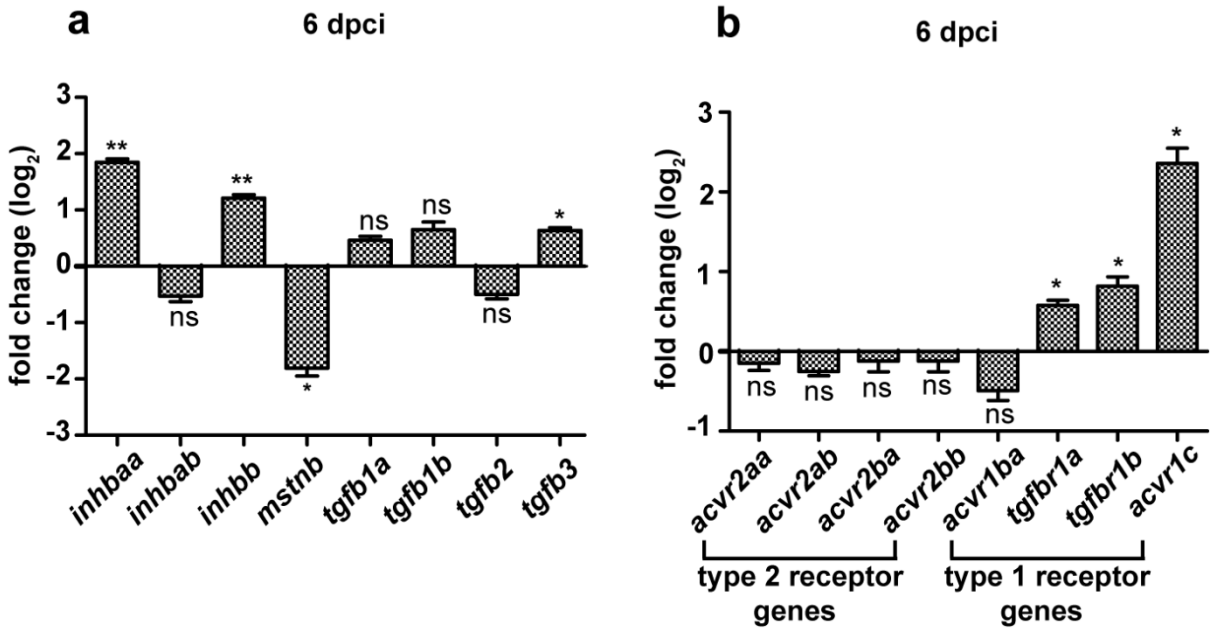

Figure 4.3. Expression analysis of TGF-β genes during cardiac regeneration. (**a**) RT–qPCR for *inhbaa, inhbab, inhbb, mstnb, tgfb1a, tgfb1b, tgfb2,* and *tgfb3* expression at 6 dpci compared to sham injured hearts (n=2 x 3 cardiac ventricles assessed as 2 biological and 2 technical replicates). (**b**) RT–qPCR for *acvr2aa, acvr2ab, acvr2ba, acvr2bb, acvr1ba, tgfbr1a, tgfbr1b* and *acvr1c* expression at 6 dpci compared to sham injured hearts (n=2 x 3 cardiac ventricles assessed as 2 biological and 2 technical replicates). Data are mean ± s.e.m., ns: no significant changes observed, *P ≤ 0.05 and **P ≤ 0.01, Student's t-test, two-tailed. Figure submitted in Dogra et al. (manuscript under revision).

4.3 Generation of *mstnb* GOF and *inhbaa* LOF fish.

Since I observed that the expression of *mstnb* decreases during cardiac regeneration, I next wanted to analyze the effect of sustained *mstnb* expression in regenerating hearts. Thus, a transgenic zebrafish line for cardiomyocyte-specific constitutive overexpression of *mstnb*, *Tg(myl7:mstnb-2A-H2B-EGFP)bns145* (*mstnb* OE hereafter) was generated (**Figure 4.4a**). The plasmid construct for this transgenic line was cloned by using Cold fusion technology (System Biosciences, CA, USA). PCR amplified full length CDS of *mstnb* was fused to self-cleaving 2A peptide along with H2B-EGFP fluorescent reporter, all under the control of myosin, light chain 7, regulatory (*myl7*) promoter. 18 pg of this construct was co-injected with 20 pg Tol2 mRNA into one-cell stage embryos. The founders were outcrossed with *Tg(-0.8myl7:nlsDsRedExpress)hsc4* to generate stable lines, which were used in the experiments (**Figure 4.4b, c**). From the RT-qPCR analysis, *mstnb* transcript levels seem to be highly increased in *mstnb* OE compared to wild-type siblings (**Figure 4.4d**), confirming that *mstnb* is overexpressed in the generated *mstnb* OE transgenic animals.

To determine the role of *inhbaa* in the regenerating hearts, a mutant allele using TALEN-induced mutagenesis was generated. A TALEN targeting the TGF-β propeptide domain was designed (**Figure 4.5a**) and cloned according to Golden Gate Assembly. The TALEN arms targeting *inhbaa* had the following RVDs: NN NG NN NN NG NN NN NI NN NN HD NI NN NG NN and NN HD NI NN NN NG NN HD NI NN HD NI NG NN NG. The TALEN mRNA injections were done in one-cell stage embryos and the activity of TALEN was analyzed by performing HRMA of the PCR products spanning the TALEN-target site in the injected F0 embryos (**Figure 4.6a**). Using HRMA, F1 animals were screened for possible genomic lesions and a 17 bp deletion allele, $inhbaa^{bns37}$ was recovered (**Figure 4.5b, Figure 4.6b**), which is predicted to encode a truncated protein (**Figure 4.5c**). *inhbaa* transcript levels seem to be significantly reduced in $inhbaa^{-/-}$ compared to $inhbaa^{+/+}$, from RT-qPCR analysis (**Figure 4.5d**). (Certain lines in this section 4.3 have been quoted verbatim from Dogra et al. (manuscript under revision)).

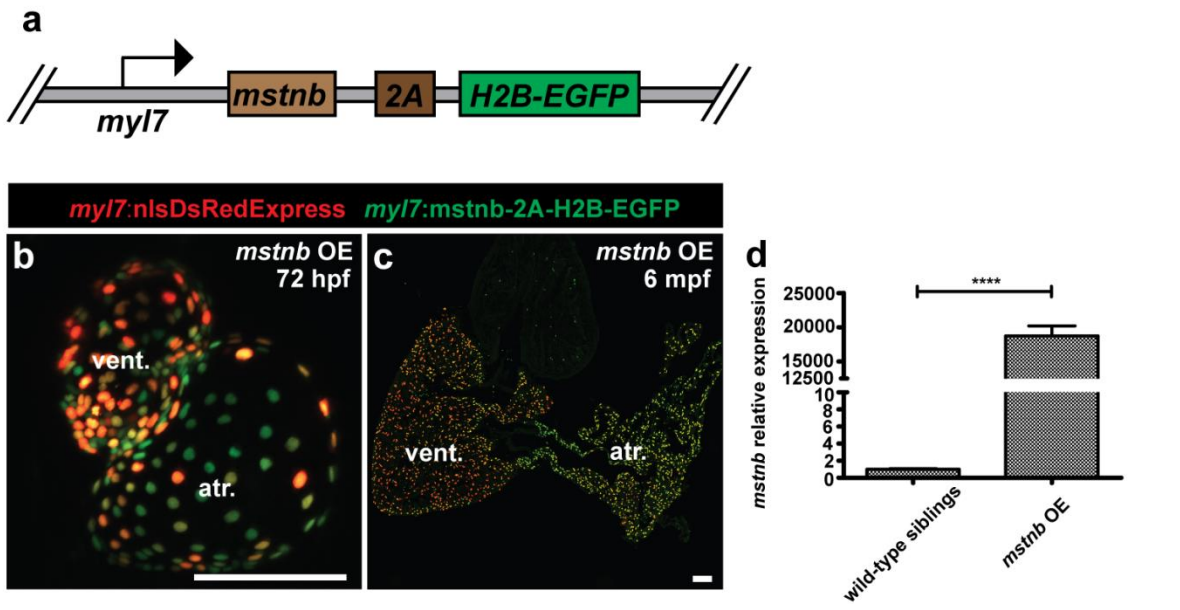

Figure 4.4. Generation and validation of *mstnb* GOF line. (**a**) Schematic of cardiomyocyte-specific *mstnb* OE transgene, *Tg(myl7:mstnb-2A-H2B-EGFP).* (**b**) Heart of 72 hpf *mstnb* OE larva in *Tg(myl7:nlsDsRedExpress)* background (native fluorescence). (**c**) Section of *mstnb* OE adult heart in *Tg(myl7:nlsDsRedExpress)* background, immunostained for DsRed (red) and GFP (green). (**d**) RT–qPCR for *mstnb* expression analysis in wild-type sibling and *mstnb* OE adult hearts (n=2 x 3 cardiac ventricles assessed as 2 biological and 2 technical replicates). Data are mean ± s.e.m., ****P ≤ 0.0001, Student's t-test, two-tailed. Scale bars, 100 µm. hpf, hours post fertilization; mpf, months post fertilization; vent., ventricle; atr., atrium. Figure submitted in Dogra et al. (manuscript under revision).

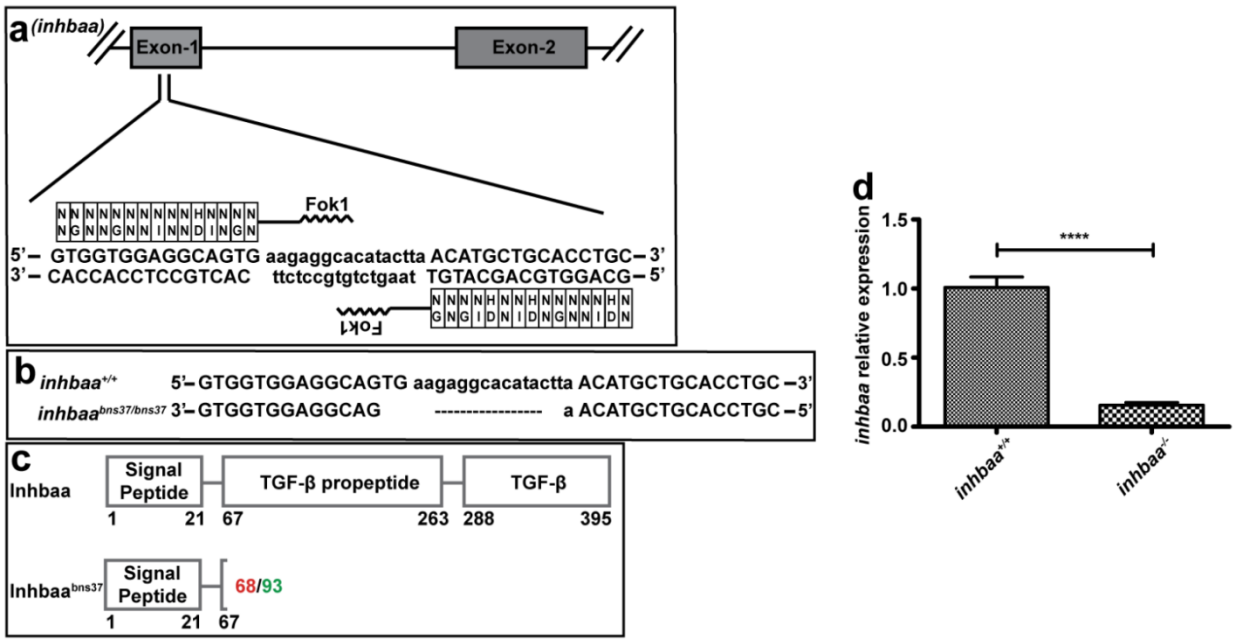

Figure 4.5. Generation and validation of *inhbaa* LOF line. (**a-c**) *inhbaa* TALEN designed to target the TGF-β propeptide domain in exon 1 (**a**), a 17 bp frameshift deletion allele (*inhbaa*^{bns37}) was identified (**b**) and is

predicted to cause the formation of truncated Inhbaa (**c**). Red number indicates the last native amino acid before the frameshift mutation; green number indicates the last amino acid before stop codon. (**d**) RT–qPCR for *inhbaa* expression analysis in *inhbaa*$^{+/+}$ and *inhbaa*$^{-/-}$ adult hearts (n=2 x 3 cardiac ventricles assessed as 2 biological and 2 technical replicates). Data are mean ± s.e.m., ****P ≤ 0.0001, Student's t-test, two-tailed. Figure submitted in Dogra et al. (manuscript under revision).

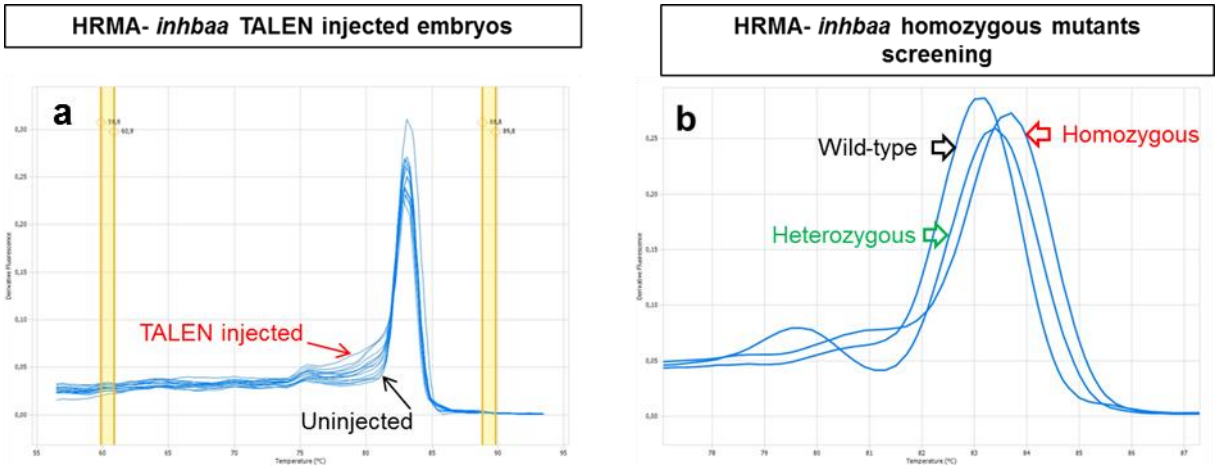

Figure 4.6. HRMA analysis of *inhbaa* TALEN-induced mutagenesis. (**a**) HRMA of PCR products of TALEN targeted region, with *inhbaa* TALEN injected embryos showing an altered melt profile (red arrow) compared to uninjected embryos (black arrow). (**b**) HRMA of PCR products of TALEN targeted region, with *inhbaa* homozygous mutants (carrying 17 bp deletion alleles), heterozygous and wild-type siblings showing different melt profiles.

4.4 *mstnb* GOF and *inhbaa* LOF do not affect cardiac development and growth.

The *mstnb* OE fish were viable and survived to adulthood. Further, the hearts of adult animals were observed, and the gross morphology of adult *mstnb* OE fish and morphology of their hearts, as assessed by histological sections appeared comparable to non-transgenic fish (**Figure 4.7a-b'**). This result indicates that cardiomyocyte-specific *mstnb* overexpression does not affect the development or growth of the zebrafish heart, unlike in mice, where its overexpression has been reported to cause interstitial fibrosis in cardiac muscle with compromised cardiac output (Biesemann et al., 2015).

Similarly, the adult *inhbaa*$^{-/-}$ mutants do not exhibit any gross morphological defects and their hearts appear indistinguishable from wild-type siblings, as assessed by histological sections (**Figure 4.8a-b'**), indicating that *inhbaa* does not play an important role in zebrafish heart

development or growth. (Certain lines in this section 4.4 have been quoted verbatim from Dogra et al. (manuscript under revision)).

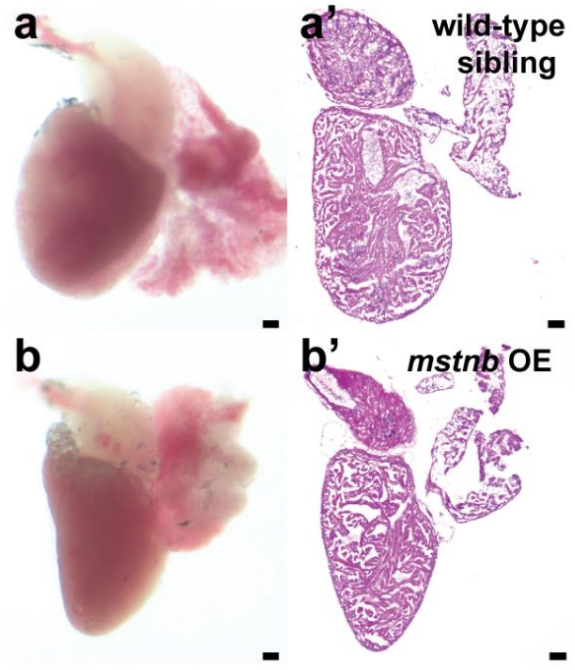

Figure 4.7. *mstnb* GOF does not affect cardiac growth. (**a- b'**) Wild-type sibling and *mstnb* OE adult hearts, and H&E staining of heart sections, with *mstnb* OE hearts showing no apparent abnormalities. Scale bars, 100 µm. Figure submitted in Dogra et al. (manuscript under revision).

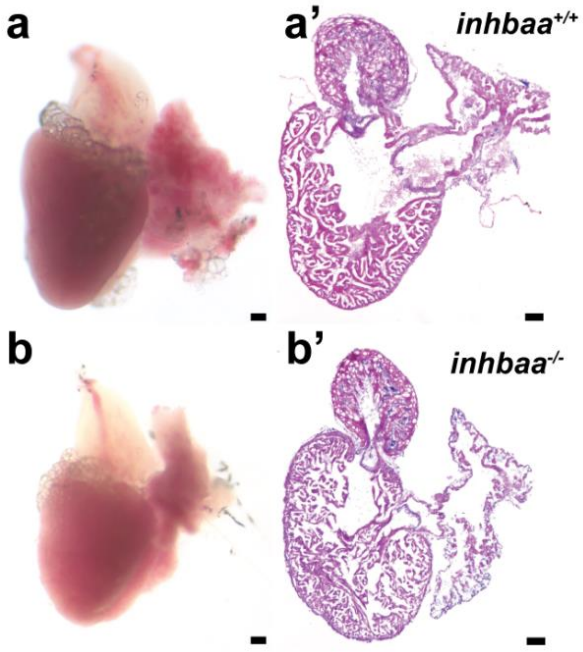

Figure 4.8. *inhbaa* LOF does not affect cardiac growth. (**a-b'**) *inhbaa*$^{+/+}$ and *inhbaa*$^{-/-}$ adult hearts, and H&E staining of heart sections, with *inhbaa*$^{-/-}$ showing no apparent abnormalities. Scale bars, 100 µm. Figure submitted in Dogra et al. (manuscript under revision).

4.5 *mstnb* GOF and *inhbaa* LOF lead to unresolved scarring during cardiac regeneration.

Zebrafish heart responds to cryoinjury with the formation of a transient scar, comprising of fibrin and collagen network, which is progressively replaced by healthy myocardial tissue within two months post cardiac injury (Chablais et al., 2011). Next, I wanted to analyze whether *mstnb* GOF and *inhbaa* LOF cause any possible defect in the process of cardiac regeneration. Thus, *mstnb* OE and *inhbaa*$^{-/-}$ hearts, along with their siblings were cryoinjured and analyzed at 45 dpci for scar clearance. On sampling, the hearts of *mstnb* OE and *inhbaa*$^{-/-}$ exhibited light colored tissue at the injury site indicating unresolved scar, whereas the wild-type hearts appeared regenerated from the surface (**Figure 4.9**). Further, by performing Acid Fuchsin Orange G (AFOG) staining on the sections of injured hearts, I observed that 45 dpci *mstnb* OE and *inhbaa*$^{-/-}$ hearts had unresolved scars, in contrast to wild-type siblings (which had the scars resolved and replaced by new myocardial tissue) (**Figure 4.10**). The *mstnb* OE and *inhbaa*$^{-/-}$ hearts had significant amounts of scarring persisting at the injury area, suggesting that *mstnb* GOF and *inhbaa* LOF negatively affect the scar resolution, thereby leading to incomplete cardiac regeneration. (Certain lines in this section 4.5 have been quoted verbatim from Dogra et al. (manuscript under revision)).

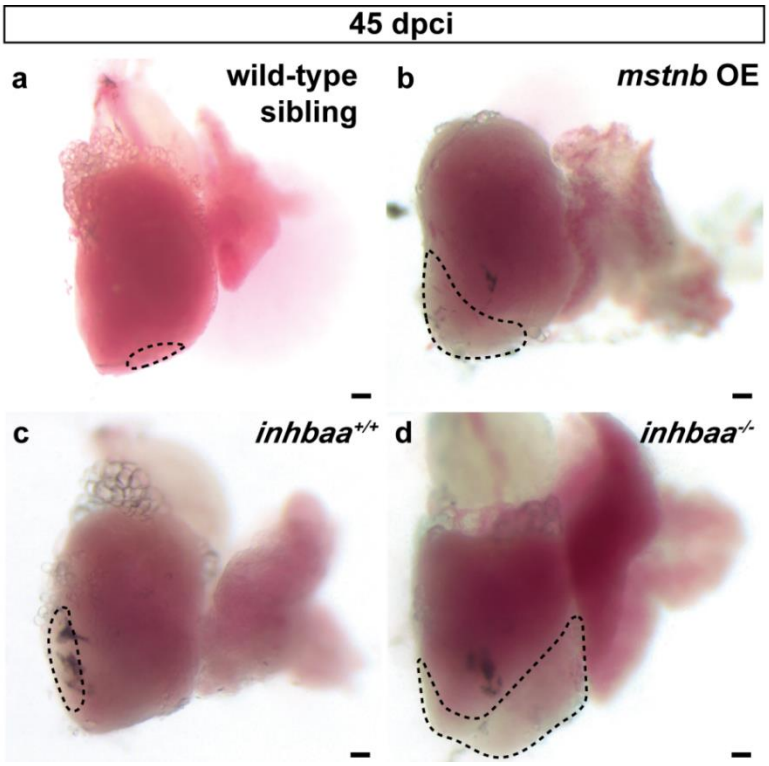

Figure 4.9. *mstnb* OE and *inhbaa*$^{-/-}$ hearts appear non-regenerated at 45 dpci. (**a-d**) Wild-type sibling, *mstnb* OE, *inhbaa*$^{+/+}$ and *inhbaa*$^{-/-}$ cryoinjured hearts at 45 dpci. Dotted regions mark non-regenerated area post cryoinjury. Scale bars, 100 µm.

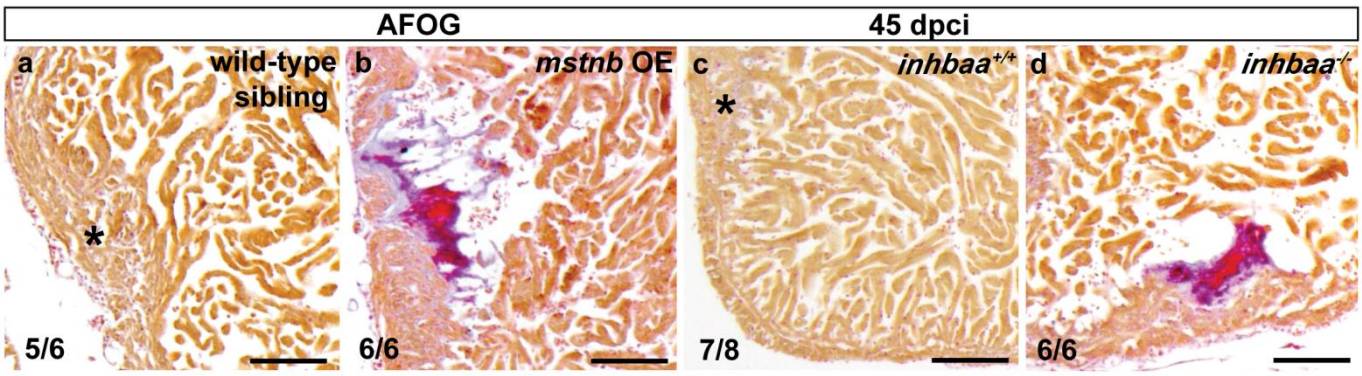

Figure 4.10. *mstnb* GOF and *inhbaa* LOF lead to unresolved scarring after cardiac injury. (**a-d**) AFOG staining of wild-type sibling, *mstnb* OE, *inhbaa*$^{+/+}$ and *inhbaa*$^{-/-}$ cryoinjured heart sections at 45 dpci. Healthy myocardium is stained in orange, fibrin in red and collagen in blue. Asterisks indicate the regions of resolved scars. The numerators indicate the number of hearts with a particular pattern of scarring and the denominators the total number of hearts analyzed. Scale bars, 100 µm. Figure submitted in Dogra et al. (manuscript under revision).

4.6 *mstnb* GOF and *inhbaa* LOF do not affect cardiomyocyte dedifferentiation during cardiac regeneration.

As reported in previous studies, post cardiac injury the cardiomyocytes in the proximity of injured area undergo dedifferentiation, re-enter the cell cycle, and proliferate to replace the injured myocardial issue (Jopling et al., 2010). Since, I observed that *mstnb* OE and *inhbaa*$^{-/-}$ hearts fail to resolve the scar, I wanted to check whether the non-regenerated scar phenotype is associated with any kind of disturbance in the cardiomyocyte dedifferentiation occuring during the early phase of regeneration. Thus, to determine the effect of *mstnb* GOF and *inhbaa* LOF on cardiomyocyte dedifferentiation, the expression of embryonic cardiac myosin heavy chain (embCMHC), a marker of dedifferentiated cardiomyocytes (Sallin et al., 2015), was analyzed by performing immunostaining on 6 dpci hearts sections of *Tg(myl7:nlsDsRedExpress)* fish for embCMHC and DsRed. No obvious difference in embCMHC expression was observed in *mstnb* OE or *inhbaa*$^{-/-}$ hearts compared to wild-type siblings after cryoinjury (**Figure 4.11**), which indicates that cardiomyocyte dedifferentiation is not disturbed by *mstnb* GOF or *inhbaa* LOF after cardiac injury. (Certain lines in this section 4.6 have been quoted verbatim from Dogra et al. (manuscript under revision)).

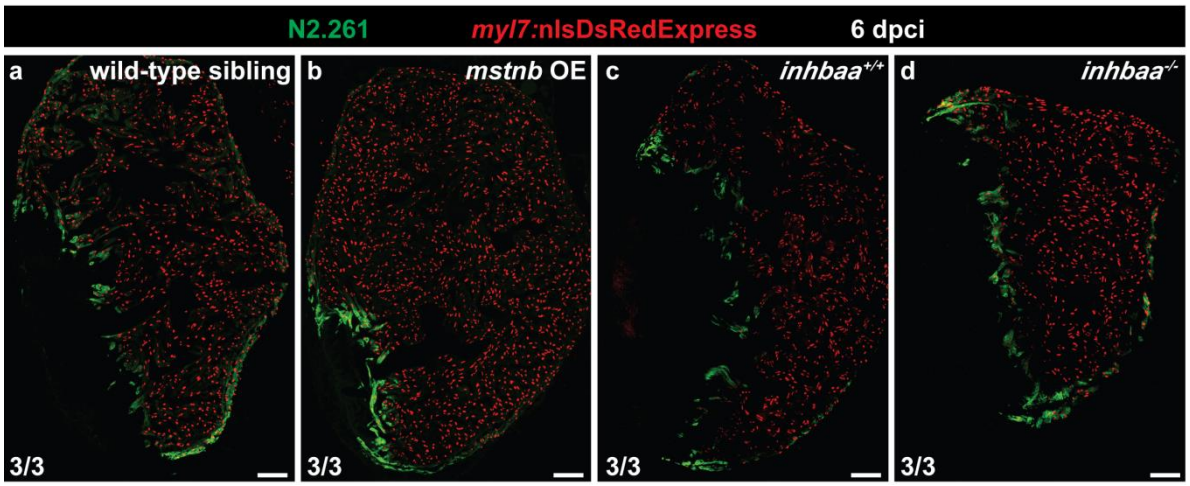

Figure 4.11. *mstnb* GOF and *inhbaa* LOF do not affect cardiomyocyte dedifferentiation during cardiac regeneration. (**a-d**) Sections of wild-type sibling (n=3), *mstnb* OE (n=3), *inhbaa*$^{+/+}$ (n=3) and *inhbaa*$^{-/-}$ (n=3) cryoinjured hearts in *Tg(myl7:nlsDsRedExpress)* background at 6 dpci, immunostained for DsRed (red) and N2.261 (green). The numerators indicate the number of hearts with a particular pattern of staining and the denominators the total number of hearts analyzed. Scale bars, 100 µm. Figure submitted in Dogra et al. (manuscript under revision).

4.7 *mstnb* GOF and *inhbaa* LOF lead to reduced cardiomyocyte proliferation during cardiac regeneration.

Furthermore, I wanted to test whether cardiomyocyte proliferation was affected in *mstnb* OE and *inhbaa*$^{-/-}$ fish at 6 dpci, by using *Tg(myl7:nlsDsRedExpress)* fish. Thus, I performed immunostaining for DsRed and PCNA (cell cycle stage marker), and quantified cardiomyocyte proliferation in 100 µm region adjacent to injured area, the region with highest levels of cardiomyocyte proliferation as reported previously (Sallin et al., 2015). I observed a 53% (±13% s.e.m.) decrease in cardiomyocyte proliferation in *mstnb* OE compared to wild-type siblings (**Figure 4.12a-c**), suggesting that *mstnb* has an inhibitory effect on the proliferation of cardiomyocytes during cardiac regeneration. Further on, there was a reduction of 49% (±11.5% s.e.m.) in cardiomyocyte proliferation in *inhbaa*$^{-/-}$ compared to *inhbaa*$^{+/+}$ animals (**Figure 4.12d-f**), indicating that the absence of *inhbaa* disturbs cardiomyocyte proliferation in the regenerating heart. Taken together, these results suggest that *mstnb* GOF and *inhbaa* LOF negatively affect cardiomyocyte proliferation, indicating that these two ligands have opposite functions during cardiac regeneration. (Certain lines in this section 4.7 have been quoted verbatim from Dogra et al. (manuscript under revision)).

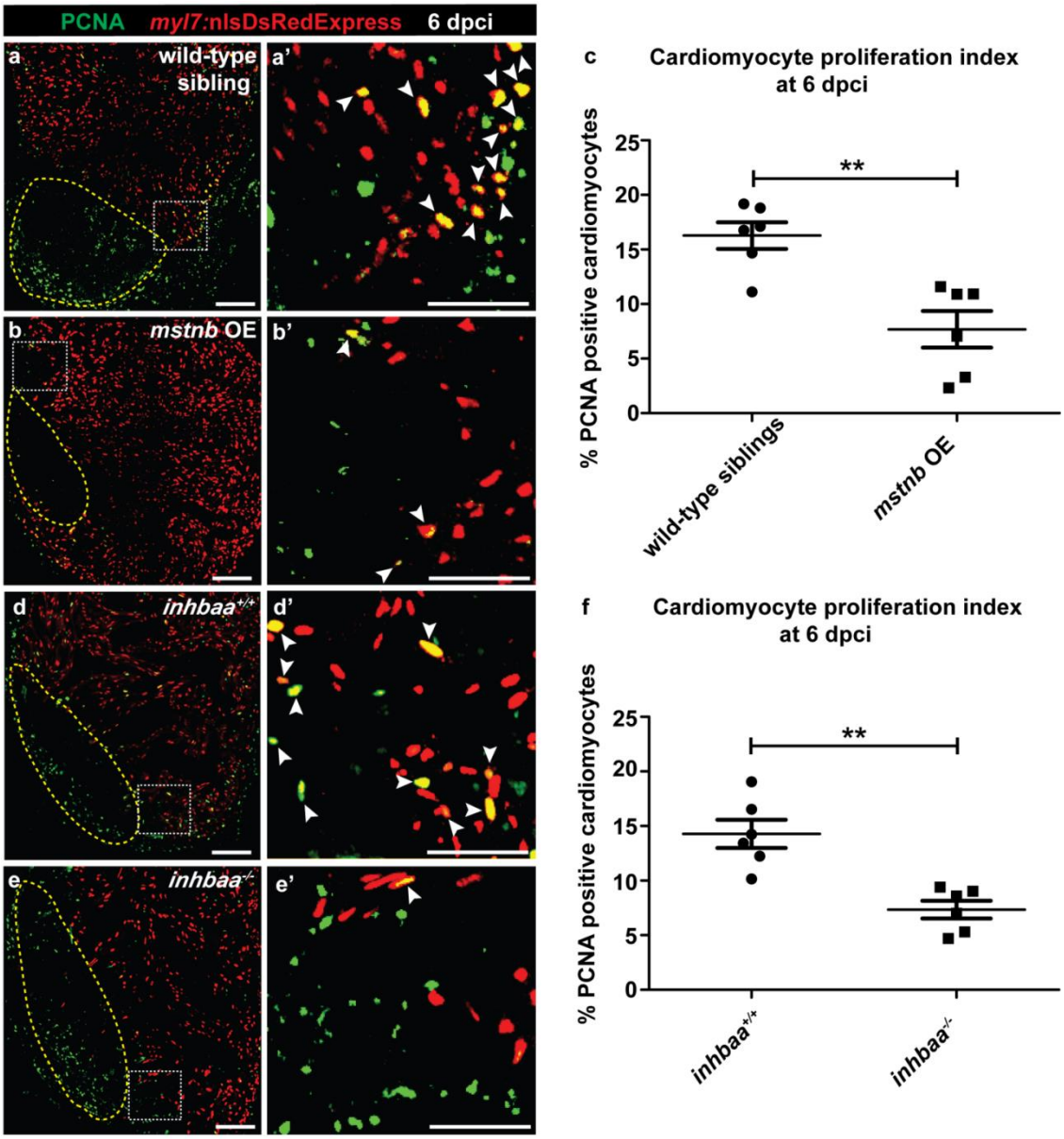

Figure 4.12. *mstnb* GOF and *inhbaa* LOF negatively affect cardiomyocyte proliferation during cardiac regeneration. (**a, b**) Sections of wild-type sibling and *mstnb* OE cryoinjured hearts in *Tg(myl7:nlsDsRedExpress)* background at 6 dpci, immunostained for DsRed (red) and PCNA (green). Yellow dotted regions delineate the injured area. (**a', b'**) Higher magnifications of white dotted boxes in a, b. White arrowheads point to proliferating cardiomyocytes ($PCNA^{+}/DsRed^{+}$). (**c**) Quantification of cardiomyocyte proliferation in wild-type sibling (n=6) and *mstnb* OE (n=6) cryoinjured hearts in the 100 µm region adjacent to the injured area at 6 dpci. (**d, e**) Sections of $inhbaa^{+/+}$ and $inhbaa^{-/-}$ cryoinjured hearts in *Tg(myl7:nlsDsRedExpress)* background at 6 dpci, immunostained for DsRed (red) and PCNA (green). (**d', e'**) Higher magnifications of white dotted boxes in d, e. (**f**) Quantification of cardiomyocyte proliferation in $inhbaa^{+/+}$ (n=6) and $inhbaa^{-/-}$ (n=6) cryoinjured hearts in the 100 µm region adjacent to the injured area at 6 dpci. All cell counts were performed on three sections from each heart and each data point on dot plot represents one heart. Data are mean ± s.e.m., **P ≤ 0.01, Student's t-test, two-tailed. Scale bars: heart sections, 100 µm; Higher magnifications, 50 µm. Figure submitted in Dogra et al. (manuscript under revision).

4.8 *mstnb* GOF and *inhbaa* LOF also affect non-cardiomyocyte proliferation during cardiac regeneration.

I further aimed to check non-cardiomyocyte proliferation in *mstnb* OE and *inhbaa*$^{-/-}$ hearts post cryoinjury. Thus, by performing DAPI counterstaining, along with PCNA and DsRed immunostaining on 6 dpci *Tg(myl7:nlsDsRedExpress)* fish, I found that overexpression of *mstnb* disturbed non-cardiomyocyte proliferation, as there was a significant reduction in non-cardiomyocyte proliferation in *mstnb* OE compared to wild-type siblings (**Figure 4.13a**). This shows that Mstnb has an inhibitory effect on the proliferation of multiple cell types during cardiac regeneration. Additionally, it was intriguing to observe that non-cardiomyocyte proliferation in *inhbaa*$^{-/-}$ was significantly enhanced compared to *inhbaa*$^{+/+}$ animals (**Figure 4.13b**). This result can be supported by the cell-specific nature of TGF-β signaling pathway (Chablais and Jazwinska, 2012). However, the exact mechanism how *inhbaa* is involved in the regulation of the non-myocardial cell cycle remains obscure and, importantly, the nature of the observed cell type remains unclear at this point.

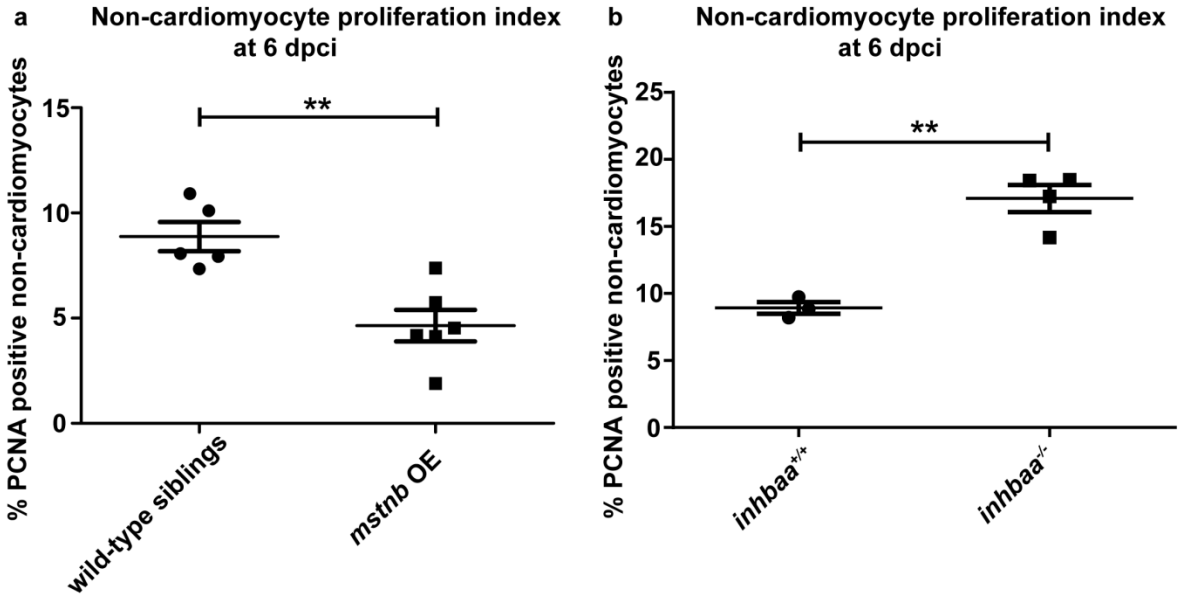

Figure 4.13. *mstnb* GOF and *inhbaa* LOF affect non-cardiomyocyte proliferation during cardiac regeneration. (**a**) Quantification of non-cardiomyocyte proliferation in wild-type sibling (n=5) and *mstnb* OE (n=6) cryoinjured hearts (immunostained for DsRed and PCNA, along with DAPI counterstaining) in the 100 µm region adjacent to the injured area at 6 dpci. (**b**) Quantification of non-cardiomyocyte proliferation in *inhbaa*$^{+/+}$ (n=3) and *inhbaa*$^{-/-}$ (n=4) cryoinjured hearts (immunostained for DsRed and PCNA, along with DAPI counterstaining) in the 100 µm region adjacent to the injured area at 6 dpci. All cell counts were performed on three sections from each heart and each data point on dot plot represents one heart. Data are mean ± s.e.m., **P ≤ 0.01, Student's t-test, two-tailed.

4.9 *mstnb* GOF and *inhbaa* LOF do not affect RA signaling during cardiac regeneration.

In addition to cardiomyocytes, other cell types including endocardial and epicardial cells also show injury responses, such as the reactivation of developmental marker genes, including *raldh2*. *raldh2* encodes for the rate limiting enzyme in RA synthesis which plays an important role in cardiac tissue regeneration by promoting cardiomyocyte proliferation (Kikuchi et al., 2011b; Lepilina et al., 2006). Hence, the expression of *raldh2* is observed in epicardium as well as in endocardium in the injured area (Kikuchi et al., 2011b). Thus, I wanted to check whether *mstnb* GOF and *inhbaa* LOF affect RA signaling during cardiac regeneration, by performing immunostaining for Raldh2 and DsRed on 14 dpci *Tg(myl7:nlsDsRedExpress)* hearts. There was no significant difference observed in Raldh2 expression in *mstnb* OE and *inhbaa*$^{-/-}$ injured hearts compared to their wild-type siblings (**Figure 4.14**), indicating that RA signaling is not affected in the epicardial and endocardial cells during cardiac regeneration by overexpression of *mstnb* and loss of *inhbaa*.

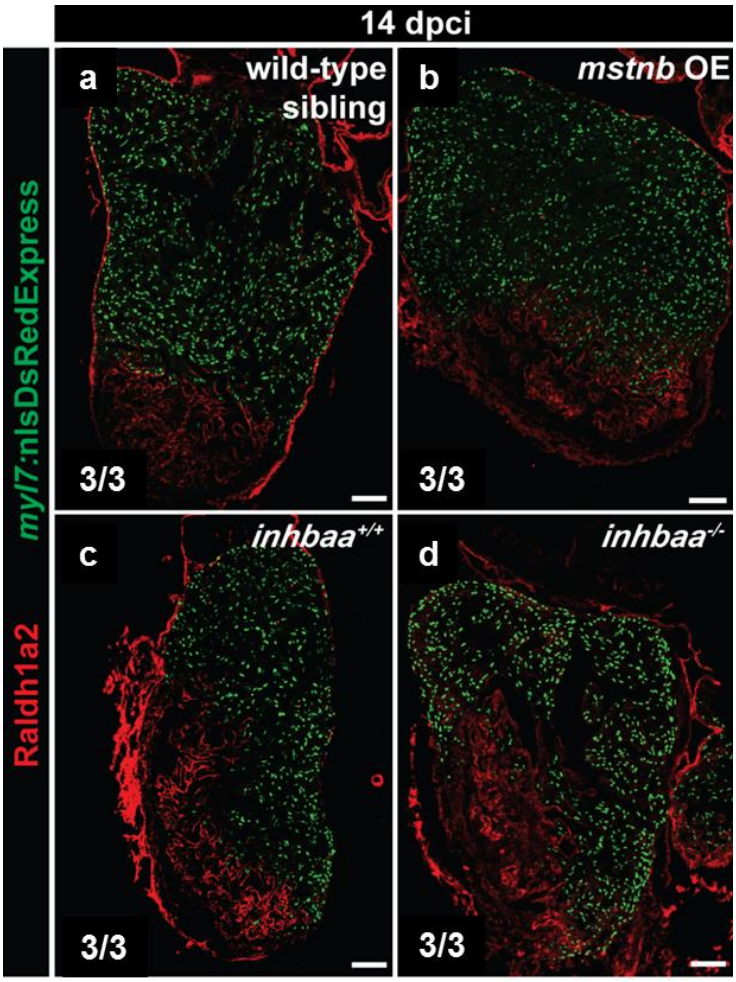

Figure 4.14. *mstnb* GOF and *inhbaa* LOF do not affect RA signaling during cardiac regeneration. (**a-d**) Sections of wild-type sibling (n=3), *mstnb* OE (n=3), *inhbaa*$^{+/+}$ (n=3) and *inhbaa*$^{-/-}$ (n=3) cryoinjured hearts in *Tg(myl7:nlsDsRedExpress)* background at 6 dpci, immunostained for DsRed (red) and Raldh2 (green). The numerators indicate the number of hearts with a particular pattern of staining and the denominators the total number of hearts analyzed. Scale bars, 100 µm.

4.10 *mstnb* GOF and *inhbaa* LOF do not affect fibronectin deposition during cardiac regeneration.

It has been previously reported that the post-infarct zone is labelled by connective tissue markers, such as extracellular matrix (ECM) protein, Fibronectin (Fb) (Chablais and Jazwinska, 2012). I therefore wanted to check whether *mstnb* GOF and *inhbaa* LOF affect Fb deposition. Thus, the sections of 14 dpci *mstnb* OE and *inhbaa*$^{-/-}$ hearts in *Tg(myl7:nlsDsRedExpress)* and *Tg(myl7:LIFEACT-GFP)* background were immunostained with Fb and DsRed/GFP. There was no significant difference observed in fibronectin expression in *mstnb* OE and *inhbaa*$^{-/-}$ hearts compared to their wild-type siblings (**Figure 4.15**). This result indicates that fibronectin deposition is not disturbed in *mstnb* GOF and *inhbaa* LOF fish during cardiac regeneration.

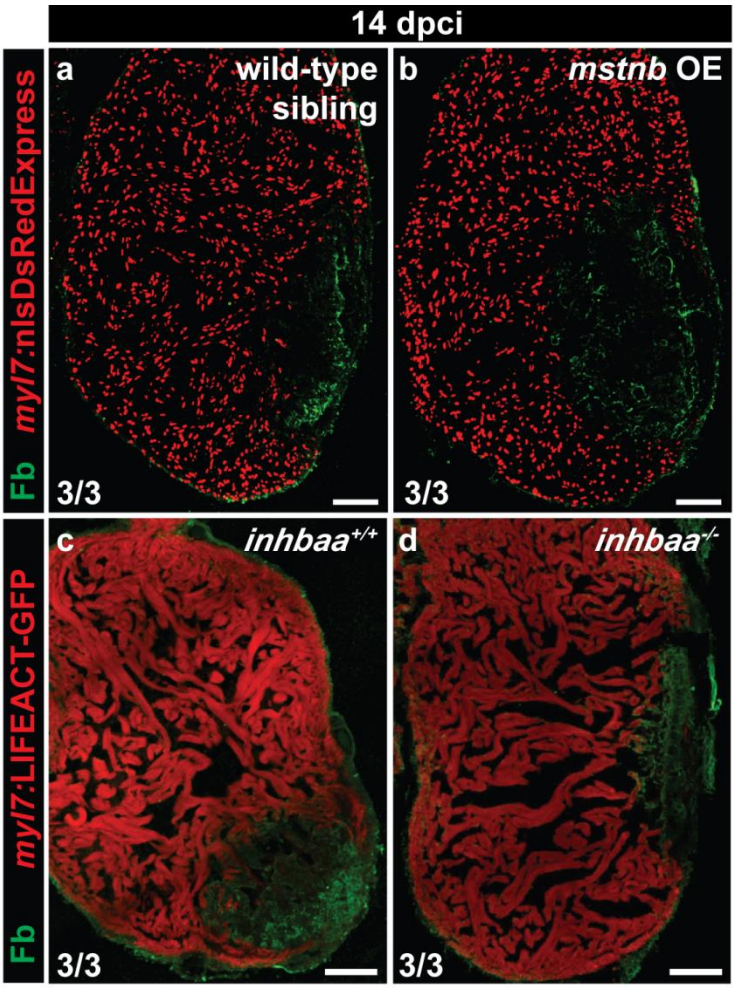

Figure 4.15. ***mstnb*** **GOF and** ***inhbaa*** **LOF do not affect fibronectin deposition during cardiac regeneration.** (**a,b**) Sections of wild-type sibling (n=3) and *mstnb* OE (n=3) cryoinjured hearts in *Tg(myl7:nlsDsRedExpress)* background at 6 dpci, immunostained for DsRed (red) and Fb (green). (**c,d**) Sections of *inhbaa*$^{+/+}$ (n=3) and *inhbaa*$^{-/-}$ (n=3) cryoinjured hearts in *Tg(myl7:LIFEACT-GFP)* background at 6 dpci, immunostained for GFP (red) and Fb (green). The numerators indicate the number of hearts with a particular pattern of staining and the denominators the total number of hearts analyzed. Scale bars, 100 μm.

4.11 Generation of *mstnb* LOF and *inhbaa* GOF fish.

The above-mentioned results indicate that *mstnb* GOF and *inhbaa* LOF suppress cardiac regeneration by negatively affecting cardiomyocyte proliferation in the injured zebrafish heart. Thus, as a complementary approach, the effect of *mstnb* LOF and *inhbaa* GOF was assessed on cardiac development and regeneration.

In order to investigate the effect of loss of *mstnb*, *mstnb* mutant fish was generated using a TALEN targeting the region after signal peptide domain (**Figure 4.16a**). The TALEN was

cloned according to Golden Gate Assembly. The TALEN arms targeting *mstnb* had the following RVDs: NN NN NI NN NI NG NI NG NI NI HD NN NN HD NN HD and HD NN HD NG NG NG HD HD NG HD HD NN NG NN NN HD. The TALEN mRNA injections were done in one-cell stage embryos and the activity of TALEN was analyzed by performing HRMA of the PCR products spanning the TALEN-target site in the injected F0 embryos (**Figure 4.17a**). Using HRMA, F1 animals were screened for possible genomic lesions and a 10 bp deletion allele, $mstnb^{bns5}$ was recovered (**Figure 4.16b, Figure 4.17b**), which is predicted to encode a truncated protein (**Figure 4.16c**). From RT-qPCR analysis, *mstnb* transcript levels seem to be significantly reduced in $mstnb^{-/-}$ compared to $mstnb^{+/+}$ (**Figure 4.16d**), suggesting mRNA decay.

Further, transgenic zebrafish line for cardiomyocyte-specific constitutive overexpression of *inhbaa*, *Tg(myl7:inhbaa-2A-H2B-EGFP)bns146* (*inhbaa* OE hereafter) was generated (**Figure 4.18a**). The plasmid construct for this transgenic line was cloned by using Cold Fusion technology. PCR amplified full length CDS of *inhbaa* was fused to self-cleaving 2A peptide along with H2B-EGFP fluorescent reporter, all under the control of *myl7* promoter. 18 pg of this construct was co-injected with 20 pg Tol2 mRNA into one-cell stage embryos. The founders were outcrossed with *Tg(-0.8myl7:nlsDsRedExpress)hsc4* to generate stable lines, which were used in the experiments (**Figure 4.18b, c**). From RT-qPCR analysis, *inhbaa* transcript levels seem to be highly increased in *inhbaa* OE compared to wild-type siblings (**Figure 4.18d**), confirming that *inhbaa* is overexpressed in the generated *inhbaa* OE transgenic animals. (Certain lines in this section 4.11 have been quoted verbatim from Dogra et al. (manuscript under revision)).

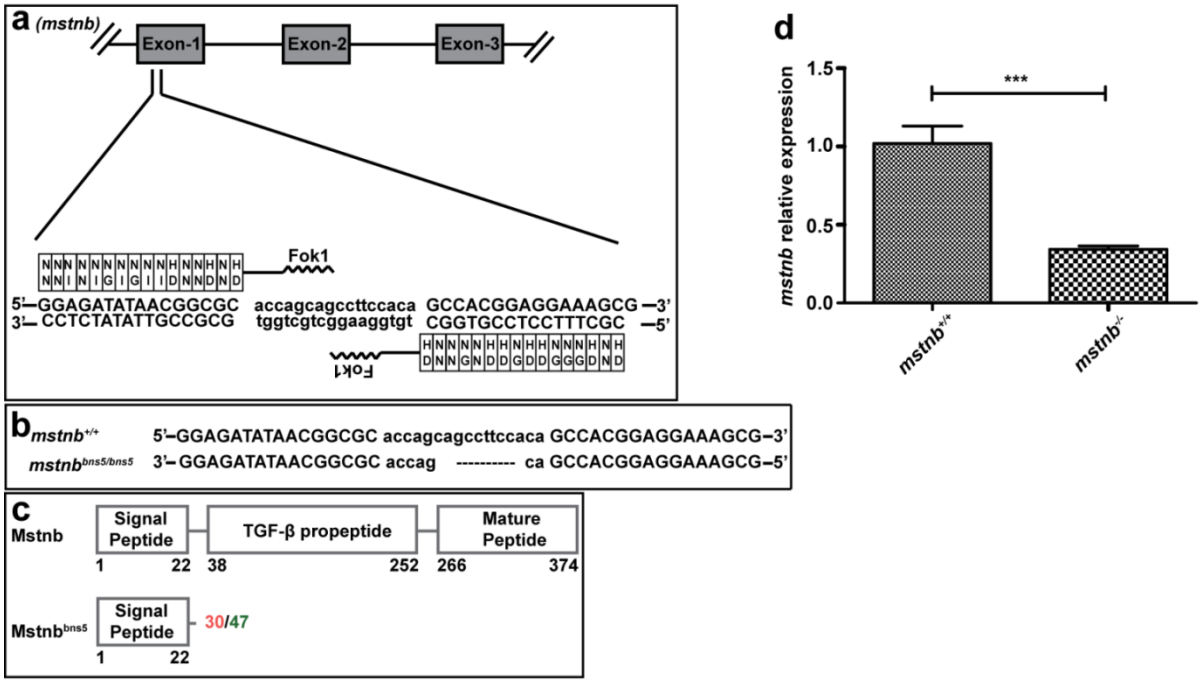

Figure 4.16. Generation and validation of *mstnb* LOF line. (**a-c**) *mstnb* TALEN designed to target the region after the signal peptide in exon 1 was generated (**a**), a 10 bp frameshift deletion allele (*mstnb*^{bns5}) was identified (**b**) and is predicted to cause the formation of a truncated protein (**c**). Red number indicates the last native amino acid before the frameshift mutation; green number indicates the last amino acid before stop codon. (**d**) RT–qPCR for *mstnb* expression analysis in *mstnb*$^{+/+}$ and *mstnb*$^{-/-}$ adult hearts (n=2 x 3 cardiac ventricles assessed as 2 biological and 2 technical replicates). Data are mean ± s.e.m., ***P ≤ 0.001, Student's t-test, two-tailed. Figure submitted in Dogra et al. (manuscript under revision).

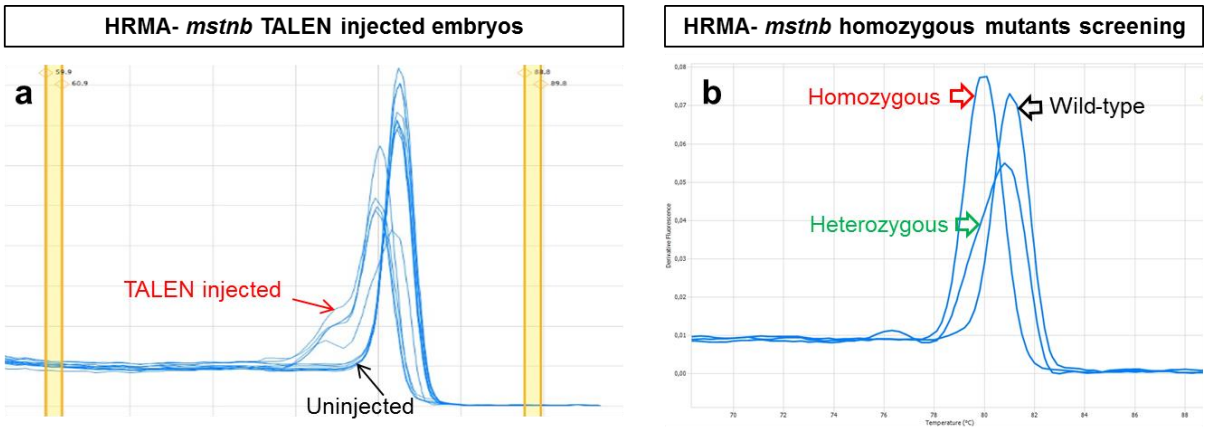

Figure 4.17. HRMA analysis of *mstnb* TALEN-induced mutagenesis. (**a**) HRMA of PCR products of TALEN targeted region, with *mstnb* TALEN injected embryos showing an altered melt profile (red arrow) compared to uninjected embryos (black arrow). (**b**) HRMA of PCR products of TALEN targeted region, with *mstnb* homozygous mutants (carrying 10 bp deletion alleles), heterozygous and wild-type siblings showing different melt profiles.

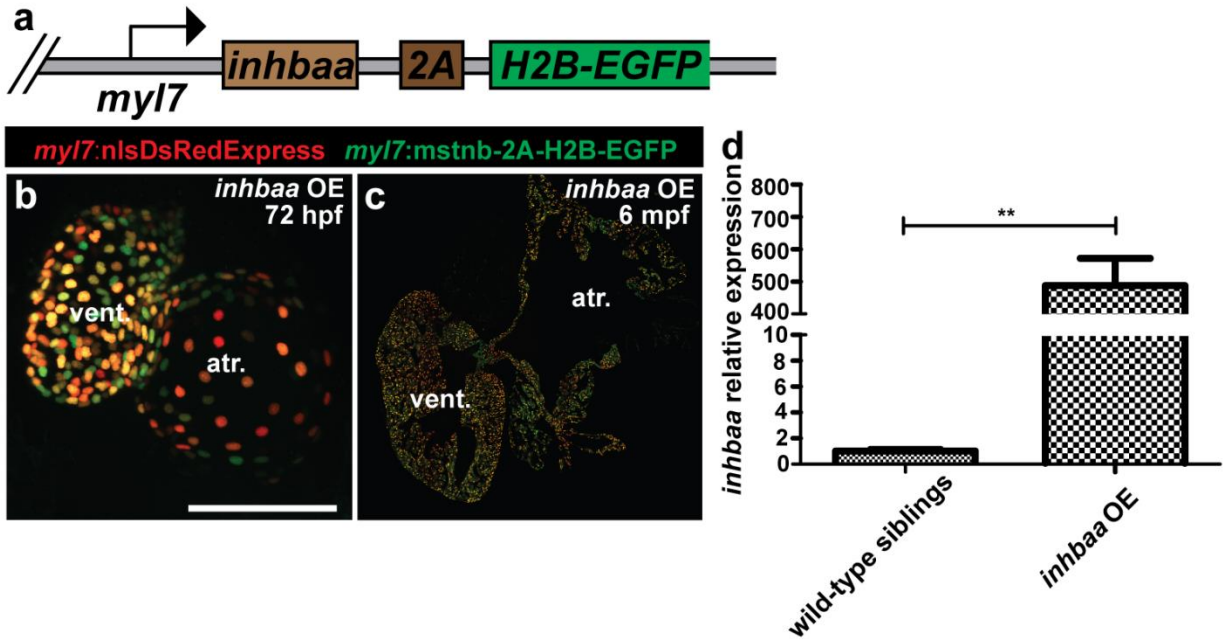

Figure 4.18. Generation and validation of *inhbaa* GOF line. (**a**) Schematic representation of cardiomyocyte-specific *inhbaa* OE transgene, *Tg(myl7:inhbaa-2A-H2B-EGFP).* (**b**) 72 hpf heart of *inhbaa* OE larva in *Tg(myl7:nlsDsRedExpress)* background (native fluorescence). (**c**) Section of *inhbaa* OE adult fish heart in *Tg(myl7:nlsDsRedExpress)* background, immunostained for DsRed (red) and GFP (green). (**d**) RT–qPCR for *inhbaa* expression analysis in wild-type sibling and *inhbaa* OE adult hearts (n=2 x 3 cardiac ventricles assessed as 2 biological and 2 technical replicates). Data are mean ± s.e.m., **P ≤ 0.01, Student's t-test, two-tailed. Scale bars, 100 µm. vent., ventricle; atr., atrium. Figure submitted in Dogra et al. (manuscript under revision).

4.12 *mstnb* LOF and *inhbaa* GOF positively affect physiological cardiomyocyte proliferation.

The adult *mstnb*$^{-/-}$ animals appear hypermuscular (**Figure 4.19**), as previously reported in other species (Chisada et al., 2011; Haidet et al., 2008; Whittemore et al., 2003), suggesting a conserved role of Mstn on skeletal muscle growth. Interestingly, the *mstnb*$^{-/-}$ fish also showed enlarged heart size with a thickened ventricular wall (**Figure 4.20a-d, f**), the principal expression domain of *mstnb* as assessed in the results mentioned earlier (**Figure 4.2c, c'**). On the other hand, the eye size remained unaffected amongst *mstnb*$^{-/-}$ *and mstnb*$^{+/+}$ animals (**Figure 4.20e**). Further, to understand whether the increase in ventricular wall thickness was a consequence of increased cardiomyocyte proliferation in the compact layer, EdU was injected in adult *Tg(myl7:nlsDsRedExpress)* fish and immunostaining was performed for DsRed and cardiomyocyte-specific myosin heavy chain (MF-20, to help in distinguishing between compact and trabecular layers of the ventricle), followed by EdU labeling on cardiac sections (**Figure 4.21a**). Both DsRed^{+} nuclei as well as % EdU^{+}/DsRed^{+} nuclei were

quantified in the compact and trabecular layers of the ventricles. Notably, *mstnb*$^{-/-}$ hearts showed a significant increase in the total number of cardiomyocytes and the number of EdU incorporating cardiomyocytes, in both the wall and trabeculae of the ventricle (**Figure 4.21b-e**). Overall, these results suggest that *mstnb* LOF promotes physiological cardiomyocyte proliferation, leading to cardiac hyperplasia in zebrafish, unlike in *Mstn*-knockout mice which respond by cardiac hypertrophy (Biesemann et al., 2014; Morissette et al., 2006; Rodgers et al., 2009).

Next, the majority of adult (3-6 mpf) *inhbaa* OE fish appear morphologically comparable to wild-type siblings; however, the *inhbaa* OE hearts are enlarged and show dense trabeculation in both chambers, whereas the eye size is unaffected (**Figure 4.22a-e**; H&E staining experiments in Figure 4.22a', a'', b', b'' were performed in collaboration with Dr. Suchit Ahuja). During late adult stages (>6 mpf), nearly 20% of the *inhbaa* OE fish developed pericardial edema with abnormally enlarged atria (**Figure 4.23**), indicating symptoms of a failing heart due to sustained *inhbaa* overexpression. In order to analyze whether the enlargement and excessive trabeculation of *inhbaa* OE hearts in young adults was linked to increased cardiomyocyte proliferation, EdU injections were performed in adult *Tg(myl7:nlsDsRedExpress)* fish, followed by immunostaining for DsRed, and EdU labeling (**Figure 4.24a**). Quantification of DsRed^{+} nuclei as well as % EdU^{+}/DsRed^{+} nuclei was performed in both chambers. Interestingly, a 50% (±11% s.e.m.) increase in total number of cardiomyocytes, as well as an increase of 83% (±14% s.e.m.) in the number of EdU incorporating cardiomyocytes was observed in the *inhbaa* OE hearts compared to wild-type siblings (**Figure 4.24b-e**). These results indicate that cardiomyocyte-specific *inhbaa* overexpression promotes cardiomyocyte proliferation, suggesting that Inhbaa can act as a potential mitogen during cardiac development and regeneration. (Certain lines in this section 4.12 have been quoted verbatim from Dogra et al. (manuscript under revision)).

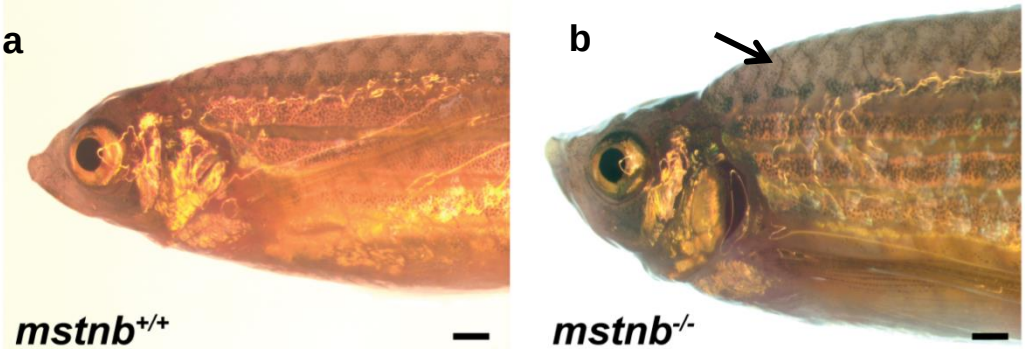

Figure 4.19. *mstnb* LOF leads to increased muscle mass in adult zebrafish. (**a, b**) *mstnb*$^{+/+}$ and *mstnb*$^{-/-}$ adult zebrafish; *mstnb*$^{-/-}$ animals show hypermuscular phenotype (black arrow points to increased muscle mass). Scale bars, 1000 µm.

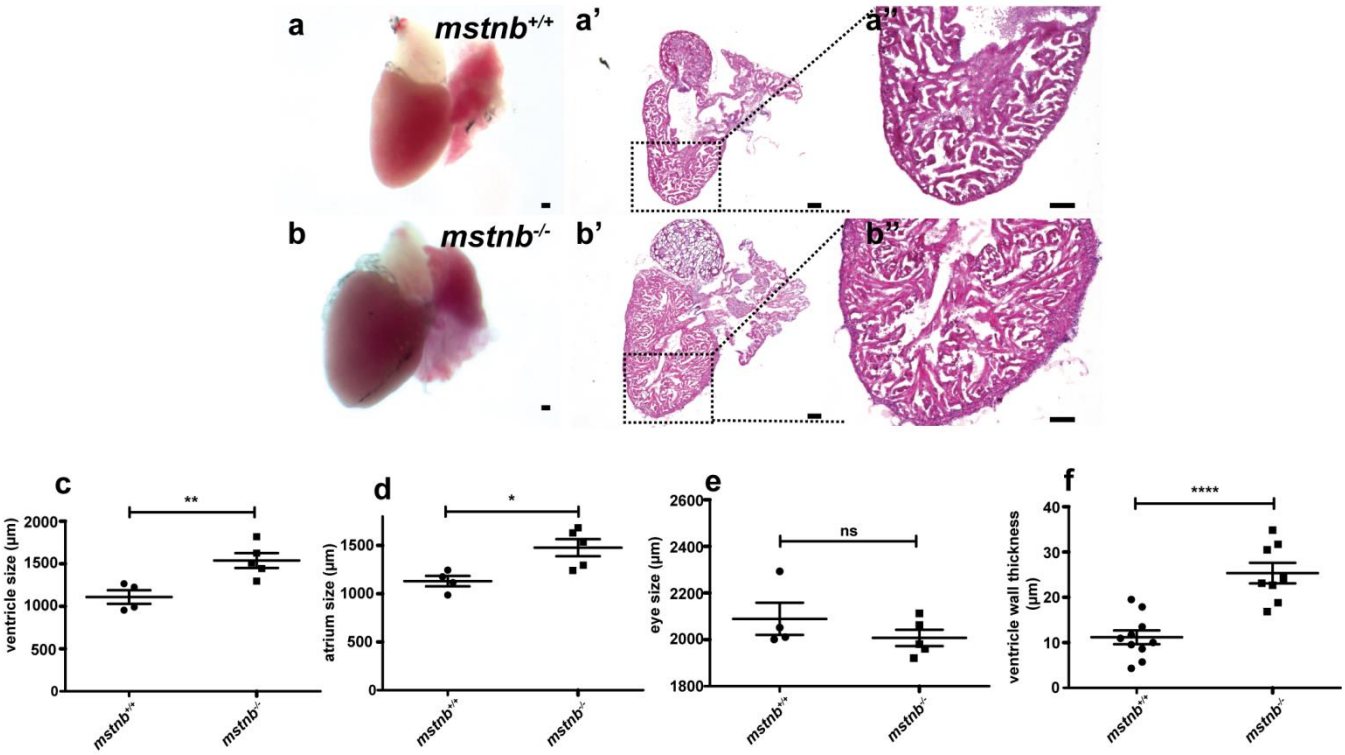

Figure 4.20. *mstnb* LOF leads to enlarged heart size and ventricular wall thickening. (**a-b''**) *mstnb*$^{+/+}$ and *mstnb*$^{-/-}$ adult hearts, H&E staining of heart sections and higher magnifications of H&E staining. (**c-e**) Quantification of the size of ventricle, atrium and eye in *mstnb*$^{+/+}$ (n=4) and *mstnb*$^{-/-}$ (n=5) adults. (**f**) Quantification of ventricular wall thickness in *mstnb*$^{+/+}$ (n=10) and *mstnb*$^{-/-}$ (n=8) adult hearts. Data are mean ± s.e.m., ns: no significant changes observed, *P ≤ 0.05, **P ≤ 0.01 and ****P ≤ 0.0001, Student's t-test, two-tailed. Scale bars, 100 µm. Figure submitted in Dogra et al. (manuscript under revision).

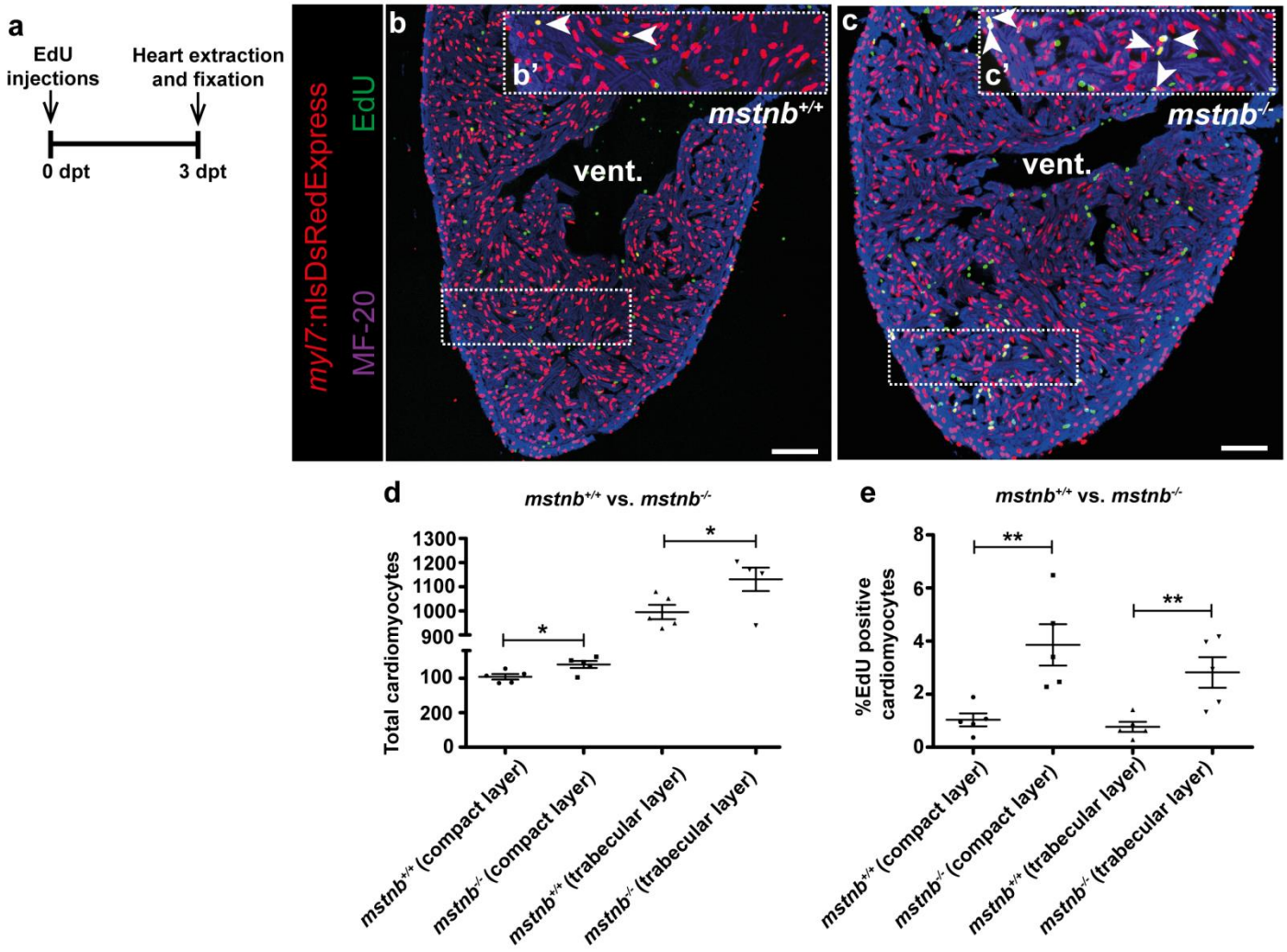

Figure 4.21. ***mstnb*** **LOF positively affects physiological cardiomyocyte proliferation.** (**a**) Experimental setup of EdU injections, followed by heart extraction and fixation. (**b, c**) Heart sections of *mstnb*$^{+/+}$ and *mstnb*$^{-/-}$ adult fish in *Tg(myl7:nlsDsRedExpress)* background, immunostained for DsRed (red) and MF-20 (blue), followed by EdU labeling (green). (**b', c'**) Higher magnifications of dotted boxes in b, c. White arrowheads point to EdU^{+}/DsRed^{+} cardiomyocytes. (**d, e**) Quantification of total cardiomyocytes (DsRed^{+}) and EdU incorporating cardiomyocytes (EdU^{+}/DsRed^{+}) in the compact and trabecular layers of *mstnb*$^{+/+}$ (n=5) and *mstnb*$^{-/-}$ (n=5) ventricles. All cell counts were performed on three sections from each heart and each data point on dot plot represents one heart. Data are mean ± s.e.m., *P ≤ 0.05 and **P ≤ 0.01, Student's t-test, two-tailed. Scale bars, 100 µm. vent., ventricle; atr., atrium. Figure submitted in Dogra et al. (manuscript under revision).

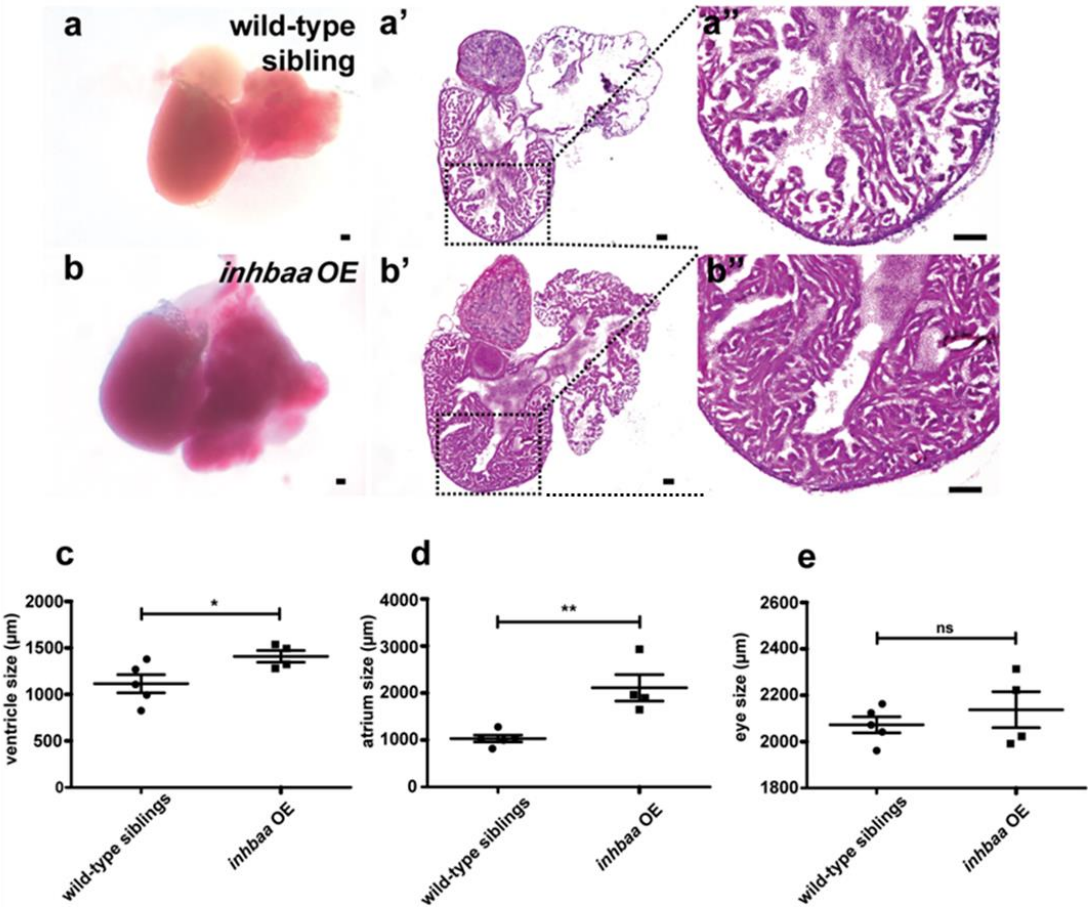

Figure 4.22. *inhbaa* GOF leads to enlarged heart size and hypertrabeculation. (**a-b''**) Wild-type sibling and *inhbaa* OE adult hearts, H&E staining of heart sections and higher magnifications of H&E staining. (**c-e**) Quantification of the size of ventricle, atrium and eye in wild-type sibling (n=5) and *inhbaa* OE (n=4) adults. Data are mean ± s.e.m., ns: no significant changes observed, ns: no significant changes observed, *P ≤ 0.05 and **P ≤ 0.01, Student's t-test, two-tailed. Scale bars, 100 µm. Figure submitted in Dogra et al. (manuscript under revision). H&E staining experiments in Figure 4.22a', a'', b', b'' were performed in collaboration with Dr. Suchit Ahuja.

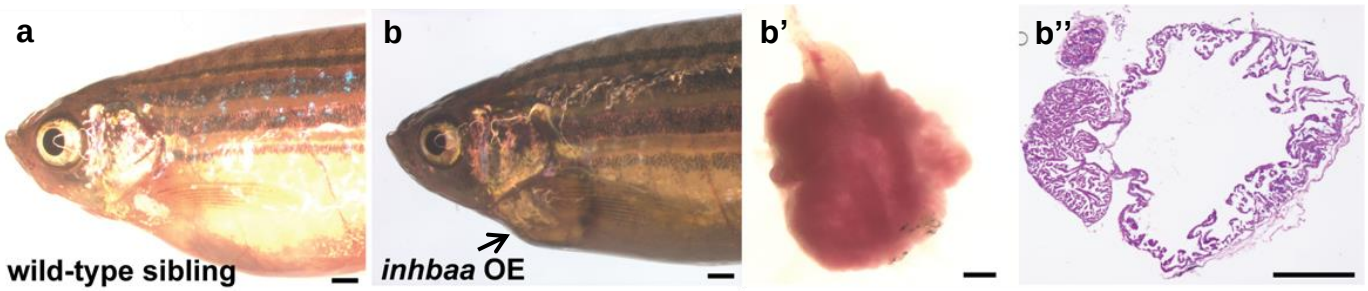

Figure 4.23. *inhbaa* GOF leads to pericardial edema with abnormally enlarged cardiac atria in late adult stages (>6 mpf). (**a, b**) Unlike wild-type siblings, *inhbaa* OE adult fish (>6 mpf) show pericardial edema (as pointed by black arrow). (**b',b''**) *inhbaa* OE fish heart and H&E of heart section showing abnormally enlarged atrium. Scale bars: fish, 1000 µm; heart and heart section, 500 µm.

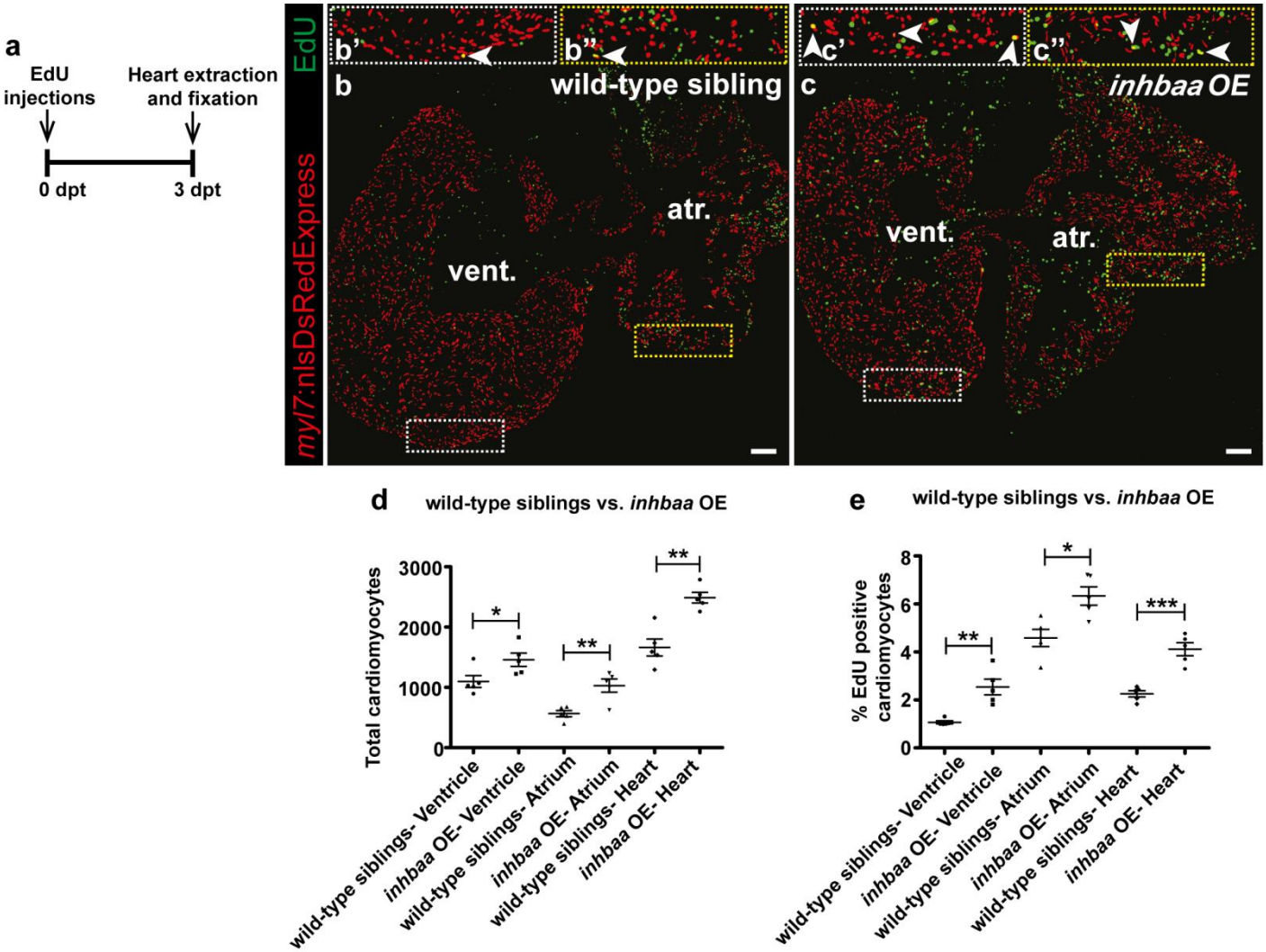

Figure 4.24. *inhbaa* GOF positively affects physiological cardiomyocyte proliferation. (**a**) Experimental setup of EdU injections, followed by heart extraction and fixation for immunostaining. (**b, c**) Heart sections of wild-type sibling and *inhbaa* OE adult fish in *Tg(myl7:nlsDsRedExpress)* background, immunostained for DsRed (red), followed by EdU labeling (green). (**b', b'', c', c''**) Higher magnifications of dotted boxes in b, c. (**d, e**) Quantification of total cardiomyocytes ($DsRed^+$) and EdU incorporating cardiomyocytes ($EdU^+/DsRed^+$) in wild-type sibling (n=5) and *inhbaa* OE (n=5) hearts. All cell counts were performed on three sections from each heart and each data point on dot plot represents one heart. Data are mean ± s.e.m., $*P \leq 0.05$, $**P \leq 0.01$, $***P \leq 0.001$, Student's t-test, two-tailed. vent., ventricle; atr., atrium. Figure submitted in Dogra et al. (manuscript under revision).

4.13 *mstnb* LOF and *inhbaa* GOF lead to enhanced cardiac regeneration.

Next, I tested whether increased cardiomyocyte proliferation helps *mstnb*$^{-/-}$ and *inhbaa* OE hearts to regenerate better. Thus, the cryoinjured hearts of *mstnb*$^{-/-}$ and *inhbaa* OE were

compared with their siblings at 30 dpci, a time point at which wild-type cryoinjured hearts still possess scarring (Chablais et al., 2011). Interestingly, *mstnb*$^{-/-}$ and *inhbaa* OE hearts had completely resolved scars at 30 dpci, unlike their sibling hearts (**Figure 4.25**), indicating that the loss of *mstnb* and overexpression of *inhbaa* lead to enhanced cardiac regeneration. Taken together, these results support the finding that *mstnb* and *inhbaa* have opposite effects on cardiomyocyte proliferation and ultimately cardiac regeneration. (Certain lines in this section 4.13 have been quoted verbatim from Dogra et al. (manuscript under revision)).

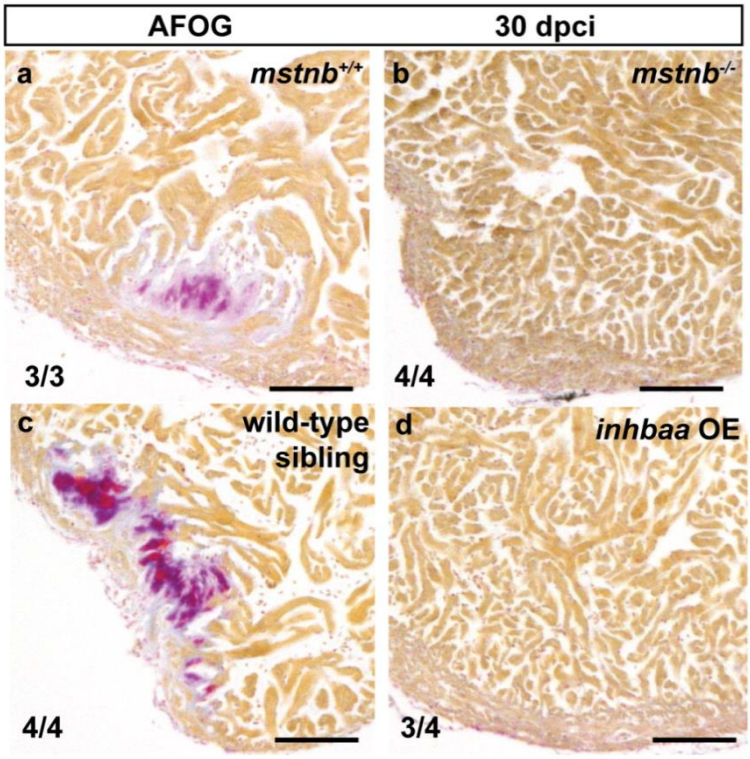

Figure 4.25. *mstnb* LOF and *inhbaa* GOF positively affect cardiac regeneration. (**a-d**) AFOG staining of *mstnb*$^{+/+}$ (n=3), *mstnb*$^{-/-}$ (n=4), wild-type sibling (n=4) and *inhbaa* OE (n=4) cryoinjured heart sections at 30 dpci. The numerators indicate the number of hearts with a particular pattern of scarring and the denominators the total number of hearts analyzed. Scale bars, 100 µm. Figure submitted in Dogra et al. (manuscript under revision).

4.14 *inhbaa* GOF promotes cardiomyocyte proliferation independent of Nrg-ErbB signaling pathway.

To further study the pro-mitogenic effect of *inhbaa* overexpression on cardiomyocyte proliferation, EdU incorporation was analyzed in larval hearts at 120 hpf. Cardiomyocyte

labeling was achieved using the *Tg(myl7:nlsDsRedExpress)* background, which again was combined with an EdU incorporation assay, followed by immunostaining for DsRed (**Figure 4.26a**). I observed an increase of 35% (±11% s.e.m.) in the number of EdU incorporating cardiomyocytes in *inhbaa* OE larvae compared to wild-type siblings (**Figure 4.26b-d**), indicating that *inhbaa* overexpression also promotes cardiomyocyte proliferation at early stages. Next, I wanted to investigate whether the effects of *inhbaa* OE on cardiomyocyte proliferation depended on the Nrg-ErbB signaling pathway, a well-known mitogen of cardiomyocyte proliferation (D'Uva et al., 2015; Gemberling et al., 2015; Liu et al., 2010). Thus, I injected *myl7:inhbaa-2A-H2B-EGFP* and *myl7:H2B-EGFP* plasmid DNA in embryos from the intercross of *erbb*^{2st61} heterozygous fish and performed EdU incorporation analysis (**Figure 4.27a**), followed by genotyping. Analyzing GFP^{+} cardiomyocytes in *erbb*^{2st61} homozygous mutants at 120 hpf, I observed that a significant amount of *erbb*$^{-/-}$ cardiomyocytes expressing *inhbaa* OE were EdU positive, whereas *erbb*$^{-/-}$ cardiomyocytes expressing GFP alone did not show any signs of EdU incorporation (**Figure 4.27b-d**). Further on, I treated *inhbaa* OE larvae and wild-type siblings with the established ErbB2 inhibitor PD168393 and analyzed cardiomyocyte proliferation (**Figure 4.28a**). There was a significant reduction in cardiomyocyte proliferation due to the chemical inhibition of ErbB2 signaling, as also described previously (Liu et al., 2010), and interestingly, *inhbaa* OE was able to rescue this effect. Overexpression of *inhbaa* led to an increase of 77.5% (±18% s.e.m.) in the cardiomyocyte EdU incorporation compared to wild-type siblings under ErbB2 blocking conditions (**Figure 4.28b-d**).

As recently reported, in zebrafish, Nrg2a signals through ErbB2 to induce cardiomyocyte trabeculation and proliferation (Rasouli and Stainier, 2017). Thus, I wanted to compare the effects of *inhbaa* and *nrg2a* overexpression, and check whether the overexpression of both ligands resulted in an additive effect on cardiomyocyte proliferation. Therefore, I crossed *inhbaa* OE and *Tg(myl7:nrg2a202-p2a-tdTomato)bns140* (*nrg2a* OE hereafter) fish, and analyzed cardiomyocyte proliferation in *Tg(myl7:nlsDsRedExpress)* larvae at 120 hpf, by performing immunostaining for DsRed, followed by EdU labeling (**Figure 4.29a**) and genotyping. In line with my earlier-mentioned observations and recently published work (Rasouli and Stainier, 2017), there was an increase of 38% (±7.5% s.e.m.) and 55% (±8% s.e.m.) in the number of EdU incorporating cardiomyocytes in *inhbaa* OE and *nrg2a* OE larvae, respectively (**Figure 4.29b-d, f**; the *nrg2a* OE transgenic line used in Figure 4.29 d, f has been provided by collaborator Seyed Javad Rasouli). However, there was no additive effect from overexpressing both ligands, and an increase of 53% (±6% s.e.m.) was observed

in the number of EdU incorporating cardiomyocytes, similar to *nrg2a* OE alone (**Figure 4.29e, f**; the *nrg2a* OE transgenic line used in Figure 4.29 e, f has been provided by collaborator Seyed Javad Rasouli). This result might indicate that cardiomyocyte proliferation reaches its maximum by *nrg2a* overexpression alone, as supported by the minimal variability across the assessed samples or an interference of Inhbaa-mediated proliferation by ErbB signaling. Altogether, these data show that Inhbaa can promote cardiomyocyte proliferation during development, even in the absence of any injury stimuli, and that the mitogenic activity of Inhbaa on cardiomyocytes is independent of ErbB receptor activity. (Certain lines in this section 4.14 have been quoted verbatim from Dogra et al. (manuscript under revision)).

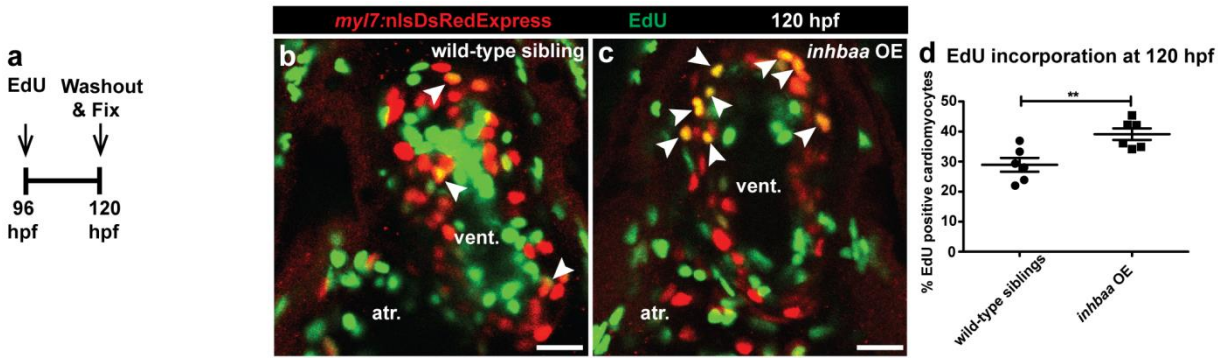

Figure 4.26. *inhbaa* GOF promotes cardiomyocyte proliferation during early stages of development. (**a**) Experimental setup of EdU incubation, washing out EdU and fixing the larvae. (**b, c**) Hearts of 120 hpf wild-type sibling and *inhbaa* OE larvae in *Tg(myl7:nlsDsRedExpress)* background, immunostained for DsRed (red), followed by EdU labeling (green). White arrowheads point to proliferating cardiomyocytes ($EdU^+/DsRed^+$). (**d**) Quantification of cardiomyocyte proliferation in 120 hpf wild-type sibling (n=6) and *inhbaa* OE (n=6) ventricles. All cell counts were performed on non-overlapping confocal planes (thickness, 1µm). Data are mean ± s.e.m., **P ≤ 0.01, Student's t-test, two-tailed. Scale bars, 20 µm. vent., ventricle; atr., atrium. Figure submitted in Dogra et al. (manuscript under revision).

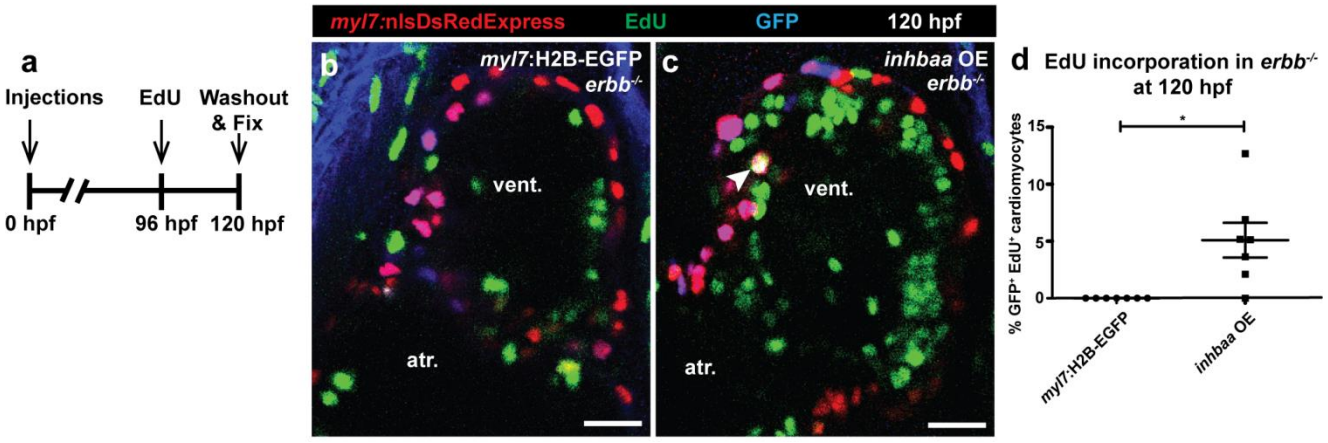

Figure 4.27. *inhbaa* GOF promotes cardiomyocyte proliferation independently of ErbB2 signaling. (**a**) Experimental setup of injections, EdU exposure, followed by fixation. (**b, c**) *Tg(myl7:nlsDsRedExpress)* hearts of *myl7:H2B-EGFP* and *myl7:inhbaa-2A-H2B-EGFP (inhbaa OE)* injected *erbb*$^{-/-}$ larvae at 120 hpf, immunostained for DsRed (red) and GFP (blue), followed by EdU labeling (green). White arrowheads point to proliferating cardiomyocytes (EdU^{+}/DsRed^{+}/GFP^{+}). (**d**) Quantification of cardiomyocyte proliferation in *myl7:H2B-EGFP* (n=7) and *inhbaa* OE (n=7) injected ventricles at 120 hpf. All cell counts were performed on non-overlapping confocal planes (thickness, 1µm) (data are mean ± s.e.m., *P ≤ 0.05, Student's t-test, two-tailed). Scale bars, 20 µm. vent., ventricle; atr., atrium. Figure submitted in Dogra et al. (manuscript under revision).

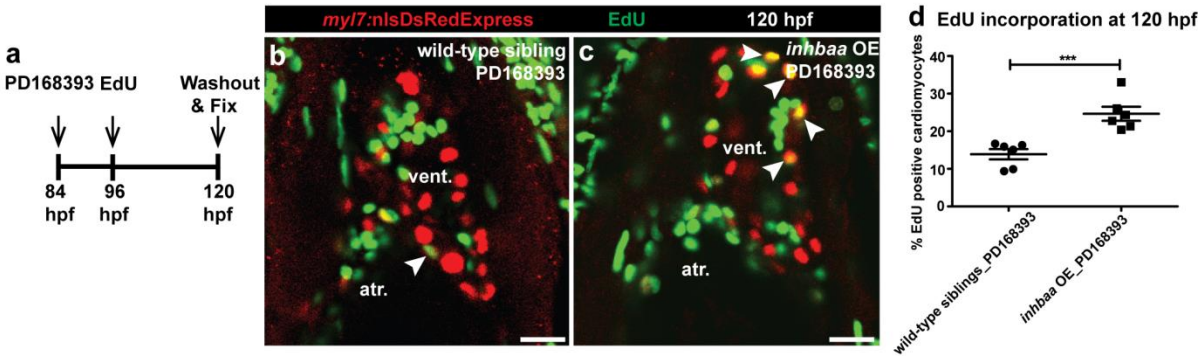

Figure 4.28. *inhbaa* GOF promotes cardiomyocyte proliferation during the inhibition of ErbB2 signaling. (**a**) Experimental setup of PD168393 treatment, EdU incubation, washing out the compounds and fixing the larvae. (**b, c**) Hearts of 120 hpf PD168393 treated wild-type sibling and *inhbaa* OE larvae in *Tg(myl7:nlsDsRedExpress)* background, immunostained for DsRed (red), followed by EdU labeling (green). (**d**) Quantification of cardiomyocyte proliferation in 120 hpf PD168393-treated wild-type sibling (n=6) and *inhbaa* OE (n=6) ventricles. All cell counts were performed on non-overlapping confocal planes (thickness, 1µm). Data are mean ± s.e.m., ***P ≤ 0.001, Student's t-test, two-tailed. Scale bars, 20 µm. vent., ventricle; atr., atrium. Figure submitted in Dogra et al. (manuscript under revision).

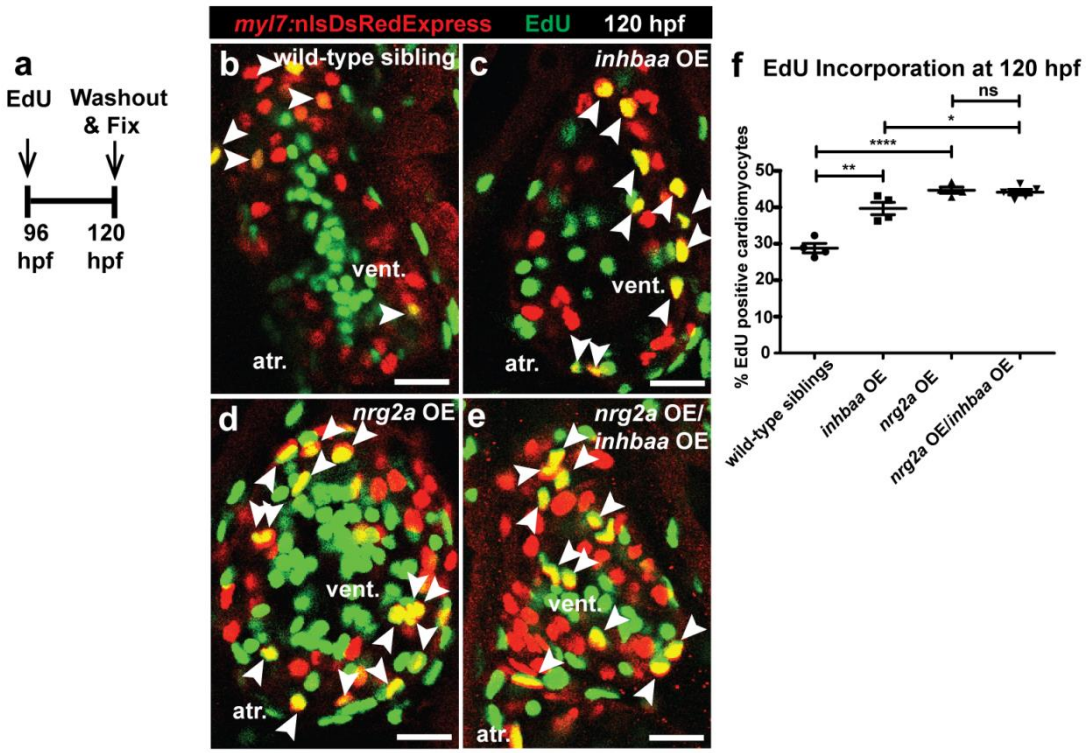

Figure 4.29. *inhbaa* GOF and *nrg2a* GOF do not lead to additive effect on cardiomyocyte proliferation. (**a**) Experimental setup of EdU treatment, washing out EdU and larvae fixation. (**b-e**) Hearts of 120 hpf wild-type sibling, *inhbaa* OE, *nrg2a* OE and *nrg2a* OE/*inhbaa* OE larvae in *Tg(myl7:nlsDsRedExpress)* background, immunostained for DsRed (red) and EdU labeled (green). (**f**) Quantification of cardiomyocyte proliferation in 120 hpf wild-type sibling (n=4), *inhbaa* OE (n=4), *nrg2a* OE (n=4) and *nrg2a* OE/*inhbaa* OE (n=5) ventricles. All cell counts were performed on non-overlapping confocal planes (thickness, 1µm). Data are mean ± s.e.m., ns: no significant changes observed, *P ≤ 0.05, **P ≤ 0.01 and ****P ≤ 0.0001, Student's t-test, two-tailed. Scale bars, 20 µm. vent., ventricle; atr., atrium. Figure submitted in Dogra et al. (manuscript under revision). The *nrg2a* OE transgenic line used in Figure 4.29 d-f has been provided by collaborator Seyed Javad Rasouli.

4.15 *inhbaa* GOF competes with *mstnb* GOF to regulate cardiomyocyte proliferation.

So far, I observed that overexpressing *inhbaa* results in enhanced cardiomyocyte proliferation through an ErbB2 independent mechanism. Further, in order to investigate whether *mstnb* and *inhbaa* collaboratively regulate cardiomyocyte proliferation, *inhbaa* OE line was crossed with the *mstnb* OE line in the *Tg(myl7:nlsDsRedExpress)* background and EdU incorporation was analyzed (**Figure 4.30a**), followed by genotyping. Intriguingly, there was a significant reduction in the number of EdU incorporating cardiomyocytes due to *mstnb* OE alone compared to wild-type siblings (**Figure 4.30b, d, f**). Moreover, it was observed that in the

presence of both *mstnb* OE and *inhbaa* OE, *mstnb* overexpression reduces the cardiomyocyte EdU incorporation induced by *inhbaa* overexpression and brings it down to wild-type levels (**Figure 4.30b-f**), suggesting that Mstnb and Inhbaa compete in controlling cardiomyocyte proliferation. (Certain lines in this section 4.15 have been quoted verbatim from Dogra et al. (manuscript under revision)).

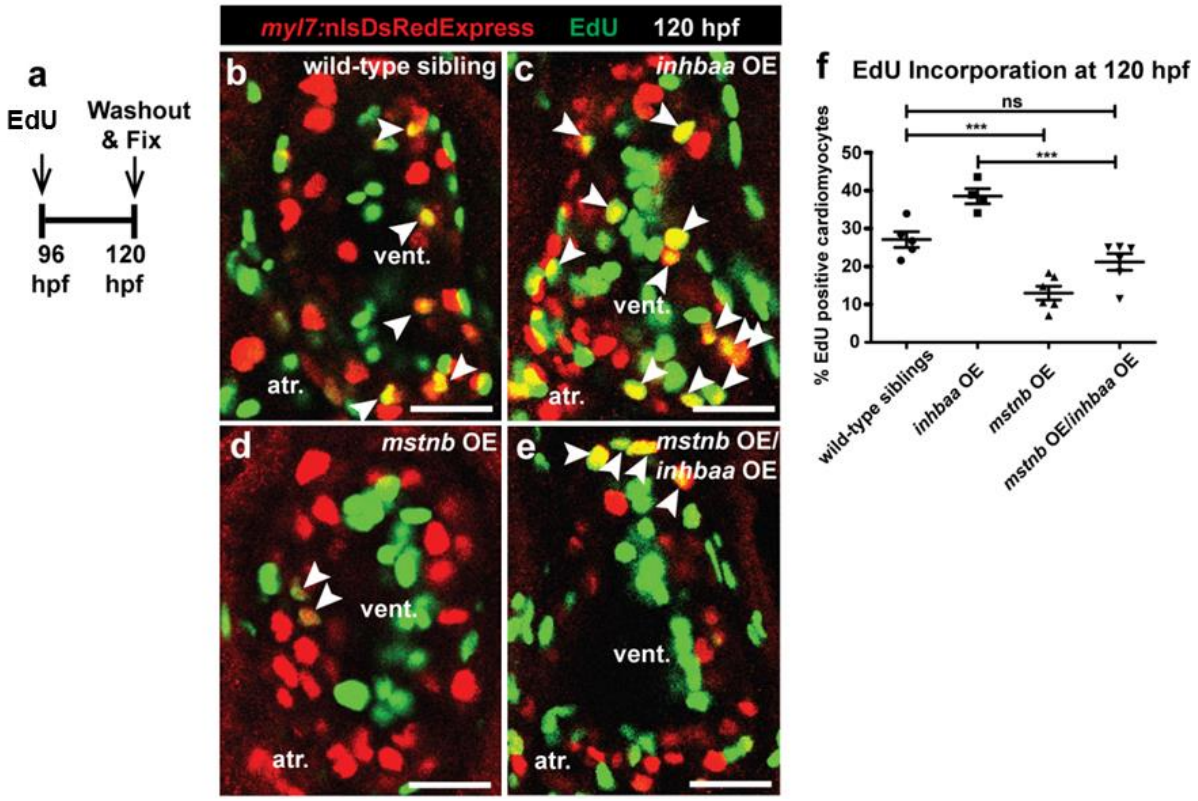

Figure 4.30. *inhbaa* GOF competes with *mstnb* GOF to regulate cardiomyocyte proliferation. (**a**) Experimental setup of EdU treatment, followed by fixation. (**b-e**) Hearts of 120 hpf wild-type sibling, *inhbaa* OE, *mstnb* OE and *mstnb* OE/*inhbaa* OE larvae in *Tg(myl7:nlsDsRedExpress)* background, immunostained for DsRed (red), followed by EdU labeling (green). (**f**) Quantification of cardiomyocyte proliferation in 120 hpf wild-type sibling (n=5), *inhbaa* OE (n=4), *mstnb* OE (n=6) and *mstnb* OE/*inhbaa* OE (n=6) ventricles. All cell counts were performed on non-overlapping confocal planes (thickness, 1µm). Data are mean ± s.e.m., ns: no significant changes observed, ***P ≤ 0.001, Student's t-test, two-tailed. Scale bars, 20 µm. vent., ventricle; atr., atrium. Figure submitted in Dogra et al. (manuscript under revision).

4.16 *mstnb* and *inhbaa* overexpression activate distinct Smad-dependent transcriptional targets.

Further on, I aimed to decipher the molecular mechanisms underlying the differential regulation of cardiomyocyte proliferation and thereby, cardiac regeneration by *mstnb* and *inhbaa*. Myostatin and Activin have been reported to work through the TGF-β signaling cascade, leading to the phosphorylation of the downstream signal transducers, Smad2 and Smad3 (Massagué and Gomis, 2006; Massagué, 2012; Rebbapragada et al., 2003). Smad2, along with Smad4 and transcription factors including FAST1/2, binds to the Activin Response Elements (ARE) present in the promoter regions of target genes (Chen et al., 1997, 1996; Labbé et al., 1998). Likewise, Smad3 binds to the Smad Binding Elements (SBE) present in the promoter regions of target genes (Jonk et al., 1998; Stroschein et al., 1999). Therefore, to identify potentially distinct transcriptional target genes of Mstnb and Inhbaa signaling, I made use of the published Smad2 reporter line, *Tg(ARE:EGFP)* (van Boxtel et al., 2015) and Smad3 reporter line *Tg(12XSBE:EGFP)* (Casari et al., 2014). After injecting *mstnb-2A-H2B-mcherry* and *inhbaa-2A-H2B-mcherry* mRNA in *Tg(ARE:EGFP)* and *Tg(12XSBE:EGFP)*embryos at the one-cell stage, I quantified *EGFP* mRNA expression at 48 hpf by RT-qPCR (**Figure 4.31**). I observed a robust induction of Smad2 reporter expression and a downregulation of Smad3 reporter expression in *mstnb-2A-H2B-mcherry* mRNA injected embryos (**Figure 4.31**). On the other hand, there was an induction of Smad3 reporter expression and a decline in Smad2 reporter expression after *inhbaa-2A-H2B-mcherry* mRNA injections (**Figure 4.31**). Further, to make sure that the P2A labelling strategy did not affect the protein function and overall specificity, I performed the aforementioned experiments with non-tagged wild-type versions and observed results similar in magnitude and specificity (**Figure 4.31**). This differential regulation of the activities of distinct Smad response elements by *mstnb* and *inhbaa* could possibly account for their opposite influence on cardiomyocyte proliferation.

To validate these above-mentioned results, I examined the transcriptional response of several known targets of TGF-β signaling in response to *mstnb* or *inhbaa* overexpression. Several TGF-β target genes have been reported to be specific targets of Smad2, including *Gsc* and *Mix.2* (Chen et al., 1996; Labbé et al., 1998) or Smad3, including *JunB* and *PAI-1* (Jonk et al., 1998; Stroschein et al., 1999). Therefore, by RT-qPCR, I analyzed the expression of these target genes and their paralogs in 48 hpf *mstnb-2A-H2B-mcherry* and *inhbaa-2A-H2B-mcherry* mRNA injected embryos. Notably, there was an upregulation of Smad2 target gene expression after *mstnb* overexpression but a downregulation of their expression by *inhbaa*

overexpression (**Figure 4.32**). Conversely, I observed an upregulation of Smad3 target gene expression after *inhbaa* overexpression but a downregulation of their expression by *mstnb* overexpression (**Figure 4.33**). Next, I investigated whether the expression of these Smad target genes gets affected by *mstnb* and *inhbaa* overexpression in the injured adult heart. Thus, by performing RT-qPCR at 4 dpci, I observed that Smad2 target gene expression was induced in *mstnb* OE hearts; however there was either no significant effect or a transcriptional downregulation observed in *inhbaa* OE hearts (**Figure 4.34**). Conversely, the expression of Smad3 target genes was induced in *inhbaa* OE hearts, but their expression was either unaffected or downregulated in *mstnb* OE hearts (**Figure 4.35**). In sum, these results suggest that Smad2 and Smad3 activities are inversely regulated by *mstnb* and *inhbaa*. (Certain lines in this section 4.16 have been quoted verbatim from Dogra et al. (manuscript under revision)).

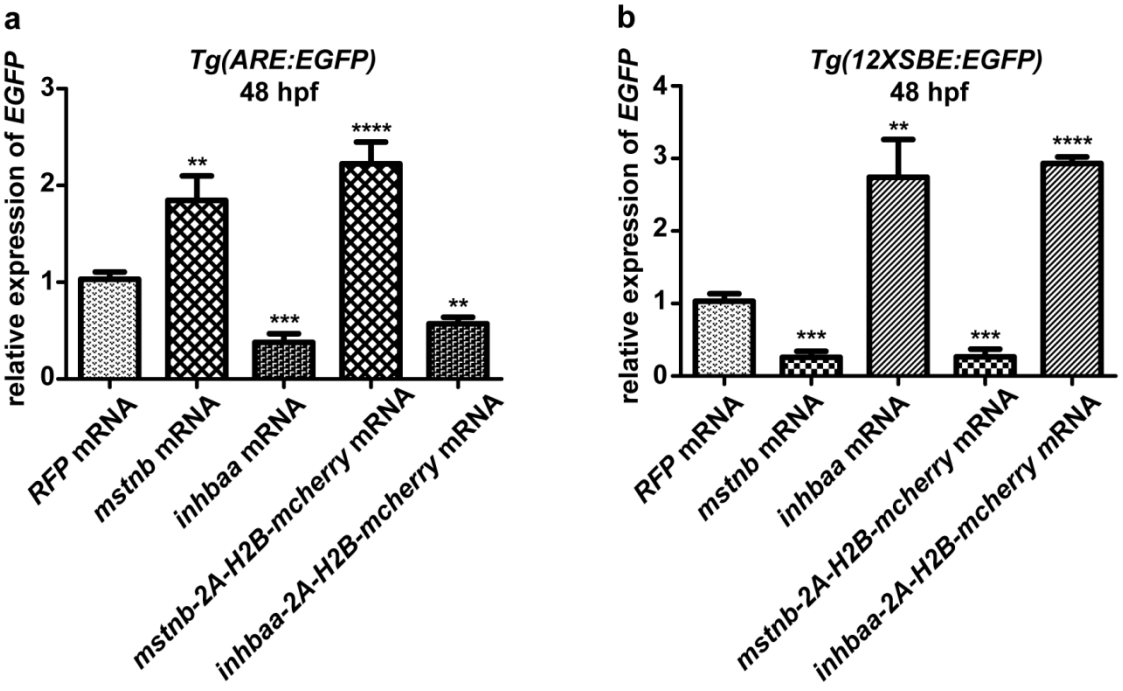

Figure 4.31. *mstnb* and *inhbaa* inversely regulate the activities of Smad2 and Smad3 response elements. (**a**) RT-qPCR analysis for relative *EGFP* mRNA expression in *mstnb* mRNA, *inhbaa* mRNA, *mstnb-2A-H2B-EGFP* mRNA and *inhbaa-2A-H2B-EGFP* mRNA injected 48 hpf *Tg(ARE:EGFP)* embryos compared to *RFP* mRNA injected (n=2 x 10 embryos assessed as 2 biological and 2 technical replicates). (**b**) RT-qPCR analysis for relative *EGFP* mRNA expression in *mstnb* mRNA, *inhbaa* mRNA, *mstnb-2A-H2B-EGFP* mRNA and *inhbaa-2A-H2B-EGFP* mRNA injected 48 hpf *Tg(12XSBE:EGFP)* embryos compared to *RFP* mRNA injected (n=2 x 10 embryos assessed as 2 biological and 2 technical replicates). Data are mean ± s.e.m., **P ≤ 0.01, ***P ≤ 0.001 and ****P ≤ 0.0001, Student's t-test, two-tailed. Figure submitted in Dogra et al. (manuscript under revision).

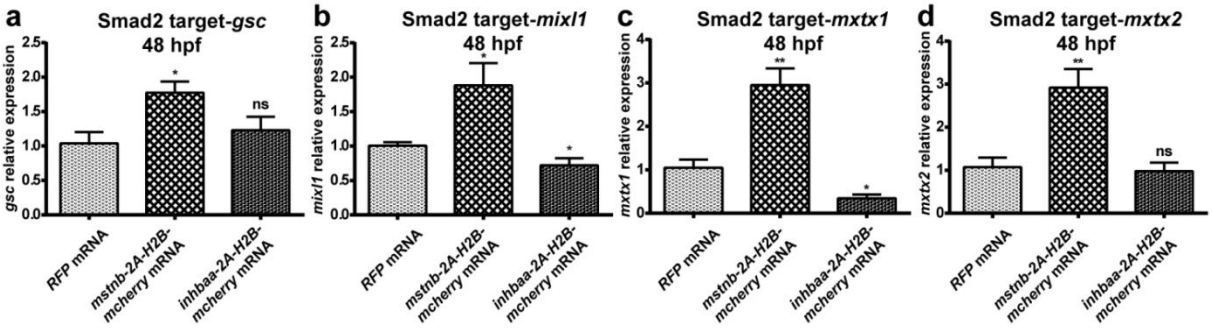

Figure 4.32. *mstnb* and *inhbaa* inversely regulate Smad2 activity during early embryonic development. (**a-d**) RT-qPCR analysis for Smad2 target gene expression in *mstnb-2A-H2B-mcherry* mRNA or *inhbaa-2A-H2B-mcherry* mRNA injected 48 hpf embryos compared to *RFP* mRNA injected (n=2 x 10 embryos assessed as 2 biological and 2 technical replicates). Data are mean ± s.e.m., ns: no significant changes observed, *P ≤ 0.05 and **P ≤ 0.01, Student's t-test, two-tailed. Figure submitted in Dogra et al. (manuscript under revision).

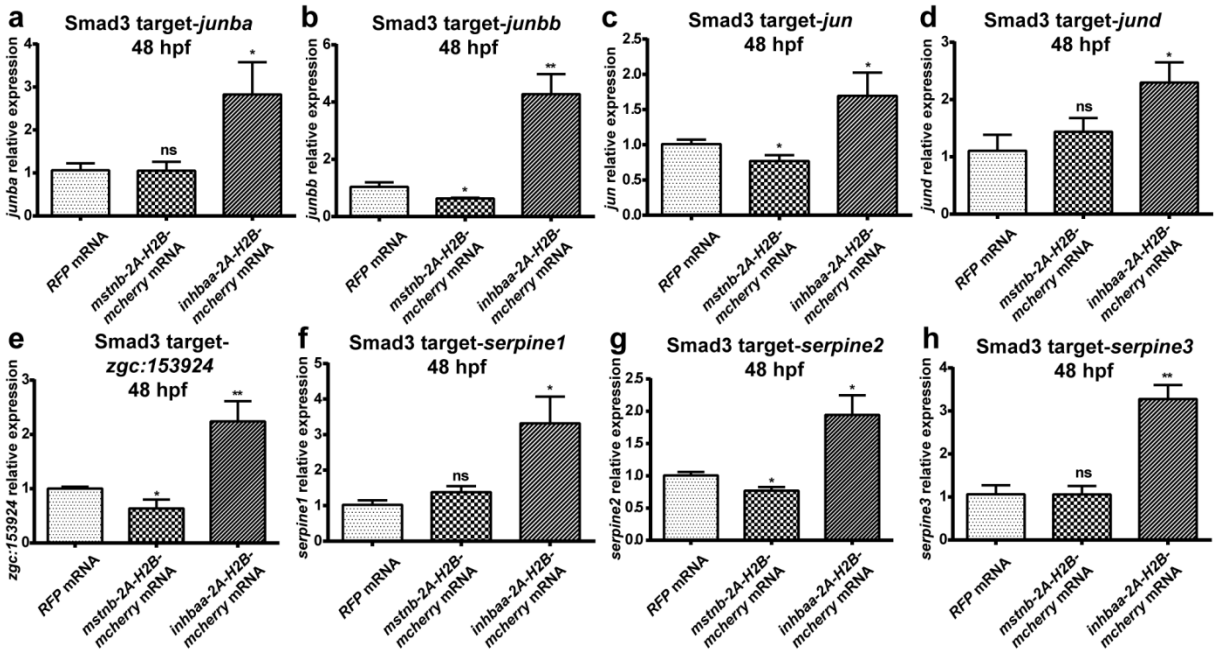

Figure 4.33. *mstnb* and *inhbaa* inversely regulate Smad3 activity during early embryonic development. (**a-h**) RT-qPCR analysis for Smad3 target gene expression in *mstnb-2A-H2B-mcherry* mRNA or *inhbaa-2A-H2B-mcherry* mRNA injected 48 hpf embryos compared to *RFP* mRNA injected (n=2 x 10 embryos assessed as 2 biological and 2 technical replicates). Data are mean ± s.e.m., ns: no significant changes observed, *P ≤ 0.05 and **P ≤ 0.01- Student's t-test, two-tailed. Figure submitted in Dogra et al. (manuscript under revision).

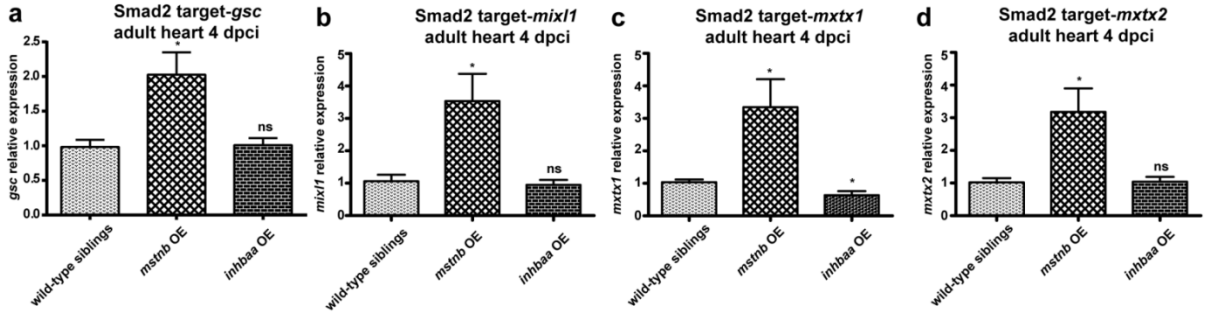

Figure 4.34. *mstnb* and *inhbaa* inversely regulate Smad2 activity in the injured adult heart. (**a-d**) RT-qPCR analysis for Smad2 target gene expression in *mstnb* OE and *inhbaa* OE 4 dpci adult hearts compared to 4 dpci wild-type hearts (n=2 x 3 cardiac ventricles assessed as 2 biological and 2 technical replicates). Data are mean ± s.e.m., ns: no significant changes observed, *P ≤ 0.05, Student's t-test, two-tailed. Figure submitted in Dogra et al. (manuscript under revision).

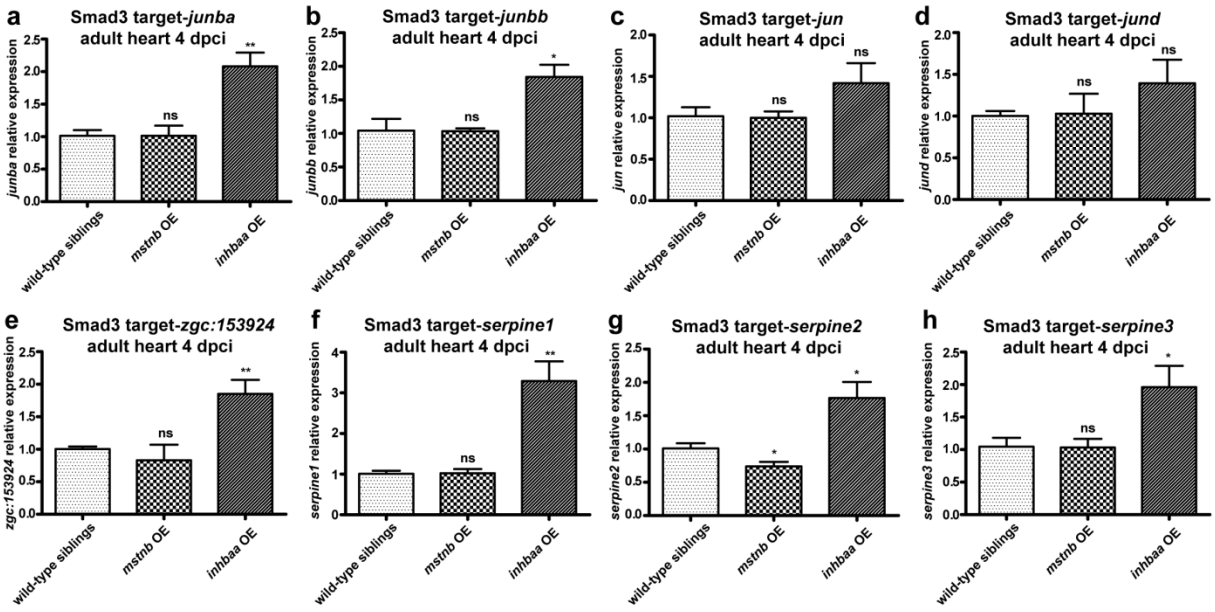

Figure 4.35. *mstnb* and *inhbaa* inversely regulate Smad3 activity in the injured adult heart. (**a-h**) RT-qPCR analysis for Smad3 target gene expression in *mstnb* OE and *inhbaa* OE 4 dpci adult hearts compared to 4 dpci wild-type hearts (n=2 x 3 cardiac ventricles assessed as 2 biological and 2 technical replicates). Data are mean ± s.e.m., ns: no significant changes observed, *P ≤ 0.05 and **P ≤ 0.01- Student's t-test, two-tailed. Figure submitted in Dogra et al. (manuscript under revision).

4.17 *mstnb* and *inhbaa* inversely regulate myocardial Smad3 phosphorylation during cardiac regeneration.

It has been previously shown that Smad3-dependent TGF-β signaling is associated with cardiac regeneration as the pharmacological inhibition of Activin type 1 receptors led to a reduction in the number of pSmad3^{+} cardiomyocytes and eventually blocked cardiac regeneration (Chablais and Jazwinska, 2012). Similarly, another study has shown that the inhibition of TGF-β signaling suppresses cardiomyocyte proliferation in zebrafish (Choi et al., 2013). Thus, to investigate whether *mstnb* and *inhbaa* influence the myocardial Smad3 phosphorylation during cardiac regeneration, I performed immunostainings for pSmad3 and MF-20 using a DAPI counterstain, followed by quantification of pSmad3^{+} cardiomyocytes proximal to the injured area in the respective gain- and loss-of-function genotypes at 14 dpci. Interestingly, the overexpression of *mstnb* suppressed myocardial Smad3 phosphorylation, as there was a reduction of 28% (±10% s.e.m.) in the number of pSmad3^{+} cardiomyocytes in *mstnb* OE compared to wild-type siblings (**Figure 4.36a-c**). However, the overexpression of *inhbaa* induced Smad3 phosphorylation, leading to an increase of 118% (±20% s.e.m.) in the number of pSmad3^{+} cardiomyocytes compared to control (**Figure 4.36d-f**). Notably, I also observed an induction of Smad3 phosphorylation in the cardiomyocytes of *mstnb*$^{-/-}$ animals, with an increase of 66% (±21% s.e.m.) in the number of pSmad3+ cardiomyocytes compared to wild-type siblings (**Figure 4.37a-c**). Further, I also observed a 26% (±7.5% s.e.m.) reduction in the number of pSmad3^{+} cardiomyocytes in *inhbaa*$^{-/-}$ compared to control (**Figure 4.37d-f**), which suggests that Inhbaa is important for inducing the phosphorylation of Smad3 during cardiac regeneration. Altogether, these results indicate that Mstnb and Inhbaa work antagonistically to one another in controlling Smad3 phosphorylation levels, a seemingly crucial event during zebrafish cardiac regeneration. (Certain lines in this section 4.17 have been quoted verbatim from Dogra et al. (manuscript under revision)).

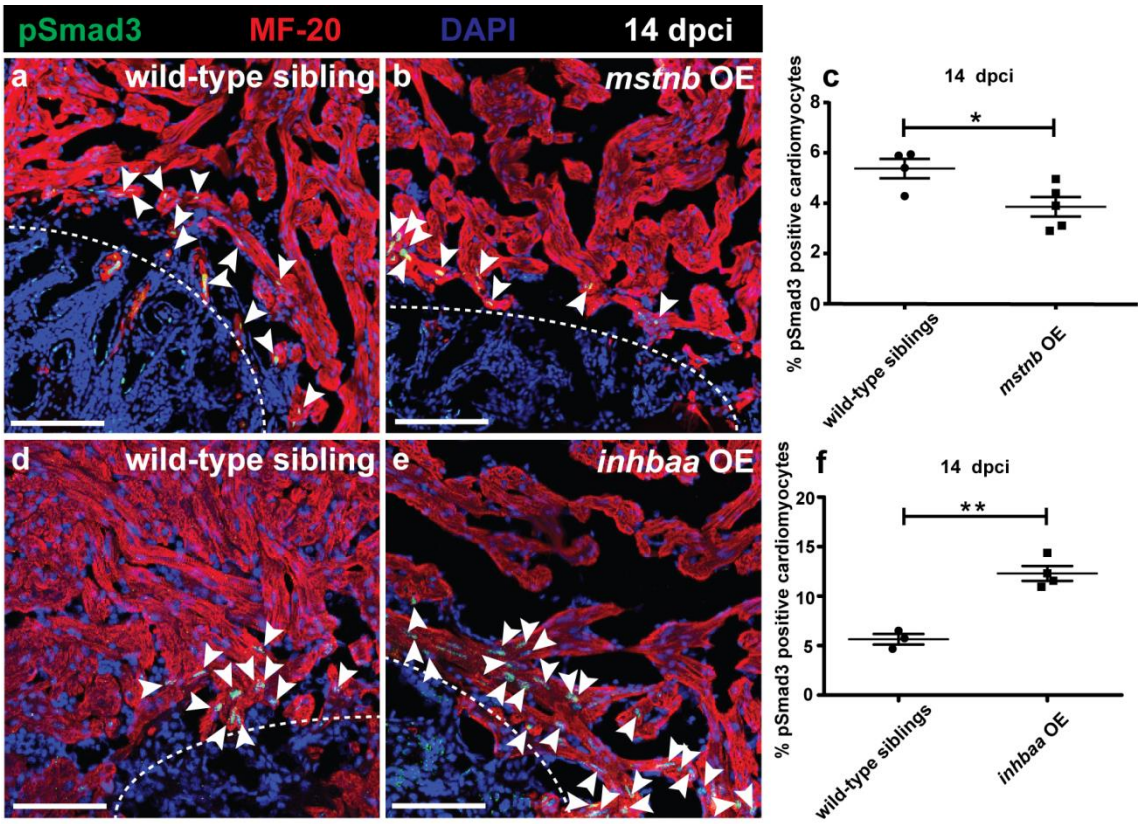

Figure 4.36. ***mstnb* OE and *inhbaa* OE inversely regulate myocardial Smad3 phosphorylation.** (**a, b**) Wild-type sibling and *mstnb* OE cryoinjured heart sections at 14 dpci, immunostained for pSmad3 (green) and MF-20 (red), followed by DAPI staining (blue). White dotted regions delineate the injured area and white arrowheads point to pSmad3^{+} cardiomyocytes near the injured area. (**c**) Quantification of pSmad3^{+} cardiomyocytes in wild-type sibling (n=4) and *mstnb* OE (n=5) cryoinjured hearts in the 100 µm region adjacent to the injured area at 14 dpci. (**d, e**) Wild-type sibling and *inhbaa* OE cryoinjured heart sections at 14 dpci, immunostained for pSmad3 (green) and MF-20 (red), followed by DAPI staining (blue). (**f**) Quantification of pSmad3^{+} cardiomyocytes in wild-type sibling (n=3) and *inhbaa* OE (n=4) cryoinjured hearts in the 100 µm region adjacent to the injured area at 14 dpci. All cell counts were performed on three sections from each heart and each data point on dot plot represents one heart. Data are mean ± s.e.m., *P ≤ 0.05, **P ≤ 0.01, Student's t-test, two-tailed). Scale bars, 100 µm. vent., ventricle; atr., atrium. Figure submitted in Dogra et al. (manuscript under revision).

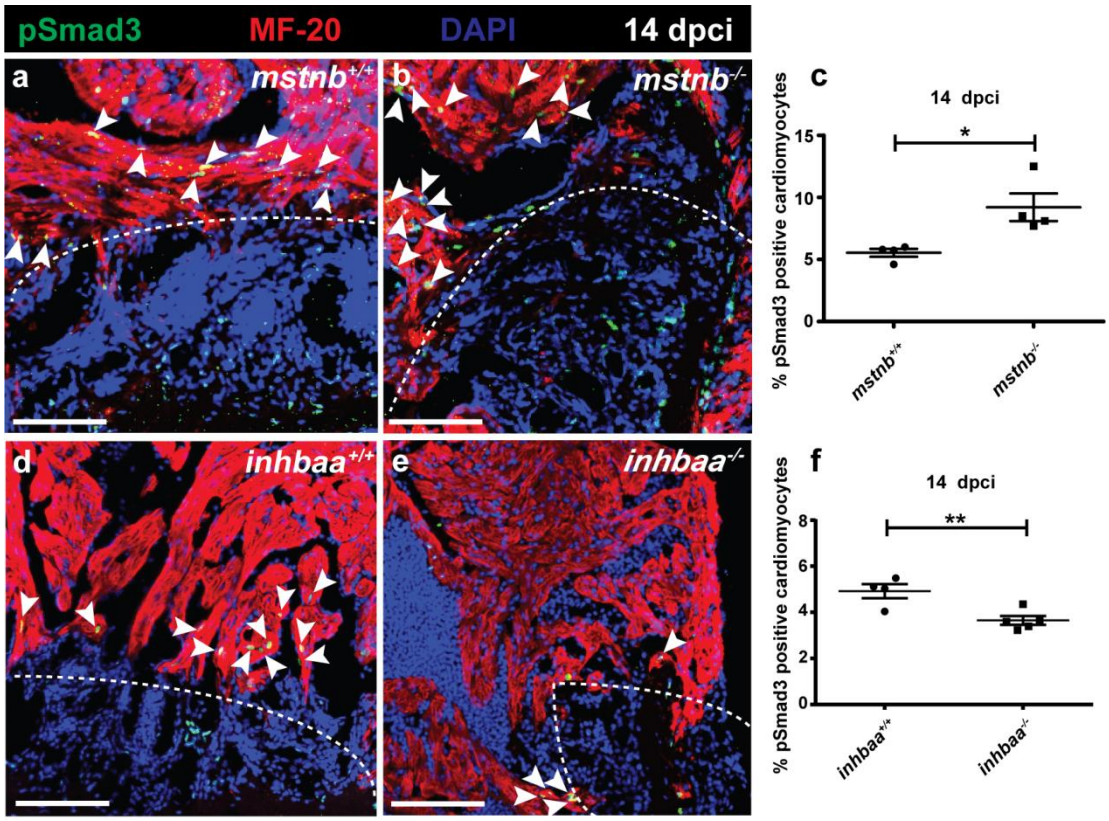

Figure 4.37. *mstnb* LOF and *inhbaa* LOF inversely regulate myocardial Smad3 phosphorylation. (**a, b**) *mstnb*$^{+/+}$ and *mstnb*$^{-/-}$ cryoinjured heart sections at 14 dpci, immunostained for pSmad3 (green) and MF-20 (red), followed by DAPI staining (blue). (**c**) Quantification of pSmad3^{+} cardiomyocytes in *mstnb*$^{+/+}$ (n=4) and *mstnb*$^{-/-}$ (n=4) cryoinjured hearts in the 100 µm region adjacent to the injured area at 14 dpci. (**d, e**) *inhbaa*$^{+/+}$ and *inhbaa*$^{-/-}$ cryoinjured heart sections at 14 dpci, immunostained for pSmad3 (green) and MF-20 (red), followed by DAPI staining (blue). (**f**) Quantification of pSmad3^{+} cardiomyocytes in *inhbaa*$^{+/+}$ (n=4) and *inhbaa*$^{-/-}$ (n=5) cryoinjured hearts in the 100 µm region adjacent to the injured area at 14 dpci. All cell counts were performed on three sections from each heart and each data point on dot plot represents one heart. Data are mean ± s.e.m., *P ≤ 0.05, **P ≤ 0.01, Student's t-test, two-tailed). Scale bars, 100 µm. vent., ventricle; atr., atrium. Figure submitted in Dogra et al. (manuscript under revision).

4.18 Pharmacological inhibition of Smad3 phosphorylation leads to reduced cardiomyocyte proliferation.

Myocardial Smad3 phosphorylation is induced at the site of injury during cardiac regeneration (Chablais and Jazwinska, 2012). The above mentioned data from regenerating *mstnb* OE and *inhbaa*$^{-/-}$ hearts show that myocardial Smad3 phosphorylation in proximity to the injured area was reduced (**Figure 4.36a-c, 4.37d-f**), as was cardiomyocyte proliferation. Therefore, to test the hypothesis that Smad3 phosphorylation is directly linked to cardiomyocyte proliferation, a small molecule inhibitor, SIS3 was used, which is reported to block TGF-β mediated Smad3

phosphorylation (Denis et al., 2016; Jinnin et al., 2006). I first checked whether SIS3 works as a specific inhibitor of Smad3 phosphorylation and by RT-qPCR analysis, I observed a significant downregulation in Smad3 target gene expression in 72 hpf SIS3-treated hearts (**Figure 4.38d-h**), however Smad2 target gene expression remained unaffected (**Figure 4.38a-c**). I also examined whether the established Activin type 1 receptor inhibitor, SB431542 affects Smad target gene expression, by performing RT-qPCR on 72 hpf SB431542-treated hearts. There was a significant downregulation in both Smad2 and Smad3 target gene expression (**Figure 4.38a-h**), confirming that this inhibitor blocks the complete TGF-β pathway as reported previously (Inman et al., 2002). Next, I treated the *Tg(myl7:nlsDsRedExpress)* larvae with 3µM concentration of SIS3 and analyzed cardiomyocyte proliferation by performing immunostaining for DsRed, followed by EdU labeling at 120 hpf (**Figure 4.39a**). Quantification of the number of EdU incorporating cardiomyocytes in the larval cardiac ventricles revealed that SIS3 treatment led to a significant reduction of 29% (±8.7% s.e.m.) in EdU incorporation (**Figure 4.39b-d**), suggesting that cardiomyocyte proliferation is dependent on Smad3 phosphorylation. (Certain lines in this section 4.18 have been quoted verbatim from Dogra et al. (manuscript under revision)).

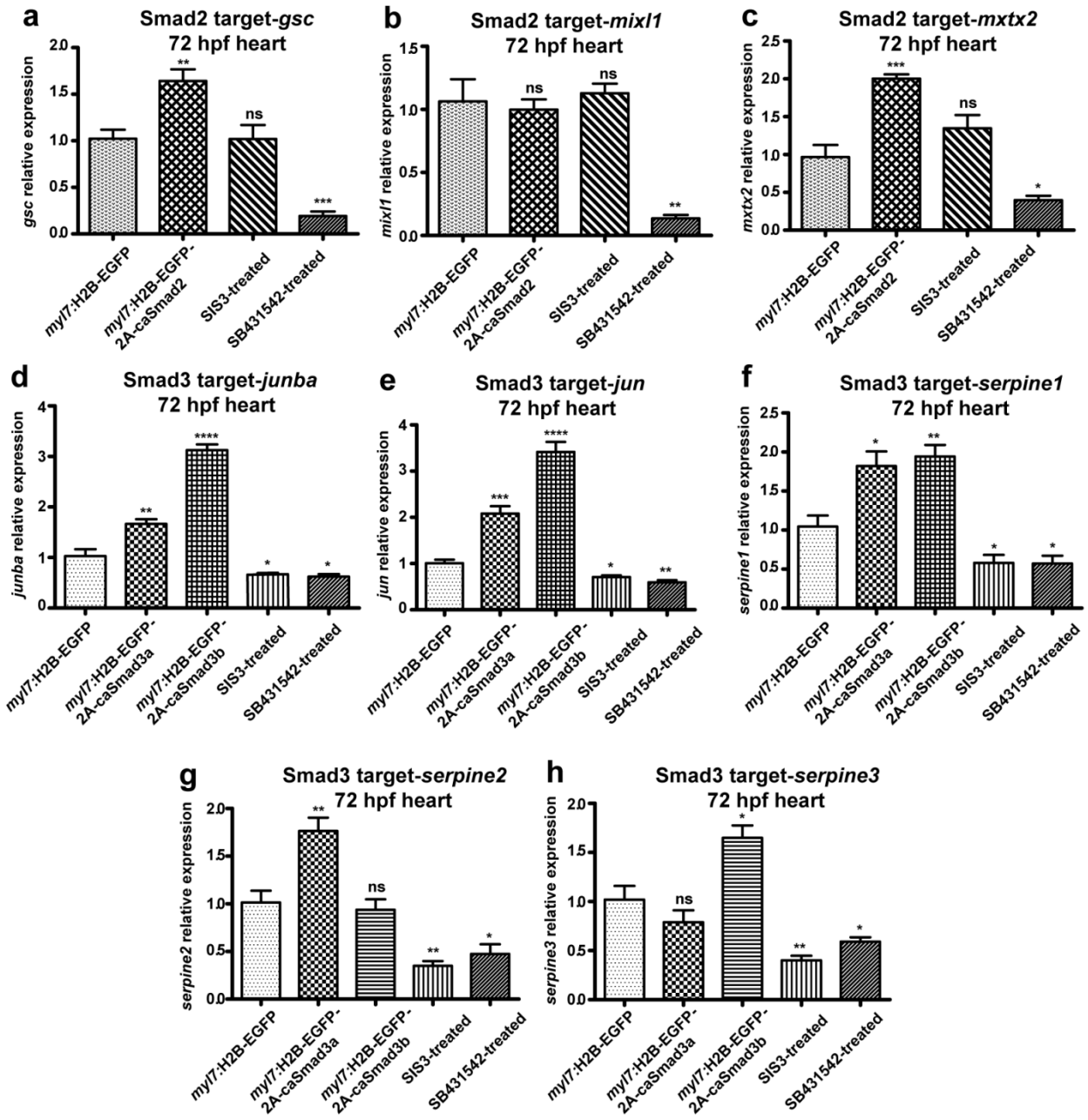

Figure 4.38. Validation of caSmad2/3 constructs and TGF-β pathway inhibitors. (**a-c**) RT-qPCR analysis for Smad2 target gene expression in *myl7:H2B-GFP*, *caSmad2*, SIS3-treated and SB431542-treated 72 hpf hearts (n=2 x 30 hearts assessed as 2 biological and 2 technical replicates). (**d-h**) RT-qPCR analysis for Smad3 target gene expression in *myl7:H2B-GFP*, *caSmad3a*, *caSmad3b*, SIS3-treated and SB431542-treated 72 hpf hearts (n=2 x 30 hearts assessed as 2 biological and 2 technical replicates). Data are mean ± s.e.m., ns: no significant changes observed, *P ≤ 0.05, **P ≤ 0.01, ***P ≤ 0.001 and ****P ≤ 0.0001, Student's t-test, two-tailed. Figure submitted in Dogra et al. (manuscript under revision).

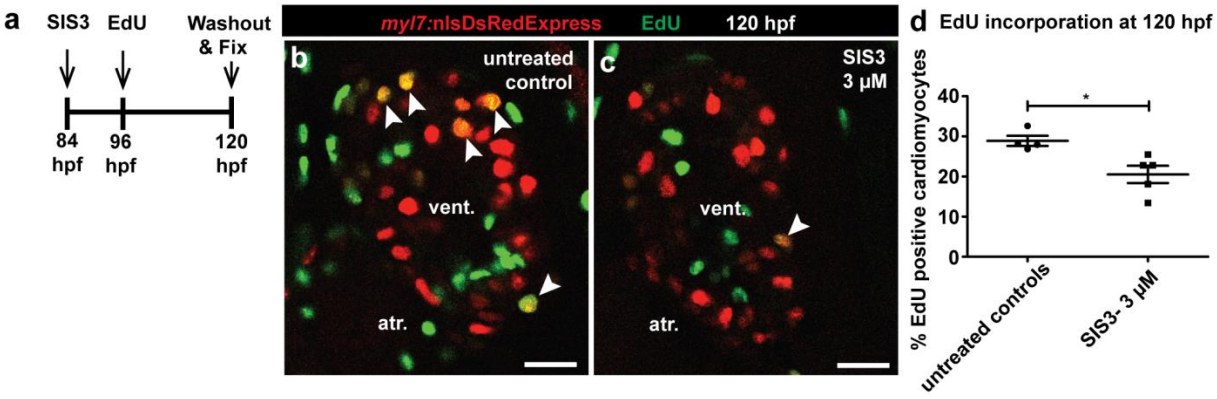

Figure 4.39. Chemical inhibition of Smad3 phosphorylation suppresses cardiomyocyte proliferation. (**a**) Experimental setup of SIS3 treatment and EdU incubation, followed by washout and larvae fixation. (**b, c**) Hearts of untreated control and 3 µM SIS3 treated 120 hpf larvae in *Tg(myl7:nlsDsRedExpress)*background, immunostained for DsRed (red), followed by EdU labeling (green). (**d**) Quantification of cardiomyocyte proliferation in untreated control (n=4) and 3 µM SIS3 treated (n=5) ventricles of 120 hpf larvae. All cell counts were performed on non-overlapping confocal planes (thickness, 1µm). Data are mean ± s.e.m., *P ≤ 0.05, Student's t-test, two-tailed. Scale bars, 20 µm. vent., ventricle; atr., atrium. Figure submitted in Dogra et al. (manuscript under revision).

4.19 Generation of constitutively active versions of Smads.

To further validate my results, I analyzed the effects of constitutively active (ca) Smad2, Smad3a and Smad3b on cardiomyocyte proliferation following mosaic overexpression. The constitutively active versions of Smads have been reported to mimic constitutive Smad phosphorylation, by creating amino acid substitutions of three carboxyl-terminal Serines with Aspartic acid (Chipuk et al., 2002). Thus, with the similar approach, I generated constructs expressing constitutively active, phosphomimetic, Smads under the cardiomyocyte-specific *myl7* promoter, namely *Tg(myl7:H2B-EGFP-2A-caSmad2)* (*caSmad2* hereafter), *Tg(myl7:H2B-EGFP-2A-caSmad3a)* (*caSmad3a* hereafter), *Tg(myl7:H2B-EGFP-2A-caSmad3b)* (*caSmad3b* hereafter), and *Tg(myl7:H2B-EGFP)* as control (**Figure 4.40**), by using Cold Fusion technology. I first tested whether the constitutively active constructs were functional and specific, by performing RT-qPCR analysis for Smad2 and Smad3 target gene expression on hearts of 72 hpf larvae obtained by outcrossing *caSmad2*, *caSmad3a* and *caSmad3b* founders. There was an upregulation in Smad2 target gene expression in caSmad2 hearts (**Figure 4.38a-c**) and similarly, an upregulation in Smad3 target gene expression in caSmad3a and caSmad3b hearts (**Figure 4.38d-h**). (Certain lines in this section 4.19 have been quoted verbatim from Dogra et al. (manuscript under revision)).

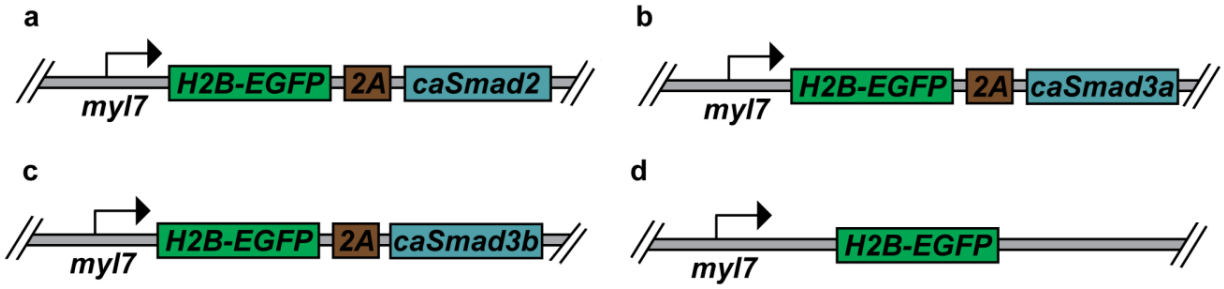

Figure 4.40. Generation of constitutively active Smad2/3 constructs. (**a-d**) Schematic of cardiomyocyte-specific constructs, *Tg(myl7:H2B-EGFP-2A-caSmad2), Tg(myl7:H2B-EGFP-2A-caSmad3a), Tg(myl7:H2B-EGFP-2A-caSmad3b)* and *Tg(myl7:H2B-EGFP).* Figure submitted in Dogra et al. (manuscript under revision).

4.20 Cardiomyocyte proliferation is inversely regulated through Smad2 and Smad3 activity.

Next, after injection of the ca constructs at the one-cell stage, cardiomyocyte proliferation was analyzed by performing immunostaining for GFP and DsRed, followed by EdU labeling in 120 hpf *Tg(myl7:nlsDsRedExpress)* larvae (**Figure 4.41a**). Interestingly, by comparing GFP^+ cardiomyocytes across all constructs, I found that cardiomyocytes expressing *caSmad2* showed a 50% (±12% s.e.m.) reduction in EdU incorporation compared to cardiomyocytes expressing GFP alone, whereas both *caSmad3a* and *caSmad3b* expression led to an increase of 70% (±18% s.e.m.) and 31% (±12% s.e.m.) in EdU incorporation, respectively (**Figure 4.41b-f**). This result clearly indicates that Smad2 and Smad3 inversely regulate cardiomyocyte proliferation in zebrafish and could potentially explain how different TGF-β ligands of the same family can have opposite effects during regeneration. (Certain lines in this section 4.20 have been quoted verbatim from Dogra et al. (manuscript under revision)).

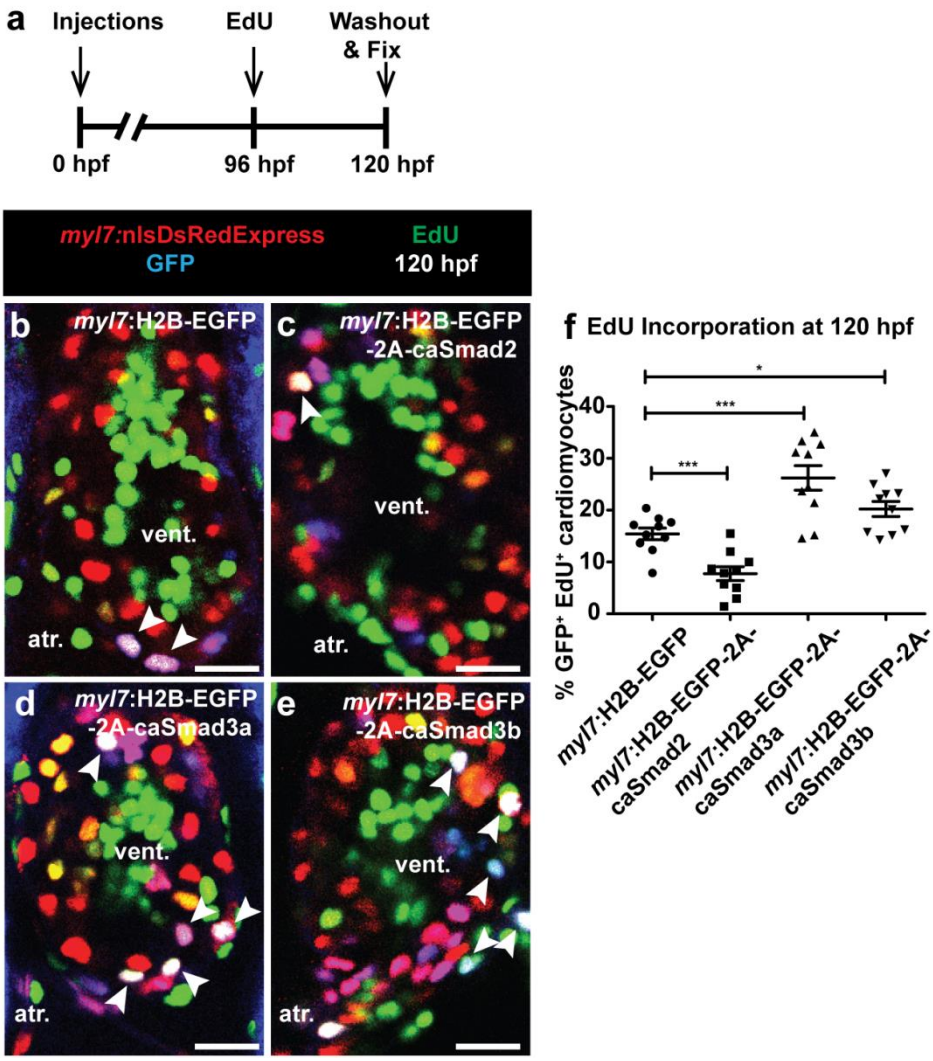

Figure 4.41. Smad2 and Smad3 inversely regulate cardiomyocyte proliferation. (**a**) Experimental setup of injections, EdU incubation and larvae fixation. (**b-e**) Hearts of *myl7:H2B-EGFP*, *myl7:H2B-EGFP-2A-caSmad2*, *myl7:H2B-EGFP-2A-caSmad3a* and *myl7:H2B-EGFP-2A-caSmad3b* injected 120 hpf larvae in *Tg(myl7:nlsDsRedExpress)* background, immunostained for DsRed (red) and GFP (blue), followed by EdU labeling (green). (**f**) Quantification of cardiomyocyte proliferation in the ventricles of *myl7:H2B-EGFP* (n=10), *caSmad2* (n=10), *caSmad3a* (n=10) and *caSmad3b* (n=10) injected 120 hpf larvae. All cell counts were performed on non-overlapping confocal planes (thickness, 1µm). Data are mean ± s.e.m., *P ≤ 0.05 and ***P ≤ 0.001, Student's t-test, two-tailed. Scale bars, 20 µm. vent., ventricle; atr., atrium. Figure submitted in Dogra et al. (manuscript under revision).

4.21 Mstnb and Inhbaa signal through different Activin type 2 receptors to regulate cardiomyocyte proliferation.

Mstn and Inhba have been shown to signal through the same type 2 receptor complex (Massagué and Gomis, 2006; Massagué, 2012; Rebbapragada et al., 2003). I further wanted

to investigate how Mstnb and Inhbaa could function antagonistically if they work through the same signaling pathway. Therefore, to better understand the ligand-receptor relationships, I carried out combined gene knockdown and overexpression experiments. Thus, I co-injected morpholinos (MOs) for the activin type 2 receptor genes (*acvr2aa, acvr2ab, acvr2ba* and *acvr2bb*; refer to **Table 4.1** for gene names) with *mstnb-2A-H2B-EGFP* mRNA or *inhbaa-2A-H2B-mcherry* mRNA in the Smad2 (van Boxtel et al., 2015) and Smad3 (Casari et al., 2014) reporter lines. By RT-qPCR analysis for *EGFP* mRNA expression, I found that co-injection of *acvr2a* MOs (*acvr2aa* and *acvr2ab*) along with *mstnb-2A-H2B-EGFP* mRNA did not influence the effect of *mstnb* overexpression, as Smad2 reporter expression was induced and Smad3 reporter expression was suppressed compared to control (**Figure 4.42a, b**). Conversely, the co-injection of *acvr2b* MOs *(acvr2ba* and *acvr2bb)* along with *mstnb-2A-H2B-mcherry* mRNA significantly reduced the effect of *mstnb* overexpression on Smad2 and Smad3 reporter activity (**Figure 4.42c, d**). These results indicate that Mstnb has a preference for binding Acvr2b over Acvr2a, as per previous studies (Lee and McPherron, 2001; Rebbapragada et al., 2003). Next, I tested the relationship between Inbhaa and the Activin type 2 receptors. I found that the co-injection of *acvr2b* MOs (*acvr2ba* and *acvr2bb*) with *inhbaa-2A-H2B-mcherry* mRNA did not influence the effect of *inhbaa* overexpression, as Smad2 reporter expression was suppressed and Smad3 reporter expression was induced (**Figure 4.42e, f**). However, the co-injection of *acvr2a* MOs (*acvr2aa* and *acvr2ab*) along with *inhbaa-2A-H2B-mcherry* mRNA significantly reduced the effect of *inhbaa* overexpression on Smad2 and Smad3 reporter activity (**Figure 4.42g, h**). These data suggest a previously unreported preference for Inhbaa to signal through Acvr2a over Acvr2b.

Additionally, I investigated the effect of these receptor knockdowns on the cardiomyocyte proliferation in *mstnb* OE and *inhbaa* OE lines, by performing EdU incorporation analysis (**Figure 4.43a**). Since, the effect of *acvr2bb* MO on Smad2 reporter expression was more significant compared to *acvr2ba* MO, I injected *acvr2bb* MO in the *mstnb* OE line and analyzed EdU incorporation in the cardiomyocytes at 72 hpf. There was a significant increase of 94% (±33% s.e.m.) in EdU incorporation in *acvr2bb* MO injected *mstnb* OE larvae compared to control (**Figure 4.43b-e**). This result is in line with the previously mentioned RT-qPCR data, i.e., Acvr2b is a specific receptor for Mstnb, and knocking down *acvr2bb* prevents the suppression of cardiomyocyte proliferation by *mstnb* overexpression. Next, I injected *acvr2aa* MO in *inhbaa* OE line and analyzed cardiomyocyte EdU incorporation at 72 hpf. There was a significant reduction of 70% (±8% s.e.m.) in cardiomyocyte EdU incorporation in *acvr2aa* MO injected *inhbaa* OE larvae compared to control (**Figure 4.43f-i**).

Similarly, this result is in line with the previously obtained RT-qPCR data that Acvr2a is a specific receptor for Inhbaa, and knocking down *acvr2aa* prevents the induction of cardiomyocyte proliferation by *inhbaa* overexpression. Overall, the preference for Mstnb and Inhbaa to signal through Acvr2b and Acvr2a, respectively, possibly explains the opposite effects of these TGF-β ligands on cardiomyocyte proliferation and ultimately on cardiac regeneration. (Certain lines in this section 4.21 have been quoted verbatim from Dogra et al. (manuscript under revision)).

Internal gene name	Ensemble gene name	Ensemble gene ID
acvr2ba	*acvr2b*	ENSDARG00000044422
acvr2bb	ACVR2B	ENSDARG00000103108

Table 4.1. Internal gene names used and their corresponding ensemble names. Table submitted in Dogra et al. (manuscript under revision).

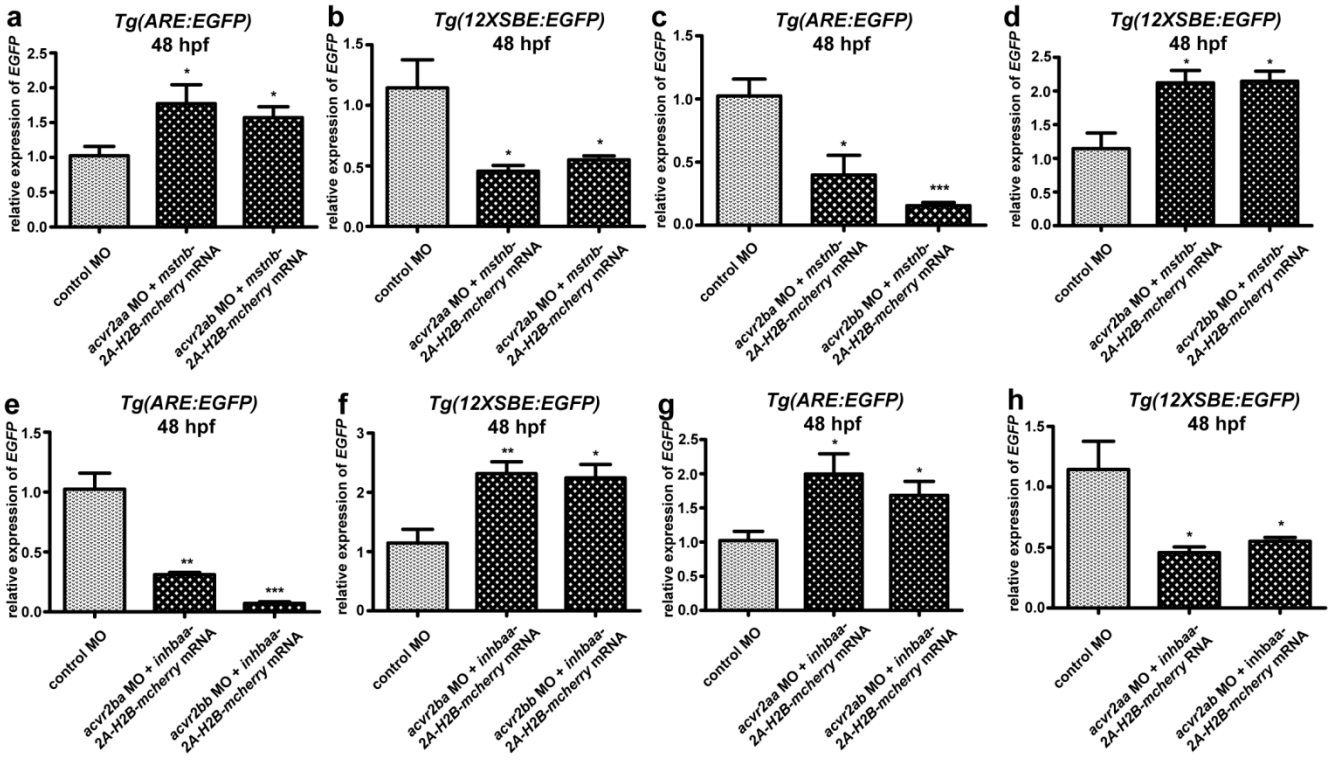

Figure 4.42. Mstnb and Inhbaa show preference for different Activin type 2 receptors. (**a-d**) RT-qPCR analysis for relative *EGFP* mRNA expression in 48 hpf *Tg(ARE:EGFP)* and *Tg(12XSBE:EGFP)* embryos injected with *acvr2aa* MO/*mstnb-2A-H2B-mcherry* mRNA, *acvr2ab* MO/*mstnb-2A-H2B-mcherry* mRNA,

acvr2ba MO/*mstnb-2A-H2B-mcherry* mRNA and *acvr2bb* MO/*mstnb-2A-H2B-mcherry* mRNA compared to control MO injected (n=2 x 10 embryos assessed as 2 biological and 2 technical replicates). (**e-h**) RT-qPCR analysis for relative *EGFP* mRNA expression in 48 hpf *Tg(ARE:EGFP)* and *Tg(12XSBE:EGFP)* embryos injected with *acvr2ba* MO/*inhbaa-2A-H2B-mcherry* mRNA, *acvr2bb* MO/*inhbaa-2A-H2B-mcherry* mRNA, *acvr2aa* MO/*inhbaa-2A-H2B-mcherry* mRNA and *acvr2ab* MO/*inhbaa-2A-H2B-mcherry* mRNA compared to control MO injected (n=2 x 10 embryos assessed as 2 biological and 2 technical replicates). All cell counts were performed on non-overlapping confocal planes (thickness, 1µm). Data are mean ± s.e.m., *P ≤ 0.05, **P ≤ 0.01 and ***P ≤ 0.001, Student's t-test, two-tailed. Scale bars, 20 µm. vent., ventricle; atr., atrium. Figure submitted in Dogra et al. (manuscript under revision).

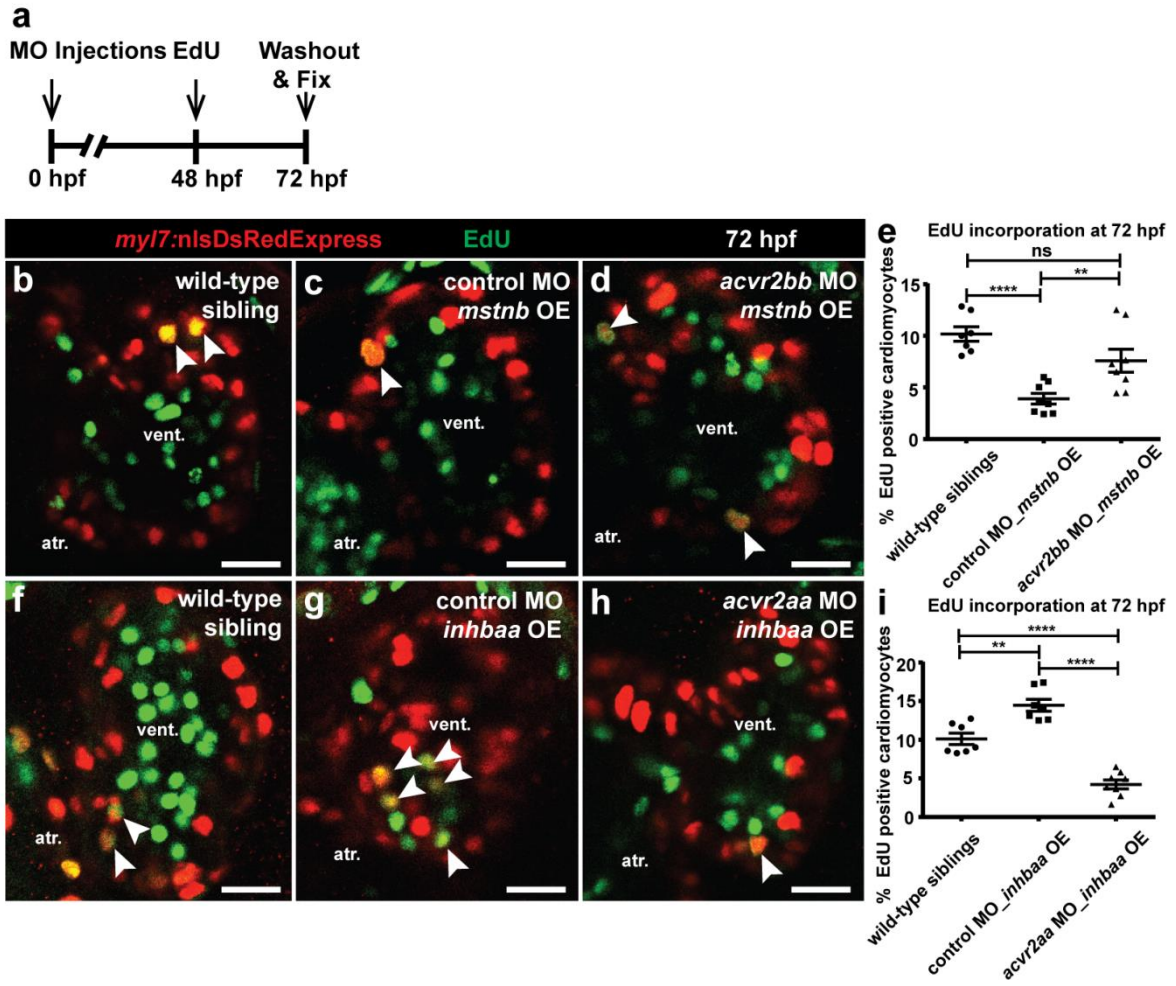

Figure 4.43. Mstnb and Inhbaa signal through different Activin type 2 receptors to regulate cardiomyocyte proliferation. (**a**) Experimental setup of injections, followed by EdU treatment and fixation. (**b-d**) *Tg(myl7:nlsDsRedExpress)* hearts of wild-type sibling, control MO injected *mstnb* OE and *acvr2bb* MO injected *mstnb* OE larvae at 72 hpf; α-DsRed (red), EdU (green). White arrowheads point to proliferating cardiomyocytes (EdU^+/$DsRed^+$). (**e**) Quantification of cardiomyocyte proliferation in wild-type sibling (n=7), control MO injected *mstnb* OE (n=8) and *acvr2bb* MO injected *mstnb* OE (n=8) ventricles at 72 hpf. (**f-h**) *Tg(myl7:nlsDsRedExpress)* hearts of wild-type sibling, control MO injected *inhbaa* OE and *acvr2aa* MO injected *inhbaa* OE larvae at 72 hpf; α-DsRed (red), EdU (green). (**i**) Quantification of cardiomyocyte proliferation in wild-type sibling (n=7), control MO injected *inhbaa* OE (n=7) and *acvr2aa* MO injected *inhbaa*

OE (n=8) ventricles at 72 hpf. All cell counts were performed on non-overlapping confocal planes (thickness, 1µm). Data are mean ± s.e.m., ns: no significant changes observed, **P ≤ 0.01 and ****P ≤ 0.0001 - Student's t-test, two-tailed. Scale bars, 20 µm. vent., ventricle; atr., atrium. Figure submitted in Dogra et al. (manuscript under revision).

5. Discussion

5.1 Current state of knowledge on cardiac regeneration.

According to WHO, CVDs are the leading cause of death globally. In 2015, approximately 17.7 million people died from CVDs, which accounts for 31% of all deaths worldwide. Of these deaths, around 7.4 million were because of CAD and 6.7 million were due to stroke (http://www.who.int/mediacentre/factsheets/fs317/en/).

CVDs refer to a group of heart and blood vessel disorders, including CAD, cerebrovascular disease, peripheral artery disease, congenital heart disease and many more disorders. Heart attacks (also known as Myocardial Infarction (MI)) and strokes are the acute events occurring due to a blockage in blood vessels which supply blood to the heart and brain. The fundamental reason for this blockage is the accumulation of fatty acids, known as plaque in the lumen of these blood vessels. The prolonged absence of blood and oxygen supply to a part of heart damages the heart muscle, eventually leading to the formation of irreplaceable non-contractile scar tissue. This fibrotic scar hinders the proper functioning of the heart, ultimately causing heart attack and fatality. The main risk factors causing heart attacks and stroke include high fat diet, excessive tobacco and alcohol intake, obesity, lack of physical activities, high blood pressure, diabetes as well as hyperlipidemia (http://www.who.int/mediacentre/factsheets/fs317/en/). Consequently, there are extensive medical advancements being introduced to cure the diseased condition, i.e., by dissolving the coronary artery plaque. Further, several active fields of research are trying to develop novel regenerative approaches focusing on the engraftment of stem cell-derived cardiomyocytes into injured hearts (Chong et al., 2014), the stimulation of cardiomyocyte proliferation *in situ* (Bersell et al., 2009), or the *in situ* trans-differentiation of fibroblasts into functional cardiomyocytes (Qian et al., 2012), so as to promote the regeneration of the infarct. However, to date there has been no successful cure for replacing the non-contractile scar formed due to the damaged heart muscle. Interestingly, the mammalian heart including that of humans is unable to regenerate after any kind of cardiac injury, unlike other organs such as kidney (Song et al., 2013) and liver (Nagasue et al., 1987). This inability of adult mammalian heart to regenerate is possibly because the cardiomyocytes present in the vicinity of the lesion are unable to dedifferentiate and divide, so as to give rise to the regenerated myocardium (Steinhauser and Lee, 2011). However, lower vertebrates including zebrafish (Poss et al., 2002) and newts (Witman et al., 2011) can recover from cardiac injury, as the injured myocardium can regenerate into a healthy muscle within a few months.

Cardiac regeneration can be studied in zebrafish by inducing cardiac injury through multiple well-established techniques, including ventricular resection, cryoinjury or genetic cardiomyocyte ablation (Chablais and Jaźwińska, 2012; González-Rosa and Mercader, 2012; Poss et al., 2002; Zhang et al., 2013). Lineage tracing experiments have shown that the remaining cardiomyocytes in the vicinity of injured area undergo dedifferentiation and proliferation to give rise to new cardiac muscle in the injured zebrafish heart (Jopling et al., 2010; Kikuchi et al., 2010). Thus, zebrafish serves as a suitable model system to closely understand the process of cardiac regeneration (Chablais and Jaźwińska, 2012; González-Rosa and Mercader, 2012; Poss et al., 2002; Zhang et al., 2013) and study the underlying molecular mechanisms, which would help in designing novel regenerative therapies for treating the ailing human heart.

Various pathways including RA signaling, EGF signaling, FGF signaling, BMP signaling, VEGF signaling, Il6 class cytokines and others have been implicated in the process of cardiac regeneration and are important for diverse processes including epicardial responses, neovascularization, cardiomyocyte proliferation and scar deposition after injury (Fang et al., 2013; Kikuchi, 2014; Kikuchi et al., 2011b; Marín-Juez et al., 2016; Wu et al., 2016). Importantly, only Nrg and its co-receptor ERBB2 have so far been reported to possess mitogenic activity, thereby inducing cardiomyocyte proliferation in both healthy and injured hearts of fish and mammals (Bersell et al., 2009; D'Uva et al., 2015; Gemberling et al., 2015; Liu et al., 2010). Subsequently, Nrg treatment is a subject of ongoing research to evaluate its therapeutic potential for injured heart treatment (Polizzotti et al., 2015). Interestingly, members of the TGF-β signaling pathway have been implicated to be involved in various developmental (Ahuja et al., 2016; Azhar et al., 2009) and disease conditions (Pohlers et al., 2009; Siegel and Massagué, 2003), but the role of its various components in cardiac regeneration is poorly understood. (Certain lines have been quoted verbatim from Dogra et al. (manuscript under revision)).

5.2 Previous knowledge on the distinct role of TGF-β signaling in cardiac regeneration and significance of this study.

So far, multiple studies have revealed a discrepancy in the role of TGF-β signaling in organ regeneration and pathology. Several spatio-temporal roles of TGF-β signaling have been reported during *Xenopus* tail regeneration, including wound epithelium formation, regulation

of cell proliferation and establishment of regeneration bud structures (Ho and Whitman, 2008). However, its loss has been associated with an expansion of hepatic progenitor cells in the regenerating mammalian liver (Thenappan et al., 2010). Additionally, TGF-β signaling has been implicated in the pathogenesis of cardiac remodeling and fibrosis after pressure overload in mammals (Koitabashi et al., 2011), whereas TGF-β receptor inhibitor treatment suppressed cardiomyocyte proliferation and ultimately blocked cardiac regeneration in adult zebrafish (Chablais and Jazwinska, 2012). Further studies suggest that TGF-β signaling cascade is crucial for the repression of inflammatory response, promotion of extracellular matrix deposition as well as induction of interstitial fibrosis in the healing infarcts (Bujak and Frangogiannis, 2007).

Altogether, the understanding of the exact role of TGF-β signaling during cardiac regeneration still remains incomplete and needs further investigation. Therefore, because of its highly diverse and seemingly contradictory functions across various cell types and species, I aimed to dissect the role of different TGF-β family members in cardiac regeneration by performing ligand-specific genetic manipulations. (Certain lines have been quoted verbatim from Dogra et al. (manuscript under revision)).

5.3 Opposing expression response and function of *mstnb* and *inhbaa* during cardiac regeneration.

With the aid of microarray, RT-qPCR and *in situ* hybridization, I identified the opposing expression response of two TGF-β genes, *mstnb* and *inhbaa* to cryoinjury. From subsequent gain- and loss-of-function approaches, I identified their contrasting roles in regulating cardiac regeneration as well as cardiomyocyte proliferation in zebrafish, which is one of the fundamental events promoting the healing of the injured heart.

My study shows that *mstnb,* which is predominately expressed in the ventricular wall of the adult zebrafish heart, is rapidly and continuously downregulated post cryoinjury throughout the process of heart regeneration, and notably its expression comes back to basal levels at the end of regeneration process (**Figure 4.1, 4.2**; *in situ* hybridization experiments in Figure 4.2c-f were performed in collaboration with Dr. Hyun-Taek Kim). However, this observation contrasts previous findings in mammals which show a rapid and significant upregulation of MSTN post MI (Bish et al., 2010; Castillero et al., 2015). Interestingly, *mstnb* has a conserved function as a negative regulator of skeletal muscle growth in fish and mammals

(Chisada et al., 2011; Haidet et al., 2008; Whittemore et al., 2003) and the prolonged absence of MSTN is reported to induce robust skeletal muscle regeneration in mice (Wagner et al., 2005). Therefore, I hypothesize that *mstnb* downregulation in zebrafish following cardiac injury facilitates cardiac regeneration, whereas elevated MSTN levels in the injured mammalian heart could possibly inhibit the process of regeneration. In support of this hypothesis, I observed that loss of *mstnb* positively regulates physiological cardiomyocyte proliferation as the *mstnb*$^{-/-}$ animals have enlarged hearts with thickened ventricular wall (**Figure 4.20, 4.21**). Further analysis on the cryoinjured *mstnb*$^{-/-}$ hearts showed that loss of *mstnb* enhances cardiac regeneration, as observed by faster scar clearance (**Figure 4.25**). As a complementary approach, I wanted to analyze the effect of overexpressing *mstnb,* and therefore generated a cardiomyocyte-specific overexpression of *mstnb*. Conversely, overexpression of *mstnb* in cardiomyocytes, led to a significant decline in cardiomyocyte proliferation, disturbed regeneration and compromised scar clearance after injury (**Figure 4.10, 4.12**). In sum, these findings strongly support that *mstnb* downregulation is imperative during cardiac regeneration, facilitating cardiomyocyte proliferation as well as scar clearance, and suggest Mstnb as a potential novel target whose inhibition can be further explored in mammalian system for developing therapeutics targeting cardiac regeneration.

The other TGF-β ligand, Inhba has been previously reported to be strongly induced at the fin amputation site and is involved in wound healing and blastemal proliferation during zebrafish fin regeneration (Jaźwińska et al., 2007). Interestingly, in this study, I found that *inhbaa* expression is upregulated in response to cardiac injury during the early stages of cardiac regeneration, and its expression reaches back to basal levels in the later stages (**Figure 4.1, 4.2**). Thus, I speculate that the presence of *inhbaa* is vital during early phase of regeneration. In support of my speculation, I found that the loss of *inhbaa* strongly correlates with reduced cardiomyocyte proliferation and compromised scar clearance within the proximity of the injured area (**Figure 4.10, 4.12**). Then I wanted to assess the effect of cardiomyocyte-specific overexpression of *inhbaa* and discovered that it indeed enhances cardiac regeneration as observed by faster scar clearance, and also results in cardiomegaly as a consequence of increased cardiomyocyte proliferation and hypertrabeculation, even in the absence of cardiac injury (**Figure 4.22, 4.24, 4.25**; H&E staining experiments in Figure 4.22a', a'', b', b'' were performed in collaboration with Dr. Suchit Ahuja). The cardiac hypertrabeculation phenotype of the *inhbaa* OE fish is reminiscent of that observed in mice mutant for FKBP12 (Chen et al., 2009), a negative regulator of the TGF-β family (Wang et al., 1996), suggesting a conserved

function of TGF-β signaling in cardiac development and possibly cardiomyocyte proliferation.

Recent reports have identified Nrg as a potent mitogen in fish and mammals (Bersell et al., 2009; Gemberling et al., 2015; Rasouli and Stainier, 2017). Thus, I performed epistasis experiments to test whether *inhbaa*-induced cardiomyocyte proliferation depends upon Nrg-ErbB signaling. These experiments performed by using *erbb*$^{-/-}$ and chemical inhibitor of ErbB signaling, revealed that Inhbaa stimulates cardiomyocyte proliferation independently of ErbB receptor activity (**Figure 4.26, 4.27, 4.28**), indicating that similar to Nrg, Inhbaa has the potential to induce cardiomyocyte proliferation directly and can have therapeutic implications as a cardiomyocyte mitogen. However, simultaneous overexpression of *nrg2a* and *inhbaa* did not yield a higher cardiomyocyte proliferative index than overexpression of *nrg2a* alone (**Figure 4.29**; the *nrg2a* OE transgenic line used in Figure 4.29 d-f has been provided by collaborator Seyed Javad Rasouli). Possibly, stimulation of cardiomyocyte proliferation becomes saturated by *nrg2a* overexpression alone, as suggested by the minimal variability observed across the different specimens (**Figure 4.29f**; the *nrg2a* OE transgenic line used in Figure 4.29f has been provided by collaborator Seyed Javad Rasouli). Alternatively, Nrg2a signaling might interfere with the potential of Inhbaa to promote cardiomyocyte proliferation. Indeed, stimulation of the MAPK signaling cascade by oncogenic mutations in Ras or by EGF receptor stimulation mediates the phosphorylation of specific residues in the linker region of Smad2 and Smad3 (Kretzschmar et al., 1999). Further, the phosphorylation of this linker region has been shown to inhibit TGF-β-induced C-terminal phosphorylation and nuclear accumulation of Smads, thereby negatively affecting the transcriptional activation of their target genes (Kretzschmar et al., 1999).

In addition, I asked the question, whether *mstnb* and *inhbaa* collaboratively regulate cardiomyocyte proliferation. Therefore, I investigated cardiomyocyte proliferation in the presence of both *mstnb* OE and *inhbaa* OE, and discovered that overexpression of *mstnb* suppresses cardiomyocyte proliferation induced by *inhbaa* OE, thereby bringing it back to wild-type levels (**Figure 4.30**). Interestingly, I found that *inhbaa* OE competes with *mstnb* OE to regulate cardiomyocyte proliferation (**Figure 4.30**).

Since *inhbaa* is upregulated after cardiac injury, both in mammals (Yndestad et al., 2004) and zebrafish, I speculate that possibly the timing and levels of its induction do not allow it to induce regeneration in the mammalian heart. In fact, the prolonged upregulation of *INHBA* has been associated with induction of fibrosis post MI in mammals, leading to cardiac

remodeling and failure (Yndestad et al., 2004). Therefore, I hypothesize that a transient upregulation of *INHBA* in injured hearts, along with a rapid inactivation of *MSTN*, as observed in zebrafish, could prove beneficial to stimulate cardiomyocyte proliferation while prolonged *INHBA* expression has negative consequences. Indeed, several of the *inhbaa* OE animals show signs of cardiomyopathy and heart failure past 6 months of age (**Figure 4.23**), an effect that could be potentiated by the presence of a higher number of myofibroblasts and other non-myocardial cells in the mammalian heart (Zhou and Pu, 2016). (Certain lines have been quoted verbatim from Dogra et al. (manuscript under revision)).

5.4 Activation of distinct Smad-dependent transcriptional targets by *mstnb* and *inhbaa.*

I further aimed to explore the molecular mechanisms underlying the differential regulation of cardiomyocyte proliferation and thereby, cardiac regeneration by *mstnb* and *inhbaa*. Myostatin and Activin signal through the TGF-β signaling cascade, leading to the phosphorylation of downstream effectors, Smad2 and Smad3 on their C-terminal residues (Massagué and Gomis, 2006; Massagué, 2012; Rebbapragada et al., 2003). It has been reported that Smad2, along with Smad4 and transcription factors such as FAST1/2, binds to the Activin Response Elements (ARE) present in the promoter regions of target genes (Chen et al., 1997, 1996; Labbé et al., 1998). Likewise, Smad3 binds to the Smad Binding Elements (SBE) present in the promoter region of target genes (Jonk et al., 1998; Stroschein et al., 1999). Therefore, I made use of the published Smad2 (van Boxtel et al., 2015) and Smad3 (Casari et al., 2014) reporter lines, to identify potentially distinct transcriptional target genes of Mstnb and Inhbaa signaling. Interestingly, I found that *mstnb* overexpression induces Smad2 reporter expression and suppresses Smad3 reporter expression, whereas *inhbaa* overexpression induces Smad3 reporter expression and downregulates Smad2 reporter expression (**Figure 4.31**). The data thus obtained made me speculate that this differential regulation of the activities of distinct Smad responsive elements by *mstnb* and *inhbaa* might account for their different influence on cardiomyocyte proliferation.

Additionally, I monitored the expression levels of the zebrafish orthologs of known Smad-specific target genes in response to *inhbaa* or *mstnb* overexpression, including *Goosecoid (Gsc)* (Labbé et al., 1998) and *Mix.2* (Chen et al., 1996) for Smad2, and *JunB* (Jonk et al., 1998) and *PAI-1* (Stroschein et al., 1999) for Smad3. I found that *mstnb* overexpression is

able to induce Smad2 target gene expression and suppress Smad3 target gene expression; however, *inhbaa* overexpression induces Smad3 target gene expression and downregulates Smad2 target gene expression, both during embryonic development as well as adult cardiac regeneration (**Figure 4.32, 4.33, 4.34, 4.35**). In sum, this study reports for the first time that the activities of Smad2 and Smad3 are inversely regulated by *mstnb* and *inhbaa*. (Certain lines have been quoted verbatim from Dogra et al. (manuscript under revision)).

5.5 Opposite effects of Smad2 and Smad3 on cardiomyocyte proliferation.

The Smad proteins are characterized by two conserved regions namely N-terminal Mad homology domain-1 (MH1) and C-terminal Mad homology domain-2 (MH2). Further these two domains are connected by a short, poorly conserved linker region. Smad2 and Smad3 have 66% amino acid sequence identity between their MH1 domains and 96% amino acid sequence identity between their MH2 domains (Brown et al., 2007). Although Smad2 and Smad3 have highly homologous MH1 and MH2 domains, the MH1 domain of Smad2 has 30 extra amino acids preventing its direct binding to DNA, unlike Smad3 which can directly bind to target DNA sequences (Brown et al., 2007). These structural differences in Smad2 and Smad3 may account for differences in their biological functions. In fact, several recent studies have revealed the antagonistic effects of Smad2 and Smad3 during multiple cellular processes, including early lineage specification, blastema formation during regeneration, tumor angiogenesis and neurogenesis (Denis et al., 2016; Liu et al., 2016; Míguez et al., 2013; Petersen et al., 2010). Keeping in mind their reported differential roles, I generated constitutively active versions of Smad2 and Smad3, by inducing phosphomimetic mutations in their C-terminal region by replacing Serines with Aspartic acid (Chipuk et al., 2002). Subsequent analysis of the effect of *caSmad2* and *caSmad3* on cardiomyocyte EdU incorporation revealed that Smad2 and Smad3 act antagonistically to one another in regulating cardiomyocyte proliferation (**Figure 4.41**).

Additionally, I also reveal that the chemical inhibition of Smad3 phosphorylation suppresses cardiomyocyte proliferation, indicating that Smad3 is indeed positively regulating the cardiomyocyte cell-cycle (**Figure 4.39**). Furthermore, Smad3-dependent TGF-β signaling has been previously reported to be associated with cardiac regeneration, as because of the pharmacological inhibition of TGF-β signaling, the myocardial Smad3 phosphorylation in the vicinity of injured area was significantly reduced, as was cardiomyocyte proliferation and

cardiac regeneration (Chablais and Jazwinska, 2012). Therefore, I assessed the respective gain- and loss-of-function genotypes of *mstnb* and *inhbaa* to determine the phosphorylation status of Smad3 during cardiac regeneration. Notably, I have identified differential effects of *mstnb* and *inhbaa* overexpression on myocardial Smad3 phosphorylation in the regenerating hearts i.e., *mstnb* overexpression suppresses myocardial Smad3 phosphorylation, whereas *inhbaa* overexpression induces this process (**Figure 4.36**). In line with the results obtained from overexpression lines, I further found that loss of *mstnb* positively regulates Smad3 phosphorylation in the cardiomyocytes proximal to the injured area, whereas loss of *inhbaa* negatively regulates this process (**Figure 4.37**). Overall, these data suggest that certainly these two ligands are inversely affecting the phosphorylation of Smad3 which seemingly mediates cardiomyocyte proliferation during cardiac regeneration. (Certain lines have been quoted verbatim from Dogra et al. (manuscript under revision)).

5.6 Differential ligand-receptor relationship and its impact on cardiomyocyte proliferation.

To determine whether the receptor specificity of Mstnb and Inhbaa is a potential reason for the opposing function and effects of these two ligands, it is essential to study the ligand-receptor relationships. Canonically, TGF-β ligands including Myostatin and Activin signal by binding the serine/threonine kinase receptors, Activin type 2 receptors. This ligand-receptor complex initiates the activation and recruitment of the other serine/threonine kinase receptors, i.e., Activin type 1 receptors. This event ultimately leads to the C-terminal phosphorylation of the signal transducers, Smad2 and Smad3. Mstn and Inhba have been reported to signal through the same Activin type 2 receptor complex (Massagué and Gomis, 2006; Massagué, 2012; Rebbapragada et al., 2003). Thus, I asked the question that how could Mstnb and Inhbaa function antagonistically to one another if they work through the same signaling cascade. Therefore, to better understand the ligand-receptor relationships, I carried out combined Activin type 2 receptor encoding gene knockdown and *mstnb* or *inhbaa* overexpression experiments. Mechanistically, I found that Mstnb has a binding preference for Acvr2b compared to Acvr2a (**Figure 4.42**), which is also shown in previous reports (Lee and McPherron, 2001; Rebbapragada et al., 2003). I further report for the first time that Inhbaa has a preference to bind Acvr2a over Acvr2b (**Figure 4.42**). Furthermore, regarding the Activin type 1 receptors, it has been reported that Acvr1b and Tgfbr1 (Tgfbr1a and Tgfbr1b)

are the type 1 receptors for Mstn, whereas Acvr1b and Acvr1c are the type 1 receptors for Inhba (Tsuchida et al., 2009). Altogether, this study reveals an interesting finding that Mstnb and Inhbaa bind to their specific Activin type 2 receptors to inversely modulate the activities of Smad2 and Smad3, thereby regulating cardiomyocyte proliferation antagonistically to each other (**Figure 4.43**).

Summarizing the findings of this study, I have identified the opposite functions for the two TGF-β ligands, Mstnb and Inhbaa, during cardiac regeneration and similarly, for their downstream effectors Smad2 and Smad3. These two ligands act through different Activin type 2 receptors to inversely regulate cardiomyocyte proliferation. Additionally, the Nrg-ErbB independent mitogenic activity of Inhbaa may provide new avenues towards developing novel strategies in the treatment of patients post MI. (Certain lines have been quoted verbatim from Dogra et al. (manuscript under revision)).

6. Conclusion

In conclusion, my study identifies the opposite effects of two TGF-β genes, *mstnb* and *inhbaa* on cardiomyocyte proliferation during cardiac development as well as regeneration. Here I show for the first time the differential expression response of *mstnb* and *inhbaa* to cardiac injury, which correlates with their opposite functions during cardiac regeneration. I show that the overexpression of *mstnb* negatively regulates cardiomyocyte proliferation and therefore disturbs cardiac regeneration. However, loss of *mstnb* not only promotes physiological cardiomyocyte proliferation but also enhances cardiac regeneration. Conversely, I reveal that loss of *inhbaa* leads to suppressed cardiomyocyte proliferation and thereby disturbs cardiac regeneration. Notably, the overexpression of *inhbaa* not only accelerates cardiac regeneration but also positively regulates cardiomyocyte proliferation even in the absence of cardiac injury. For the first time, I identify Inhbaa as a mitogen which promotes cardiomyocyte proliferation independent of the well-established Nrg-ErbB signaling.

My data also uncover the underlying molecular mechanisms responsible for the differential functions of Mstnb and Inhbaa. Here I unraveled that Mstnb and Inhbaa inversely control the activities of Smad2 and Smad3 transcriptional factors through alternate Activin type 2 receptor complexes, thereby regulating cardiomyocyte proliferation.

Altogether, I reveal novel and unexpected opposite roles for two TGF-β ligands during cardiac regeneration, resulting in a pro-mitogenic as well as an anti-mitogenic effect on cardiomyocytes. Thus, my study should stimulate further research on targeting specific TGF-β family members to generate novel regenerative therapeutic strategies.

6.1 Proposed model

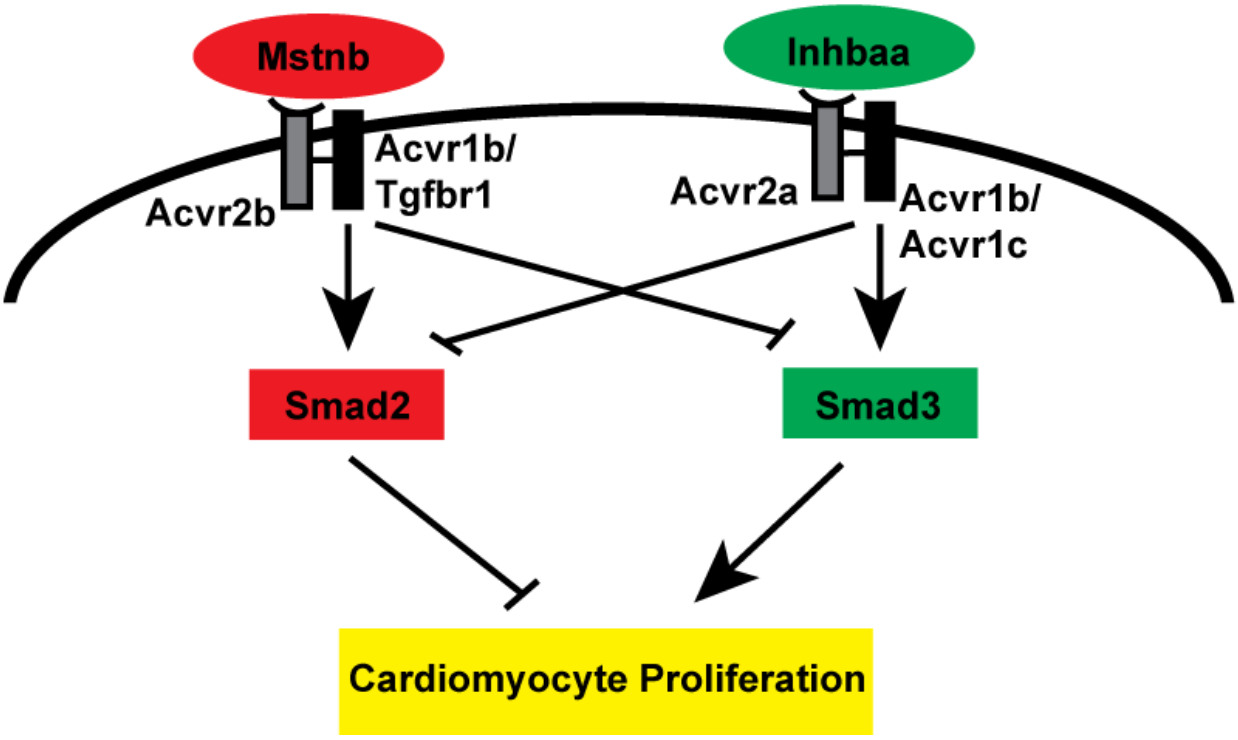

Figure 6.1. Opposite effects of TGF-β ligands on cardiomyocyte proliferation during development and repair. Mstnb binds to Acvr2b, leading to the activation of Acvr1b/Tgfbr1, which promotes Smad2 and suppresses Smad3 activation. Inversely, Inhbaa binds to Acvr2a, recruiting Acvr1b/Acvr1c, thereby inducing Smad3 and suppressing Smad2 activation. This process is followed by the differential regulation of cardiomyocyte proliferation by Smad2 and Smad3. Figure submitted in Dogra et al. (manuscript under revision).

I. Zusammenfassung

Gegenteilige Effekte von *mstnb* und *inhbaa* auf die Proliferation von Kardiomyozyten während Entwicklung und Reparatur

Einleitung

Das erwachsene Säugetierherz ist unfähig, verletztes Muskelgewebe nach einem Myokardinfarkt (MI) zu regenerieren. Stattdessen wird der verletzte Muskel durch eine nicht-kontraktile und funktionell inerte, fibrotische Narbe ersetzt, welche die Leistung des Herzens stört und Arrhythmien verursacht (Steinhauser and Lee, 2011). Daher ist der MI eine der häufigsten Todesursachen weltweit (Mozaffarian et al., 2016). Einige Forschungsfelder versuchen neue regenerative Methoden zu entwickeln, um dieses Problem zu lösen und fokussieren sich dabei vorrangig auf die Stimulation der Proliferation von Kardiomyozyten *in situ* (Bersell et al., 2009), auf das Anwachsen von Stammzell-abgeleiteten Kardiomyozyten im verletzten Herzen (Chong et al., 2014) oder auf die *in situ*-Transdifferenzierung von Fibroblasten zu funktionalen Kardiomyozyten (Qian et al., 2012).

Im Gegensatz zu Säugetieren sind niedere Wirbeltiere, wie der Zebrafisch (Poss et al., 2002), dazu befähigt, das verletzte Herzgewebe effektiv zu regenerieren und das nach verschiedensten Verletzungsarten, wie beispielsweise der ventrikularen Resektion (Poss et al., 2002), der Kryoverletzung (Chablais et al., 2011) oder genetischer Kardiomyozytenablation (Wang et al., 2011). Linienverfolgungsexperimente ergaben, dass verschonte Kardiomyozyten in der Umgebung rund um den verletzten Bereich eine Dedifferenzierung und Proliferation durchlaufen, wodurch sie neue Kardiomyozyten bilden, welche den verletzen Muskel ersetzen (Jopling et al., 2010; Kikuchi et al., 2010). Dies macht den Zebrafisch zu einem geeigneten Modellorganismus, um die verschiedenen molekularen Mechanismen zu analysieren, welche dem Prozess der Herzregeneration unterliegen und somit neue regenerative Therapien zu ermöglichen.

Es wurde berichtet, dass verschiedene Signalwege, wie die der Retinolsäure, des Interleukin 6 und des epidermalen Wachstumsfaktors (EGF) in der Herzregeneration involviert sind (Kikuchi et al., 2011b; Fang et al., 2013; Kikuchi, 2014; Marín-Juez et al., 2016; Wu et al., 2016). Allerdings ist bis heute nur für Neuregulin (Nrg) und seinen Co-Rezeptor ERBB2 bekannt, dass sie eine mitogene Aktivität aufweisen, indem sie die

Kardiomyozytenproliferation sowohl in gesunden, als auch in verletzten Herzen von Fischen und Säugetieren induzieren (Bersell et al., 2009; et al., 2015; Gemberling et al., 2015; Liu et al., 2010). Dies macht Nrg zu einem zentralen Objekt der aktuellen Forschung, um sein therapeutisches Potential für die Behandlung menschlicher Herzpatienten festzustellen (Polizzotti et al., 2015). Der TGF-β-Signalweg ist insbesondere in mehrere Zustände der Entwicklung (Ahuja et al., 2016; Azhar et al., 2009) und Krankheit (Pohlers et al., 2009; Siegel and Massagué, 2003) verwickelt, allerdings bleibt die Rolle seiner verschiedenen Komponenten in der Regulation der Herzregeneration noch immer unklar. Die Liganden der Wirbeltier-TGF-β/Activin-Unterfamilie (TGF-β-Unterfamilie) bestehen aus Activinen (INHBA, INHBB), GDFs (Myostatin/GDF8, GDF11) und TGF-β (TGFB1, TGFB2 und TGFB3), welche den Activin-Typ-2-Rezeptor (ACVR2A, ACVR2B, TGFBR2) binden, was zu der Rekrutierung und Aktivierung des Activin-Typ-1-Rezeptors (ACVR1B, TGFBR1, ACVR1C) führt. Dieser Prozess ist gefolgt von der Phosphorylierung der stromabwärts gelegenen Effektoren Smad2/3, welche Smad4 binden und in den Nucleus translozieren, wodurch sie die Zielgenexpression modulieren (Massagué and Gomis, 2006; Massagué, 2012; Sartori et al., 2014).

Eine Verstärkung der TGF-β-Signalwirkung inklusive der Hochregulierung von Myostatin (MSTN) (Castillero et al., 2015) , Inhibin betaA (INHBA) (Yndestad et al., 2004) und TGF-β (Li et al., 1997) wurde nach einem MI im Säugerherzen beobachtet, was Hypertrophie, Apoptose und eine Endothel-Mesenchym-Transition weiter fördert (Euler-Taimor and Heger, 2006; Zeisberg et al., 2007). Zusätzlich reduziert die Kardiomyozyten-spezifische Deletion von *Tgfbr2* die pathologische Herzremodellierung als Antwort auf eine anhaltende Drucküberlastung (Koitabashi et al., 2011). Dagegen ist die TGF-β-Signalwirkung im Zebrafisch essentiell während der Herzregeneration, da die pharmakologische Inhibition des Aktivin-Typ-1-Rezeptors die Proliferation der Kardiomyozyten unterdrückt und die Herzregeneration beeinträchtigt (Chablais and Jazwinska, 2012). MSTN, ein gut untersuchter negativer Regulator des Skelettmuskelwachstums (Haidet et al., 2008; Whittemore et al., 2003) wurde mit der Entwicklung von kardialer Hypertrophie in Säugetieren in Verbindung gebracht (Biesemann et al., 2014; Rodgers et al., 2009). Weiterhin verstärkt die Abwesenheit von MSTN die Regeneration von Skelettmuskeln in Mäusen (Wagner et al., 2005) und ein kürzlich entwickelter monoklonaler Antikörper gegen MSTN zeigt therapeutisches Potential in der Behandlung von Skelettmuskelatrophie (Latres et al., 2015). *inhba*, auch bekannt als *activin betaA*, fördert die Wundschließung über die Regulierung der Phosphorylierung von c-jun und der Blastemproliferation und reguliert so positiv die Regeneration der

Zebrafischflossen (Jaźwińska et al., 2007). Zusammengenommen bleibt die Rolle der TGF-β-Signalwirkung und seiner zahlreichen Liganden während der Herzregeneration unklar. Daher identifiziere ich hier, indem ich Genexpressionsprofile erstelle, die entgegenwirkenden Expressionsantworten zweier TGF-β-Gene, *mstnb* und *inhbaa*, auf die Verletzung des Herzens, mit dem Ziel einer detaillierten Untersuchung ihrer Funktion während der Regeneration des Herzens.

Hier zeige ich, dass Mstnb und Inhbaa gegenteilige Effekte auf die Regeneration des Herzens ausüben, da der Verlust von *mstnb* und die Aktivierung von *inhbaa* die Proliferation der Kardiomyozyten positiv reguliert und dadurch zu einer verstärkten Herzregeneration führen. Weiterhin zeige ich auf, dass Mstnb und Inhbaa durch alternierende Activin-Rezeptorkomplexe wirken, um die Aktivitäten der Smad2- und Smad3-Transkriptionsfaktoren zu kontrollieren und dadurch die Proliferation der Kardiomyozyten antiproportional zu regulieren.

Ergebnisse und Diskussion

Um die Gene zu identifizieren, welche während der Herzregeneration erwachsener Zebrafische unterschiedlich reguliert werden, habe ich eine Microarray-basierte Expressionsanalyse verschiedener Zebrafischherzen 4 Tage nach einer Kryoverletzung (4 dpci) im Vergleich zu 4 Tagen nach einer Scheinverletzung (4 dpsi) durchgeführt (Abbildung 4.1a). Interessanterweise habe ich gegensätzliche Expressionsantworten von *mstnb* und *inhbaa* auf Kryoverletzungen beobachtet (Abbildung 4.1b), was durch die Durchführung einer Real-Time quantitativen PCR (RT-qPCR) von schein- und kryoverletzten Ventrikeln zu verschiedenen Zeitpunkten nach der Verletzung bestätigt werden konnte. Ähnlich zu meinen Microarray-Daten habe ich eine schnelle und kontinuierliche Herunterregulierung der *mstnb*-Transkriptionslevel während des Prozesses der Regeneration beobachtet (Abbildung 4.2a). Allerdings kehrte die Expression nach 60 dpci auf ein basales Level zurück (Abbildung4.2a), sobald die Regeneration abgeschlossen war (Chablais et al., 2011), was zu der These führt, dass eine kontinuierliche Herunterregulation der Expression von *mstnb* ausschlaggebend für die Herzregeneration ist. Im Gegensatz dazu erreichte die mRNA-Expression von *inhbaa* nach 4 dpci ihren Höchststand und kehrt nach 8 dpci zu Scheinleveln zurück (Abbildung 4.2b), was zeigt, dass *inhbaa* eine Schlüsselrolle während der frühen Phase der Herzregeneration spielt. Weiterhin wurde das spatio-temporale Expressionsmuster von *mstnb*

und *inhbaa* durch die Durchführung einer *in situ*-Hybridisierung in Querschnitten weiter analysiert (Abbildung 4.2c-f; *in situ*-Hybridisierungsexperimente wurden in Kollaboration mit Dr. Hyun-Taek Kim durchgeführt). Die Expression von *mstnb* wurde in der Ventrikelwand der verletzten Herzen detektiert (Abbildung 4.2c) und war nach der Kryoverletzung unter ein messbares Level gefallen (Abbildung 4.2d). Dagegen wurde keine Expression von *inhbaa* in den unverletzten Herzen gefunden (Abbildung 4.2e), es wurde aber in bedeutendem Maße proximal zu dem verletzten Gebiet nach 4 dpci detektiert (Abbildung 4.2f). Alles in allem zeigen die Expressionsmuster beider Gene deutlich verschiedene spatio-temporale Veränderungen während der kardialen Regeneration, was mit den Methoden Microarray-Profiling, RT-qPCR und *in situ*-Hybridisierung festgestellt wurde.

Meiner Beobachtung folgend, dass sich während der kardialen Regeneration die *mstnb*-Expression verringert und die *inhbaa*-Expression erhöht, wollte ich die Effekte einer Überexpression von *mstnb* und eines Verlustes von *inhbaa* im regenerierenden Herzen untersuchen. Daher habe ich eine transgene Zebrafischlinie für die Kardiomyozyten-spezifische konstitutive Überexpression von *mstnb*, *Tg(myl7:mstnb-2A-H2B-EGFP)bns145* (ab hier *mstnb* OE) generiert (Abbildung 4.4). Ich habe außerdem eine *inhbaa*-Mutantenlinie im Zebrafisch mithilfe der TALEN-Methode generiert, mit welcher ich die TGF-β-Propeptid-Domäne von Inhbaa ins Ziel genommen habe (Abbildung 4.5a). Ein 17-Basenpaar-Deletionsallel, $inhbaa^{bns37}$, wurde dadurch gefunden, für welches vermutet wurde, dass es für ein verkürztes Protein codiert (Abbildung 4.5b,c). Interessanterweise habe ich beobachtet, dass die Herzen der *mstnb* OE und der $inhbaa^{-/-}$ nach 45 dpci nicht dazu fähig waren, ihre Narbe zu beseitigen, was im Kontrast zu Wildtyp-Geschwistern derselben regenerativen Stufe steht (Abbildung 4.10). Weiterhin habe ich getestet, ob eine *inhbaa*-Defizienz oder eine *mstnb*-Überexpression die Proliferation der Kardiomyozyten nach einer Kryoverletzung modulieren kann. Es wurde eine signifikante Reduktion der Kardiomyozytenproliferation in den Herzen von *mstnb* OE und $inhbaa^{-/-}$beobachtet, verglichen mit ihren Wildtyp-Geschwistern nach 6 dpci (Abbildung 4.12). Zusammengenommen zeigen diese Ergebnisse, dass eine Gain-of-Function-Mutation (GOF) von *mstnb* und eine Loss-of-Function-Mutation (LOF) von *inhbaa* die Proliferation von Kardiomyozyten negativ beeinflusst und die Regeneration des Herzens stört, woraus eine verringerte Narbenbeseitigung resultiert.

Komplementär dazu habe ich die Effekte einer *mstnb*-LOF und einer *inhbaa*-GOF auf die kardiale Entwicklung und Regeneration untersucht. Ich habe eine *mstnb*-Mutantenlinie im Zebrafisch mithilfe von TALEN generiert, mit welchem ich die Region nach der

Signalpeptiddomäne ins Ziel genommen habe und wodurch ich ein 10 Basenpaar-Deletionsallel gefunden habe, *mstnb*^{bns5}, für welches vermutet wurde, dass es für ein verkürztes Protein codiert (Abbildung 4.16). Erwachsene *mstnb*$^{-/-}$-Tiere zeigten ein vergrößertes Herz mit verdickter Ventrikelwand (Abbildung 4.20). Um besser zu verstehen, ob die verdickte Ventrikelwand durch eine erhöhte Proliferation der Kardiomyozyten in der kompakten Schicht bedingt ist, habe ich eine EdU-Inkorporationsanalyse der Kardiomyozyten durchgeführt. Verglichen mit den Geschwistern zeigten die Herzen der *mstnb*$^{-/-}$-Tiere eine signifikante Erhöhung der totalen Anzahl an Kardiomyozyten und eine erhöhte EdU-Inkorporation in die Kardiomyozyten, sowohl in der Wand als auch in den Trabeculae der Ventrikel (Abbildung 4.21). Als nächstes habe ich eine transgene Zebrafischlinie für eine Kardiomyozyten-spezifische konstitutive Überexpression von *inhbaa*, *Tg(myl7:inhbaa-2A-H2B-EGFP)bns146* (ab hier *inhbaa* OE), kreiert (Abbildung 4.18). Erwachsene *inhbaa* OE-Tiere zeigten signifikant vergrößerte Herzen und eine dichte Trabekulierung in beiden Kammern (Abbildung 4.22; H&E Färbungsexperimente in Abbildung 4.22a', a'', b', b'' wurden in Kollaboration mit Dr. Suchit Ahuja durchgeführt). Erneut habe ich die Kausalität der Herzvergrößerung und der Hypertrabekulierung in den *inhbaa*-Herzen untersucht, indem ich eine EdU-Inkorporationsanalyse durchgeführt habe. Es wurde eine signifikante Erhöhung der totalen Anzahl an Kardiomyozyten und der EdU-Inkorporation in die Kardiomyozyten in *inhbaa* OE-Herzen festgestellt, verglichen mit der Kontrolle (Abbildung 4.24). Ich habe daraufhin getestet, ob eine erhöhte Proliferation der Kardiomyozyten den *mstnb*$^{-/-}$ - und *inhbaa* OE-Herzen nach der Verletzung hilft. Dadurch habe ich herausgefunden, dass *mstnb*$^{-/-}$ - und *inhbaa* OE-Herzen ihre Narbe nach 30 dpci komplett beseitigt hatten, im Gegensatz zu ihren Geschwistern (Abbildung 4.25). Alles in allem decken diese Ergebnisse auf, dass *mstnb*-LOF und *inhbaa*-GOF die physiologische Proliferation der Kardiomyozyten positiv beeinflussen und zu einer erhöhten kardialen Regeneration führen.

Nachdem ich nachgewiesen habe, dass die *inhbaa* OE die Proliferation der Kardiomyozyten fördert, wollte ich feststellen, ob ihre Funktion von dem Nrg-ErbB-Signalweg abhängt. Indem ich *erbb2*^{st61}-Mutanten und einen ErbB2-Inhibitior verwendet habe, kam ich zu der Beobachtung, dass *inhbaa* OE dazu fähig ist, die Proliferation der Kardiomyozyten selbst bei Abwesenheit der ErbB-Signalwirkung zu induzieren (Abbildung 4.27, 4.28). Interessanterweise führte eine kombinierte Überexpression von *inhbaa* und *nrg2a* zu einer EdU-Inkorporation in die Kardiomyozyten ähnlich zu der *nrg2a* OE alleine (Abbildung 4.29; die transgene Linie *nrg2a* OE, welche in Abbildung 4.29 d-f verwendet wurde, wurde durch den Kollaborateur Seyed Javad Rasouli bereitgestellt), was darauf hinweist, dass entweder die

Proliferation der Kardiomyozyten ihr Maximum durch *nrg2a* OE alleine erreicht oder die ErbB-Signalwirkung in die Inhbaa-vermittelte Proliferation eingreift, wie es zuvor bereits beschrieben wurde (Kretzschmar et al., 1999) . Weiterhin habe ich herausgefunden, dass in den Larven, welche aus der Kreuzung zwischen *mstnb* OE- und *inhbaa* OE-Tieren entstanden sind, die *mstnb* OE die *inhbaa* OE-induzierte Myokard-EdU-Inkorporation auf ein Level ähnlich dem der Wildtyp-Geschwister reduziert (Abbildung 4.30), was zu der These führt, dass Mstnb und Inhbaa im Wettbewerb um die Kontrolle über die Proliferation von Kardiomyozyten stehen.

Als nächstes habe ich darauf abgezielt, die molekularen Mechanismen zu entziffern, welche der differentiellen Regulation der Kardiomyozytenproliferation und daraus folgend der kardialen Regeneration durch *mstnb* und *inhbaa* zugrunde liegen. Myostatin und Activin agieren über die TGF-β-Signalkaskade, was zu einer Phosphorylierung der Signaltransduktoren Smad2 und Smad3 führt (Massagué and Gomis, 2006; Massagué, 2012; Rebbapragada et al., 2003). Smad2 bindet die Activin Response Elements (ARE), zusammen mit Smad4 und Transkriptionsfaktoren wie FAST1/2, während Smad3 die Smad Binding Elements (SBE) bindet, welche in der Promotorregion ihrer Zielgene lokalisiert sind (Chen et al., 1997, 1996; Jonk et al., 1998; Labbé et al., 1998; Stroschein et al., 1999). Um die potentiell verschiedenen transkriptionellen Ziele der Mstnb- und Inhbaa-Signalwege zu identifizieren, habe ich jeweils den Effekt einer *mstnb*- und einer *inhbaa*-Überexpression auf die Smad2 und Smad3-Reporteraktivitäten überprüft, indem ich die publizierte Smad2-Reporterlinie *Tg(ARE:EGFP)fci100* (van Boxtel et al., 2015) und die Smad3-Reporterlinie *Tg(12XSBE:EGFP)ia16* (Casari et al., 2014) verwendet habe. Die Überexpression von *mstnb* führte zu einer signifikanten Induktion der Smad2-Reporterexpression, während eine Herunterregulierung der Smad3-Reporterexpression beobachtet wurde (Abbildung 4.31). Im Gegensatz dazu induzierte eine Überexpression von *inhbaa* die Smad3- und unterdrückte die Smad2-Reporteraktivität (Abbildung 4.31). Ich habe diese Daten validiert, indem ich den Effekt einer Überexpression von jeweils *mstnb* und *inhbaa* auf die Smad2- und Smad3-spezifische Zielgenexpression (Chen et al., 1996; Jonk et al., 1998; Labbé et al., 1998; Stroschein et al., 1999) analysiert habe, beides sowohl während früher embryonaler Entwicklungsstadien, als auch in verletzten erwachsenen Herzen. Insbesondere habe ich eine Hochregulierung der Smad2-Zielgenexpression durch die *mstnb*-Überexpression, dagegen eine Herunterregulierung derselben nach der *inhbaa*-Überexpression festgestellt (Abbildung 4.32,4.34). Im Gegensatz dazu wurde eine Hochregulierung der Smad3-Zielgenexpression durch die *inhbaa*-Überexpression und eine Herunterregulierung derselben durch die *mstnb*-

Überexpression beobachtet (Abbildung 4.33,4.35). Diese Ergebnisse führen gemeinsam zu der These, dass die Aktivitäten von Smad2 und Smad3 antiproportional durch *mstnb* und *inhbaa* reguliert sind.

Ich wollte zudem testen, ob *mstnb* und *inhbaa* die myokardiale Phosphorylierung von Smad3 beeinflussen, da Smad3-abhängige TGF-β-Signalwege zuvor bereits mit der Herzregeneration im Zebrafisch in Verbindung gebracht wurden (Chablais and Jazwinska, 2012). Ich habe beobachtet, dass eine *mstnb*-Überexpression die Phosphorylierung von Smad3 in den Kardiomyozyten inhibiert, während eine Überexpression von *inhbaa* diesen Prozess fördert (Abbildung 4.36). Zudem habe ich herausgefunden, dass ein Verlust von *mstnb* die myokardiale Phosphorylierung von Smad3 positiv reguliert und ein Verlust von *inhbaa* diesen Prozess negativ reguliert (Abbildung 4.37). Daher schließe ich daraus, dass Mstnb und Inhbaa antagonistisch zueinander agieren, um die Phosphorylierung von Smad3, einem scheinbar ausschlaggebenden Ereignis während der kardialen Regeneration, zu kontrollieren.

Weiterhin habe ich beobachtet, dass die pharmakologische Inhibition der Phosphorylierung von Smad3 die EdU-Inkorporation der Kardiomyozyten unterdrückt, was darauf hinweist, dass die Proliferation der Kardiomyozyten auf der Phosphorylierung von Smad3 beruht (Abbildung 4.39). Ich habe als nächstes analysiert, welchen Effekt die transiente Überexpression der konstitutiv aktiven Versionen von (ca) Smad2, Smad3a und Smad3b auf die Kardiomyozytenproliferation haben. Es erfolgte eine signifikante Reduktion der EdU-Inkorporation in die Kardiomyozyten, welche *caSmad2* exprimieren, während sowohl die *caSmad3a*-, als auch *caSmad3b*-Expression in einer Induktion der EdU-Inkorporation der Kardiomyozyten resultierte (Abbildung 4.41). Dies führt zu der Vermutung, dass Smad2 und Smad3 die Proliferation der Kardiomyozyten im Zebrafisch entgegengesetzt regulieren und ist eine potentielle Erklärung dafür, wie verschiedene TGF-β-Liganden entgegengesetzte Effekte während der kardialen Regeneration erzielen können.

Abschließend wollte ich untersuchen, wie Mstnb und Inhbaa antagonistisch zueinander funktionieren können, wenn sie über dieselbe Signalkaskade wirken[24,25,42]. Daher habe ich, um die Liganden-Rezeptor-Beziehung besser zu verstehen, einen kombinierten Activin-Typ-2-Rezeptor-Genknockdown und jeweils *mstnb*- und *inhbaa*-Überexpressionsexperimente durchgeführt. Ich fand heraus, dass der Knockdown von *acvr2b* (*acvr2ba* und *acvr2bb*) den Effekt der *mstnb*-Überexpression auf die Reporterexpression von Smad2 und Smad3 beeinflusst, während der Knockdown von *acvr2a* (*acvr2aa* und *acvr2ab*) den Effekt der *inhbaa*-Überexpression auf die Reporterexpression von Smad2 und Smad3 beeinflusst

(Abbildung 4.42). Weiterhin habe ich den Effekt dieser Rezeptor-Knockdowns auf die EdU-Inkorporation von Kardiomyozyten in den *mstnb* OE- und den *inhbaa* OE-Linien analysiert (Abbildung 4.43a) und herausgefunden, dass ein *acvr2bb*-Knockdown die Unterdrückung der Kardiomyozytenproliferation durch die *mstnb*-Überexpression verhindert (Abbildung 4.43b-e), was zu der Vermutung führt, dass Mstnb eine Bindung mit Acvr2b gegenüber einer Bindung mit Acvr2a präferiert, wie in vorherigen Studien gezeigt wurde (Lee and McPherron, 2001; Rebbapragada et al., 2003). Allerdings verhindert der Knockdown von *acvr2aa* die Induktion der Kardiommyozytenproliferation durch *inhbaa* OE (Abbildung 4.43f-i), was vermuten lässt, dass Inhbaa bevorzugt über Acvr2a statt über Acvr2b wirkt. Insgesamt indizieren meine Daten, dass Mstnb Acvr2b bindet und dadurch die Aktivierung von Smad2 fördert und von Smad3 unterdrückt, während Inhbaa Acvr2a bindet und dadurch die Aktivierung von Smad3 fördert und von Smad2 unterdrückt.

Fazit

Abschließend habe ich hier die gegenteilige Effekte der beiden TGF-β-Gene *mstnb* und *inhbaa* auf die Proliferation der Kardiomyozyten während der kardialen Entwicklung und Regeneration identifiziert. Ich zeige hier zum ersten Mal die verschiedenen Expressionsantworten von *mstnb* und *inhbaa* auf Verletzungen des Herzens, welche mit ihren entgegengesetzten Funktionen während der kardialen Regeneration korrelieren. Ich zeige, dass die Überexpression von *mstnb* und ein Verlust von *inhbaa* die Kardiomyozytenproliferation negativ beeinflusst und daher die kardiale Regeneration stört. Dagegen fördern ein Verlust an *mstnb* und eine Überexpression von *inhbaa* nicht nur die physiologische Kardiomyozytenproliferation, sondern sie beschleunigen auch die Erholung des Herzens. Zusätzlich fördert eine Überexpression von *inhbaa* die Proliferation der Kardiomyozyten unabhängig des wohlbekannten Nrg-ErB-Signalweges. Ich habe weiterhin herausgefunden, dass Mstnb und Inhbaa die Aktivitäten der Smad2- und Smad3-Transkriptionsfaktoren durch alternierende Activin-Typ-2-Rezeptorkomplexe kontrollieren, und dadurch die Proliferation der Kardiomyozyten regulieren.

II. English Summary

Opposite effects of *mstnb* and *inhbaa* on cardiomyocyte proliferation during development and repair.

Introduction

The adult mammalian heart is unable to regenerate damaged muscle tissue after myocardial infarction (MI). Instead, the damaged muscle is replaced by a non-contractile and functionally inert fibrotic scar, which disturbs the performance of the heart and causes arrhythmia (Steinhauser and Lee, 2011). Consequently MI is one of the leading causes of deaths worldwide (Mozaffarian et al., 2016). Several fields of research are trying to develop novel regenerative approaches to address this problem and are majorly focusing on the stimulation of cardiomyocyte proliferation *in situ* (Bersell et al., 2009), the engraftment of stem cell-derived cardiomyocytes into the injured hearts (Chong et al., 2014), or the *in situ* trans-differentiation of fibroblasts into functional cardiomyocytes (Qian et al., 2012).

However, unlike mammals, lower vertebrates including zebrafish (Poss et al., 2002) can effectively regenerate the damaged cardiac tissue after multiple types of injury, such ventricular resection (Poss et al., 2002), cryoinjury (Chablais et al., 2011), or genetic cardiomyocyte ablation (Wang et al., 2011). Lineage tracing experiments have suggested that spared cardiomyocytes in the vicinity of the injured area undergo dedifferentiation and proliferation, thereby giving rise to new cardiomyocytes which replace the injured muscle (Jopling et al., 2010; Kikuchi et al., 2010). This makes zebrafish a suitable model organism to dissect the various molecular mechanisms underlying the process of cardiac regeneration, which would contribute in developing novel regenerative therapies.

Several signaling pathways such as retinoic acid, interleukin 6 and epidermal growth factor (EGF) signaling have been reported to be involved in cardiac regeneration (Fang et al., 2013; Kikuchi, 2014; Kikuchi et al., 2011b; Marín-Juez et al., 2016; Wu et al., 2016). However, to date, only Neuregulin (Nrg) and its co-receptor ERBB2 have been reported to possess mitogenic activity by inducing cardiomyocyte proliferation in both healthy and injured hearts of the fish and mammals (Bersell et al., 2009; D'Uva et al., 2015; Gemberling et al., 2015; Liu et al., 2010). This makes Nrg a fundamental subject of ongoing research to assess its therapeutic potential for the treatment of human heart patients (Polizzotti et al., 2015).

Notably, TGF-β signaling pathway has been implicated in various developmental (Ahuja et al., 2016; Azhar et al., 2009) and disease conditions (Pohlers et al., 2009; Siegel and Massagué, 2003), however the role of its various components in regulating cardiac regeneration still remains unclear. The vertebrate TGF-β/Activin subfamily (TGF-β subfamily) of ligands includes Activins (INHBA, INHBB), GDFs (Myostatin/GDF8, GDF11) and TGF-β (TGFB1, TGFB2 and TGFB3) which bind Activin type 2 receptors (ACVR2A, ACVR2B, TGFBR2), leading to the recruitment and activation of Activin type 1 receptors (ACVR1B, TGFBR1, ACVR1C). This process is followed by the phosphorylation of downstream effectors Smad2/3, which bind to Smad4 and translocate to the nucleus, thereby modulating the target gene expression (Massagué and Gomis, 2006; Massagué, 2012; Sartori et al., 2014).

Enhanced TGF-β signaling, including the upregulation of Myostatin (MSTN) (Castillero et al., 2015), Inhibin betaA (INHBA) (Yndestad et al., 2004) and TGF-β (Li et al., 1997) has been observed post MI in the mammalian heart, which further stimulates hypertrophy, apoptosis and endothelial-mesenchymal transition (Euler-Taimor and Heger, 2006; Zeisberg et al., 2007). Additionally, cardiomyocyte-specific deletion of *Tgfbr2* reduces pathological cardiac remodeling in response to sustained pressure overload (Koitabashi et al., 2011). However, in zebrafish, TGF-β signaling is essential during cardiac regeneration as the pharmacological inhibition of Activin type 1 receptors suppresses cardiomyocyte proliferation and compromises cardiac regeneration (Chablais and Jazwinska, 2012). MSTN, a well-known negative regulator of skeletal muscle growth (Haidet et al., 2008; Whittemore et al., 2003), has been implicated in the development of cardiac hypertrophy in mammals (Biesemann et al., 2014; Rodgers et al., 2009). Moreover, the absence of MSTN enhances skeletal muscle regeneration in mice (Wagner et al., 2005) and a recently developed monoclonal antibody against MSTN shows therapeutic potential in skeletal muscle atrophy treatment (Latres et al., 2015). *inhba*, also known as *activin betaA*, promotes wound closure by regulating c-jun phosphorylation and blastema proliferation, therefore positively regulates zebrafish fin regeneration (Jaźwińska et al., 2007). Altogether, the role of TGF-β signaling and its various ligands during cardiac regeneration remains unclear. Thus, by using gene expression profiling, I identify here the opposing expression response of two TGF-β genes, *mstnb* and *inhbaa* to cardiac injury, calling for a detailed investigation of their function during cardiac regeneration.

Here, I show that Mstnb and Inhbaa exert opposite effects on cardiac regeneration, as the loss of *mstnb* and the activation of *inhbaa* positively regulate cardiomyocyte proliferation, thereby leading to enhanced cardiac regeneration. Further, I identify that Mstnb and Inhbaa signal through alternate Activin receptor complexes to control the activities of Smad2 and Smad3 transcription factors, and therefore inversely regulate cardiomyocyte proliferation.

Results and Discussion

To identify the genes differentially regulated during adult zebrafish cardiac regeneration, I performed microarray-based expression analysis of 4 days post cryoinjured (dpci) vs. 4 days post sham injured (4 dpsi) hearts (Figure 4.1a). Interestingly, I detected opposing expression response of *mstnb* and *inhbaa* to cryoinjury (Figure 4.1b), which was confirmed by performing real-time quantitative PCR (RT-qPCR) on sham and cryoinjured ventricles at different time points post injury. Similar to my microarray data, I observed a rapid and continuous downregulation of *mstnb* transcript levels throughout the process of regeneration (Figure 4.2a). However, its expression returned to basal levels at 60 dpci (Figure 4.2a), when regeneration was completed (Chablais et al., 2011), suggesting that a continuous downregulation of *mstnb* expression is crucial for cardiac regeneration. Conversely, *inhbaa* mRNA expression peaked at 4 dpci and returned to sham levels at 8 dpci (Figure 4.2b), indicating a principal role for *inhbaa* during the early phase of cardiac regeneration. Further, the spatio-temporal expression pattern of *mstnb* and *inhbaa* was analyzed by performing *in situ* hybridization on sections (Figure 4.2c-f; *in situ* hybridization experiments were performed in collaboration with Dr. Hyun-Taek Kim). *mstnb* expression was detected in the ventricular wall of the uninjured hearts (Figure 4.2c) and was reduced below detectable levels after cryoinjury (Figure 4.2d). However, no expression of *inhbaa* could be detected in uninjured hearts (Figure 4.2e), while it was prominently detected proximal to the injured area at 4 dpci (Figure 4.2f). Altogether, the expression patterns of both the genes as assessed by microarray profiling, RT-qPCR and *in situ* hybridization, clearly show different spatio-temporal changes during cardiac regeneration.

Following my observation that the expression of *mstnb* decreases and the expression of *inhbaa* increases during cardiac regeneration, I wanted to analyze the effect of *mstnb* overexpression and loss of *inhbaa* expression in regenerating hearts. Thus, I generated a transgenic zebrafish line for cardiomyocyte-specific constitutive overexpression of *mstnb*,

Tg(myl7:mstnb-2A-H2B-EGFP)bns145 (*mstnb* OE hereafter) (Figure 4.4). I also generated *inhbaa* mutant fish, using a TALEN targeting the TGF-β propeptide domain of Inhbaa (Figure 4.5a). A 17 bp deletion allele, *inhbaa*^{bns37} was thus recovered, which is predicted to encode a truncated protein (Figure 4.5b, c). Interestingly, I observed that 45 dpci *mstnb* OE and *inhbaa*$^{-/-}$ hearts were unable to resolve their scar, in contrast to wild-type siblings of the same regenerative stage (Figure 4.10). Further, I tested whether *inhbaa* deficiency or *mstnb* overexpression modulate cardiomyocyte proliferation post cryoinjury. There was a significant reduction in cardiomyocyte proliferation in *mstnb* OE and *inhbaa*$^{-/-}$ hearts compared to their wild-type siblings at 6 dpci (Figure 4.12). Taken together, these results show that *mstnb* gain-of-function (GOF) and *inhbaa* loss-of-function (LOF) negatively affect cardiomyocyte proliferation and interfere with cardiac regeneration, consequently causing a reduction in scar clearance.

As a complementary approach, I examined the effects of *mstnb* LOF and *inhbaa* GOF on cardiac development and regeneration. I generated *mstnb* mutant fish using a TALEN targeting the region after the signal peptide domain and recovered a 10 bp deletion allele, *mstnb*^{bns5}, which is predicted to encode a truncated protein (Figure 4.16). Adult *mstnb*$^{-/-}$ animals show increased heart size with a thickened ventricular wall (Figure 4.20). To better understand whether the increase in ventricular wall thickness was due to increased cardiomyocyte proliferation in the compact layer, I carried out cardiomyocyte EdU incorporation analysis. Compared to siblings, hearts of *mstnb*$^{-/-}$ animals showed a significant increase in the total number of cardiomyocytes as well as EdU incorporation in cardiomyocytes, in both the wall and the trabeculae of the ventricle (Figure 4.21). Next, I generated a transgenic zebrafish line for cardiomyocyte-specific constitutive overexpression of *inhbaa*, *Tg(myl7:inhbaa-2A-H2B-EGFP)bns146* (*inhbaa* OE hereafter) (Figure 4.18). Adult *inhbaa* OE animals have significantly enlarged hearts and show dense trabeculation in both chambers (Figure 4.22; H&E staining experiments in Figure 4.22a', a'', b', b'' were performed in collaboration with Dr. Suchit Ahuja). Again, I investigated the causality of cardiac enlargement and hypertrabeculation in *inhbaa* OE hearts, by performing EdU incorporation analysis. There was a significant increase in the total number of cardiomyocytes as well as EdU incorporation in cardiomyocytes in *inhbaa* OE hearts compared to control (Figure 4.24). I next tested whether increased cardiomyocyte proliferation helps *mstnb*$^{-/-}$ and *inhbaa* OE hearts after injury. I thus found that 30 dpci *mstnb*$^{-/-}$ and *inhbaa* OE hearts had completely resolved scars, unlike their siblings (Figure 4.25).

Taken together, these results reveal that *mstnb* LOF and *inhbaa* GOF positively affect physiological cardiomyocyte proliferation and lead to enhanced cardiac regeneration.

Having established that *inhbaa* OE promotes cardiomyocyte proliferation, I wanted to assess whether its function depended on the Nrg-ErbB signaling pathway. Using *erbb2*^{st61} mutants as well as ErbB2 inhibitor, I observed that *inhbaa* OE is able to induce cardiomyocyte proliferation even in the absence of ErbB signaling (Figure 4.27, 4.28). Interestingly, the combined overexpression of *inhbaa* and *nrg2a* showed cardiomyocyte EdU incorporation similar to *nrg2a* OE alone (Figure 4.29; the *nrg2a* OE transgenic line used in Figure 4.29 d-f has been provided by collaborator Seyed Javad Rasouli), indicating that either cardiomyocyte proliferation reaches its maximum by *nrg2a* OE alone or ErbB signaling interferes with Inhbaa-mediated proliferation, as reported previously (Kretzschmar et al., 1999). Further, in the larvae obtained from the cross between *mstnb* OE and *inhbaa* OE animals, I found that *mstnb* OE reduces myocardial EdU incorporation induced by *inhbaa* OE to levels similar to wild-type siblings (Figure 4.30), suggesting that Mstnb and Inhbaa compete in controlling cardiomyocyte proliferation.

I next aimed to decipher the molecular mechanisms underlying the differential regulation of cardiomyocyte proliferation and thus, cardiac regeneration by *mstnb* and *inhbaa*. Myostatin and Activin act through the TGF-β signaling cascade, leading to the phosphorylation of signal transducers Smad2 and Smad3 (Massagué and Gomis, 2006; Massagué, 2012; Rebbapragada et al., 2003). Smad2, along with Smad4 and transcription factors such as FAST1/2, binds to Activin Response Elements (ARE), whereas Smad3 binds to the Smad Binding Elements (SBE) present in the promoter region of their target genes (Chen et al., 1997, 1996; Jonk et al., 1998; Labbé et al., 1998; Stroschein et al., 1999). To identify potentially distinct transcriptional targets of Mstnb and Inhbaa signaling, I assessed the effect of *mstnb* or *inhbaa* overexpression on Smad2 and Smad3 reporter activities, by using the published Smad2 reporter line, *Tg(ARE:EGFP)fci100* (van Boxtel et al., 2015) and Smad3 reporter line, *Tg(12XSBE:EGFP)ia16* (Casari et al., 2014). *mstnb* overexpression led to a significant induction of Smad2 reporter expression, whereas a downregulation of Smad3 reporter expression (Figure 4.31). Conversely, *inhbaa* overexpression induced Smad3 reporter activity and suppressed Smad2 reporter activity (Figure 4.31). I validated this data by analyzing the effect of *mstnb* or *inhbaa* overexpression on Smad2- and Smad3-specific target gene expression (Chen et al., 1996; Jonk et al., 1998; Labbé et al., 1998; Stroschein et al., 1999),

both during early embryonic development and in the injured adult heart. Notably, I observed an upregulation of Smad2 target gene expression by *mstnb* overexpression but a downregulation of their expression after *inhbaa* overexpression (Figure 4.32, 4.34). In contrast, there was an upregulation of Smad3 target gene expression by *inhbaa* overexpression but a downregulation of their expression by *mstnb* overexpression (Figure 4.33, 4.35). These results collectively suggest that the activities of Smad2 and Smad3 are inversely regulated by *mstnb* and *inhbaa*.

I further wanted to test whether *mstnb* and *inhbaa* affect the myocardial Smad3 phosphorylation, as Smad3-dependent TGF-β signaling has been previously linked to cardiac regeneration in zebrafish (Chablais and Jazwinska, 2012). I observed that *mstnb* overexpression inhibits Smad3 phosphorylation in cardiomyocytes, whereas *inhbaa* overexpression promotes this process (Figure 4.36). Notably, I also found that loss of *mstnb* positively regulates myocardial Smad3 phosphorylation and loss of *inhbaa* negatively regulates this process (Figure 4.37). Therefore, I conclude that Mstnb and Inhbaa act antagonistically to one another to control Smad3 phosphorylation, a seemingly crucial event during cardiac regeneration.

Further, I observed that the pharmocological inhibition of Smad3 phosphorylation suppressed cardiomyocyte EdU incorporation, indicating that cardiomyocyte proliferation relies on Smad3 phosphorylation (Figure 4.39). I next analyzed the effects of constitutively active (ca) Smad2, Smad3a and Smad3b on cardiomyocyte proliferation following mosaic overexpression. There was a significant reduction in EdU incorporation in cardiomyocytes expressing *caSmad2*, whereas both *caSmad3a* and *caSmad3b* expression resulted in the induction of cardiomoycyte EdU incorporation (Figure 4.41), suggesting that Smad2 and Smad3 inversely regulate cardiomyocyte proliferation in zebrafish and could potentially explain how different TGF-β ligands can have opposite effects during cardiac regeneration.

Ultimately, I wanted to investigate how Mstnb and Inhbaa could function antagonistically to one another if they work through the same signaling cascade (Massagué and Gomis, 2006; Massagué, 2012; Rebbapragada et al., 2003). Thus, to better understand the ligand-receptor relationship, I performed combined activin type 2 receptor gene knockdown and *mstnb* or *inhbaa* overexpression experiments. I found that the knockdown of *acvr2b* (*acvr2ba* and *acvr2bb*) influenced the effect of *mstnb* overexpression on Smad2 and Smad3 reporter

expression, whereas the knockdown of *acvr2a* (*acvr2aa* and *acvr2ab*) influenced the effect of *inhbaa* overexpression on Smad2 and Smad3 reporter expression (Figure 4.42). Further, I analyzed the effect of these receptor knockdowns on cardiomyocyte EdU incorporation in the *mstnb* OE and *inhbaa* OE lines (Figure 4.43a) and found that *acvr2bb* knockdown prevents the suppression of cardiomyocyte proliferation by *mstnb* overexpression (Figure 4.43b-e) , which indicates that Mstnb has a preference for binding Acvr2b over Acvr2a, as per previous studies (Lee and McPherron, 2001; Rebbapragada et al., 2003). However, *acvr2aa* knockdown prevents the induction of cardiomyocyte proliferation by *inhbaa* OE (Figure 4.43f-i), suggesting a previously unreported preference for Inhbaa to signal through Acvr2a over Acvr2b. Overall, my data indicates that Mstn binds to Acvr2b, thereby promoting Smad2 and suppressing Smad3 activation, while Inhbaa binds to Acvr2a, thus promoting Smad3 and suppressing Smad2 activation.

Conclusion

In conclusion, I identify here the opposite effects of two TGF-β genes, *mstnb* and *inhbaa* on cardiomyocyte proliferation during cardiac development and regeneration. Here I show for the first time the differential expression response of *mstnb* and *inhbaa* to cardiac injury, which correlates with their opposite functions during cardiac regeneration. I show that overexpression of *mstnb* and loss of *inhbaa* negatively affect cardiomyocyte proliferation and therefore disturb cardiac regeneration. However, loss of *mstnb* and overexpression of *inhbaa* not only promote physiological cardiomyocyte proliferation, but also accelerate cardiac recovery. Additionally, the overexpression of *inhbaa* promotes cardiomyocyte proliferation independently of the well-known Nrg-ErbB signaling pathway. I further identify that Mstnb and Inhbaa inversely control the activities of Smad2 and Smad3 transcription factors through alternate Activin type 2 receptor complexes, thus regulating cardiomyocyte proliferation.

III. References

Ahuja, S., Dogra, D., Stainier, D.Y., Reischauer, S., 2016. Id4 functions downstream of Bmp signaling to restrict TCF function in endocardial cells during atrioventricular valve development. Dev. Biol. 412, 71–82.

Anderson, R.M., Bosch, J.A., Goll, M.G., Hesselson, D., Dong, P.D., Shin, D., Chi, N.C., Shin, C.H., Schlegel, A., Halpern, M., Stainier, D.Y., 2009. Loss of Dnmt1 catalytic activity reveals multiple roles for DNA methylation during pancreas development and regeneration. Dev. Biol. 334, 213–23.

Antsiferova, M, Werner, S, 2012. The bright and the dark sides of activin in wound healing and cancer. J Cell Sci.

Azhar, M., Runyan, R.B., Gard, C., Sanford, L.P., Miller, M.L., Andringa, A., Pawlowski, S., Rajan, S., Doetschman, T., 2009. Ligand-specific function of transforming growth factor beta in epithelial-mesenchymal transition in heart development. Dev. Dyn. 238, 431–42.

Azhar, M., Schultz, J.J., Grupp, I., Dorn, G.W., Meneton, P., Molin, D.G., Groot, A.C., Doetschman, T., 2003. Transforming growth factor beta in cardiovascular development and function. Cytokine & growth factor reviews 14, 391–407.

Bae, Y.-K.K., Kani, S., Shimizu, T., Tanabe, K., Nojima, H., Kimura, Y., Higashijima, S., Hibi, M., 2009. Anatomy of zebrafish cerebellum and screen for mutations affecting its development. Dev. Biol. 330, 406–26.

Bashir, M, Damineni, S, Mukherjee, G, Kondaiah, P, 2015. Activin-A signaling promotes epithelial–mesenchymal transition, invasion, and metastatic growth of breast cancer. Npj Breast Cancer.

Beltrami, A.P., Urbanek, K., Kajstura, J., Yan, S.M., Finato, N., Bussani, R., Nadal-Ginard, B., Silvestri, F., Leri, A., Beltrami, C.A., Anversa, P., 2001. Evidence that human cardiac myocytes divide after myocardial infarction. N. Engl. J. Med. 344, 1750–7.

Bergmann, O., Bhardwaj, R.D., Bernard, S., Zdunek, S., Barnabé-Heider, F., Walsh, S., Zupicich, J., Alkass, K., Buchholz, B.A., Druid, H., Jovinge, S., Frisén, J., 2009. Evidence for cardiomyocyte renewal in humans. Science 324, 98–102.

Bersell, K., Arab, S., Haring, B., Kühn, B., 2009. Neuregulin1/ErbB4 signaling induces cardiomyocyte proliferation and repair of heart injury. Cell 138, 257–70.

Bicknell, K.A., Coxon, C.H., Brooks, G., 2004. Forced expression of the cyclin B1-CDC2 complex induces proliferation in adult rat cardiomyocytes. Biochem. J. 382, 411–6.

Biesemann, N., Mendler, L., Kostin, S., Wietelmann, A., Borchardt, T., Braun, T., 2015. Myostatin induces interstitial fibrosis in the heart via TAK1 and p38. Cell Tissue Res. 361, 779–87.

Biesemann, N., Mendler, L., Wietelmann, A., Hermann, S., Schäfers, M., Krüger, M., Boettger, T., Borchardt, T., Braun, T., 2014. Myostatin regulates energy homeostasis in the heart and prevents heart failure. Circ. Res. 115, 296–310.

Bish, L.T., Morine, K.J., Sleeper, M.M., Sweeney, H.L., 2010. Myostatin is upregulated following stress in an Erk-dependent manner and negatively regulates cardiomyocyte growth in culture and in a mouse model. PLoS ONE 5, e10230.

Boxtel, A.L. van, Chesebro, J.E., Heliot, C., Ramel, M.-C.C., Stone, R.K., Hill, C.S., 2015. A Temporal Window for Signal Activation Dictates the Dimensions of a Nodal Signaling Domain. Dev. Cell 35, 175–85.

Brown, K.A., Pietenpol, J.A., Moses, H.L., 2007. A tale of two proteins: differential roles and regulation of Smad2 and Smad3 in TGF-beta signaling. J. Cell. Biochem. 101, 9–33.

Bujak, M., Frangogiannis, N.G., 2007. The role of TGF-beta signaling in myocardial infarction and cardiac remodeling. Cardiovasc. Res. 74, 184–95.

Burns, G.C., MacRae, C.A., 2006. Purification of hearts from zebrafish embryos. Biotechniques 40, 274.

Carnac, G., Vernus, B., Bonnieu, A., 2007. Myostatin in the pathophysiology of skeletal muscle. Curr. Genomics 8, 415–22.

Casari, A., Schiavone, M., Facchinello, N., Vettori, A., Meyer, D., Tiso, N., Moro, E., Argenton, F., 2014. A Smad3 transgenic reporter reveals TGF-beta control of zebrafish spinal cord development. Dev. Biol. 396, 81–93.

Castillero, E., Akashi, H., Wang, C., Najjar, M., Ji, R., Kennel, P.J., Sweeney, H.L., Schulze, P.C., George, I., 2015. Cardiac myostatin upregulation occurs immediately after myocardial ischemia and is involved in skeletal muscle activation of atrophy. Biochem. Biophys. Res. Commun. 457, 106–11.

Chablais, F., Jazwinska, A., 2012. The regenerative capacity of the zebrafish heart is dependent on TGFβ signaling. Development 139, 1921–30.

Chablais, F., Jaźwińska, A., 2012. Induction of myocardial infarction in adult zebrafish using cryoinjury. J Vis Exp.

Chablais, F., Veit, J., Rainer, G., Jaźwińska, A., 2011. The zebrafish heart regenerates after cryoinjury-induced myocardial infarction. BMC Dev. Biol. 11, 21.

Chen, X, Weisberg, E, Fridmacher, V, Watanabe, M, 1997. Smad4 and FAST-1 in the assembly of activin-responsive factor. Nature.

Chen, H., Zhang, W., Li, D., Cordes, T.M., Mark Payne, R., Shou, W., 2009. Analysis of ventricular hypertrabeculation and noncompaction using genetically engineered mouse models. Pediatr Cardiol 30, 626–34.

Chen, X., Rubock, M.J., Whitman, M., 1996. A transcriptional partner for MAD proteins in TGF-beta signalling. Nature 383, 691–6.

Chipuk, J.E., Cornelius, S.C., Pultz, N.J., Jorgensen, J.S., Bonham, M.J., Kim, S.-J.J., Danielpour, D., 2002. The androgen receptor represses transforming growth factor-beta signaling through interaction with Smad3. J. Biol. Chem. 277, 1240–8.

Chisada, S.-I., Okamoto, H., Taniguchi, Y., Kimori, Y., Toyoda, A., Sakaki, Y., Takeda, S., Yoshiura, Y., 2011. Myostatin-deficient medaka exhibit a double-muscling phenotype with hyperplasia and hypertrophy, which occur sequentially during post-hatch development. Dev. Biol. 359, 82–94.

Choi, W.-Y.Y., Gemberling, M., Wang, J., Holdway, J.E., Shen, M.-C.C., Karlstrom, R.O., Poss, K.D., 2013. In vivo monitoring of cardiomyocyte proliferation to identify chemical modifiers of heart regeneration. Development 140, 660–6.

Chong, J.J., Murry, C.E., 2014. Cardiac regeneration using pluripotent stem cells--progression to large animal models. Stem Cell Res 13, 654–65.

Chong, J.J., Yang, X., Don, C.W., Minami, E., Liu, Y.-W.W., Weyers, J.J., Mahoney, W.M., Biber, B. Van, Cook, S.M., Palpant, N.J., Gantz, J.A., Fugate, J.A., Muskheli, V., Gough, G.M., Vogel, K.W., Astley, C.A., Hotchkiss, C.E., Baldessari, A., Pabon, L., Reinecke, H., Gill, E.A., Nelson, V., Kiem, H.-P.P., Laflamme, M.A., Murry, C.E., 2014. Human embryonic-stem-cell-derived cardiomyocytes regenerate non-human primate hearts. Nature 510, 273–7.

Curado, S., Anderson, R.M., Jungblut, B., Mumm, J., Schroeter, E., Stainier, D.Y., 2007. Conditional targeted cell ablation in zebrafish: a new tool for regeneration studies. Dev. Dyn. 236, 1025–35.

Denis, J.-F.F., Sader, F., Gatien, S., Villiard, É., Philip, A., Roy, S., 2016. Activation of Smad2 but not Smad3 is required to mediate TGF-β signaling during axolotl limb regeneration. Development 143, 3481–3490.

Derynck, R., Zhang, Y.E., 2003. Smad-dependent and Smad-independent pathways in TGF-beta family signalling. Nature 425, 577–84.

Dickover, M.S., Zhang, R., Han, P., Chi, N.C., 2013. Zebrafish cardiac injury and regeneration models: a noninvasive and invasive in vivo model of cardiac regeneration. Methods Mol. Biol. 1037, 463–73.

D'Uva, G., Aharonov, A., Lauriola, M., Kain, D., Yahalom-Ronen, Y., Carvalho, S., Weisinger, K., Bassat, E., Rajchman, D., Yifa, O., Lysenko, M., Konfino, T., Hegesh, J., Brenner, O., Neeman, M., Yarden, Y., Leor, J., Sarig, R., Harvey, R.P., Tzahor, E., 2015. ERBB2 triggers mammalian heart regeneration by promoting cardiomyocyte dedifferentiation and proliferation. Nat. Cell Biol. 17, 627–38.

Eghbali, M, Tomek, R, Sukhatme, VP, Woods, C, 1991. Differential effects of transforming growth factor-beta 1 and phorbol myristate acetate on cardiac fibroblasts. Regulation of fibrillar collagen mRNAs and expression of …. Circulation ….

Euler-Taimor, G., Heger, J., 2006. The complex pattern of SMAD signaling in the cardiovascular system. Cardiovasc. Res. 69, 15–25.

Fang, Y., Gupta, V., Karra, R., Holdway, J.E., Kikuchi, K., Poss, K.D., 2013. Translational profiling of cardiomyocytes identifies an early Jak1/Stat3 injury response required for zebrafish heart regeneration. Proc. Natl. Acad. Sci. U.S.A. 110, 13416–21.

Gemberling, M., Karra, R., Dickson, A.L., Poss, K.D., 2015. Nrg1 is an injury-induced cardiomyocyte mitogen for the endogenous heart regeneration program in zebrafish. Elife 4.

Gentry, LE, Lioubin, MN, Purchio, AF, 1988. Molecular events in the processing of recombinant type 1 pre-pro-transforming growth factor beta to the mature polypeptide. Molecular and cellular ….

González-Rosa, J.M., Martín, V., Peralta, M., Torres, M., Mercader, N., 2011. Extensive scar formation and regression during heart regeneration after cryoinjury in zebrafish. Development 138, 1663–74.

González-Rosa, J.M., Mercader, N., 2012. Cryoinjury as a myocardial infarction model for the study of cardiac regeneration in the zebrafish. Nat Protoc 7, 782–8.

González-Rosa, J.M., Peralta, M., Mercader, N., 2012. Pan-epicardial lineage tracing reveals that epicardium derived cells give rise to myofibroblasts and perivascular cells during zebrafish heart regeneration. Dev. Biol. 370, 173–86.

Gupta, V., Gemberling, M., Karra, R., Rosenfeld, G.E., Evans, T., Poss, K.D., 2013. An injury-responsive gata4 program shapes the zebrafish cardiac ventricle. Curr. Biol. 23, 1221–7.

Haidet, A.M., Rizo, L., Handy, C., Umapathi, P., Eagle, A., Shilling, C., Boue, D., Martin, P.T., Sahenk, Z., Mendell, J.R., Kaspar, B.K., 2008. Long-term enhancement of skeletal muscle mass and strength by single gene administration of myostatin inhibitors. Proc. Natl. Acad. Sci. U.S.A. 105, 4318–22.

Han, P., Bloomekatz, J., Ren, J., Zhang, R., Grinstein, J.D., Zhao, L., Burns, C.G., Burns, C.E., Anderson, R.M., Chi, N.C., 2016. Coordinating cardiomyocyte interactions to direct ventricular chamber morphogenesis. Nature 534, 700–4.

Hein, S., Arnon, E., Kostin, S., Schönburg, M., Elsässer, A., Polyakova, V., Bauer, E.P., Klövekorn, W.-P.P., Schaper, J., 2003. Progression from compensated hypertrophy to failure in the pressure-overloaded human heart: structural deterioration and compensatory mechanisms. Circulation 107, 984–91.

Heinrich, P.C., Behrmann, I., Haan, S., Hermanns, H.M., Müller-Newen, G., Schaper, F., 2003. Principles of interleukin (IL)-6-type cytokine signalling and its regulation. Biochem. J. 374, 1–20.

Hill, J.J., Davies, M.V., Pearson, A.A., Wang, J.H., Hewick, R.M., Wolfman, N.M., Qiu, Y., 2002. The myostatin propeptide and the follistatin-related gene are inhibitory binding proteins of myostatin in normal serum. J. Biol. Chem. 277, 40735–41.

Hirano, T, Ishihara, K, Hibi, M, 2000. Roles of STAT3 in mediating the cell growth, differentiation and survival signals relayed through the IL-6 family of cytokine receptors. Oncogene.

Ho, D.M., Whitman, M., 2008. TGF-beta signaling is required for multiple processes during Xenopus tail regeneration. Dev. Biol. 315, 203–16.

Hoover, L.L., Burton, E.G., Brooks, B.A., Kubalak, S.W., 2008. The expanding role for retinoid signaling in heart development. The Scientific World Journal 8, 194–211.

Hudson, J.E., Porrello, E.R., 2013. The non-coding road towards cardiac regeneration. J Cardiovasc Transl Res 6, 909–23.

Inman, G.J., Nicolás, F.J., Callahan, J.F., Harling, J.D., Gaster, L.M., Reith, A.D., Laping, N.J., Hill, C.S., 2002. SB-431542 is a potent and specific inhibitor of transforming growth factor-beta superfamily type I activin receptor-like kinase (ALK) receptors ALK4, ALK5, and ALK7. Mol. Pharmacol. 62, 65–74.

Itou, J., Oishi, I., Kawakami, H., Glass, T.J., Richter, J., Johnson, A., Lund, T.C., Kawakami, Y., 2012. Migration of cardiomyocytes is essential for heart regeneration in zebrafish. Development 139, 4133–42.

Jaźwińska, A., Badakov, R., Keating, M.T., 2007. Activin-betaA signaling is required for zebrafish fin regeneration. Curr. Biol. 17, 1390–5.

Jia, M, Souchelnytstkyi, S, 2011. Comments on the cross-talk of TGF and EGF in cancer. Experimental oncology 33, 170–173.

Jinnin, M., Ihn, H., Tamaki, K., 2006. Characterization of SIS3, a novel specific inhibitor of Smad3, and its effect on transforming growth factor-beta1-induced extracellular matrix expression. Mol. Pharmacol. 69, 597–607.

Jones, KL, Kretser, D.D., Patella, S, 2004. Activin A and follistatin in systemic inflammation. Molecular and cellular ….

Jonk, L., Itoh, S., Heldin, C.-H., Dijke, P. ten, Kruijer, W., 1998. Identification and Functional Characterization of a Smad Binding Element (SBE) in the JunB Promoter That Acts as a Transforming Growth Factor-β, Activin, and Bone Morphogenetic Protein-inducible Enhancer. J Biol Chem 273, 21145–21152.

Jopling, C., Sleep, E., Raya, M., Martí, M., Raya, A., Izpisúa Belmonte, J.C., 2010. Zebrafish heart regeneration occurs by cardiomyocyte dedifferentiation and proliferation. Nature 464, 606–9.

Jopling, C., Suñé, G., Faucherre, A., Fabregat, C., Belmonte, J., 2012. Hypoxia induces myocardial regeneration in zebrafish. Circulation CIRCULATIONAHA. 112.107888.

Kang, Y, Chen, CR, Massagué, J, 2003. A self-enabling TGFβ response coupled to stress signaling: Smad engages stress response factor ATF3 for Id1 repression in epithelial cells. Molecular cell.

Kardami, E, 1990. Stimulation and inhibition of cardiac myocyte proliferation in vitro. Molecular and cellular biochemistry.

Karra, R., Knecht, A.K., Kikuchi, K., Poss, K.D., 2015. Myocardial NF-κB activation is essential for zebrafish heart regeneration. Proc. Natl. Acad. Sci. U.S.A. 112, 13255–60.

Kastner, P., Grondona, J.M., Mark, M., Gansmuller, A., LeMeur, M., Decimo, D., Vonesch, J.L., Dollé, P., Chambon, P., 1994. Genetic analysis of RXR alpha developmental function:

convergence of RXR and RAR signaling pathways in heart and eye morphogenesis. Cell 78, 987–1003.

Kikuchi, K., 2014. Advances in understanding the mechanism of zebrafish heart regeneration. Stem Cell Res 13, 542–55.

Kikuchi, K., Gupta, V., Wang, J., Holdway, J.E., Wills, A.A., Fang, Y., Poss, K.D., 2011a. tcf21+ epicardial cells adopt non-myocardial fates during zebrafish heart development and regeneration. Development 138, 2895–902.

Kikuchi, K., Holdway, J.E., Major, R.J., Blum, N., Dahn, R.D., Begemann, G., Poss, K.D., 2011b. Retinoic acid production by endocardium and epicardium is an injury response essential for zebrafish heart regeneration. Dev. Cell 20, 397–404.

Kikuchi, K., Holdway, J.E., Werdich, A.A., Anderson, R.M., Fang, Y., Egnaczyk, G.F., Evans, T., Macrae, C.A., Stainier, D.Y., Poss, K.D., 2010. Primary contribution to zebrafish heart regeneration by gata4(+) cardiomyocytes. Nature 464, 601–5.

Koitabashi, N., Danner, T., Zaiman, A.L., Pinto, Y.M., Rowell, J., Mankowski, J., Zhang, D., Nakamura, T., Takimoto, E., Kass, D.A., 2011. Pivotal role of cardiomyocyte TGF-β signaling in the murine pathological response to sustained pressure overload. J. Clin. Invest. 121, 2301–12.

Kretzschmar, M., Doody, J., Timokhina, I., Massagué, J., 1999. A mechanism of repression of TGFbeta/ Smad signaling by oncogenic Ras. Genes Dev. 13, 804–16.

Kubin, T., Pöling, J., Kostin, S., Gajawada, P., Hein, S., Rees, W., Wietelmann, A., Tanaka, M., Lörchner, H., Schimanski, S., Szibor, M., Warnecke, H., Braun, T., 2011. Oncostatin M is a major mediator of cardiomyocyte dedifferentiation and remodeling. Cell Stem Cell 9, 420–32.

Labbé, E., Silvestri, C., Hoodless, P.A., Wrana, J.L., Attisano, L., 1998. Smad2 and Smad3 positively and negatively regulate TGF beta-dependent transcription through the forkhead DNA-binding protein FAST2. Mol. Cell 2, 109–20.

Laflamme, M.A., Murry, C.E., 2011. Heart regeneration. Nature 473, 326–35.

Latres, E., Pangilinan, J., Miloscio, L., Bauerlein, R., Na, E., Potocky, T.B., Huang, Y., Eckersdorff, M., Rafique, A., Mastaitis, J., Lin, C., Murphy, A.J., Yancopoulos, G.D., Gromada, J., Stitt, T., 2015. Myostatin blockade with a fully human monoclonal antibody induces muscle hypertrophy and reverses muscle atrophy in young and aged mice. Skelet Muscle 5, 34.

Lee, S.J., McPherron, A.C., 2001. Regulation of myostatin activity and muscle growth. Proc. Natl. Acad. Sci. U.S.A. 98, 9306–11.

Lepilina, A., Coon, A.N., Kikuchi, K., Holdway, J.E., Roberts, R.W., Burns, C.G., Poss, K.D., 2006. A dynamic epicardial injury response supports progenitor cell activity during zebrafish heart regeneration. Cell 127, 607–19.

Li, R.K., Li, G., Mickle, D.A., Weisel, R.D., Merante, F., Luss, H., Rao, V., Christakis, G.T., Williams, W.G., 1997. Overexpression of transforming growth factor-beta1 and insulin-like growth factor-I in patients with idiopathic hypertrophic cardiomyopathy. Circulation 96, 874–81.

Lian, X., Hsiao, C., Wilson, G., Zhu, K., Hazeltine, L.B., Azarin, S.M., Raval, K.K., Zhang, J., Kamp, T.J., Palecek, S.P., 2012. Robust cardiomyocyte differentiation from human pluripotent stem cells via temporal modulation of canonical Wnt signaling. Proc. Natl. Acad. Sci. U.S.A. 109, E1848–57.

Liu, J., Bressan, M., Hassel, D., Huisken, J., Staudt, D., Kikuchi, K., Poss, K.D., Mikawa, T., Stainier, D.Y., 2010. A dual role for ErbB2 signaling in cardiac trabeculation. Development 137, 3867–75.

Liu, L., Liu, X., Ren, X., Tian, Y., Chen, Z., Xu, X., Du, Y., Jiang, C., Fang, Y., Liu, Z., Fan, B., Zhang, Q., Jin, G., Yang, X., Zhang, X., 2016. Smad2 and Smad3 have differential sensitivity in relaying TGFβ signaling and inversely regulate early lineage specification. Sci Rep 6, 21602.

Lyons, D.A., Pogoda, H.-M., Voas, M.G., Woods, I.G., Diamond, B., Nix, R., Arana, N., Jacobs, J., Talbot, W.S., 2005. erbb3 and erbb2 are essential for schwann cell migration and myelination in zebrafish. Current Biology 15, 513–524.

Marín-Juez, R., Marass, M., Gauvrit, S., Rossi, A., Lai, S.-L.L., Materna, S.C., Black, B.L., Stainier, D.Y., 2016. Fast revascularization of the injured area is essential to support zebrafish heart regeneration. Proc. Natl. Acad. Sci. U.S.A. 113, 11237–11242.

Massagué, J, 2008. TGFβ in cancer. Cell.

Massagué, J., 2000. How cells read TGF-beta signals. Nat. Rev. Mol. Cell Biol. 1, 169–78.

Massagué, J., 2012. TGFβ signalling in context. Nat. Rev. Mol. Cell Biol. 13, 616–30.

Massagué, J., Gomis, R.R., 2006. The logic of TGFbeta signaling. FEBS Lett. 580, 2811–20.

McCroskery, S., Thomas, M., Maxwell, L., Sharma, M., Kambadur, R., 2003. Myostatin negatively regulates satellite cell activation and self-renewal. J. Cell Biol. 162, 1135–47.

McPherron, AC, Lee, SJ, 1997. Double muscling in cattle due to mutations in the myostatin gene. Proceedings of the National ….

McPherron, A.C., Lawler, A.M., Lee, S.J., 1997. Regulation of skeletal muscle mass in mice by a new TGF-beta superfamily member. Nature 387, 83–90.

Miyazono, K., Kamiya, Y., Morikawa, M., 2010. Bone morphogenetic protein receptors and signal transduction. Journal of biochemistry 147, 35–51.

Mollova, M., Bersell, K., Walsh, S., Savla, J., Das, L.T., Park, S.-Y.Y., Silberstein, L.E., Remedios, C.G. Dos, Graham, D., Colan, S., Kühn, B., 2013. Cardiomyocyte proliferation contributes to heart growth in young humans. Proc. Natl. Acad. Sci. U.S.A. 110, 1446–51.

Morikawa, M., Koinuma, D, Miyazono, K., Heldin, C.-H., 2013. Genome-wide mechanisms of Smad binding. Oncogene 32, 1609–1615.

Morissette, M.R., Cook, S.A., Foo, S., McKoy, G., Ashida, N., Novikov, M., Scherrer-Crosbie, M., Li, L., Matsui, T., Brooks, G., Rosenzweig, A., 2006. Myostatin regulates cardiomyocyte growth through modulation of Akt signaling. Circ. Res. 99, 15–24.

Mozaffarian, D., Benjamin, E.J., Go, A.S., Arnett, D.K., Blaha, M.J., Cushman, M., Das, S.R., Ferranti, S. de, Després, J.-P.P., Fullerton, H.J., Howard, V.J., Huffman, M.D., Isasi, C.R., Jiménez, M.C., Judd, S.E., Kissela, B.M., Lichtman, J.H., Lisabeth, L.D., Liu, S., Mackey, R.H., Magid, D.J., McGuire, D.K., Mohler, E.R., Moy, C.S., Muntner, P.,

Mussolino, M.E., Nasir, K., Neumar, R.W., Nichol, G., Palaniappan, L., Pandey, D.K., Reeves, M.J., Rodriguez, C.J., Rosamond, W., Sorlie, P.D., Stein, J., Towfighi, A., Turan, T.N., Virani, S.S., Woo, D., Yeh, R.W., Turner, M.B., 2016. Heart Disease and Stroke Statistics-2016 Update: A Report From the American Heart Association. Circulation 133, e38–360.

Murry, CE, Keller, G, 2008. Differentiation of embryonic stem cells to clinically relevant populations: lessons from embryonic development. Cell.

Míguez, D.G., Gil-Guiñón, E., Pons, S., Martí, E., 2013. Smad2 and Smad3 cooperate and antagonize simultaneously in vertebrate neurogenesis. J. Cell. Sci. 126, 5335–43.

Münch, J, Grivas, D, González-Rajal, Á., 2017. Notch signalling restricts inflammation and serpine1 in the dynamic endocardium of the regenerating zebrafish heart. ….

Nagasue, N, Yukaya, H, Ogawa, Y, Kohno, H, 1987. Human liver regeneration after major hepatic resection. A study of normal liver and livers with chronic hepatitis and cirrhosis. Annals of ….

Nieto, MA, 2011. The ins and outs of the epithelial to mesenchymal transition in health and disease. Annual review of cell and developmental biology.

Orkin, S.H., Hochedlinger, K., 2011. Chromatin connections to pluripotency and cellular reprogramming. cell 145, 835–850.

Ozdamar, B., Bose, R., Barrios-Rodiles, M., Wang, H.-R.R., Zhang, Y., Wrana, J.L., 2005. Regulation of the polarity protein Par6 by TGFbeta receptors controls epithelial cell plasticity. Science 307, 1603–9.

Padua, D., Zhang, X., Wang, Q., Nadal, C., Gerald, W., Gomis, R., Massagué, J., 2008. TGFβ Primes Breast Tumors for Lung Metastasis Seeding through Angiopoietin-like 4. Cell 133, 66–77.

Pangas, S.A., Jorgez, C.J., Tran, M., Agno, J., Li, X., Brown, C.W., Kumar, T.R., Matzuk, M.M., 2007. Intraovarian activins are required for female fertility. Mol. Endocrinol. 21, 2458–71.

Parker, TG, Packer, SE, Schneider, MD, 1990. Peptide growth factors can provoke“ fetal” contractile protein gene expression in rat cardiac myocytes. Journal of Clinical ….

Petersen, M., Pardali, E., Horst, G. van der, Cheung, H., Hoogen, C. van den, Pluijm, G. van der, Ten Dijke, P., 2010. Smad2 and Smad3 have opposing roles in breast cancer bone metastasis by differentially affecting tumor angiogenesis. Oncogene 29, 1351–61.

Pohlers, D., Brenmoehl, J., Löffler, I., Müller, C.K., Leipner, C., Schultze-Mosgau, S., Stallmach, A., Kinne, R.W., Wolf, G., 2009. TGF-beta and fibrosis in different organs - molecular pathway imprints. Biochim. Biophys. Acta 1792, 746–56.

Polizzotti, B.D., Ganapathy, B., Walsh, S., Choudhury, S., Ammanamanchi, N., Bennett, D.G., Remedios, C.G. dos, Haubner, B.J., Penninger, J.M., Kühn, B., 2015. Neuregulin stimulation of cardiomyocyte regeneration in mice and human myocardium reveals a therapeutic window. Sci Transl Med 7, 281ra45.

Porrello, E.R., Mahmoud, A.I., Simpson, E., Hill, J.A., Richardson, J.A., Olson, E.N., Sadek, H.A., 2011. Transient regenerative potential of the neonatal mouse heart. Science 331, 1078–80.

Porrello, E.R., Olson, E.N., 2014. A neonatal blueprint for cardiac regeneration. Stem cell research 13, 556–570.

Poss, K.D., Wilson, L.G., Keating, M.T., 2002. Heart regeneration in zebrafish. Science 298, 2188–90.

Qian, L., Huang, Y., Spencer, C.I., Foley, A., Vedantham, V., Liu, L., Conway, S.J., Fu, J.D., Srivastava, D., 2012. In vivo reprogramming of murine cardiac fibroblasts into induced cardiomyocytes. Nature 485, 593–8.

Rasouli, S.J., Stainier, D.Y.R.Y., 2017. Regulation of cardiomyocyte behavior in zebrafish trabeculation by Neuregulin 2a signaling. Nat Commun 8, 15281.

Rebbapragada, A, Benchabane, H, 2003. Myostatin signals through a transforming growth factor β-like signaling pathway to block adipogenesis. … and cellular biology.

Rebbapragada, A., Benchabane, H., Wrana, J.L., Celeste, A.J., Attisano, L., 2003. Myostatin signals through a transforming growth factor beta-like signaling pathway to block adipogenesis. Mol. Cell. Biol. 23, 7230–42.

Reischauer, S., Arnaout, R., Ramadass, R., Stainier, D.Y., 2014. Actin binding GFP allows 4D in vivo imaging of myofilament dynamics in the zebrafish heart and the identification of Erbb2 signaling as a remodeling factor of myofibril architecture. Circ. Res. 115, 845–56.

Rodgers, BD, Garikipati, DK, 2008. Clinical, agricultural, and evolutionary biology of myostatin: a comparative review. Endocrine reviews.

Rodgers, B.D., Interlichia, J.P., Garikipati, D.K., Mamidi, R., Chandra, M., Nelson, O.L., Murry, C.E., Santana, L.F., 2009. Myostatin represses physiological hypertrophy of the heart and excitation-contraction coupling. J. Physiol. (Lond.) 587, 4873–86.

Rubin, N., Darehzereshki, A., Bellusci, S., Kaartinen, V., Ling Lien, C., 2013. FGF10 Signaling Enhances Epicardial Cell Expansion during Neonatal Mouse Heart Repair. J Cardiovasc Dis Diagn 1.

Ryckebusch, L, Wang, Z, Bertrand, N, 2008. Retinoic acid deficiency alters second heart field formation. Proceedings of the ….

Sallin, P., Preux Charles, A.-S.S. de, Duruz, V., Pfefferli, C., Jaźwińska, A., 2015. A dual epimorphic and compensatory mode of heart regeneration in zebrafish. Dev. Biol. 399, 27–40.

Sartori, R., Gregorevic, P., Sandri, M., 2014. TGFβ and BMP signaling in skeletal muscle: potential significance for muscle-related disease. Trends Endocrinol. Metab. 25, 464–71.

Scheel, C, Eaton, EN, Li, S., Chaffer, CL, Reinhardt, F, 2011. Paracrine and autocrine signals induce and maintain mesenchymal and stem cell states in the breast. Cell.

Schindler, C, Jr, D.J., 1995. Transcriptional responses to polypeptide ligands: the JAK-STAT pathway. Annual review of biochemistry.

Schnabel, K., Wu, C.-C.C., Kurth, T., Weidinger, G., 2011. Regeneration of cryoinjury induced necrotic heart lesions in zebrafish is associated with epicardial activation and cardiomyocyte proliferation. PLoS ONE 6, e18503.

Senyo, S.E., Lee, R.T., Kühn, B., 2014. Cardiac regeneration based on mechanisms of cardiomyocyte proliferation and differentiation. Stem Cell Res 13, 532–41.

Senyo, S.E., Steinhauser, M.L., Pizzimenti, C.L., Yang, V.K., Cai, L., Wang, M., Wu, T.-D.D., Guerquin-Kern, J.-L.L., Lechene, C.P., Lee, R.T., 2013. Mammalian heart renewal by pre-existing cardiomyocytes. Nature 493, 433–6.

Sharma, M., Kambadur, R., Matthews, K.G., Somers, W.G., Devlin, G.P., Conaglen, J.V., Fowke, P.J., Bass, J.J., 1999. Myostatin, a transforming growth factor-beta superfamily member, is expressed in heart muscle and is upregulated in cardiomyocytes after infarct. J. Cell. Physiol. 180, 1–9.

Siegel, P.M., Massagué, J., 2003. Cytostatic and apoptotic actions of TGF-beta in homeostasis and cancer. Nat. Rev. Cancer 3, 807–21.

Song, JJ, Guyette, JP, Gilpin, SE, Gonzalez, G, 2013. Regeneration and experimental orthotopic transplantation of a bioengineered kidney. Nature medicine.

Song, K., Nam, Y.-J.J., Luo, X., Qi, X., Tan, W., Huang, G.N., Acharya, A., Smith, C.L., Tallquist, M.D., Neilson, E.G., Hill, J.A., Bassel-Duby, R., Olson, E.N., 2012. Heart repair by reprogramming non-myocytes with cardiac transcription factors. Nature 485, 599–604.

Soonpaa, M.H., Field, L.J., 1997. Assessment of cardiomyocyte DNA synthesis in normal and injured adult mouse hearts. Am. J. Physiol. 272, H220–6.

Soonpaa, M.H., Kim, K.K., Pajak, L., Franklin, M., Field, L.J., 1996. Cardiomyocyte DNA synthesis and binucleation during murine development. Am. J. Physiol. 271, H2183–9.

Sridurongrit, S., Larsson, J., Schwartz, R., Ruiz-Lozano, P., Kaartinen, V., 2008. Signaling via the Tgf-beta type I receptor Alk5 in heart development. Dev. Biol. 322, 208–18.

Stefano, V. Di, Giacca, M., Capogrossi, M.C., Crescenzi, M., Martelli, F., 2011. Knockdown of cyclin-dependent kinase inhibitors induces cardiomyocyte re-entry in the cell cycle. J. Biol. Chem. 286, 8644–54.

Steinhauser, M.L., Lee, R.T., 2011. Regeneration of the heart. EMBO Mol Med 3, 701–12.

Stroschein, S.L., Wang, W., Luo, K., 1999. Cooperative binding of Smad proteins to two adjacent DNA elements in the plasminogen activator inhibitor-1 promoter mediates

transforming growth factor beta-induced smad-dependent transcriptional activation. J. Biol. Chem. 274, 9431–41.

Takeuchi, J.K., Lou, X., Alexander, J.M., Sugizaki, H., Delgado-Olguín, P., Holloway, A.K., Mori, A.D., Wylie, J.N., Munson, C., Zhu, Y., Zhou, Y.-Q.Q., Yeh, R.-F.F., Henkelman, R.M., Harvey, R.P., Metzger, D., Chambon, P., Stainier, D.Y., Pollard, K.S., Scott, I.C., Bruneau, B.G., 2011. Chromatin remodelling complex dosage modulates transcription factor function in heart development. Nat Commun 2, 187.

Tan, EJ, Thuault, S, Caja, L, Carletti, T, Heldin, CH, 2012. Regulation of transcription factor Twist expression by the DNA architectural protein high mobility group A2 during epithelial-to-mesenchymal transition. Journal of Biological ….

Thenappan, A., Li, Y., Kitisin, K., Rashid, A., Shetty, K., Johnson, L., Mishra, L., 2010. Role of transforming growth factor beta signaling and expansion of progenitor cells in regenerating liver. Hepatology 51, 1373–82.

Thiery, JP, Acloque, H, Huang, R., Nieto, MA, 2009. Epithelial-mesenchymal transitions in development and disease. cell.

Thuault, S, Tan, EJ, Peinado, H, Cano, A, 2008. HMGA2 and Smads co-regulate SNAIL1 expression during induction of epithelial-to-mesenchymal transition. Journal of Biological ….

Tsuchida, K., Nakatani, M., Hitachi, K., Uezumi, A., Sunada, Y., Ageta, H., Inokuchi, K., 2009. Activin signaling as an emerging target for therapeutic interventions. Cell Commun. Signal 7, 15.

Vale, W., Rivier, J., Vaughan, J., McClintock, R., Corrigan, A., Woo, W., Karr, D., Spiess, J., 1986. Purification and characterization of an FSH releasing protein from porcine ovarian follicular fluid. Nature 321, 776–779.

Villarreal, FJ, Dillmann, WH, 1992. Cardiac hypertrophy-induced changes in mRNA levels for TGF-beta 1, fibronectin, and collagen. American Journal of Physiology- ….

Viloria-Petit, AM, David, L, Jia, JY, 2009. A role for the TGFβ-Par6 polarity pathway in breast cancer progression. Proceedings of the ….

Vincent, T, Neve, E., Johnson, JR, Kukalev, A, 2009. A SNAIL1–SMAD3/4 transcriptional repressor complex promotes TGF-β mediated epithelial–mesenchymal transition. Nature cell ….

Wagner, K.R., Liu, X., Chang, X., Allen, R.E., 2005. Muscle regeneration in the prolonged absence of myostatin. Proc. Natl. Acad. Sci. U.S.A. 102, 2519–24.

Walsh, S., Pontén, A., Fleischmann, B.K., Jovinge, S., 2010. Cardiomyocyte cell cycle control and growth estimation in vivo--an analysis based on cardiomyocyte nuclei. Cardiovasc. Res. 86, 365–73.

Wang, J., Karra, R., Dickson, A.L., Poss, K.D., 2013. Fibronectin is deposited by injury-activated epicardial cells and is necessary for zebrafish heart regeneration. Dev. Biol. 382, 427–35.

Wang, J., Panáková, D., Kikuchi, K., Holdway, J.E., Gemberling, M., Burris, J.S., Singh, S.P., Dickson, A.L., Lin, Y.-F.F., Sabeh, M.K., Werdich, A.A., Yelon, D., Macrae, C.A., Poss, K.D., 2011. The regenerative capacity of zebrafish reverses cardiac failure caused by genetic cardiomyocyte depletion. Development 138, 3421–30.

Wang, T., Li, B.Y., Danielson, P.D., Shah, P.C., Rockwell, S., Lechleider, R.J., Martin, J., Manganaro, T., Donahoe, P.K., 1996. The immunophilin FKBP12 functions as a common inhibitor of the TGF beta family type I receptors. Cell 86, 435–44.

Wang, X., Fischer, G., Hyvönen, M., 2016. Structure and activation of pro-activin A. Nat Commun 7, 12052.

Whittemore, L.-A.A., Song, K., Li, X., Aghajanian, J., Davies, M., Girgenrath, S., Hill, J.J., Jalenak, M., Kelley, P., Knight, A., Maylor, R., O'Hara, D., Pearson, A., Quazi, A., Ryerson, S., Tan, X.Y., Tomkinson, K.N., Veldman, G.M., Widom, A., Wright, J.F., Wudyka, S., Zhao, L., Wolfman, N.M., 2003. Inhibition of myostatin in adult mice increases skeletal muscle mass and strength. Biochem. Biophys. Res. Commun. 300, 965–71.

Witman, N., Murtuza, B., Davis, B., Arner, A., Morrison, J.I., 2011. Recapitulation of developmental cardiogenesis governs the morphological and functional regeneration of adult newt hearts following injury. Dev. Biol. 354, 67–76.

Wu, C.-C.C., Kruse, F., Vasudevarao, M.D., Junker, J.P., Zebrowski, D.C., Fischer, K., Noël, E.S., Grün, D., Berezikov, E., Engel, F.B., Oudenaarden, A. van, Weidinger, G., Bakkers, J., 2016. Spatially Resolved Genome-wide Transcriptional Profiling Identifies BMP Signaling as Essential Regulator of Zebrafish Cardiomyocyte Regeneration. Dev. Cell 36, 36–49.

Xi, Q, Wang, Z, Zaromytidou, AI, Zhang, X., 2011. A poised chromatin platform for TGF-β access to master regulators. Cell.

Yang, L, Pang, Y, Moses, HL, 2010. TGF-β and immune cells: an important regulatory axis in the tumor microenvironment and progression. Trends in immunology.

Yin, V.P., Lepilina, A., Smith, A., Poss, K.D., 2012. Regulation of zebrafish heart regeneration by miR-133. Dev. Biol. 365, 319–27.

Ying, QL, Nichols, J, Chambers, I, Smith, A, 2003. BMP induction of Id proteins suppresses differentiation and sustains embryonic stem cell self-renewal in collaboration with STAT3. Cell.

Yingling, J.M., Datto, M.B., Wong, C., Frederick, J.P., Liberati, N.T., Wang, X.F., 1997. Tumor suppressor Smad4 is a transforming growth factor beta-inducible DNA binding protein. Mol. Cell. Biol. 17, 7019–28.

Yndestad, A., Ueland, T., Øie, E., Florholmen, G., Halvorsen, B., Attramadal, H., Simonsen, S., Frøland, S.S., Gullestad, L., Christensen, G., Damås, J.K., Aukrust, P., 2004. Elevated levels of activin A in heart failure: potential role in myocardial remodeling. Circulation 109, 1379–85.

Young, RA, 2011. Control of the embryonic stem cell state. Cell.

Yuasa, S, Fukuda, K, 2009. Multiple roles for BMP signaling in cardiac development. Drug Discovery Today: Therapeutic Strategies.

Zeisberg, E.M., Tarnavski, O., Zeisberg, M., Dorfman, A.L., McMullen, J.R., Gustafsson, E., Chandraker, A., Yuan, X., Pu, W.T., Roberts, A.B., Neilson, E.G., Sayegh, M.H., Izumo, S., Kalluri, R., 2007. Endothelial-to-mesenchymal transition contributes to cardiac fibrosis. Nat. Med. 13, 952–61.

Zhang, R., Han, P., Yang, H., Ouyang, K., Lee, D., Lin, Y.-F.F., Ocorr, K., Kang, G., Chen, J., Stainier, D.Y., Yelon, D., Chi, N.C., 2013. In vivo cardiac reprogramming contributes to zebrafish heart regeneration. Nature 498, 497–501.

Zhou, P., Pu, W.T., 2016. Recounting Cardiac Cellular Composition. Circ. Res. 118, 368–70.

Acknowledgements

I would like to thank a lot of people who have been a part of my journey of doing PhD here.

Firstly, I would like to thank Prof. Dr. Didier Stainier for giving me the opportunity to pursue PhD in his laboratory. I am also grateful to him for his constant support, critical suggestions and guidance throughout my PhD. I have learned a lot from him, about not only being a good scientist on bench but also to be able to efficiently pen down my thoughts in scientific writing.

Another person who has played an equally important role in my PhD project is my direct supervisor, Dr. Sven Reischauer. I would like to thank him for always being there to guide and support me during my PhD. I highly appreciate his critical supervision as well as friendly attitude towards me, which gave me a lot of confidence to follow my path.

I would also like to thank Prof. Dr. Virginie Lecaudey for taking her precious time and accepting to review my thesis.

I take the opportunity to thank my friends, Suchit Ahuja, Veronica Uribe Sokolov, Claudia Carlantoni and Sri Teja Mullapudi, for always being there and with whom I have had many treasurable memories. I also express my gratitude to my friends and colleagues for all their support and sharing happy moments: Srinivas Allanki, Giulia Boezio, Claudia Gerri, Krishna Srinivasan, Anoop Cherian, Vanesa Jiménez Amilburu, Rashmi Priya, Sophie Ramas, Felix Gunawan, Michelle Marass, Alessandra Gentile, Jasmin Gäbges, Hadil El Sammak, Kenny Mattonet, Jason Lai, Anabela Bensimon Brito, Sébastien Gauvrit, Javad Rasouli, Hyun-Taek Kim, Pourya Sarvari, Rubén Marín Juez, Michelle Collins, Paolo Panza, Radhan Ramadass, Carol Yang, Raoul Frietas, Marion Delous, Alethia Villasenor, Avdesh Avdesh, Chinmoy Patra, Arica Beisaw, Almary Guerra, Mohamed El Brolosy, Ayele Taddese Tsedeke, Brijesh Kumar, Ryuichi Fukuda, Oliver Stone, Silvia Parajes, Nana Fukuda, Khrievono Kikhi, Sharon Meaney Gardian, Hans-Martin Maischein, Sabine Fischer, Beate Grohmann, Marianne Ploch, Carmen Büttner, Rita Retzloff, Martin Laszczyk, Bilge Reischauer and Franziska Hainer.

Last but not the least, I would like to express my gratitude and love to my family. I would like to thank my parents and siblings who have always stood by me throughout my life and have always supported and encouraged me to follow my dreams.